



AN ADVANCED LOWER AND UPPER BOUND SHAKEDOWN  
ANALYSIS METHOD TO ENHANCE THE R5 HIGH  
TEMPERATURE ASSESSMENT PROCEDURE

by

JAMES MICHAEL URE

Submitted to the Department of Mechanical and Aerospace Engineering in Partial  
Fulfilment of the Degree of

DOCTOR OF ENGINEERING (ENGD) IN NUCLEAR ENGINEERING

at the

UNIVERSITY OF STRATHCLYDE

August 2013

This thesis is the result of the author's original research. It has been composed by the author and has not been previously submitted for examination which has led to the award of a degree.

The copyright of this thesis belongs to the author under the terms of the United Kingdom Copyright Acts as qualified by University of Strathclyde Regulation 3.50. Due acknowledgement must always be made of the use of any material contained in, or derived from, this thesis.

Signed:

Date:

## **Acknowledgements**

A doctorate is very often thought of as an individual endeavour, but the reality is that the completion of this project and thesis would not have been possible without the help and guidance of a number of people.

I would like to extend my thanks to the University of Strathclyde Mechanical and Aerospace Dept, in particular my supervisor Dr Haofeng Chen and IMechE mentor Dr Andrew McLaren. Their guidance over the past 4 years has been invaluable in getting to the stage I'm at now. Considerable thanks also go to David Tipping from EDF for his advice and support over the years. I'm also grateful to David, Marc Chevalier, Peter Budden Dave Dean and others from the Assessment Technology Group for making me feel welcome during my visit to Barnwood. I look forward to keeping in touch with you all once my studies are complete.

I think any doctoral student would agree that completing their project just wouldn't be possible without fellow PhD students to share the highs and lows (and to provide a welcome distraction when the code just isn't working!). Among the many people are Niall Hamilton, Alistair Pugh, Alan Jappy, Michael Lytwyn, Steven Owens and many others. I wish you all the best of luck for your future careers.

To my friends outside of the department, former course-mates and swimming friends, I have really enjoyed all the triathlon training and general good times. Whether you realise it or not you have all helped me through the past 4 years.

Finally my sincerest go to thanks to my family, especially my parents, whose advice, support and timely words of wisdom have been invaluable. Thank you to you all.

*"...Structural engineering is the art of modelling materials we do not wholly understand into shapes we cannot precisely analyse, so as to withstand forces we cannot properly assess, in such a way that the public at large has no reason to suspect the extent of our ignorance..."*

**Dr A.R Dykes in his address to the Institute of Structural Engineers, 1978.**

## **Abstract**

A nuclear power station contains some of the most extreme environments and operating conditions seen by metallic components. In order to ensure the continued safe operation of these plant components rigorous structural integrity assessments are performed. Part of this structural assessment involves demonstrating that the component in question will not fail by ratcheting.

In the UK the R5 procedure forms the cornerstone of these integrity assessments. The R5 rules for shakedown, whilst easily implemented, can give an overly pessimistic estimate of the shakedown status. This means that a computationally expensive nonlinear finite element analysis must be conducted. The Linear Matching Method (LMM) is one of the recently developed Direct Methods for shakedown analysis. This upper bound method has the ability to give more accurate shakedown limits than the simplified R5 route and with less computational expense than nonlinear finite element analysis.

This thesis details the steps taken to take the LMM from being a research based method into a tool which can be used for regular integrity analyses within EDF. Firstly a conservative lower bound to the shakedown limit is derived and added to the LMM. The theoretical development and numerical implementation of this calculation is detailed. Convergence improvements are also investigated to improve the numerical difficulties often suffered by lower bound shakedown calculations. The LMM is implemented in Abaqus through user subroutines. To make the LMM suitable for regular use a user interface has been created via a plug-in for Abaqus. This plug-in automatically configures the model for the analysis, meaning that the user now has access to LMM analyses without having to carry out the code changes which were required with the research version of the method.

The resulting analysis tool has been delivered to EDF so their engineers can now access accurate shakedown analyses through a convenient user-interface.

University of Strathclyde Supervisor: Dr Haofeng Chen, Senior Lecturer

EDF Energy Supervisor: Mr David Tipping, Structural Integrity Software Engineer

# Table of Contents

1	Technical, Economic and Political Background .....	1
1.1	Introduction .....	1
1.2	The UK Nuclear Industry .....	2
1.3	Safe Electricity Generation from Nuclear Power .....	4
1.3.1	Shakedown and the R5 Procedure.....	6
1.4	Drivers for Project Creation .....	7
1.5	The Linear Matching Method .....	9
1.6	Project Aims and Objectives .....	10
2	Shakedown in Structural Engineering.....	12
2.1	Introduction .....	12
2.2	The Shakedown Phenomenon .....	12
2.3	The Shakedown Theorems.....	16
2.4	The R5 High Temperature Assessment Procedure .....	17
2.4.1	Shakedown Criteria in R5.....	19
2.5	Finite Element Analysis for Shakedown Limit Calculation .....	21
2.6	Direct Methods .....	24
2.6.1	Direct Methods for Limit Load and Strict Shakedown .....	24
2.6.2	Direct Methods for Global Shakedown.....	28
2.6.3	The Linear Matching Method for Use in Industry.....	32
2.7	Summary .....	33
3	The LMM Strict Shakedown Procedure, Analyses and Verifications .....	35
3.1	Introduction .....	35
3.2	The LMM Strict Shakedown Procedure .....	35
3.2.1	The General Cyclic State for Strict Shakedown.....	35

3.2.2	LMM Upper Bound Method.....	37
3.2.2.1	The Upper Bound Theorem .....	37
3.2.2.2	The Iterative Upper Bound Procedure.....	37
3.2.2.3	Numerical Implementation of the Method .....	39
3.2.3	Lower Bound Method .....	43
3.3	Validation of the LMM Strict Shakedown Procedure .....	44
3.3.1	Limit Loads of Notched Bars .....	44
3.3.1.1	3D Notched Round Bar .....	46
3.3.1.2	Axisymmetric Notched Round Bar .....	46
3.3.1.3	Plane Strain Double Notched Plate.....	47
3.3.1.4	Plane Stress Double Notched Plate.....	48
3.3.1.5	Notched Bar Summary .....	48
3.3.2	The Bree Cylinder .....	48
3.3.3	Comparisons with Experimental Data.....	50
3.3.3.1	Limit Load Comparisons.....	50
3.3.3.2	Shakedown Limit Comparisons .....	53
3.4	The LMM Strict Shakedown Method Applied to Pipe Bends.....	56
3.4.1	Existing Pipe Bend Solutions .....	57
3.4.2	LMM Analysis .....	60
3.4.3	Description of FEA Model, Parametric Study and Loading .....	61
3.4.4	Internal Pressure and Moment Loading .....	63
3.4.4.1	Effect of the Ratio $r/t$ .....	65
3.4.4.2	Effect of the Ratio $R/r$ .....	66
3.4.4.3	Comparison of Opening, Closing and Reversed Bending.....	67
3.4.5	Internal Pressure and Thermal Loading .....	69
3.4.5.1	Temperature Dependent Yield Stress.....	69
3.4.5.2	Effect of $R/r$ .....	70
3.4.5.3	Effect of $r/t$ .....	70
3.4.6	Pipe Bend Conclusions .....	71

3.5	Summary and Discussion .....	72
4	The LMM Global Shakedown Analysis Procedure .....	73
4.1	Introduction .....	73
4.2	LMM Upper Bound Global Shakedown Analysis.....	73
4.2.1	The General Cyclic State .....	73
4.2.2	Upper Bound Theorem for Loading in Excess of Strict Shakedown.....	75
4.2.3	The Two Stage Global Shakedown Limit Calculation .....	77
4.2.4	Numerical Implementation.....	77
4.2.4.1	Stage 1 - Procedure for Establishing the Steady State Cycle .....	78
4.2.4.2	Stage 2 - Calculation of the Global Shakedown Limit .....	81
4.3	Lower Bounds to Global Shakedown .....	82
4.4	A Lower Bound to the LMM Global Shakedown Procedure .....	83
4.4.1	Conditions for a Lower Bound to Global Shakedown .....	83
4.4.2	Lower Bound in the LMM Global Shakedown Procedure.....	85
4.5	Numerical Example .....	88
4.5.1	Verification of the Position of the Constant Residual Stress Field.....	88
4.5.2	Plate with a Central Hole .....	89
4.6	Convergence Improvements.....	91
4.6.1	Sources of Convergence Issues .....	92
4.6.2	Proposed Solutions .....	93
4.6.3	Numerical Testing .....	95
4.6.4	Results and Selection of Final Scheme.....	96
4.7	Summary and Discussion .....	100
5	Analyses and Validations of the LMM Global Shakedown Method.....	101
5.1	Introduction .....	101
5.2	Validations .....	101

5.2.1	Limit Loads of Notched Bars .....	101
5.2.2	The Bree Cylinder .....	102
5.3	Global Shakedown of a Pipe Intersection .....	104
5.3.1	Review of Existing Pipe Intersection Solutions .....	105
5.3.2	The Pipe Intersection Model and Material Properties .....	106
5.3.3	Internal Pressure and Thermal Loading .....	108
5.3.3.1	Results .....	110
5.3.3.2	Validation .....	111
5.3.4	Internal Pressure and Moment Loading .....	114
5.3.4.1	Results .....	115
5.3.4.2	Material Property Study.....	116
5.3.5	Pipe Intersection Summary.....	118
5.4	Summary and Discussion .....	119
6	The Creation of a LMM Structural Analysis Tool .....	120
6.1	Introduction .....	120
6.2	Preliminary Considerations .....	120
6.2.1	Previous LMM Versions .....	120
6.2.2	Customising Abaqus.....	121
6.3	Re-structuring of the Subroutines .....	124
6.4	Graphical User Interface via an Abaqus Plug-in.....	127
6.5	Installation and Testing.....	138
6.6	Summary and Discussion .....	139
7	Application of the Complete LMM Analysis Tool.....	140
7.1	Background .....	140
7.2	Finite Element Model.....	141
7.2.1	Geometry .....	141
7.2.2	Material Properties .....	142

7.2.3	Loads and Boundary Conditions .....	143
7.3	EDF Shakedown Analysis.....	144
7.3.1	R5 Simple Checks .....	145
7.3.2	R5 Shakedown Check Involving a Residual Stress Field .....	145
7.3.3	Elastic-Plastic FEA.....	146
7.4	Analysis using the LMM .....	147
7.4.1	Strict Shakedown Analysis .....	147
7.4.2	Steady State Cycle and Global Shakedown Limit .....	151
7.5	Summary and Discussion .....	155
8	Conclusions, Discussion and Future Work .....	156
8.1	Summary of the Thesis.....	156
8.2	Future work.....	158
9	References .....	161
Appendix A.	Equations for limit pressure and moment of a pipe bend .....	I
Appendix B.	Iterative Evaluation of the Varying Residual Stress Field.....	III
Appendix C.	Algebraic Expansion of Equation ( 4.44) .....	V
Appendix D.	The LMM Subroutines.....	VII
Appendix E.	Structure of the LMM Plug-in .....	XXV

## List of Figures

Figure 1.1 - Schematic of a Nuclear Power Station.....	5
Figure 1.2 - 3D Model of the EPR Reactor .....	6
Figure 1.3 - LMM Modulus Adjustment and Stress Redistribution .....	9
Figure 2.1 - Structural Responses to Cyclic Loading .....	13
Figure 2.2 - Bree Interaction Diagram.....	15
Figure 2.3 - Plastic Strain History at a Critical Location in Cyclic FEA Model.....	23
Figure 2.4 - ECM Limit Load for a Beam in Bending and Tension .....	26
Figure 2.5 - Map of Results from DCA Analysis of the Bree Cylinder.....	29
Figure 2.6 - Hybrid Method Stage 2 Yield Stress Calculation.....	30
Figure 3.1 - Load and Boundary Condition Schematic.....	35
Figure 3.2 - Geometry, Mesh and Material Properties of the Notched Bars.....	45
Figure 3.3 - 3D Notched Bar Results Comparison.....	46
Figure 3.4 - Axisymmetric Notched Bar Results Comparison .....	47
Figure 3.5 - Plane Strain Notched Bar Results Comparison .....	47
Figure 3.6 - Plane Stress Notched Bar Results Comparison.....	48
Figure 3.7 - Bree Cylinder Loading, Load History and Results .....	49
Figure 3.8 - Modified Bree Cylinder Loading, Load History and Results.....	50
Figure 3.9 - Pipe Intersection a) Geometry and b) Typical Material Stress-Strain Curve .....	51
Figure 3.10 - Application of a Pure Moment.....	51
Figure 3.11 - FEA Models A and B1 .....	52
Figure 3.12 - Geometry of Nozzles 5 and 6.....	53
Figure 3.13 - FEA Models of Nozzles 5 and 6 .....	55
Figure 3.14 - Location of Reverse Plasticity in Nozzle 5.....	56
Figure 3.15 - Pipe Bend Geometry and h Value.....	57

Figure 3.16 - Pipe Bend Change in Cross Section Under Bending.....	58
Figure 3.17 - Sample Results from [66].....	59
Figure 3.18 - Pipe Bend FEA Model Showing Symmetry Planes .....	61
Figure 3.19 - Moment Loading and History .....	62
Figure 3.20 - R/r=2, r/t=5 Limit load, Shakedown Limit and Location of Failure.....	63
Figure 3.21 - Comparison of the LMM with the Results in [66].....	64
Figure 3.22 - Effect of r/t on the Limit and Shakedown Boundaries .....	65
Figure 3.23 - Effect of R/r on the Shakedown Boundaries .....	66
Figure 3.24 - Comparison of Opening, Closing and Reversed Bending.....	67
Figure 3.25 - Comparison of LMM Results with the Equations of Lei [100] .....	68
Figure 3.26 - Effect of Temperature Dependent Yield on the Strict Shakedown Limit for R/r=3 r/t=10 .....	69
Figure 3.27 - Effect of R/r on Thermal Loading Strict Shakedown.....	70
Figure 3.28 - Effect of r/t on Thermal Loading Strict Shakedown.....	71
Figure 4.1 - Bree Stress Fields .....	88
Figure 4.2 - Holed Plate Geometry, Mesh and Load History .....	90
Figure 4.3 - Holed Plate Interaction Diagram and Convergence .....	91
Figure 4.4 - Setting $\mu_{Max}$ as a Function of Stress .....	94
Figure 4.5 - Trial Schemes for Limiting $\mu_{rate}$ .....	95
Figure 4.6 - Test Load Cases for the Holed Plate .....	95
Figure 4.7 - Nodal Paths Used to Compare Stresses.....	96
Figure 4.8 - Comparison of Trial 1,2 and 3 with the Original Scheme and Step by Step .....	97
Figure 4.9 - Comparison of Trials 4-7 with the Original Scheme and Step by Step Results...	98
Figure 4.10 - Comparison of Trials 8-10 with the Original Scheme and Step by Step Results	98
Figure 4.11 - Load Multiplier Comparison of Original Scheme and Trial 4 .....	99
Figure 4.12 - Comparison of Elemental Averaging, Trial 4 and the Original Scheme .....	100

Figure 5.1 - Bree Cylinder Global Shakedown Results Comparison.....	103
Figure 5.2 - Modified Bree Global Shakedown Results Comparison .....	104
Figure 5.3 - Pipe Intersection Geometry.....	107
Figure 5.4 - Pipe Intersection Quarter Model and Mesh .....	109
Figure 5.5 - Elastic Stresses due to a) Internal Pressure, b) Linear Temperature Difference and c) Uniform Elevated Temperature .....	109
Figure 5.6 - Strict and Global Interaction Diagram .....	110
Figure 5.7 - Ratchet Mechanism at Point A, C and E .....	111
Figure 5.8 - Points Used for Comparison with Step by Step FEA .....	112
Figure 5.9 - Plastic Strain Response of Points D, E, F and G.....	112
Figure 5.10 - Predicted Failure Mechanism at a) Point F, b) the LMM at $\Delta\theta/\Delta\theta_0 = 2.5$ and c) Point G.....	113
Figure 5.11 - a) Half Model Mesh and b) Elastic Stress from Bending Moment.....	114
Figure 5.12 - Global Shakedown Interaction Diagram for Pressure Moment Loading.....	115
Figure 5.13 - Failure Mechanism at a) Point N, b) Point O and c) Point P .....	116
Figure 5.14 - Global Shakedown Interaction Diagram for Original Pipe, Case 1 and Case 2.....	117
Figure 5.15 - Normalised Interaction Diagram of Original Pipe, Case 1 and Case 2 .....	118
Figure 6.1 - The "Create Plate" Plug-in Dialog Box .....	122
Figure 6.2 - Overall Structure of a LMM Solution .....	124
Figure 6.3 - High Level Overview of LMM Plug-in from the Users Perspective .....	128
Figure 6.4 - Main Dialog Box and Possible Error Messages .....	129
Figure 6.5 - Material Properties Dialog Box and Possible Error Messages .....	130
Figure 6.6 - a) Material Properties Dialog with Ramberg Osgood Option and b) "Tip" Box .....	130
Figure 6.7 - Loadcycle Dialog and Load Scaling Options .....	131
Figure 6.8 - "Tip" Box for Loadcycle .....	132

Figure 6.9 - Analysis Parameters Dialog Boxes for a) Strict Shakedown, b) Steady State Cycle and c) Steady State Cycle + Ratchet.....	133
Figure 6.10 - Load and Predefined Field Manager Dialogs .....	135
Figure 6.11 - Keyword Block After the *ENERGY FILE Command has been Added .....	137
Figure 6.12 - Monitor Dialog Box Showing the LMM Summary Report .....	138
Figure 7.1 - Geometry and Dimensions of Header .....	141
Figure 7.2 - a) Header Mesh b) Weld Mesh Detail.....	142
Figure 7.3 - Reference Points, Multi-Point Constraints and Moment Coordinate System..	143
Figure 7.4 - Stress Classification Line for Linearised Stresses .....	144
Figure 7.5 - Elastic Stress at the Hot Pressure Condition.....	145
Figure 7.6 - Residual Stress State after Removal of all Loads (temp 382.2 degrees) .....	146
Figure 7.7 - Contour of Plastic Strain and Plastic Strain History At the Critical Location ....	147
Figure 7.8 - a) Main Dialog Box and b) Materials Dialog Box.....	148
Figure 7.9 - a) Load Cycle Dialog and b) Job Dialog .....	148
Figure 7.10 - Abaqus Monitor Dialog for the Strict Shakedown Analysis .....	150
Figure 7.11 - a) LMM Mechanism Prediction at the Strict Shakedown Limit and b) Location of Peak Plastic Strain from Elastic-Plastic Analysis .....	150
Figure 7.12 - Steady Cycle and Ratchet Limit a) Main and b) Materials Dialogs .....	151
Figure 7.13 - Steady Cycle and Ratchet a) Load Cycle Dialog and b) Job Dialog.....	152
Figure 7.14 - a) Contour Plot of Plastic Strain and b) Plastic Strain History of Elastic PLastic Analysis .....	154
Figure 7.15 - Plastic Strain History of the Second Elastic Plastic Analysis .....	154
Figure E-1 - Structure of a Generic Abaqus Plug-in.....	XXVI
Figure E-2 - doCustomChecks Dialog Box Descision .....	XXVIII
Figure E-3 - doCustomChecks for a)LMM_main and b)LMM_mats dialog boxes .....	XXX
Figure E-4 - doCustomChecks for a) LMM_loadCycle and b) LMM_job .....	XXXI

## List of Tables

Table 1.1 - Operational UK Nuclear Power Stations .....	3
Table 3.1 - Limit Load Comparison.....	53
Table 3.2 - Material Properties .....	54
Table 3.3 - Comparison of Shakedown Pressures.....	55
Table 3.4 - Temperature Dependent Yield Stress .....	63
Table 5.1 - Comparison of Notched Bar Limit Load Solutions .....	102
Table 5.2 - Temperature Dependent Yield Stress Values .....	107
Table 5.3 - Comparison of Predicted Plastic Strain Ranges for Points H to M.....	114
Table 6.1 - Functions Available in Each LMM Analysis .....	127
Table 6.2 - LMM Text File Example .....	134
Table 6.3 - Material Properties Section of the LMM Text File .....	136
Table 7.1 - Temperature Dependent Material Properties for the Header Branch .....	142
Table 7.2 - Bending Moments Applied to Model (all in Nm) .....	144
Table D-1 - UEXTERNALDB operations.....	VIII

## Nomenclature

$a_0$	Initial defect size
$b$	Bar width/diameter at notch
$C$	Compliance matrix
$E$	Young's modulus
$\bar{F}$	Constant (time invariant) applied load
$h$	Pipe bend factor
$I$	Functional defined during LMM derivation
$J$	Jacobian (or stiffness) matrix
$k$	Iteration number
$K$	Bulk modulus
$m$	Current cycle number
$M$	Total number of cycles
$n$	Current time point in the load cycle
$N$	Total number of time points in the load cycle
$P$	Cyclic mechanical load
$P_L$	Equivalent local primary membrane stress defined in R5
$P_B$	Equivalent primary bending stress defined in R5
$Q$	Equivalent secondary stress defined in R5
$r$	Notch radius for notched bars, or pipe mean radius for pipes and pipe bends
$R$	Bend radius
$S$	Surface of a volume where loads and boundary conditions are applied
$S_T$	Part of the surface where loads are applied
$S_U$	Part of the surface where boundary conditions are applied
$t$	Current time in the cycle
$\Delta t$	Total cycle time
$T$	Temperature
$u$	displacement
$V$	Volume
$x$	Location within the volume, $V$
$w$	Bar width/diameter remote from the notch
$\epsilon$	strain
$\epsilon^P$	Plastic strain
$\dot{\epsilon}$	Strain rate

$\theta$	Cyclic thermal load
$\lambda$	Load multiplier
$\mu$	Shear modulus
$\bar{\mu}$	A value of "effective" shear modulus defined during the LMM derivation
$\nu$	Poisson's ratio
$\bar{\rho}$	Constant (time invariant) residual stress
$\rho^r$	Varying (time dependent) residual stress
$\sigma$	stress
$\hat{\sigma}$	Applied elastic stress
$\sigma^c$	Stress state at yield
$\sigma^{\text{in}}$	Stress value defined during LMM derivation
$\sigma_y$	Yield stress
$()'$ (dash)	Deviatoric components
$()_{ij}$	components
$()^i, ()^f$	Initial and final values of the increment
$()^{\text{UB}}, ()^{\text{LB}}$	Upper bound and lower bound
$\bar{\sigma}(\ )$	Effective (Von-Mises) value of the stress in the bracket
$\bar{\varepsilon}(\ )$	Effective (Von-Mises) value of the strain in the bracket

# 1 Technical, Economic and Political Background

## 1.1 Introduction

A nuclear power station is a large and complex feat of engineering. It contains a large number of safety critical systems and components operating simultaneously for extended periods of time in a harsh environment. The safe operation of these components and systems must be ensured so that the plant can continue to safely generate electricity, and part of the process to do this involves ensuring the structural integrity of the plant. Furthermore, much of the existing UK nuclear power generation is now reaching the end of its design life and the current uncertainties in the timescales for replacement generation capacity means that there is an incentive to keep these plants operating. Structural integrity analyses play an important role in these life extension safety cases, and there is a need for accurate yet conservative analysis techniques.

A great number of components in nuclear power stations are subjected to cyclic loading, often at elevated temperatures. This combination introduces a number of possible failure mechanisms for metallic components including creep rupture and fatigue. The R5 procedure [1], which is used to perform some of the structural integrity calculations, must account for all these relevant failure mechanisms.

Ratcheting, where plastic strain accumulates with each cycle of loading until failure occurs, is one such failure mechanism [2]. The past two decades has seen a substantial increase in research into methods which calculate safe loading limits so that ratcheting does not occur, i.e. a shakedown analysis. These shakedown methods are able to accurately determine the safe loading conditions, and so would be a valuable addition to the R5 procedure. The development of one such method, namely the Linear Matching Method, and its implementation as a tool for use by EDF engineers is the focus of this research.

This introductory chapter outlines the background to this research by:

- Summarising the state of the current nuclear fleet and the position of nuclear new build.
- Describing the manner in which structural integrity assessments contribute to the continued operation of the current nuclear fleet.

- Outlining how current research in the field of shakedown analysis can be used to improve these structural integrity assessments.
- Clarifying the specific objectives of this project to allow wider adoption of this current research in EDF for their structural calculations.

## **1.2 The UK Nuclear Industry**

Electricity through nuclear power has been commercially generated in the UK since 1956 when Calder Hall power station was first connected to the grid [3][4]. At this time all electricity generation was operated by the public owned utility the Central Electricity Generation Board (CEGB). During the 1950's and 60's a further 9 nuclear power stations were built, all of which were of the Magnox reactor design [3].

A more efficient reactor design, the Advanced Gas-Cooled Reactor (AGR) was introduced in the UK which is able to generate 2 to 3 times more electricity than the Magnox design [4]. Construction of this type of power station began in the late 1960's, with the final AGR connected to the grid in 1988. A single Pressure Water Reactor (PWR) was also built at Sizewell, which was connected to the grid in 1995 [5]. After these AGR and PWR reactors no more nuclear plants have been built. All but one of the Magnox plants have reached the end of their operational life and the remaining Magnox station at Wylfa is due to begin decommissioning in 2014 [6]. This will leave the 7 AGR and 1 PWR, all owned and operated by EDF Energy, as the remaining nuclear fleet in the UK. Table 1.1 gives details of the current operational nuclear stations in the UK.

At the turn of the century the government was initially indecisive on the topic of whether to invest in new nuclear power stations. The energy white paper published in 2003 [7] outlined that the existing nuclear fleet would be kept until the end of its life, at which point it would be decommissioned without being replaced. The reliance would instead be on renewable sources and combined heat and power (CHP). The reasons cited for this were that nuclear power was economically unattractive and that uncertainty existed about long term plans for nuclear waste.

This position changed in 2007, when the government published an energy white paper - Meeting the Energy Challenge [8]. This gave the preliminary view that nuclear power could have a role to play in the future energy mix of the UK and announced a public consultation on the matter. In January 2008 the findings of the consultation were released and based on

this the government decided that nuclear should play a part in the UK energy mix [9]. The reasons for this change in opinion included energy security, the desire to have a diverse energy mix and that nuclear power is the only low carbon baseload generation proven on a commercial scale. The government took action to facilitate private investment in nuclear plants including, for example, the creation of the Office for Nuclear Regulation [10] and identifying several sites which could accommodate new reactors.

**Table 1.1 - Operational UK Nuclear Power Stations**

Station	Type	Operator	Net Capacity (MW)	Start of Generation	Estimated Decommissioning Date
Wylfa	Magnox	Magnox Ltd	473	1971	2014
Hunterston B	AGR	EDF	890 (1190)*	1976	2023
Hinkley Point B	AGR	EDF	880 (1220)*	1976	2023
Hartlepool	AGR	EDF	1180	1983	2019
Heysham 1	AGR	EDF	1155	1983	2019
Dungeness B	AGR	EDF	1040	1983	2018
Heysham 2	AGR	EDF	1220	1988	2023
Torness	AGR	EDF	1185	1988	2023
Sizewell B	PWR	EDF	1198	1995	2035

*\*Hinkley Point B and Hunterston B have been restricted to around 70% load because of boiler temperature restrictions.*

The Office for Nuclear Regulation (ONR) was formed from several existing nuclear related government departments and subsequently created the Generic Design Assessment (GDA) process for any new reactor designs [11]. This process, which can take up to 4 years, ensures that the general design of a plant is safe and is a mandatory first step for any new

nuclear station in the UK. Once complete, a reactor design can be built at multiple locations and only needs to obtain site specific consents and approvals.

Currently two consortia plan to build new nuclear stations. EDF plan to build two European Pressurised Reactors (EPR) at Hinkley Point with a combined generating capacity of 3260 MW and a further two at Sizewell [12]. The EPR reactor has passed the GDA (and to date is the only reactor design to do so) [13]. Hitachi also plans to build new nuclear plants, in the form of Advanced Boiling Water Reactors, but only began the Generic Design Assessment for this design in April 2013 [14][15].

Even when a reactor design has passed the GDA process, it is not clear how long it will take to construct and commission a new power station. The EPR reactor is currently under construction in several countries, all of which, barring the Chinese, have reported delays to the schedule [16][17]. The Advanced Boiling Water Reactors currently in operation worldwide took between 4 and 5 years to build and commission [18][19], but must still complete the GDA process. There is an incentive, then, to keep the existing fleet in operation for as long as is safe to do so. Based on the existing decommissioning dates, it is entirely possible that several of the existing fleet will reach the end of their life before any new plants are in operation, leading to a deficit in electricity generation. Therefore EDF are actively pursuing life extension of their plants.

### **1.3 Safe Electricity Generation from Nuclear Power**

The principles of electricity generation from nuclear power are relatively simple, and a simplified schematic of a nuclear power station is shown in Figure 1.1.

The basic principle is that the heat generated by the fission chain reaction is used to create high pressure steam which is in turn used to drive turbines and a generator. In this way a nuclear station is very similar to conventional power stations, the fundamental difference being the manner in which the heat is created.

The reactor core contains the fissile fuel (typically enriched uranium) in long channels. The UK Advanced Gas-cooled Reactor (AGR) design uses a graphite core and alongside the fuel, has parallel channels for control rods [4]. These control rods are made from materials such as boron which are highly neutron absorbent. The degree to which the control rods are removed from the core determines the number of free neutrons available to continue the chain reaction.

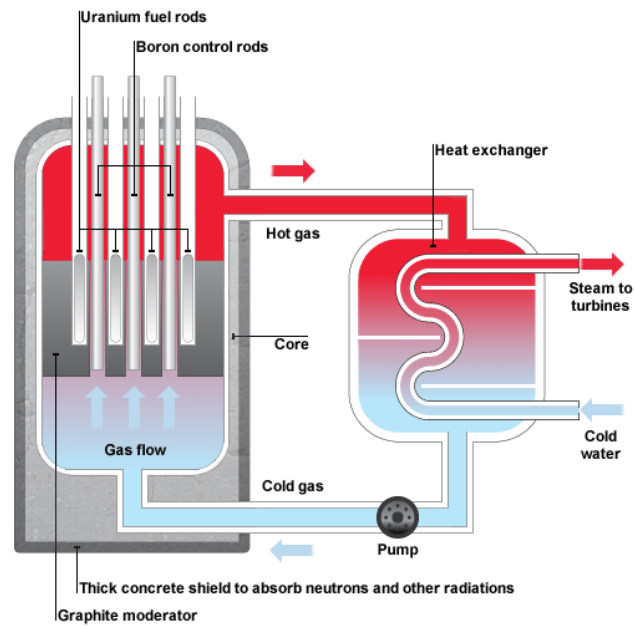


**Figure 1.1 - Schematic of a Nuclear Power Station**

The fission chain reaction generates substantial levels of heat, which is used to increase the temperature of the coolant. In the British AGR design carbon dioxide is used as the core coolant, and as it passes over the fuel in the core channels it reaches temperatures of over 600 degrees Celsius. The carbon dioxide then passes into a heat exchanger, also known as a steam generator because the thermal energy of the CO<sub>2</sub> is used to convert water into high pressure steam. Once it has passed through the steam generator, the cooler CO<sub>2</sub> is then pumped back into the core. This coolant loop is known as the primary circuit.

The secondary circuit uses the high pressure steam from the steam generator to drive the turbine and generator to generate electricity. In this respect the nuclear power station is similar to conventional power generation.

This description of a nuclear power station is heavily simplified. In reality a nuclear power station is hugely complex with many inter-dependent systems simultaneously in operation. Figure 1.2 shows a schematic of the new European Pressurised Reactor (EPR) which is due to be built by EDF at their Hinkley Point and Sizewell sites [12]. In this diagram the scale and complexity of a nuclear station becomes apparent, and this diagram does not include a great number of the auxiliary and safety systems which are vital to the plant operation. Overall a nuclear power station contains numerous valves, pressure vessels, heat exchangers and kilometres of piping with countless intersections, bends, welds, flanged

joints and supports. The structural integrity of all of these components and systems must be ensured if the plant is to be operated safely.



**Figure 1.2 - 3D Model of the EPR Reactor**

Ensuring the structural integrity of the vast number of components is a difficult engineering challenge, not least because of the environments they operate in. Such conditions result in high pressures, bending moments, high temperatures and potentially large temperature gradients. As mentioned, the CO<sub>2</sub> coolant operates in excess of 600 degrees, which is well into the creep range for the stainless steels typically used for these components [20]. During operation there will be variation in these operating conditions alongside some larger, less frequent, events such as shutdowns and start-ups. The cyclic nature of the loading introduces fatigue as a potential failure mechanism, especially when a nuclear power station has a nominal design life of 40 years [3]. EDF must prove that each nuclear station is safe to operate in order to retain the nuclear license for the site. The generation and maintenance of structural integrity safety cases for all components contributes to the safety case for the site as a whole. The component safety cases are generated by rigorous inspections combined with structural integrity calculations by EDF engineers.

### **1.3.1 Shakedown and the R5 Procedure**

R5 [1] is a structural integrity assessment procedure developed for use in the UK nuclear industry, and is now used more widely by other industries concerned with high temperature structural integrity. First developed in 1990, R5 is now in its third issue and provides the backbone of structural integrity assessments in EDF used to create the safety

cases for plant components. The procedure has been developed to assess metallic structures containing defects (such as cracks) which operate at high temperatures, meaning the effects of creep are introduced to its behaviour.

The R5 procedure uses a simplified approach based on linear elastic analysis with accompanying techniques to incorporate the nonlinearity of plasticity and creep [2][21]. This makes the procedure less restrictive than the rule based approach of many design codes and assessment procedures, but less computationally expensive than full nonlinear analysis using Finite Element Analysis (FEA). If the simplified techniques in R5 are not sufficient to substantiate the component then advice is also given for full nonlinear analysis. R5 is used to assess a component based on a number of potential mechanisms including gross plastic collapse, creep rupture and crack growth.

A key part of the R5 procedure is to demonstrate that a component is not ratcheting. Ratcheting (or incremental plastic collapse) is where plastic strains accumulate with each cycle of loading. Continued cycling causes these plastic strains to grow unbounded until the structure fails through gross plastic deformation. Showing a component does not ratchet is achieved by demonstrating that it is either within strict shakedown or global shakedown. Strict shakedown is the structural phenomenon where a component is initially loaded beyond the elastic limit (thus causing permanent plastic strains in the structure) but responds in an entirely elastic manner after the first few loading cycles. Global shakedown is where there are plastic strains in each load cycle, but these are entirely reversed so that no accumulation of plastic strain occurs from one cycle to the next. Demonstration of shakedown is one of the first calculations in the R5 procedure and is used in subsequent steps (for example the shakedown reference stress used in the creep assessment stages). If shakedown cannot be demonstrated using the simplified approaches then R5 cannot be used any further for the assessment. Instead a more computationally expensive and time consuming route using nonlinear FEA must be used.

#### **1.4 Drivers for Project Creation**

From a financial point of view, if EDF are able to keep their existing nuclear power stations running for longer than their original design life, then more income will be generated from a plant which would otherwise be shutdown and decommissioned. Aside from financial concerns, there is a growing political pressure resulting from the possibility of existing plant closures before replacement generation has been constructed and commissioned. The long

lead times of a nuclear power station mean that the new generation capacity may not be ready before the existing AGR's reach their published decommissioning dates.

Life extensions of 5 years have already been achieved for Heysham 1 and Hartlepool stations [22] and 7 years for Hinkley Point B and Hunterston B [23] (these are included in the respective decommissioning years in Table 1.1). In addition to these extensions, EDF have announced that they expect to extend the life of all AGR plants by a further 5 to 7 years, and extend the life of the Sizewell PWR station by 20 years [24]. To substantiate an extension to the operational life of a plant, a rigorous safety case must be assembled which demonstrates the ability of the plant to continue safely operating beyond the original design life. Structural integrity assessments using the R5 procedure are heavily involved in this safety case.

Aside from the issue of life extension, a significant level of work is conducted to demonstrate that the plants are safe to continue operating between planned shutdowns and outages. Structural assessments are performed on components which are inspected during these shutdowns, contributing either to the safety cases to justify continued operation or to highlight components to be replaced. Once again the procedures in R5 are used to conduct these assessments.

The importance of R5 within EDF means that there is a lot of investment to improve its procedures and keep it up to date with the most recent advances in structural integrity research. The R5 research program investigates many topics, including advances in the analysis of cracks [25], effects of welds [26] and probabilistic methods of structural analysis [27]. Part of this research program concerns the development of methods to better predict the shakedown status of components. At times the shakedown methods in the R5 procedure can prove overly pessimistic in the prediction of the shakedown limit, meaning that the component is not shown to be within shakedown according to the R5 criteria. When this happens it is necessary to use nonlinear FEA which, in shakedown assessments, can produce ambiguous results and involve large computing times.

An improvement to this situation can be found in the form of the so called "Direct Methods" for shakedown assessment. These methods are able to give more accurate predictions of shakedown than are currently given in the simplified routes of R5 and can do so with clearer results and less computational expense than full nonlinear FEA. Therefore

including one of these Direct Methods as an option in R5 would be beneficial in cases where shakedown is difficult to determine conventionally.

## 1.5 The Linear Matching Method

The Linear Matching Method (LMM) is a Direct Method for shakedown assessment and has been a part of the R5 research program for a number of years [28][29]. The LMM is an upper bound procedure initially developed from the Elastic Compensation Method [30], and has the ability to give accurate upper bounds to the shakedown limits. The LMM has seen significant theoretical and numerical development over the years making it among the most successful of the Direct Methods available today.

The premise of the LMM is that a nonlinear material response, such as metal plasticity, can be mimicked by a series of linear analyses where the modulus is changed throughout the structure. This is demonstrated pictorially in Figure 1.3.

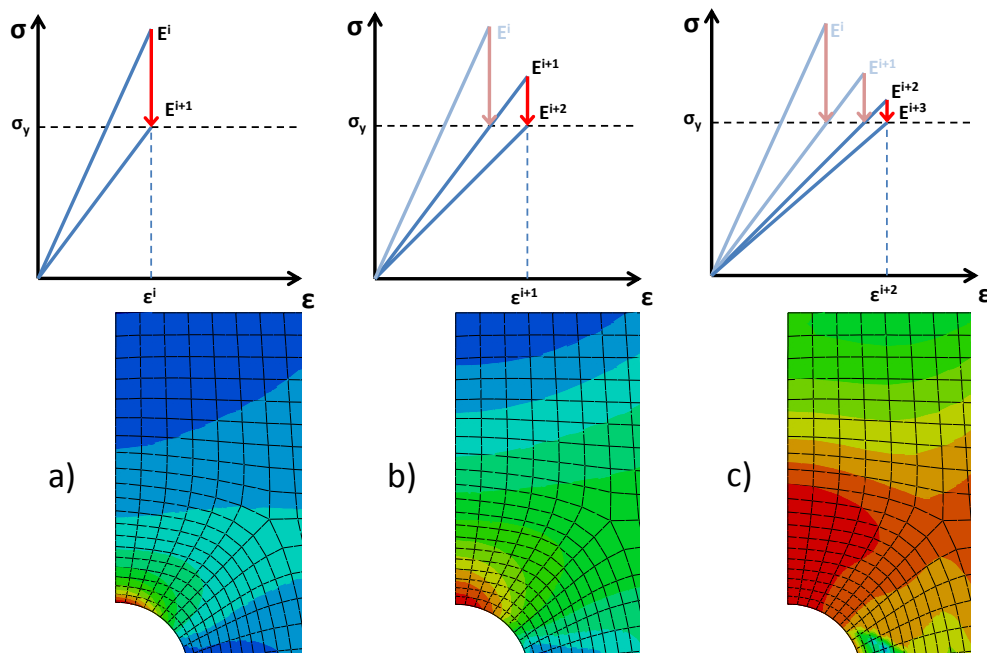


Figure 1.3 - LMM Modulus Adjustment and Stress Redistribution

The process begins with a linear elastic analysis for the applied loads. The modulus at each point in the structure is then modified so that the stress matches the yield stress (Figure 1.3a). The next elastic analysis uses these modified modulus values and the stress begins to redistribute in the structure (Figure 1.3b). The modulus is then modified again and the process repeats, allowing the stresses to redistribute similarly to an elastic-plastic material.

The LMM is implemented in Abaqus commercial finite element software [31] through use of user subroutines. Through this implementation it has been successfully applied to many practical engineering structures, including some examples of EDF plant components [32][33]. This has proven the capabilities of the method as a practical engineering analysis tool, with the potential for regular use within EDF for their routine structural assessments.

## **1.6 Project Aims and Objectives**

The LMM has the potential to be a useful tool for EDF engineers if proof of shakedown is problematic by other means. However, there are some barriers to wider adoption of the method.

The first of these is that the LMM is fundamentally an upper bound procedure. This means that the shakedown limits generated will be greater than or equal to the exact limit. Whilst the convergence of the LMM has been shown to be robust and stable, an upper bound solution is nonetheless a non-conservative solution by nature. The nuclear industry favours conservative lower bounds to shakedown and so if the LMM is to be user regularly within EDF then lower bound solutions must also be available.

The second issue, which is faced by all the Direct Methods, is that they all require some level of programming ability in order to use them. The LMM is implemented in Abaqus through user-subroutines and historically requires several changes to the code to run an analysis. This presents opportunities for errors when users who are inexperienced with coding, or the LMM itself, use the subroutines. Tipping [34] alleviated this problem to an extent by rationalising earlier versions of the LMM subroutines so that the code changes required per analysis were minimised. The LMM job was instead set up through the use of a text file containing information about the load cycle and convergence criteria. This, whilst an improvement on the original LMM implementation, can be further improved upon if a user interface is created to automatically set up the analysis, making it easier and quicker for the user to run a LMM analysis.

With these points in mind, this project has three major objectives:

1. Add conservative lower bounds to the LMM calculations. These lower bounds should run concurrently with the upper bound so that the user is given both lower and upper bounds to the shakedown limit.

2. Provide validations of the shakedown limits predicted by the LMM. This is somewhat linked to objective 1 in that any new development to a numerical procedure must be validated to ensure the results are as expected. This validation requirement also extends to the upper bound, so that EDF can have confidence in the shakedown limits predicted by the LMM as a whole.
3. Provide a user interface to the LMM to eliminate the manual code changes required to perform a LMM analysis.

Chapter 2 of this thesis gives an overview of shakedown in structures. This includes the structural response itself and how this is used at present in pressure vessel design and assessment. The current research in shakedown is also discussed. Chapter 3 examines the LMM strict shakedown procedure theoretically and gives some theoretical and numerical validation examples.

Chapter 4 discusses the LMM global shakedown method. A lower bound to this limit is derived and implemented, and investigations into convergence are performed. The aim of chapter 5 is to provide validation of the global shakedown method through analytical and numerical comparisons.

Chapter 6 details the creation of a user interface to the LMM through an Abaqus plug-in. Details are given about the structure of the plug-in and the re-structuring of the subroutines to allow automated use. Chapter 7 demonstrates the use of this LMM tool to analyse a plant example from EDF.

A summary of the findings and outputs from this project, and a discussion of areas for future work, are given in chapter 8.

## **2 Shakedown in Structural Engineering**

### **2.1 Introduction**

Shakedown is a structural phenomenon seen in elastic-plastic materials which are loaded cyclically. It occurs if loads cause the elastic limit of the material to be exceeded, and is very often exploited as a means of allowing a structure to carry more load than would be allowed if the component were restricted to stresses below yield. This is particularly true for pressure vessels, where the basic concepts of shakedown are commonplace in the codes used in their design and assessment.

The subject of shakedown in metallic structures is not a new one. Some of the theoretical solutions and theorems have existed for half a century or more. Shakedown solutions, however, are difficult to achieve analytically and so development of the field was slow until the more widespread adoption of numerical analysis tools such as Finite Element Analysis (FEA).

FEA itself does not hold the complete solution when shakedown calculations are involved because it can be difficult to determine when steady state cyclic behaviour has been achieved. This has led to the development of many "Direct Methods", which are usually based within FEA and are so called because of their ability to remove ambiguity from the numerical calculations. Other advantages of these Direct Methods includes improved solution times over the conventional FEA approach. Included among these methods is the Linear Matching Method, and collectively these methods represent the main focus in shakedown research today.

This chapter will explore the subject of shakedown from concepts and theorems through to their implementation in the Direct Methods. Some of the current challenges in shakedown research will be highlighted in the context of the goals of this project, which allows these ideas to be expanded upon in subsequent chapters.

### **2.2 The Shakedown Phenomenon**

The focus of the majority of shakedown research has been on metallic materials, i.e. materials which show an elastic-plastic response, have large levels of ductility (relative to brittle materials such as ceramics) and for which the von-Mises yield condition is applicable. However research into other materials and geotechnical problems [35] also exists. Metallic

materials are the primary concern of the nuclear industry and so form the focus of this work.

In structural mechanics the limit load of a structure is a commonly used calculation to characterise fitness for service. The limit load gives the maximum allowable monotonically applied load that the structure can bear before a plastic hinge forms, at which point no further increase in load can be sustained by the structure. When a component is loaded cyclically however, failure can be seen at load levels which are lower than the limit load. Depending on the magnitude and nature of the cyclic loading, several different structural responses may be seen.

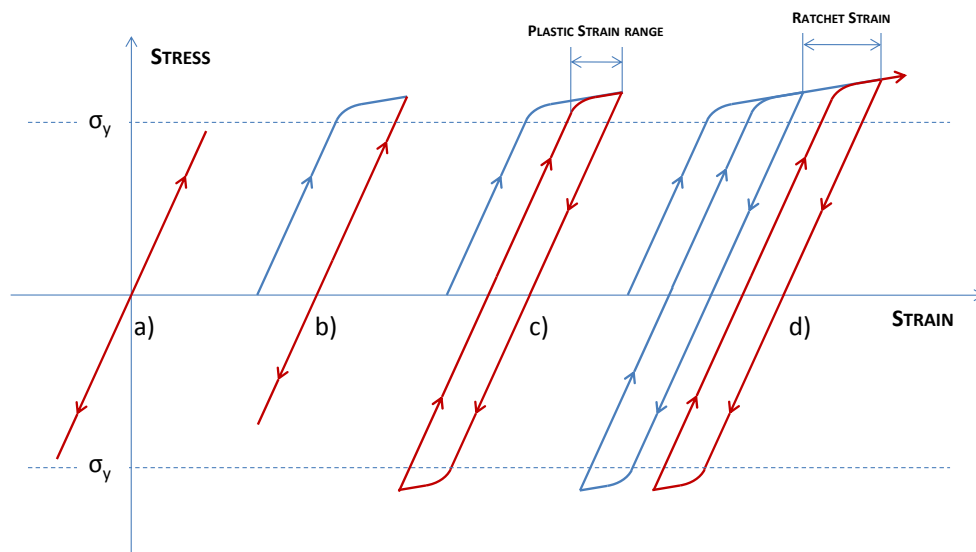


**Figure 2.1 - Structural Responses to Cyclic Loading**

If the applied loads are small enough then the whole component will remain within the elastic limit during the entire load cycle, as shown in Figure 2.1a. Increasing the magnitude of the loading beyond the elastic limit will cause plastic strains to form in parts of the structure and one of three steady state responses will be observed.

- Strict shakedown, also known as elastic shakedown. The plastic strains are accumulated in the first few cycles along with the formation of a residual stress field due to the yielding. After these first cycles the residual stress causes the structure to respond to subsequent loading cycles in an entirely elastic manner, as shown in Figure 2.1b, therefore preventing any further plastic strains forming.

- Global Shakedown, also known as plastic shakedown or alternating plasticity. This is where the plastic straining does not stop after the first few cycles but instead is seen in every load cycle. In the steady state response there is equal plastic straining in the forward and reverse directions, as shown in Figure 2.1c. This means that the strains form a closed loop over the cycle and no net increase in plastic strain is seen from one cycle to the next.
- Ratcheting. When ratcheting occurs there is a net accumulation of plastic strain with each load cycle which would eventually lead to failure of the structure by gross plastic collapse. This is shown in Figure 2.1d.

It is worth noting that within a structure it is rare that only one of the steady state responses will be observed. Instead several responses may be seen depending on the applied loads and the severity and location of stress concentrations. It is common that the bulk of a structure will remain elastic at all times whilst stress concentrations will cause plasticity and one of the other three responses will develop. The shakedown status of the component is dictated by the most severe response seen in the entire structure. For example, if the entire component is entirely elastic but one small region around a stress raiser is ratcheting, then the whole component is said to be ratcheting.

In structural assessments it is important to be able to assess which behaviour a component is exhibiting. An entirely elastic response and strict shakedown are allowable states for a component to be in. Indeed, strict shakedown is the most favourable state because the response of the component is entirely elastic despite the load levels being large enough to initially exceed the elastic limit in some locations. Global shakedown is usually allowed provided that a low cycle fatigue assessment is performed because of the presence of the reverse plasticity. In almost all cases ratcheting is not allowed. One of the first stages in any structural assessment is, therefore, to determine the shakedown status of the component.

One of the most famous classifications of these responses came from Bree, who conducted a simplified analysis of a nuclear fuel casing [36]. The casing, which is cylindrical, is subject to a linear through wall temperature difference which is cyclic with time and a steady state axial tension. By assuming that the casing wall thickness is small relative to the radius and that the hoop stress is dominant compared to the axial stress, Bree was able to reduce the problem to a 1-dimensional analysis. Doing this allowed Bree to analytically calculate the levels of thermal and pressure loading which would result in the different responses of

Figure 2.1. This resulted in the now famous Bree interaction diagram, which is a common method of graphically displaying the responses to different loading levels. An example interaction diagram is shown in Figure 2.2.

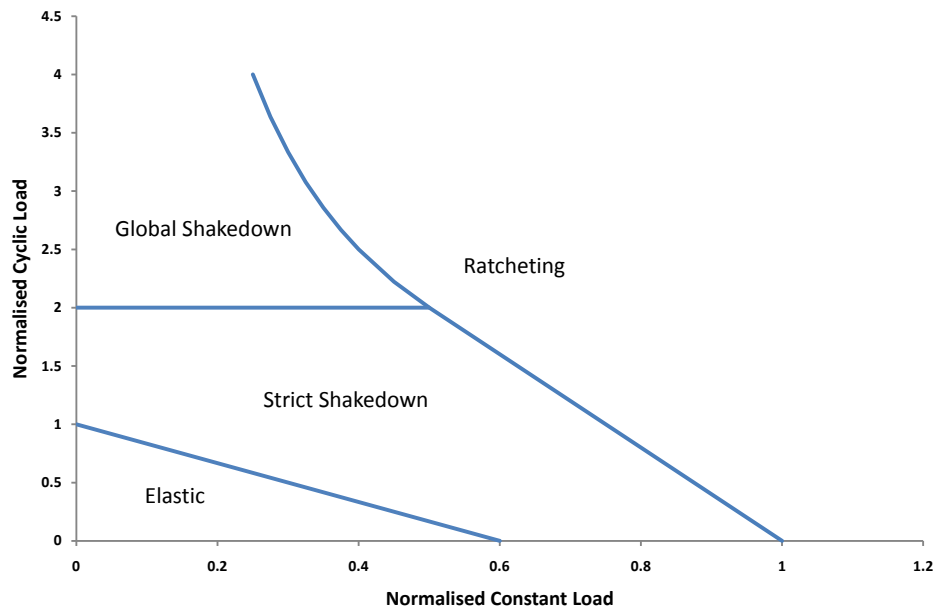


**Figure 2.2 - Bree Interaction Diagram**

In Figure 2.2 the horizontal axis represents the steady state pressure stress and the vertical axis represents the cyclic thermal stress, both of which have been normalised against the yield stress. This interaction diagram clearly shows the relative levels of cyclic thermal and steady state pressure loading which will result in each behaviour.

This study, despite being heavily simplified, still includes many important features of shakedown and highlights characteristics which are applicable to a large number of shakedown assessments:

- The boundary between strict and global shakedown is exactly twice the yield stress. For a perfectly plastic material (and low levels of constant loading) the stress can cycle between compressive and tensile yield and still remain elastic.
- When the level of cyclic loading becomes zero the strict shakedown limit coincides with the limit load. The limit load can be considered to be a special case of strict shakedown due to there being only one point in the load cycle.
- As the level of cyclic loading increases the global shakedown limit becomes asymptotic to the vertical axis. This applies to situations where the cyclic load is

self equilibrating and cannot itself cause the limit state to be reached (classified as a secondary stress in the ASME code [37] and R5). An example of this is a through wall temperature difference, which is the case for the Bree analysis. In cases where the cyclic load is mechanical (which has the ability to cause limit in its own right) the global shakedown boundary is not asymptotic, but instead intercepts the vertical axis at the limit load. Examples of this are seen in the interaction diagrams of a pipe intersection in chapter 5.

This analysis by Bree has been adopted by many design and assessment codes as the cornerstone of their shakedown analysis. For example, the Design by Analysis section of ASME VIII [37] uses these exact stress limits to prevent thermal stress ratcheting.

### **2.3 The Shakedown Theorems**

The analytical examples, such as those of Bree, provide useful insights into the shakedown phenomenon and result in rules of thumb which can be applied more broadly to engineering calculations. These analytical examples, however, only exist for basic geometries and load conditions which limits their applicability somewhat. Despite this, the importance of calculating the shakedown status has led to the phenomenon being studied by many researchers with the aim of creating robust shakedown/non-shakedown criteria which are more generally applicable to any applied loading or geometry. The most widely used of these theorems are those of Melan [38] and Koiter [39] which give conditions for strict shakedown [40]. Such is the extent of these theorems within the field that all Direct Methods discussed in Section 2.6 are based on one of these two theorems.

Melan's theorem states that:

*For a given cyclic load set the structure will shakedown if a constant self-equilibrating residual stress field can be found such that the yield condition is not violated for any combination of cyclic elastic and residual stresses.*

Therefore if a residual field, which is in equilibrium when all external loads are removed, can be calculated which means that the yield condition is satisfied when the applied elastic stresses are added, then the structure will be in strict shakedown. Melan's theorem is often referred to as the Lower Bound shakedown theorem, because the predicted shakedown limits are always equal to or less than the exact strict shakedown limit.

Koiter's theorem states that:

*For a prescribed load set  $P(t)$  with a cyclic period  $t$ , if any kinematically admissible strain rate can be found during a time interval  $(0, t)$  such that the strain field is compatible with a displacement field  $u$  (which satisfies the applied displacement boundary conditions) and*

$$\int_0^t \sum P\dot{u} \geq \int_0^t \int_V \dot{D} dV dt$$

*where  $\dot{D}$  is the rate of plastic dissipation per unit volume corresponding to the admissible strain rate  $\dot{\epsilon}$ , then shakedown has not occurred.*

Therefore Koiter's theorem requires the definition of a kinematically determinate mode of deformation for the component (i.e. compatible sets of displacement and strain increments) and performs an energy balance of internal and external work done. Koiter's theorem is often referred to as the upper bound theorem because it predicts shakedown limits which are equal to or greater than the exact strict shakedown limit.

The broader applicability of these theorems in terms of geometry and loading mean that they have formed the foundation of modern shakedown analysis methods, as discussed in section 2.6. Melan's theorem in particular, being conservative by nature, is a popular choice for the Direct Methods and is also used as the basis of the shakedown criteria used in R5.

## **2.4 The R5 High Temperature Assessment Procedure**

The R5 procedure [1] is a UK nuclear industry standard frequently used for high temperature structural integrity assessments of Advanced Gas-Cooled Reactor (AGR) components [2][21]. Together R5 and R6 (for the assessment of low temperature fracture) [41] provide the cornerstone of integrity assessment for the UK AGR fleet. Being a high temperature procedure, the R5 procedure considers the effects of creep, fatigue and the creep-fatigue interaction to determine the remaining operational life of the component in question.

R5 is divided into five volumes:

Volume 1: Overview

Volume 2/3: Creep-fatigue crack initiation procedure for defect free structures

Volume 4/5: Procedure for assessing defects under creep and creep-fatigue loading

Volume 6: Assessment procedure for dissimilar metal welds

Volume 7: Behaviour of similar welds: guidance for steady creep of ferritic pipework.

Broadly speaking the R5 procedure contains two stages. This first stage is an assessment of the time for a defect to occur in an initially defect free component, detailed in volume 2/3. The second stage is the assessment of the time for a given defect to grow to a critical size, detailed in volume 4/5. Volumes 6 and 7 are essentially specialised applications of volumes 2/3 and 4/5 respectively. Overall, the procedure checks the component for, and may limit the operating life based on, the following:

- i. Excessive plastic deformation from a single application of a set of loads
- ii. Creep rupture
- iii. Ratcheting from cyclic loading
- iv. Creep deformation enhanced by cyclic loading
- v. Crack initiation in defect free material due to creep or creep-fatigue mechanisms
- vi. Crack growth due to creep and creep fatigue mechanisms.

R5 uses a simplified approach based on elastic stress analysis and criteria associated with this such as reference stress methods. The procedures are laid out as a series of analysis options which are applicable to one or more of the above failure mechanisms. Where the initial, simple options are not sufficient then more advanced options are used which lead to less restrictive results. Should these options also prove to be insufficient then advice is given regarding full cyclic inelastic computation. This strategy strikes a compromise between the pessimism of elastic analysis and the complexity of cyclic inelastic analysis.

Volume 2/3 is concerned with the first of the two assessment stages, the assessment of crack initiation in defect free components. The procedures it contains provide an estimate of the number of cycles to form a crack of a predefined size (i.e. does not provide an estimate of the number of cycles to failure). Elastic analyses are performed as a starting point for the volume 2/3 assessment. These stresses are categorised into primary and secondary in a similar manner to the ASME code [21]. Limits are placed on these stress categories to ensure that excessive plastic deformation will not occur before the component reaches steady state behaviour (mechanism i). Creep rupture (mechanism ii) is

assessed using reference stress techniques where the creep reference stress is dependent on the creep ductility of the material.

Volume 2/3 includes several methods to guard against incremental plastic collapse (mechanism iii). If strict shakedown cannot be demonstrated then global shakedown is allowed provided that an elastic core remains to constrain the cyclic plasticity. Mechanism iv is the phenomenon whereby cyclic loading may repeatedly generate high stress levels in a component containing a creep dwell in the cycle. This significantly increases the creep strains per cycle and therefore can reduce the service life. The shakedown stress solutions are used to calculate a creep usage factor, ensuring that creep rupture does not occur due to this phenomenon.

Crack initiation (mechanism v) is said to have occurred when a defect of size  $a_0$  or larger has formed. This is assessed by independently calculating the damage caused by creep and fatigue. The interaction of creep and fatigue is accounted for through use of an interaction diagram.

The initiation of a crack of size  $a_0$  does not in itself represent the failure of the component but rather indicates the starting point of a defect growth assessment using volume 4/5 if required (mechanism vi) i.e. if no defect will form in the service life of the component then the assessment is complete and no further action is required. If however, volume 2/3 predicts that a defect will initiate within the service time of the component then a volume 4/5 assessment is required to determine the crack growth in the service life. In addition to being a sequential assessment to volume 2/3, volume 4/5 is also a stand-alone procedure for assessment of existing defects found through inspection and NDT.

#### **2.4.1 Shakedown Criteria in R5**

The first two stages in the volume 2/3 procedure involve defining the service cycles that the component will experience and performing the elastic analyses for these. Once complete, step 3 then demonstrates that the component will not suffer plastic collapse by placing limits on the different stress categories (i.e. primary and secondary). In addition to those relevant to plastic collapse, there is also a limit set on the stress range seen by the component, namely:

$$\Delta(P_L + P_B + Q) \leq 2.0\sigma'_y \quad (\text{for ferritic steels}) \quad (2.1)$$

$$\Delta(P_L + P_B + Q) \leq 2.7\sigma'_y \quad (\text{for austenitic steels}) \quad (2.2)$$

Where  $\Delta(P_L+P_B+Q)$  is the total stress range seen at a given point in the structure and  $\sigma'_y$  is equal to the yield stress for most ferritic and austenitic steels (but may be modified depending on the creep properties of the steel). These limits are present to ensure that it is possible for the steady cyclic state to be within global shakedown. These stress limit criteria may be bypassed by performing an inelastic analysis to find the limit load, but it is relevant nonetheless that checks are present at the early stages of the procedure.

Steps 4 and 5 present simple checks to determine the significance of the creep loading and to ensure that creep rupture endurance is satisfactory. Once complete, the shakedown status of the component is explicitly checked in steps 6 and 7.

Step 6 is a simple check for shakedown and also checks for insignificant cyclic loading. The shakedown check begins by assuming that the residual stress field is null and compares the linearised cyclic elastic stresses to a modified yield stress  $K_s\sigma_y$ .

$$\hat{\sigma}_{lin}(x,t) \leq K_s\sigma_y \quad (2.3)$$

The scalar factor,  $K_s$ , is introduced as a measure of the ability of the material to form steady cyclic behaviour i.e. the extent of cyclic softening or hardening exhibited. Condition (2.3) is allowed to be violated (i.e. the elastic stresses can exceed the modified yield stress) provided that this occurs in less than 20% of the section thickness. This ensures that an elastic core is present in the remaining 80% to constrain the cyclic plastic strains. If this condition is satisfied then the more advanced shakedown check is not required and therefore step 7 can be omitted.

Additionally in step 6, if equation (2.3) is satisfied for the entire structure (rather than just 80% of the section), then checks for insignificant cyclic loading are performed. These checks include limits on the stress range (when the yield stress in the creep dwell is considered), the fatigue damage and the steady state stress during creep dwell. If these criteria can be satisfied then steps 8 to 14 inclusive can also be omitted.

Inability to satisfy the shakedown conditions in step 6 then requires step 7 to be carried out. This more detailed shakedown assessment introduces the use of residual stress fields to allow Melan's theorem to be satisfied. Several options exist to generate these residual

stresses, and any number of attempts to find a constant residual stress may be made (and so an iterative process is likely). However if a residual stress,  $\rho$ , which is self-equilibrating and constant with time can be found so that the modified yield stress is satisfied over the entire component at all time points:

$$\hat{\sigma}(x,t) + \bar{\rho}(x) \leq K_s \sigma_y \quad (2.4)$$

then strict shakedown has occurred. If this is the case then the checks for insignificant cyclic loading from step 6 can be carried out. In addition, this condition may be relaxed and the stresses over 20% of any given cross section may exceed yield (i.e. the remaining 80% must satisfy equation (2.4)). This exception may only be granted if the criteria of equations (2.1) or (2.2) (whichever is applicable) is satisfied i.e. if a nonlinear analysis is needed to find the limit load then strict shakedown must be satisfied over the entire structure.

All the criteria outlined above are based on Melan's lower bound theorem from section 2.3, which is used because it provides an inherent conservatism in the shakedown calculations when strict shakedown is achieved. The 80% rule, not present in Melan's theorem, is present so that limited regions of reverse plasticity can form and so allowing the component to operate in global shakedown. This 80% rule has been decided upon based on engineering judgement of simple cases such as the Bree cylinder and beams in bending rather than rigorous theoretical justification.

The conservative nature of the shakedown rules in R5 mean that it is sometimes not possible to demonstrate shakedown using this route. If global shakedown cannot be demonstrated using either steps 6 or 7 then all subsequent steps in volume 2/3 to calculate the effects of creep and fatigue cannot be used, and a more detailed cyclic inelastic analysis must be used to determine the continued operation of the component.

## 2.5 Finite Element Analysis for Shakedown Limit Calculation

The use of inelastic FEA is becoming an increasingly common theme across the design and assessment codes for pressure vessels and piping, which are incorporating design by analysis techniques as a viable alternative to their design by rule procedures. Two prevalent methods used in these design or assessment by analysis options are cyclic inelastic FEA and the Abaqus Direct Cyclic Analysis (DCA) method [42].

Inelastic FEA involves subjecting a model with elastic-plastic material properties to repeated cycles of loading. The plastic strains (if any) develop as a consequence of the loads and after the simulation of a number of load cycles the model will tend towards one of the cyclic states depicted in Figure 2.1. The use of inelastic FEA presents a large number of possibilities due to the vast number of material models available, the ability to include creep dwells in the cycle and the ability to include any number of applied loads and boundary conditions in any combination. This freedom also has disadvantages in terms of solution time and computational expense, especially for models with large numbers of finite elements and/or complex load cycles. In these situations the need to model the transient load cycle to obtain the non-linear material response can become very time consuming. Further disadvantages come when determining when the structure has actually reached its steady state response. The transient response, depicted in Figure 2.3, is present in any cyclic FEA model involving plasticity. In some cases this transient phase may be very small (in the Bree problem for example), but in complex models and load cycles the tendency is for this phase to last for increasing numbers of cycles, requiring that more cycles be solved. Additionally, the determination of the steady state response often requires a level of judgement from the engineer, usually by comparing strains or displacements at critical locations in consecutive cycles. In many situations the behaviour may be asymptotic to a shakedown response, but the final outcome is not entirely clear.

DCA in Abaqus shares many similarities with cyclic inelastic FEA in that it retains the freedom associated with the finite element method in terms of load cycle generation and available material models. The computational expense of DCA is reduced somewhat by the fact that it solves directly for the stabilised cyclic state, negating the time spent in the transient phase of the response. DCA achieves this by assuming the displacement field of the component during the load cycle takes the form of a Fourier series function. This displacement function is solved for in an iterative manner where one iteration obtains the residuals associated with the current displacement function, and these are then used to update the function for the subsequent iteration. In situations where many load cycles are needed to obtain the steady state response in an inelastic FEA model then DCA provides a viable alternative. The accuracy of DCA is determined by the number of Fourier terms in the displacement function, the number of time points used to sample the load cycle to determine this function and the convergence tolerance used.

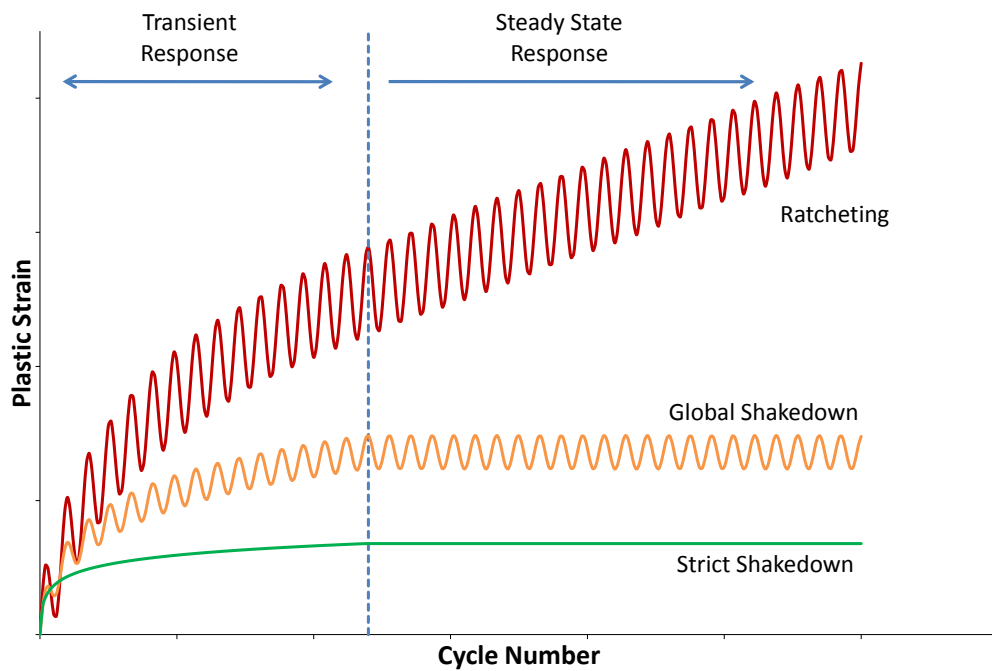


**Figure 2.3 - Plastic Strain History at a Critical Location in Cyclic FEA Model**

DCA is a useful method in determining the shakedown status because it calculates the plastic strains at the stabilised response, so the analyst can determine if strict or global shakedown has occurred. To this end, DCA has been used as the basis of a global shakedown method [43], see section 2.6.2. In the situation of a ratcheting response DCA will not converge - the displacement grows each cycle and so the process cannot converge on a stable Fourier series. Even when a stable response is possible it has been shown that increasing levels of plasticity (as the loading moves further into the reverse plasticity region or closer to the ratchet boundary for example) requires a greater number of iterations to achieve convergence [43], and convergence in these regions can be slow [44].

Overall the use of computer based methods (using FEA) offers useful advantages including the removal of stress classifications and the ability to include all relevant structural features. Despite this, the two prevalent methods described here have many disadvantages individually when used for shakedown analysis. Other drawbacks which are shared by both methods includes their inability to predict the proximity of the current load cycle to the strict or global shakedown limit. With these methods an iterative process must be used to find these limits manually. This has prompted the creation of so called Direct Methods for shakedown analysis, which are able to provide the proximity to these limits in a single calculation.

## **2.6 Direct Methods**

Despite the existence of the shakedown bounding theorems for well over 50 years, it was not until computing power and FEA techniques became established that these theorems could be used in any meaningful shakedown analysis method. The creation of these direct methods was prompted by the conflicting needs of a shakedown analysis of speed of solution and clarity of the shakedown status. The methods included in the design codes and in R5 offer a fast means of assessing shakedown by elastic analysis. However these methods are often overly conservative. Cyclic FEA offers less restrictive results but can involve lengthy computation times and ambiguous results. Direct methods have been created to offer a shakedown calculation which offers the flexibility of cyclic FEA but with improved solution times.

Existing Direct Methods are generally divided into those for strict shakedown and those for global shakedown, and these are discussed in the following sections.

### **2.6.1 Direct Methods for Limit Load and Strict Shakedown**

Mathematical programming techniques for limit and shakedown are among the most common methods in this field. Such techniques have been studied for several decades and pre-date the other Direct Methods for limit and shakedown.

Mathematical programming techniques are based upon finite element discretisations of a model and are capable of finding both lower and upper bounds to the strict shakedown limit [45]. The basic principle is that these limits can be found for the finite element mesh by an optimisation algorithm which has constraints placed on it by the applied loads, boundary conditions and the criteria of the bounding theorem used. For example, to find the lower bound shakedown limit the optimisation problem must find a constant residual stress field which maximises the applied load levels whilst also keeping the stresses below the yield stress. The upper bound seeks to minimise the plastic dissipation energy whilst producing kinematically admissible strain fields. The proof of duality of the solutions means that both the lower and upper bounds can be solved concurrently, with the optimal solution being the optimal for both bounds [46].

Mathematical programming methods historically have always been difficult to implement robustly within a finite element framework. A great deal of specialised programming is required to implement the complex theoretical framework of the optimisation algorithms.

Therefore the application of this method was, until relatively recently, restricted to simple geometries and load cases. The LISA project (Limit and Shakedown Analysis) [47][48] was launched to combat this by producing a more robust implementation of the method in the PERMAS finite element code as well as investigate theoretical extensions. During and since the LISA project, several verification and demonstration examples have been produced by mathematical programming methods including limit loads of a torispherical head [49], shakedown of a pipe intersection [46][50] and shakedown of a mixing device [48]. The mixing device in particular represents the largest example analysed using this method, and demonstrates that realistic problems can be solved using the method. Mathematical programming methods offer an advantage over the other Direct Methods described in this chapter in that the kinematic hardening material model can be included [51] whereas the other Direct Methods have only used perfect plasticity to date. Despite this, and the efforts of the LISA project, the complexity in implementation of the method is significant in comparison to other methods described here which has hindered its uptake in industry. This has resulted in the creation of a number of new methods which are simpler both theoretically and in their implementation, making them more amenable to industrial use.

One of the first methods in this category was the GLOSS r-node (Generalised Local Stress Strain) method of Seshadri [52]. This method is based on two elastic analyses which are used to determine the limit load of a structure. This method is based on the idea of dividing the structure into two, the "local" and "remainder", where the local portion experiences the largest inelastic effects. The inelastic effects in this local region are then approximated through modulus adjustment, and the size of the plastic zone due to stress redistribution is estimated based on some approximate plastic zone size calculations. This method was improved upon in [53] and gave reasonable approximations to limit loads when compared with inelastic FEA, but has not been extended to the calculation of shakedown limits.

A method for calculation of limit loads was proposed by Marriott [54] which made use of elastic analyses with modified modulus values. Using this as a basis, along with aspects of the GLOSS r-node method, MacKenzie et al [30] were able to extend these limit load methods to enable calculation of the strict shakedown limit. The resulting method, named the Elastic Compensation Method (ECM), was able to provide lower and upper bounds to the limit load and the strict shakedown limit.

The ECM used a series of linear elastic analyses where the elastic modulus of each element is systematically modified according to

$$E_{i+1} = E_i \frac{\sigma_n}{\sigma_i} \quad (2.5)$$

Where  $E_i$  refers to the current elastic modulus of the element,  $E_{i+1}$  is the subsequent modulus,  $\sigma_i$  is the current effective stress and  $\sigma_n$  is a nominal reference value of stress, often chosen to be the yield stress. Iterative elastic analyses using this system to adjust the modulus within each element allows the stress in highly loaded elements to reduce and spread to elements with low stress.

The ECM has been used to calculate the limit loads and strict shakedown limits of a number of components including simple beam and bar structures [55], axisymmetric shells including nozzles [56][57] and 3D pipe intersections [58][59]. In general the upper bound ECM formulations are able to give good estimates of the limit loads and shakedown limits whilst the lower bounds tend to give overly conservative results. This is demonstrated in Figure 2.4, which shows the limit surface for a beam under combined bending and tension predicted by the ECM.

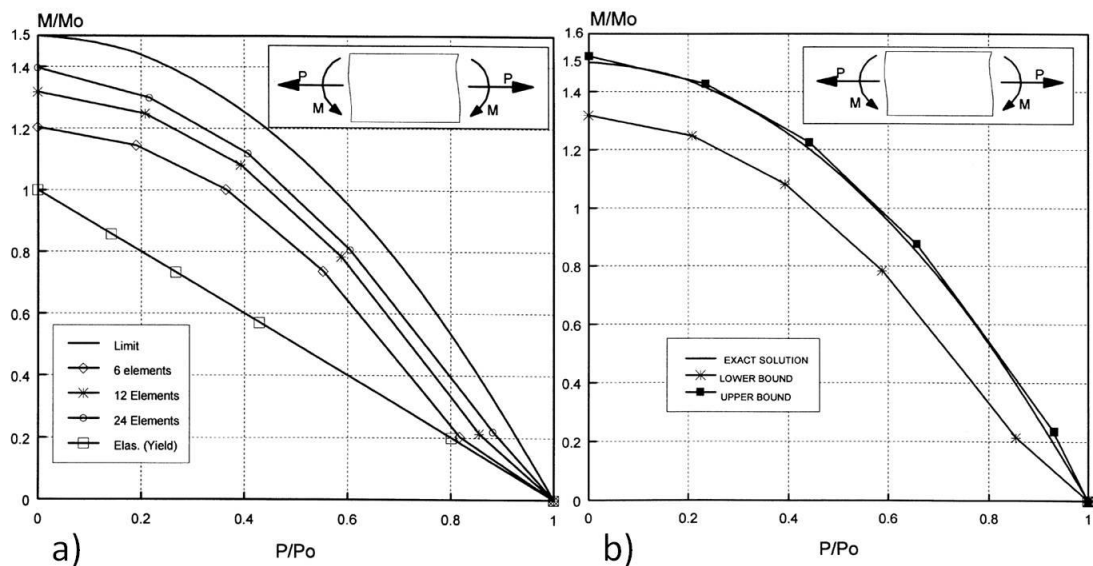


Figure 2.4 - ECM Limit Load for a Beam in Bending and Tension

Figure 2.4a shows that the refinement of the mesh through the thickness of the beam produces lower bounds which approach the exact limit, but with diminishing returns of

accuracy with increasing element density. The upper bounds, shown in Figure 2.4b, agree well with the exact solution. In [60] the behaviour of the lower bounds is attributed to the nature of the stress fields generated by the modulus adjustment procedure. The elemental basis of modulus adjustment can produce stress fields which are discontinuous through a section which, whilst approximating the continuous solution, are not able to generate lower bounds with the same accuracy as the upper bounds.

The creators of the ECM also pioneered another strict shakedown method based on nonlinear superposition of stress [61][62]. The method to produce the strict shakedown limit based on proportional loading is as follows. The first stage of this method is to perform a limit load analysis for the loading in question. As the limit load analysis progresses, ever increasing levels of the loads are applied until the plasticity is such that equilibrium can no longer be satisfied and the limit load has been reached. The limit load analysis, by definition, ensures that the yield function is satisfied to maintain equilibrium at all loads up to the limit load. The stress field is stored at a number of time points up to the limit load. The second stage of the procedure then performs an elastic analysis for the same loads and the elastic stress at each of the points in the limit load analysis is found by proportionality. The shakedown limit is found by subtracting this elastic stress from the corresponding point in the limit load analysis, which gives the residual stress field. This residual stress field is checked against the yield condition, and if satisfied, then both loaded and unloaded ends of the cycle satisfy yield and this load level is within strict shakedown. Each stored time point up to the limit load is checked in this way, and the maximum load level which still gives a residual stress which satisfies yield is the lower bound strict shakedown load. This method is also able to take non-proportional loading into account [61]. In this case the elastic-plastic analysis contains steady state and cyclic loading, and only the elastic stress for the cyclic loading is subtracted to find the stress at the unloaded state.

Nonlinear Superposition was used and validated by application to several geometries including a plate with a central hole, nozzles in spherical shells [63] and thick walled cylinders with radial cross holes [64]. The method gave favourable results when compared to cyclic elastic-plastic FEA, and is able to predict more accurate shakedown limits than the ECM [61]. At present, however, this method is only formulated for two load extremes, but is nonetheless a useful method for determining strict shakedown limits and is still widely used today [65][66].

The Linear Matching Method (LMM) began as an evolution of the Elastic Compensation Method of MacKenzie et al [30] to calculate the limit load and strict shakedown limit. The theoretical foundations for an upper bound method are given by Ponter and Carter [67][68] who investigated the implementation and convergence properties of such a method. Further theoretical development, a convergence proof and implementation within the commercial finite element software Abaqus [31] was provided by Ponter et al [69] and Ponter and Engelhardt [70]. Consolidation of these developments and extension to the calculation of 3D structures led to the Linear Matching Method strict shakedown procedure [71].

The premise of the LMM, similarly to the ECM, is that a nonlinear material response can be mimicked by an iterative procedure based entirely on linear solutions. During each iteration the modulus is varied within the volume of the structure so that the stress is matched to the yield stress. The next elastic solution in the iterative procedure uses this modified value of modulus, and the stresses redistribute in the same way as they would with an elastic-plastic material. During each iteration the energies associated with plastic dissipation and external work done are calculated and used in the upper bound theorem to calculate a load multiplier, which is used to scale the applied loads in the subsequent increment. The combination of modulus adjustment and load scaling produces a series of upper bounds to the strict shakedown limit, which have been proven to monotonically converge to the least upper bound [69]. Relatively recently a lower bound calculation was added by Chen [28], meaning that the strict shakedown procedure is capable of providing a lower and upper bounds which are calculated in parallel.

The LMM strict shakedown procedure has been successfully applied to many structures including a superheater tubeplate [28][72], welded pipes [73] and composite cylinders with radial cross holes [74].

## **2.6.2 Direct Methods for Global Shakedown**

The strict shakedown status is a very useful quantity to calculate. It is the most desirable steady state response to cyclic loading and it forms a central role in EDF's R5 procedure. Methods to calculate strict shakedown are therefore very desirable. R5 also allows components to operate in global shakedown, and so methods which extend beyond strict shakedown to calculate this limit are equally desirable, and a brief summary of the existing methods is given here.

As outlined in section 2.5, Direct Cyclic Analysis (DCA) has recently been implemented in Abaqus as an alternative means of determining the steady state response of a structure to cyclic loading. DCA determines the stabilised cyclic response directly by approximating the displacement of the component using a Fourier series function. An iterative procedure produces increasingly accurate estimates until the steady state is achieved. In a situation where a stabilised response does not exist (i.e. when ratcheting is occurring) then the solution fails to converge.

Martin [43] has used DCA as the basis of a global shakedown method. The process uses repeated DCA calculations and uses the convergence/non-convergence of the solution as an indicator of the steady state response to that level of loading. A search function is employed (which in [43] is a bisection algorithm) which alters the levels of applied loading for subsequent analyses based on the convergence/non-convergence of the previous calculation. In this way the global shakedown limit is located using a "map" of results, as shown in Figure 2.5. The distinction between strict and global shakedown, whilst not given directly by this method, is determined by simply examining the plastic strains of the solutions. This method has been shown to successfully locate the global shakedown limit for complex components, namely a nozzle in a spherical shell subject to thermal transients and internal pressure.

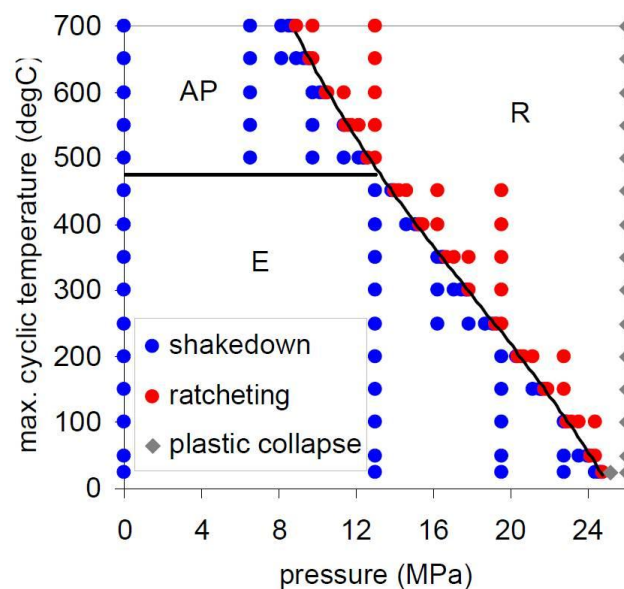
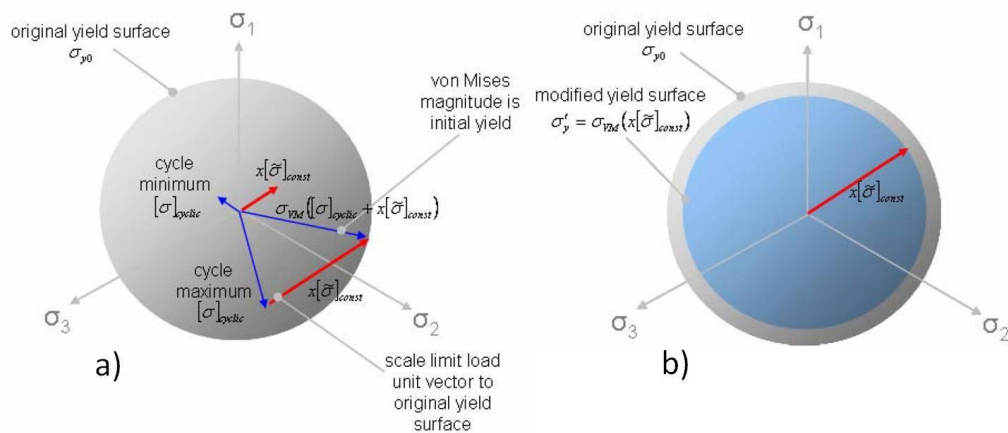


Figure 2.5 - Map of Results from DCA Analysis of the Bree Cylinder

One further method developed by Martin and Rice [75], named the Hybrid Method, is able to find the global shakedown limit in a more direct way. The load cycle is decomposed into cyclic and steady state loading (in a similar way to section 4.2.3) and a two stage calculation process is used.

The cyclic loading is considered in the first stage using a DCA analysis to find the stabilised cyclic response. With the cyclic stress fields known, an intermediate step is carried out where a unit vector of the steady state loading is added to each extreme of the load cycle. This unit stress vector is then scaled to the yield surface for each time point to find the level of constant loading which could be applied at that time point (Figure 2.6a). The minimum value of additional constant stress given by this vector scaling is then taken as the effective yield stress for stage 2 (Figure 2.6b). This process is followed for all integration points in the finite element model, giving a modified yield stress over the entire volume. The second calculation stage then performs a limit load assessment for the steady state loading using these modified yield stress values.



**Figure 2.6 - Hybrid Method Stage 2 Yield Stress Calculation**

This method was able to give a good approximation to the global shakedown limit when compared to the DCA method in [75]. This method also had the advantage of computational savings because the global shakedown limit was determined directly rather than by an iterative process.

Using the Hybrid Method as a basis, Jappy et al [76][77] were able to derive and implement a lower bound global shakedown method. This method also uses a two stage calculation process where the applied loading is split into its cyclic and steady state components. The second stage of this procedure also performs a limit load analysis with a modified yield

stress. The primary difference between the method derived by Jappy et al and the Hybrid Method is that this modified yield stress is updated during the solution procedure to take into account the stress redistribution which occurs during the limit load stage. Favourable results were found when compared with the Hybrid Method and the LMM upper bounds for examples such as a plate with a central hole and a pressurised 2-bar geometry.

Reinhardt and Adibi-Asl have recently proposed a lower bound global shakedown method named the Non-Cyclic Method [78][79]. This method shares some similarities with the LMM global shakedown procedure in that the loading is decomposed into cyclic and constant parts, a two stage calculation process is used and an iterative elastic procedure with spatially varying modulus is used in their second stage. The foundation of the method is a tentative extension of Melan's theorem beyond strict shakedown, and begins by conducting a cyclic elastic-plastic finite element analysis for only the cyclic loads to find the cyclic stress history. Half the stress range from this analysis is brought forward to a second stage, which is a limit load analysis to find the remaining capacity of the structure to support the constant loading. The majority of the applications of this method in the literature are to relatively simple geometries such as the Bree cylinder and 3-bar problems [80][81].

The Linear Matching Method is somewhat unique among the direct methods in that it has the ability to calculate both strict and global shakedown limits. The foundation of the global shakedown procedure is the theoretical extension of Koiter's theorem beyond the strict shakedown limit, as provided by Ponter and Chen [82]. This was then implemented as a numerical technique for two extremes in the load cycle in Abaqus by Chen and Ponter [83] in a similar fashion to the strict shakedown method. Further development in [84] and [29] allowed the extension of this method to any number of load extremes in the cycle.

The LMM global shakedown method in its current form requires the decomposition of the applied loads into cyclic and steady state components. This is a requirement of the theoretical extension to the upper bound strict shakedown theorem in [82]. Similarly to many of the other Direct Methods for global shakedown, the method then has two stages. The first assesses the steady state response to the cyclic loading along with the elastic, plastic and total strain ranges associated with this. A modulus adjustment scheme identical to that of the strict shakedown gives this stage a speedy assessment of the steady cycle. The second stage then finds the maximum additional steady state loading which will not

cause ratcheting. This second stage is essentially a LMM strict shakedown analysis where the applied stresses are augmented by the varying residual stress from stage 1.

The LMM global shakedown method has been applied on several occasions to components including defective pipelines [85], cracked welded pipes [86], a nozzle in a spherical shell [87] and superheater tubeplates [32][33].

### **2.6.3 The Linear Matching Method for Use in Industry**

The driving force behind the creation of all of the above methods is so that industry can have a robust and accurate method of calculating shakedown loads for design and assessment purposes. This is evidenced by the fact that a large number of publications are dedicated to application of these methods to pressure vessel or pipe geometries. In fact several of the methods originate from within industry rather than academia. Examples of this are the DCA method of Martin (Rolls Royce), the Hybrid Method (Rolls Royce) and the Non-Cyclic Method (Atomic Energy of Canada). The DCA Method and the Hybrid method have been developed with the Rolls Royce Hierarchal Finite Element Framework (HFEF) in mind [88][89], so that they can be incorporated into their analysis procedures used to assess plant components.

The LMM has been adopted by EDF in the past for use alongside the R5 procedure. Their interest in the method began in the early stages of development from the Elastic Compensation Method, and has continued through development of the global shakedown method. The LMM was proven as a useful tool when the analysis of an AGR superheater tubeplate from EDF was undertaken [32][33] using both the strict and global shakedown methods. In [32] the LMM procedure was used to produce the strict and global shakedown limits and the plastic strain range, which agreed well with full elastic-plastic analysis. In [33], this analysis was taken further to calculate creep strain and follow up factors of this component. Once again the LMM produced results which compared favourably with full step by step FEA. Recent work by Chen and Ponter [84] Gorash and Chen [90][91] has advanced the creep capability of the LMM which has been used to successfully predict the creep fatigue life of experiments performed on welded cruciform specimens. This level of capability demonstrates the LMM's ability to be used alongside the R5 procedure, and has resulted in the choice of the LMM for use in this work to fulfil EDF's need for a shakedown analysis method.

The use of the LMM within EDF on a more routine basis became possible when the Abaqus subroutines were rationalised by Tipping [34] into a method for use by EDF engineers. Until this point the use of the LMM required moderate changes to the subroutines for each new analysis, and several different subroutines existed for different element types. Since this rationalisation of the subroutines, EDF and its partners has used the LMM for some assessments, for example [92], but use of the method is still relatively uncommon. The method created by Tipping, whilst much more user friendly than the original implementation, still requires some alteration of the subroutines for each analysis. EDF engineers instead prefer to use the familiar cyclic FEA and only use the LMM when the shakedown status is difficult to obtain. The lack of a lower bound to the LMM global shakedown procedure provides another reason for the limited use in routine assessments.

This has prompted the objectives of this project to add a complementary lower bound to the LMM global shakedown procedure and to create a user interface. This will give the necessary conservatism for routine use and eliminate the need to manually perform any code changes, and will allow EDF engineers to use the LMM in the familiar Abaqus CAE interface. Validation is an important step when any new method is developed to build confidence in the results it produces. It is hoped that such validation, combined with a user interface, will encourage EDF engineers to make use of the LMM for their assessments.

## **2.7 Summary**

The subject of shakedown and ratcheting is not new in structural integrity. The theorems which provide generally applicable shakedown/non-shakedown conditions have existed for many decades. The design and assessment codes have made use of shakedown for many years to increase the allowable working envelope of a structure whilst still preventing ratcheting. These design code implementations usually base their shakedown rules on analytical examples such as the Bree cylinder. R5 has taken this a stage further by providing a very literal interpretation of Melan's theorem, allowing the user to generate residual stress field estimates to demonstrate strict or global shakedown.

These shakedown methods in the design codes can prove to be overly conservative, however. Increased computing power has allowed the use of cyclic inelastic FEA, but this alone is not always sufficient to determine the shakedown status of a component conclusively. This, combined with the fact that FEA cannot give the proximity to the shakedown limit, has prompted the creation of the Direct Methods which can calculate the

proximity to the shakedown limit directly and with improved solution times over standard FEA.

EDF have identified that these Direct Methods are a useful tool for their structural assessments. The Linear Matching Method has been identified as the Direct Method most amenable for use within EDF and the R5 procedure. This is due to the fact that both strict and global shakedown limits can be calculated, and a historic compatibility of the LMM with R5 in terms of material properties and output data. The addition of a lower bound global shakedown calculation, verification of the method and the creation of a user interface will bring the LMM to a standard where it can be used regularly within EDF.

### 3 The LMM Strict Shakedown Procedure, Analyses and Verifications

#### 3.1 Introduction

Countless situations arise in power plants and pressure vessel designs where components are exposed to a set of cyclic thermal and mechanical loads. Where this is the case then it is desirable for the component to operate in a state of strict shakedown i.e. the component responds elastically at all points in the load cycle after the development of some initial plastic strains. This represents the best performance in terms of fatigue life whilst still allowing plasticity in the structure.

This chapter presents the Linear Matching Method strict shakedown procedure. A summary of the theoretical and numerical implementation is given which is followed by several validation cases. These validations compare the LMM to analytical and experimental limit loads and shakedown limits. Finally the LMM procedure is then applied to a pipe bend geometry as an industrially relevant demonstration case.

#### 3.2 The LMM Strict Shakedown Procedure

##### 3.2.1 The General Cyclic State for Strict Shakedown

Consider a body of volume,  $V$ , and surface,  $S$ , which is subject to a cyclic history of loading with a cycle time  $0 \leq t \leq \Delta t$ . This load history consists of mechanical loads,  $\lambda P(x,t)$ , and a temperature history,  $\lambda \theta(x,t)$ , where  $\lambda$  is a positive scalar load parameter. The mechanical loads act on part of the surface,  $S_T$ , and the temperature history acts within the entire volume. The remaining surface,  $S_U$ , is constrained to have zero displacement rate (i.e.  $\dot{u} = 0$ ). This situation is shown pictorially in Figure 3.1.

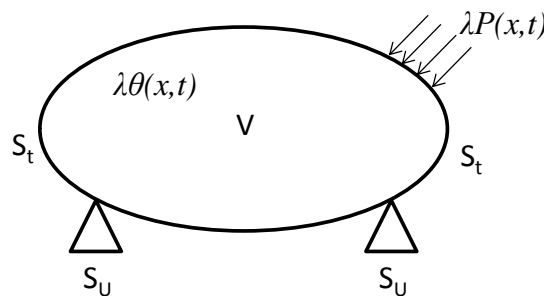


Figure 3.1 - Load and Boundary Condition Schematic

The material in question is assumed to be elastic-perfectly plastic with yield stress  $\sigma_y$  and satisfy the von-Mises yield condition,

$$f(\sigma_{ij}) = \bar{\sigma}(\sigma_{ij}) - \sigma_y = 0 \quad (3.1)$$

where  $\bar{\sigma}(\sigma_{ij}) = \sqrt{\frac{3}{2} \sigma'_{ij} \sigma'_{ij}}$  is the von-Mises effective stress and  $\sigma'_{ij}$  are the deviatoric stresses. The plastic strains are governed by the associated flow rule,

$$\dot{\epsilon}_{ij}^P = \dot{\alpha} \frac{df(\sigma_{ij})}{d\sigma'_{ij}} \quad (3.2)$$

where  $\dot{\alpha}$  is a plastic multiplier. The loading  $\lambda P(x_i, t)$  and  $\lambda \theta(x_i, t)$  is assumed to vary within the cycle time,  $t$ , such that  $0 \leq \Delta t \leq t$ . The scalar  $\lambda$  is applied so that a range of load histories may be considered. These loadings give rise to their corresponding elastic stresses which gives the applied stress history

$$\lambda \hat{\sigma}_{ij}(x, t) = \lambda \hat{\sigma}_{ij}^P(x, t) + \lambda \hat{\sigma}_{ij}^\theta(x, t) \quad (3.3)$$

Where  $\hat{\sigma}_{ij}^P(x, t)$  and  $\hat{\sigma}_{ij}^\theta(x, t)$  are the stresses corresponding to  $P(x, t)$  and  $\theta(x, t)$  respectively. For any cyclic problem the continued application of these loads will result in the following stress fields within the component

$$\sigma_{ij}(x, t) = \lambda \hat{\sigma}_{ij}(x, t) + \bar{\rho}_{ij}(x) + \rho_{ij}^r(x, t) \quad (3.4)$$

Where  $\bar{\rho}_{ij}$  is a constant (i.e. time independent) residual stress field and  $\rho_{ij}^r(x, t)$  is a varying residual stress which describes the changes which occur during the cycle. Residual stresses, by their nature, must be self equilibrating. For load cycles which are within the strict shakedown limit the varying residual stress field is zero, and therefore the cyclic stress history is fully described by the sum of the applied cyclic stresses and the time independent residual stress field

$$\sigma_{ij}(x, t) = \lambda \hat{\sigma}_{ij}(x, t) + \bar{\rho}_{ij}(x) \quad (3.5)$$

## 3.2.2 LMM Upper Bound Method

### 3.2.2.1 The Upper Bound Theorem

The upper bound method is expressed in terms of an incompressible and kinematically admissible strain rate history,  $\dot{\varepsilon}_{ij}^c$ , which does not need to be compatible, but is associated with a compatible strain increment  $\Delta\varepsilon_{ij}^c$  such that

$$\int_0^{\Delta t} \dot{\varepsilon}_{ij}^c dt = \Delta\varepsilon_{ij}^c \quad (3.6)$$

And this strain increment is associated with the corresponding displacement increment

$$\Delta\varepsilon_{ij}^c = \frac{1}{2} \left( \frac{\partial \Delta u_i^c}{\partial x_j} + \frac{\partial \Delta u_j^c}{\partial x_i} \right) \quad (3.7)$$

Considering the cyclic loading history described above in section 3.2.1, the upper bound theorem is given by

$$\lambda^{UB} \int_V \int_0^{\Delta t} (\hat{\sigma}_{ij} \dot{\varepsilon}_{ij}^c) dt dV = \int_V \int_0^{\Delta t} (\sigma_{ij}^c \dot{\varepsilon}_{ij}^c) dt dV \quad (3.8)$$

where  $\sigma_{ij}^c$  is the stress at yield associated with  $\dot{\varepsilon}_{ij}^c$ , and  $\hat{\sigma}_{ij}$  is the elastic stress associated with the applied loading from equation (3.3). Combining this with the associated flow rule for a von-Mises yield criterion, equation (3.2), the upper bound can be re-written as

$$\lambda^{UB} = \frac{\int_V \int_0^{\Delta t} \sigma_y \bar{\dot{\varepsilon}}(\dot{\varepsilon}_{ij}^c) dt dV}{\int_V \int_0^{\Delta t} (\hat{\sigma}_{ij} \dot{\varepsilon}_{ij}^c) dt dV} \quad (3.9)$$

Where  $\bar{\dot{\varepsilon}} = \sqrt{(2/3)\dot{\varepsilon}'_{ij}\dot{\varepsilon}'_{ij}}$  is the effective strain rate.

### 3.2.2.2 The Iterative Upper Bound Procedure

The LMM upper bound method uses an iterative sequence of linear solutions where the shear modulus,  $\mu$ , is varied at every point within the volume so that the stresses re-

distribute in the same way as an elastic- plastic material, which in the case of the LMM is perfect plasticity.

The iterative procedure begins with a linear elastic stress solution, which gives an effective stress and strain rate at each point of  $\bar{\sigma}(\sigma_{ij}^k)$  and  $\bar{\dot{\epsilon}}$  respectively. The initial shear modulus at each point is  $\mu^k$ . A subsequent value of shear modulus,  $\mu^{k+1}$  is evaluated such that the effective stress at the point is equal to the yield stress whilst keeping  $\bar{\dot{\epsilon}}$  at a constant value.

Subsequent iterations define a new kinematically admissible history of plastic strain rate,  $\dot{\epsilon}_{ij}^f$ :

$$\dot{\epsilon}_{ij}^{f'} = \frac{1}{\mu} \left( \lambda_i^{UB} \hat{\sigma}_{ij}' + \bar{\rho}_{ij}^f \right)' \quad \text{where } \dot{\epsilon}_{kk}^f = 0 \quad (3.10)$$

Where the superscripts i and f refer to initial and final values respectively, the "dash" refers to deviatoric components, and  $\bar{\rho}_{ij}^f$  is the constant residual stress. Here the upper bound  $\lambda = \lambda_{UB}^i$  which is the upper bound multiplier corresponding to the strain rate of the previous iteration. Integrating equation (3.10) over the cycle produces a relation between  $\Delta \epsilon_{ij}^{f'}$  and  $\bar{\rho}_{ij}^{f'}$ :

$$\Delta \epsilon_{ij}^{f'} = \frac{1}{\bar{\mu}} \left( \bar{\rho}_{ij}^{f'} + \sigma_{ij}^{in'} \right) \quad (3.11)$$

Where

$$\sigma_{ij}^{in'} = \bar{\mu} \left[ \int_0^{\Delta t} \frac{1}{\mu(t)} \lambda_i^{UB} \hat{\sigma}_{ij}'(t) dt \right] \quad \text{and} \quad \frac{1}{\bar{\mu}} = \int_0^{\Delta t} \frac{1}{\mu(t)} dt \quad (3.12)$$

The solution of this linear problem gives  $\dot{\epsilon}_{ij}^f$ , which is substituted into equation (3.9) to give a new upper bound multiplier  $\lambda_f^{UB}$ . Convergence proofs [69] have shown that  $\lambda_f^{UB} \leq \lambda_i^{UB}$ , meaning that the continued iteration of this process produces a monotonically reducing upper bound multiplier which converges to the minimum upper bound (or in the case of numerical application the least upper bound associated with the finite element mesh).

### 3.2.2.3 Numerical Implementation of the Method

The iterative procedure described above has been implemented in the Abaqus finite element software through use of user subroutines to carry out the LMM calculations.

The Abaqus software is used widely throughout industry as a versatile tool for finite element analysis of components. The nuclear industry is no exception and Abaqus is used within EDF for integrity analyses of plant components. As well as containing a vast array of material models and analysis options, the Abaqus package also allows the user to program their own subroutines to create bespoke loading, boundary conditions, contact conditions and even custom elements. The LMM requires the ability to specify and alter the shear modulus at each integration point and also to control convergence using volume integrals of stresses and strain rates (equation (3.9)). Therefore the LMM is implemented in Abaqus using these subroutines, more specifically the UMAT subroutine, for creation of user defined material behaviour, and the URDFIL subroutine, for accessing and processing of results during solution. The UEXTERNALDB subroutine, for pre-processing of an analysis, is also extensively used but does not form part of the solution procedure. The function of the UEXTERNALDB routine is discussed in chapter 6.

The UMAT subroutine allows the specification of any constitutive model, and so can be used when the existing library of material models within Abaqus does not capture the material behaviour. The routine is called twice or more times for every integration point at which the User-material option is specified (which is defined by the user via the Abaqus CAE interface). Within the UMAT routine the Jacobian matrix,  $[J]$ , must be specified which relates the stress increment and the strain increment:

$$[J] = \frac{\partial \Delta \sigma}{\partial \Delta \varepsilon} \quad (3.13)$$

Using the Jacobian and the incremental strains calculated by Abaqus the incremental stresses can be calculated, which are updated at the end of each increment to provide the total stress solution. The UMAT routine also allows the user to store any results in the Abaqus output database (.odb) file for the user to view as contour plots in post-processing.

The URDFIL is called once at the end of each increment and allows access to the results up to and including the most recent analysis increment. This routine also includes an option to

terminate the analysis, and so provides a convenient way of querying results and ending the analysis if the convergence criteria are met.

The implementation of the LMM within Abaqus and the user subroutines begins by examining the time history of the applied loads  $\lambda P(x_j, t)$  and temperatures  $\lambda \theta(x_j, t)$  over the cycle. Rather than being a continuous function of time, the numerical implementation of the LMM instead discretises the cycle into a series of time points and assumes that the applied loading follows a series of straight line paths in load space. It follows that the applied elastic stresses then also follows a sequence of straight lines in stress space. If the yield surface is strictly convex then the consequence of this is that the only instances where plastic strains can develop are at the vertices of this stress history. Put simply, it is assumed that the extremes of the load cycle are the only times during the cycle where plastic strains develop, with the remainder of the cycle time spend within the yield surface. Therefore it is only these extremes of the load cycle which need to be considered when performing a LMM analysis.

With this in mind, the load cycle divided into a series of time points,  $n=1, 2, \dots, N$ . The strain history then becomes the sum of the increments of plastic strain

$$\Delta \varepsilon_{ij}^c = \sum_{n=1}^N \Delta \varepsilon_{ij}^n \quad (3.14)$$

The linear problem of finding a new kinematically admissible strain rate,  $\Delta \varepsilon_{ij}^f$  can be found by equation (3.11), where equations (3.12) are now:

$$\sigma_{ij}^{in'} = \bar{\mu} \left[ \sum_{n=1}^N \frac{1}{\mu^n} \lambda \hat{\sigma}_{ij}^{n'} \right] \quad \text{where} \quad \frac{1}{\bar{\mu}} = \sum_{n=1}^N \frac{1}{\mu^n} \quad \text{and} \quad \mu^n = \frac{\sigma_y}{\bar{\varepsilon}(\Delta \varepsilon_{ij}^{i'n})} \quad (3.15)$$

With these modifications into a numerical set of equations, the iterative procedure can then be implemented in Abaqus via the UMAT and URDFIL subroutines. This was first achieved by Engelhardt [93] and has since been the primary mode of implementing the LMM.

To begin the iterative process, the generation of the elastic stress fields,  $\hat{\sigma}_{ij}^{external}$  must be generated which correspond to each time point,  $n$ , in the discretised load cycle. These

elastic stresses are used as the initial input to the LMM iterative process,  $\hat{\sigma}_{ij}^n = \hat{\sigma}_{ij_{external}}^n$ . These elastic solutions must be solved for the same mesh and constraint boundary conditions as will be used for the LMM analysis.

For a single iteration, k+1, the following process is used in the UMAT subroutine in the Abaqus analysis. First, the load multiplier is made equal to that calculated at the end of increment k,  $\lambda_k^{UB}$ . This is used to scale the elastic stresses in the current increment. The shear modulus at each integration point is updated using the strain increment of the previous iteration which gives:

$$\mu_{k+1}^n = \frac{\sigma_y}{\bar{\varepsilon}_k^n} \text{ where } \bar{\varepsilon}_k^n = \bar{\varepsilon}(\Delta \varepsilon_{ij_k}^n) \quad (3.16)$$

and

$$\bar{\mu}_{k+1} = \sum_{n=1}^N \frac{1}{\mu_{k+1}^n} \quad (3.17)$$

Next the updated Jacobian can be calculated using the values of  $\mu_{k+1}^n$ . For a 3-dimensional stress state the Jacobian is as follows:

$$[J]_{k+1} = \frac{E(1-\nu)}{(1+\nu)(1-2\nu)} \begin{bmatrix} 1 & \frac{\nu}{1-\nu} & \frac{\nu}{1-\nu} & 0 & 0 & 0 \\ \frac{\nu}{1-\nu} & 1 & \frac{\nu}{1-\nu} & 0 & 0 & 0 \\ \frac{\nu}{1-\nu} & \frac{\nu}{1-\nu} & 1 & 0 & 0 & 0 \\ 0 & 0 & 0 & \frac{1-2\nu}{2(1-\nu)} & 0 & 0 \\ 0 & 0 & 0 & 0 & \frac{1-2\nu}{2(1-\nu)} & 0 \\ 0 & 0 & 0 & 0 & 0 & \frac{1-2\nu}{2(1-\nu)} \end{bmatrix} \quad (3.18)$$

Where the Poisson's ratio,  $\nu$ , approaches 0.5 to satisfy plastic incompressibility. We define

$\sigma_{ij_{k+1}}^{in}$  as:

$$\sigma_{ij_{k+1}}^{in} = \bar{\mu}_{k+1} \left[ \sum_{n=1}^N \frac{1}{\mu_{k+1}^n} \lambda_k^{UB} \hat{\sigma}_{ij}^n \right] \quad (3.19)$$

Which, along with the Jacobian, allows the constant residual stress to be calculated:

$$\bar{\rho}_{ij_{k+1}} = [J]_{k+1} \Delta \varepsilon_{ij_{k+1}} - \sigma_{ij_{k+1}}^{in} \quad (3.20)$$

The strain rate associated with n vertices of the load history is

$$\Delta \varepsilon_{ij}^n = [C]_{k+1} (\bar{\rho}_{ij_{k+1}} + \lambda_k^{UB} \hat{\sigma}_{ij}^n) \quad (3.21)$$

Where  $[C]_{k+1}$  is the compliance matrix derived using  $\mu_{k+1}^n$  in a similar way to the Jacobian.

From this, the effective strain increment  $\bar{\varepsilon}_{k+1}^n$  which will be used in the modulus adjustment calculation (equation (3.16)) in the subsequent iteration. Furthermore, the quantities

$$\sigma_y \sum_{n=1}^N \bar{\varepsilon}_{k+1}^n \quad \text{and} \quad \sum_{n=1}^N \Delta \varepsilon_{ij}^n \lambda_k^{UB} \hat{\sigma}_{ij}^n \quad (3.22)$$

are stored for each integration point in the structure. When these calculations have been completed for every integration point, the URDFIL routine is then called. Within the URDFIL routine the Abaqus results file is accessed where volume integrals of the two quantities in (3.22) are extracted, allowing the load multiplier to be calculated:

$$\lambda_{k+1}^{UB} = \frac{\int_V \left( \sigma_y \sum_{n=1}^N \bar{\varepsilon}_{k+1}^n \right) dV}{\int_V \left( \sum_{n=1}^N \Delta \varepsilon_{ij}^n \lambda_k^{UB} \hat{\sigma}_{ij}^n \right) dV} \quad (3.23)$$

For the very first iteration of this process, i.e. k=1, the only difference to this process is that  $\lambda_1^{UB} = 1.0$  and  $\mu_{k+1}^n = 1/E$  where E is the elastic modulus of the material in question. Apart from these changes to  $\lambda^{UB}$  and equation (3.16), the process is unchanged in the first iteration.

### 3.2.3 Lower Bound Method

The lower bound shakedown theorem demonstrates shakedown by finding a self equilibrating residual stress field which, when superimposed with the applied cyclic elastic stresses, satisfies the yield condition at all points in the load cycle:

$$f\left(\hat{\sigma}_{ij}(x,t) + \bar{\rho}_{ij}(x)\right) \leq 0 \quad (3.24)$$

Therefore, to obtain a lower bound to the LMM strict shakedown solution, a constant residual stress field must be found which satisfies equation (3.24) above for the applied elastic stresses from equation (3.4)

$$f\left(\lambda\hat{\sigma}_{ij}(x,t) + \bar{\rho}_{ij}(x)\right) \leq 0 \quad (3.25)$$

Where  $\lambda$  is a scalar load multiplier. In the LMM, perfect plasticity is used and so the yield condition is checked by simply comparing the von-Mises stress to the yield stress. Therefore if equation (3.25) above can satisfy the temperature dependent von-Mises yield condition at all points in the structure

$$\bar{\sigma}\left(\lambda\hat{\sigma}_{ij}(x,t) + \bar{\rho}_{ij}(x)\right) \leq \sigma_y(T) \quad (3.26)$$

where  $\bar{\sigma}(\sigma_{ij}) = \sqrt{2/3\sigma'_{ij}\sigma'_{ij}}$  is the von-Mises effective stress and  $T_1$  is the temperature at that location in the structure, then Melan's theorem will be satisfied and the applied loading  $\lambda\hat{\sigma}_{ij}(x,t)$  is a lower bound to the shakedown limit.

During the upper bound iterative process, a new estimate of the constant residual stress field at each point in the structure,  $\bar{\rho}_{ij_{k+1}}$ , is obtained by equation (3.20). This superimposed with the applied elastic stresses scaled by the current upper bound multiplier,  $\lambda_k^{UB}\hat{\sigma}_{ij}^n$ , gives the total stress field at that point in the structure. Dividing the yield stress by this stress gives the factor by which this stress must be scaled in order to satisfy yield. Therefore the next estimate of the lower bound multiplier,  $\lambda_{k+1}^{LB}$ , given by multiplying this factor by the upper bound multiplier

$$\lambda_{k+1}^{LB} = \lambda_k^{UB} \frac{\sigma_y(T)}{\bar{\sigma}(\lambda_k^{UB} \hat{\sigma}_{ij}^n + \bar{\rho}_{ij,k+1})} \quad (3.27)$$

is the level by which this stress field must be scaled to satisfy the temperature dependent yield condition at that point in the structure and at the load instance. During each iteration of the upper bound calculation  $\lambda^{LB}$  can be calculated for each integration point and load instance. The lowest  $\lambda^{LB}$  value from all values calculated indicates the point where the stresses must be scaled back the most in order to satisfy Melan's theorem, and so this  $\lambda^{LB}$  is therefore the lower bound multiplier for the entire structure.

Continued iteration of the upper bound procedure will generally produce increasingly accurate estimates of the constant residual stress field, which will in turn produce an improvement in the lower bound load multiplier. Monotonic increases in the lower bound are not always observed, however, due to inaccuracies in the stress solutions at individual integration points which can dictate the lower bound of an entire model. The best lower bound from all previous and current increments is therefore used.

### 3.3 Validation of the LMM Strict Shakedown Procedure

Any numerical procedure requires extensive validation to build confidence in its ability to predict the phenomenon in question. In order to do this for the LMM strict shakedown method three comparisons are given here. The first two, namely notched bar limit loads and the Bree Cylinder, validate the numerical solutions of the LMM against theoretically derived limits. The third case presents a comparison between the LMM and experimentally derived limit loads and shakedown limits. This allows the overall analysis tool and its implementation in FEA, including the assumptions and approximations inherent in this, to be tested in similar circumstances as will be seen when in use in EDF.

#### 3.3.1 Limit Loads of Notched Bars

Calculation of the shakedown limit usually takes both cyclic and steady state loading into account. A special case of this is when the cyclic component of the loading reduces to zero, leaving only the steady state component. In this case the shakedown limit coincides with the limit load. This provides an opportunity to validate the LMM because theoretical limit loads have been derived for a large variety of geometries and can be used as a comparison. In addition, the limit load is a value which can be calculated readily using FEA packages.

The LMM is required to operate over a large range of continuum element types, namely 3D, plane strain, axisymmetric and plane stress elements. In order to verify the implementation of the code over all these element types, and due to the availability of theoretical solutions for each dimensionality, the limit loads of notched bars under axial tension is considered here. This geometry was considered by Tipping [34] after his initial consolidation of the LMM subroutines, and re-using this geometry allows the subsequent addition of lower bounds in [28] to be compared. The theoretical solutions of Miller [94] are presented alongside a LMM strict shakedown analysis and a standard limit analysis in Abaqus. The LMM and Abaqus limit analyses are performed using identical meshes. Figure 3.2 shows the geometry, FE mesh and material properties used in the analyses. For the 3D model the mesh shown is swept circumferentially. In the LMM analyses a convergence tolerance of  $1e-5$  between consecutive upper bounds was used.

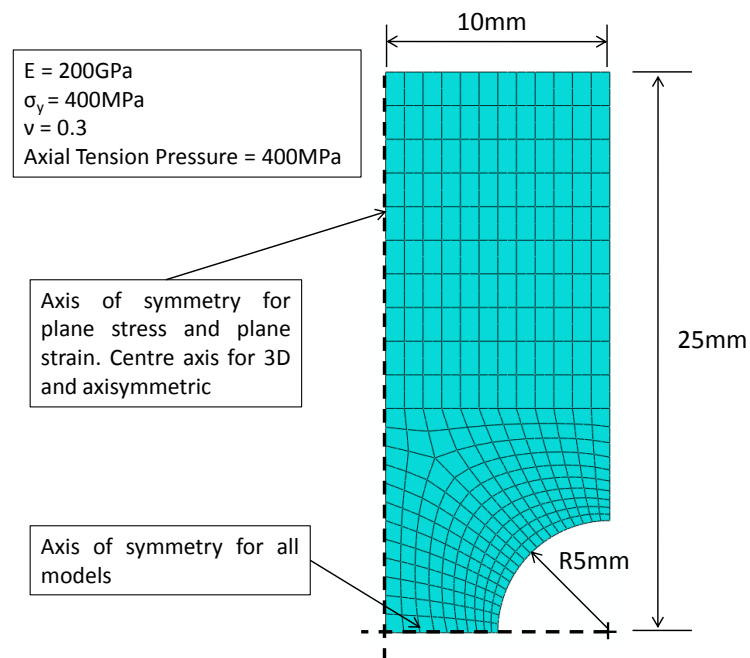


**Figure 3.2 - Geometry, Mesh and Material Properties of the Notched Bars**

An axial tension is applied through a pressure load on the top surface of the bar. The theoretical solutions presented here from [94] have been converted by Tipping [34] to give the limit load factor on the applied tensile pressure (which is equal to the yield stress). In these equations  $b$  is the bar width/diameter at the notch,  $w$  is the bar width/diameter remote from the notch and  $r$  is the notch radius.

### 3.3.1.1 3D Notched Round Bar

A circular bar with a circumferential notch under axial tension is analysed. The theoretical limit load multiplier is given by

$$\lambda = \left(\frac{b}{w}\right)^2 \left( \left(1 + \frac{4r}{b}\right) \ln\left(1 + \frac{b}{4r}\right) \right) \quad (3.28)$$

The limit load multipliers for all methods are given in Figure 3.3, which also compares the plastic strain contours from the LMM (Figure 3.3a) and Abaqus limit analyses (Figure 3.3b).

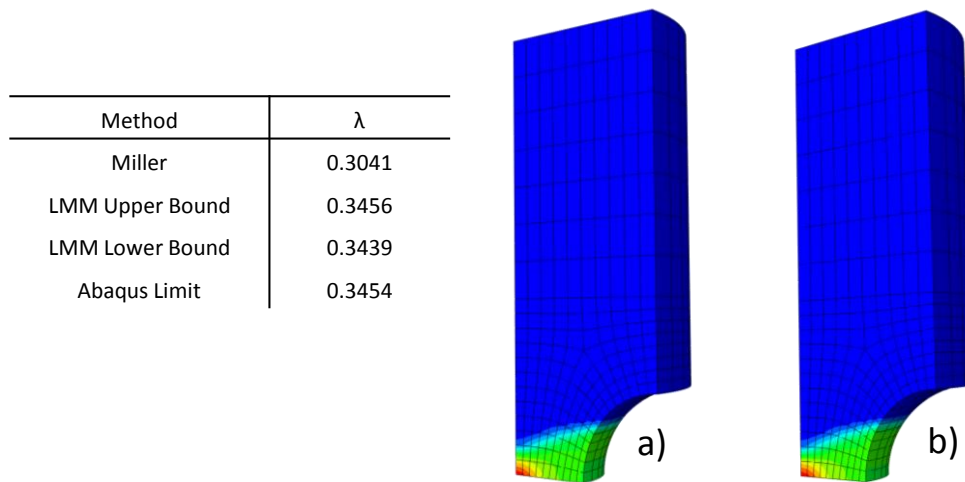


Figure 3.3 - 3D Notched Bar Results Comparison

### 3.3.1.2 Axisymmetric Notched Round Bar

The 3D case considered in section 3.3.1.1 is analysed as an axisymmetric geometry. Therefore the theoretical limit load multiplier is given by equation (3.28). Figure 3.4 shows the predicted limit load multipliers along with the plastic strain contours predicted by the LMM (Figure 3.4a) and Abaqus limit analysis (Figure 3.4b).

Method	$\lambda$
Miller	0.3041
LMM Upper Bound	0.3456
LMM Lower Bound	0.3439
Abaqus Limit	0.3454

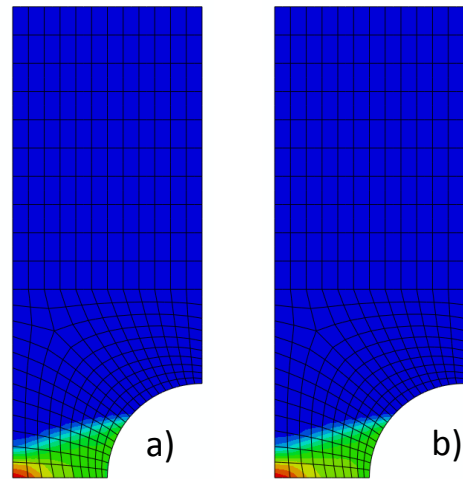


Figure 3.4 - Axisymmetric Notched Bar Results Comparison

### 3.3.1.3 Plane Strain Double Notched Plate

The theoretical limit load multiplier for a double edge notched flat plate under plane strain conditions is given by

$$\lambda = 1.155 \frac{b}{w} \left( \left( 1 + \frac{2r}{b} \right) \ln \left( 1 + \frac{b}{2r} \right) \right) \quad (3.29)$$

Figure 3.5 shows the predicted limit load multipliers and compares the plastic strain contours predicted by the LMM (Figure 3.5a) and Abaqus limit analysis (Figure 3.5b).

Method	$\lambda$
Miller	0.8006
LMM Upper Bound	0.8025
LMM Lower Bound	0.7985
Abaqus Limit	0.8028

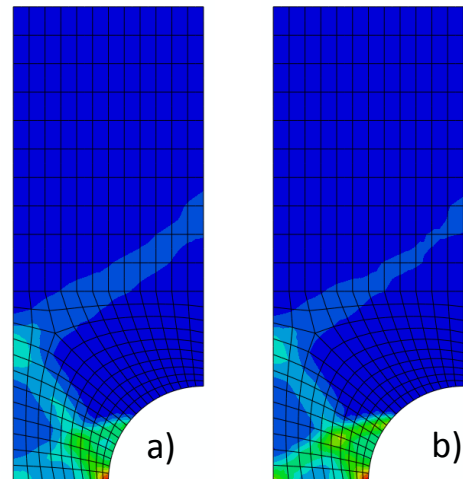


Figure 3.5 - Plane Strain Notched Bar Results Comparison

### 3.3.1.4 Plane Stress Double Notched Plate

The theoretical limit load multiplier for a double edge notched flat plate under plane stress conditions is given by

$$\lambda = \frac{b}{w} \left( 1 + \frac{0.226b}{(b + 2r)} \right) \quad (3.30)$$

Figure 3.6 shows the predicted limit load multipliers and compares the plastic strain contours predicted by the LMM (Figure 3.6a) and Abaqus limit analysis (Figure 3.6b).

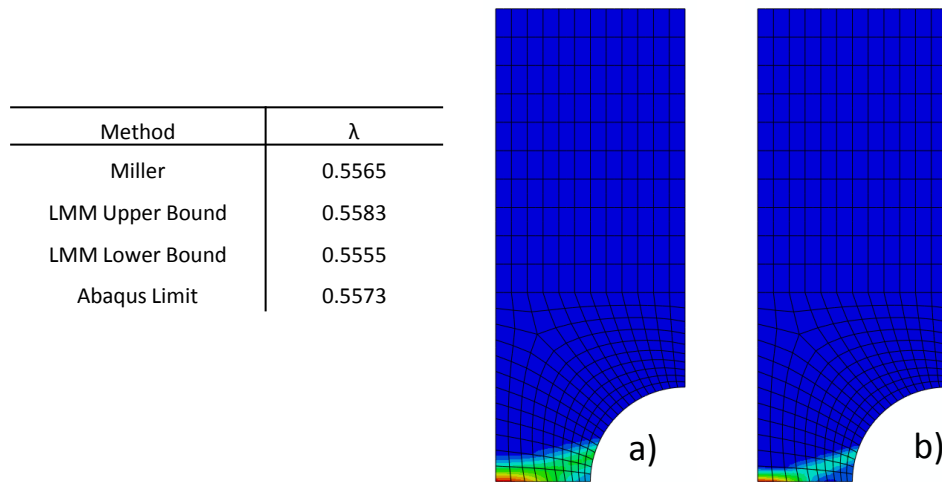


Figure 3.6 - Plane Stress Notched Bar Results Comparison

### 3.3.1.5 Notched Bar Summary

In all cases the limit load multipliers predicted by both Abaqus limit analysis and the LMM strict shakedown method agree well with each other and also with the theoretical predictions of Miller. In addition, the contour plots of plastic strain show a good resemblance to one another. These factors combined give confidence in the ability of the LMM to predict the limit loads of structures for all dimensionalities considered.

### 3.3.2 The Bree Cylinder

As described in chapter 2, the Bree cylinder is a very well established solution in the field of shakedown and ratcheting and forms the basis of the shakedown sections of many design and assessment codes. The Bree cylinder also provides a rare opportunity to compare a numerical shakedown method to a theoretical solution.

The Bree Cylinder is an analysis of a cylindrical nuclear fuel casing, where the casing is assumed to be thin in comparison to its radius. The cylinder is subject to an internal pressure and a through wall temperature distribution. The additional simplification of assuming that the hoop stress is dominant compared to the axial stress is made (in reality the hoop stress is twice the axial stress for a thin pressurised cylinder with closed ends). These simplifications allow the analysis to be reduced to a one-dimensional problem which can be solved analytically. The loads and load history are depicted in Figure 3.7.

A steady state axial tension is applied which is representative of the hoop stress. A temperature difference between the inner and outer walls of the can,  $\Delta\theta$ , causes a linear temperature distribution through the thickness. This temperature distribution is cyclic with time, resulting in two extremes in the load history. This idealised situation can be replicated for analysis with the LMM. The simplifications reduce the situation to a plane stress problem, and so this will be adopted for the LMM analysis.

A comparison of the theoretical strict shakedown limit of Bree and that of the LMM is shown in Figure 3.7. The vertical axis represents the level of cyclic thermal stress and the horizontal axis represents the level of steady state axial stress. Both axes have been normalised against the yield stress.

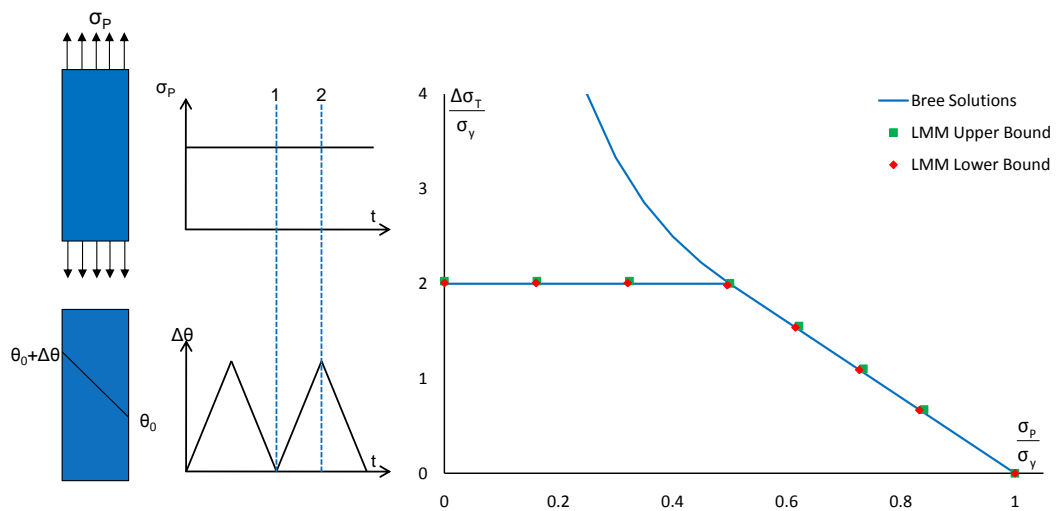


**Figure 3.7 - Bree Cylinder Loading, Load History and Results**

The derivation of Bree has recently been extended by Bradford [95] to consider the axial tension also as a cyclic load. In this derivation the axial tension and thermal gradient are cycled in phase with each other, as shown in Figure 3.8.

The LMM strict shakedown is compared to the analytical solution produced by Bradford in Figure 3.8. In this figure both the horizontal axis represents the level of cyclic axial stress and the vertical axis represents the level of cyclic thermal stress. Both axes have been normalised against the yield stress.

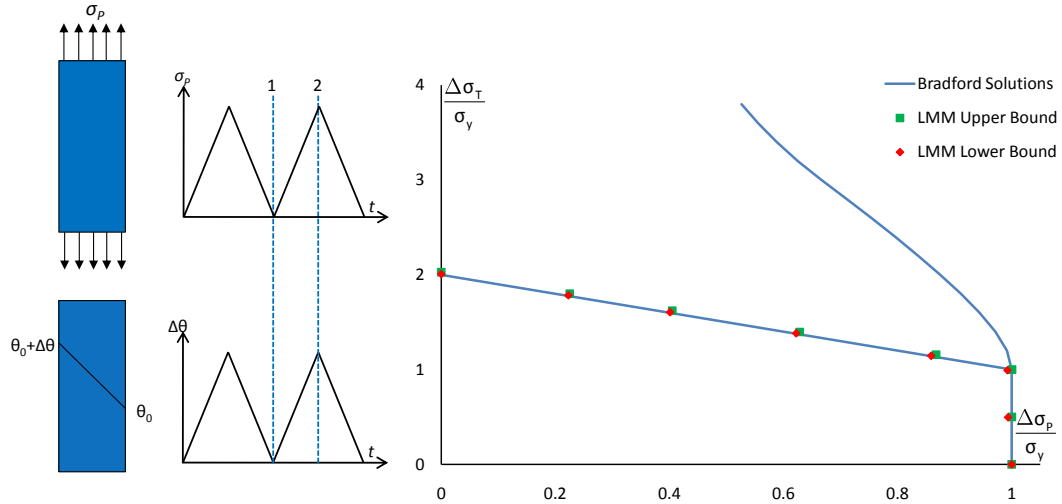


Figure 3.8 - Modified Bree Cylinder Loading, Load History and Results

Examining Figure 3.7 and Figure 3.8 shows that the LMM lower and upper bounds agree well with both theoretical strict shakedown boundaries.

### 3.3.3 Comparisons with Experimental Data

The comparison of the LMM against theoretical solutions provides a valuable validation, particularly for verifying the implementation of the bounding theorems within the finite element method. The next stage in the validation process is to compare the LMM with experimental solutions. Doing this determines if the simplifications and approximations inherent in the method are reasonable when compared to the kind of situations encountered in structural integrity calculations of real components.

#### 3.3.3.1 Limit Load Comparisons

The limit load tests used for comparison here are those performed by the Welding Research Council [96]. The limit loads of pipe intersections subject to internal pressure and in-plane bending were investigated, and two of these tests are used here. For continuity the naming convention used in [96] is also used here with Intersection A being subject to internal pressure and Intersection B1 being subject to an in-plane moment.

The intersections were manufactured from ASTM A-36 steel. A full anneal was performed before the final finishing cut to remove the residual stresses inherent in the plate and caused by machining. The material properties for each intersection were found by machining tensile testing specimens from the same billet as were used in its manufacture. These specimens were also fully annealed before testing. Figure 3.9 shows the dimensions and typical stress strain response of the steel. The yield stresses were determined using an average of six tests where no test deviated from the mean by more than 2%. The yield stresses for A and B1 from these tests are 198MPa and 167MPa respectively.

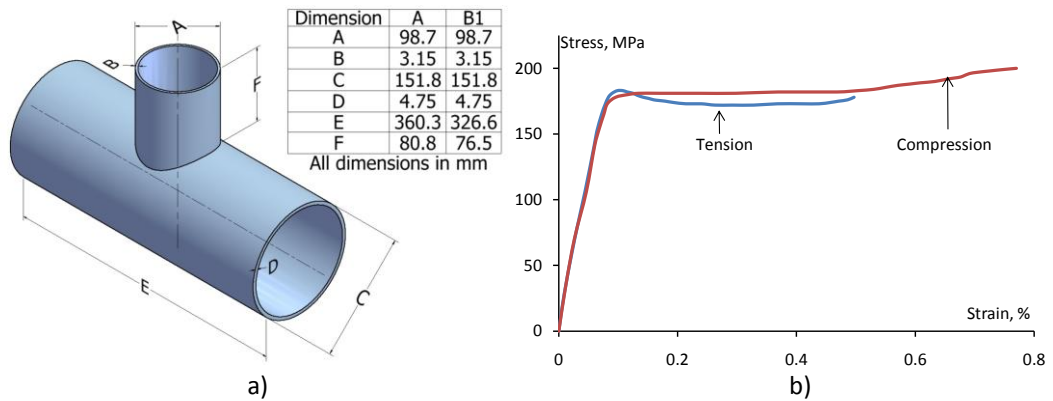


**Figure 3.9 - Pipe Intersection a) Geometry and b) Typical Material Stress-Strain Curve**

The internal pressure loading was applied to A by welding plates to the open ends of the pipes and then supplying pressurised fluid through one end. The moment loading was applied to the branch pipe of B1 using two hydraulic rams acting in opposite directions. These, in turn, were connected via pin joints to a loading arm attached to the free end of the branch pipe, shown schematically in Figure 3.10a. This arrangement applied a pure couple to the branch pipe.

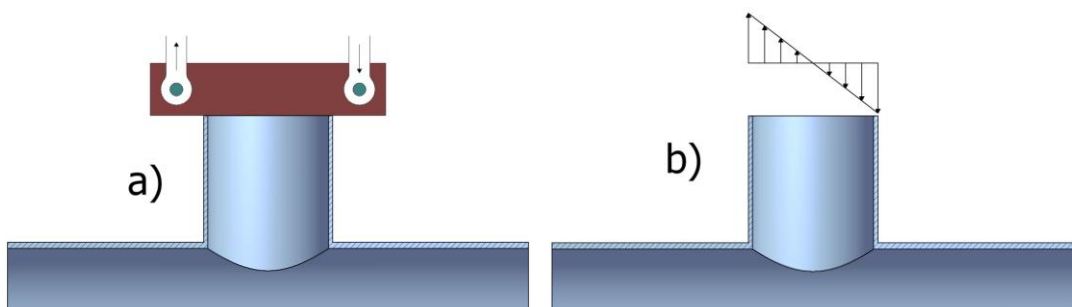


**Figure 3.10 - Application of a Pure Moment**

Using the information given in [96], the pipe intersections were modelled in Abaqus for assessment with the LMM. The dimensions of both intersections are reported with great accuracy, which allowed an exact geometry to be created and meshed in Abaqus CAE using symmetry where appropriate. Model A was modelled using a one-quarter model due to the uniform loading. Model B1 used one-half symmetry due to the symmetry of the applied moment loading along the axis of the main pipe (shown in Figure 3.11).

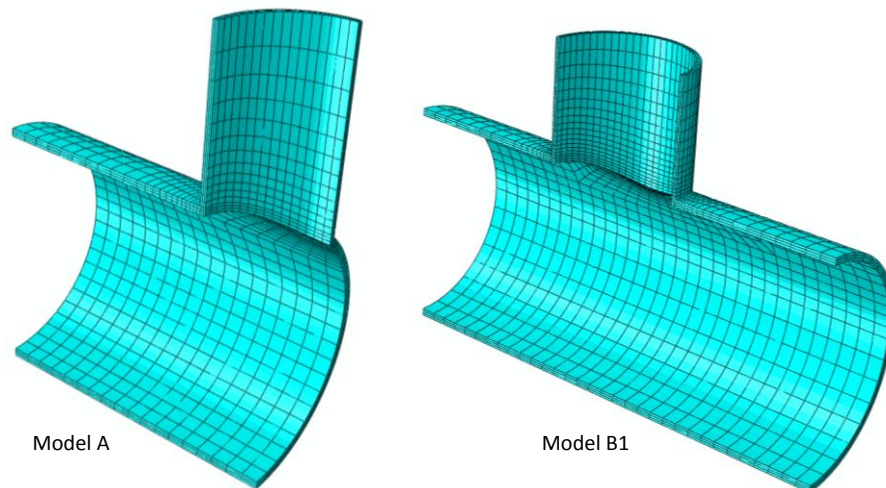


**Figure 3.11 - FEA Models A and B1**

A perfectly plastic material model was used for both limit pressure and limit moment analyses using the yield stresses quoted. Looking at Figure 3.9b it can be seen that for the range of strains shown in the tensile and compressive tests that a perfectly plastic material, despite being a very simple model, is a reasonable approximation to this material response.

The loading and boundary conditions were chosen to most accurately represent the conditions of each test. In model A internal pressure loading was applied to all internal surfaces, and due to the closure of the ends in the tests, the closed end condition was applied by applying the equivalent axial tension to the free ends of the pipes. Free radial expansion of the pipes was allowed, as per the tests, and the free ends of the pipes were constrained to remain in-plane during longitudinal expansion. In model B1, the ends of the main pipe were fully fixed. The bending moment was applied to the intersecting pipe using the DLOAD subroutine, which allowed a pure couple to be applied in the form of a linear pressure distribution across the free end, as shown in Figure 3.10b.

Table 3.1 shows the limit loads predicted by the LMM and the experiments. The limit load predicted by an Abaqus limit analysis, using the same mesh as the LMM analysis, is also

included as an additional comparison. In [96] three values of the experimental limit load are calculated using different interpretations of the load-deflection and load-strain data. For conservatism the lowest of the three values is quoted in Table 3.1.

**Table 3.1 - Limit Load Comparison**

Test	Abaqus Limit	LMM		Experiment	
		Upper Bound	Lower Bound		
A	7.19	7.191	7.122	8.0	(MPa)
B1	2970.0	2968.05	2939.29	3184.0	(Nm)

It is thought that the limit loads predicted by the LMM and Abaqus limit analysis show a reasonable agreement with each other and show a conservative result compared to the experimental limit loads.

### 3.3.3.2 Shakedown Limit Comparisons

The shakedown tests used for comparison are those performed by the C.E.G.B. [97] for oblique nozzles in spherical shells under internal pressure, and two of these tests are used here. Once again, for continuity, the naming convention used in [97] is adopted here namely Nozzles 5 and 6.

The dimensions of the two vessels are shown in Figure 3.12. The boiler plate (shell material) and forged bar (nozzle material) were selected in [97] to have closely matched material properties, which are shown in Table 3.2.

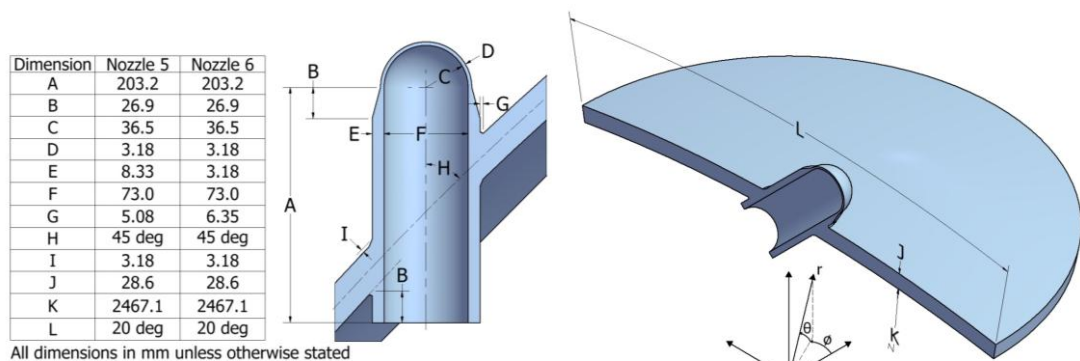


**Figure 3.12 - Geometry of Nozzles 5 and 6**

The tests were performed to find the shakedown pressure of these nozzles. Many strain gauges were attached to the nozzles prior to testing and these strain readings were used to determine the shakedown status of the vessel.

**Table 3.2 - Material Properties**

Material	Yield Stress (MPa)	Ultimate Tensile Strength (MPa)
Nozzle	265.18	492.67
Shell	273.36	484.95

Beginning at ambient pressure, the vessel was pressurised to the current test pressure and then back to ambient conditions. The initial pressure cycle began at ambient, pressurised to 400psi and then returned to ambient. If shakedown was observed with this level of pressure cycling, then the maximum pressure in the cycle was increased by 50psi and the cycling was repeated. In these tests shakedown was said to occur when identical strains were recorded in three consecutive cycles. If this shakedown criterion was not met within 8 pressure cycles, it was concluded that the vessel would not attain shakedown.

The nozzles were modelled in Abaqus CAE where the dimensions of the welds (not fully documented in the published results) were estimated based on likely leg lengths for the thickness of the shell and nozzle. The symmetry of both nozzles was used by creating half models with the appropriate symmetry boundary condition. The full spherical shell was reduced to a small section through the use of a spherical coordinate system and boundary conditions at the edge which permitted radial expansion but fixed motion in the theta and phi dimensions. The FEA models are shown in Figure 3.13.

A perfectly plastic material model was adopted for the analysis using the yield stresses given in Table 3.2. The ultimate tensile strength quoted shows that the material work hardens, but the absence of any further data prevents the use of hardening material models. Welded regions and heat affected zones very often have a higher yield stress than the surrounding parent material, but in this situation no information regarding this was provided. Therefore the material properties of the weld were assumed to be the same as those for the nozzle material which, being the lower of the two yield stresses, introduces a small conservatism into the analysis.

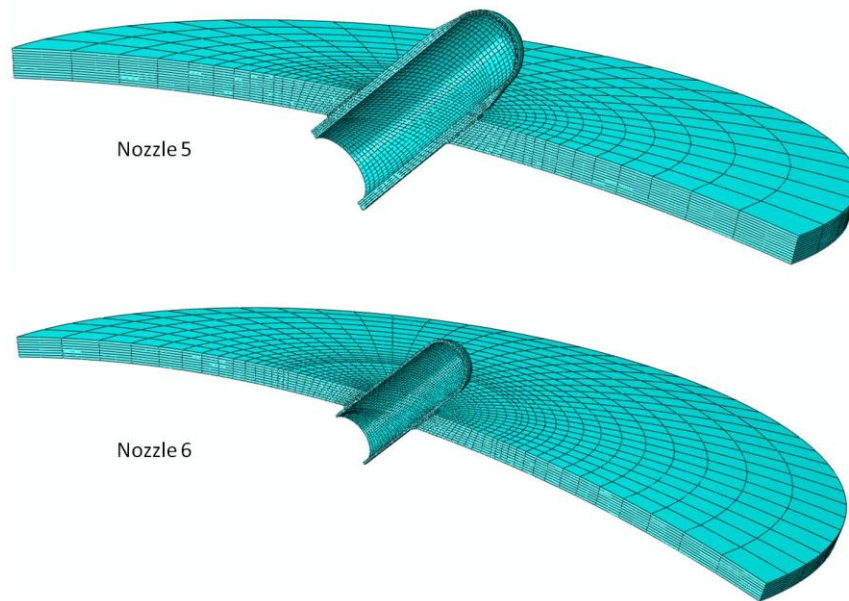


**Figure 3.13 - FEA Models of Nozzles 5 and 6**

An internal pressure was applied to all inner surfaces of the model. This pressure was established within a load cycle in the LMM analysis so that it would cycle from zero to a maximum pressure and then to zero once again. This load cycle is scaled by the LMM to find the shakedown limit, which in turn results in the shakedown pressure for the nozzle.

Table 3.3 shows a comparison of the shakedown limit pressures found by experiment and through LMM calculation. The experimental lower bound corresponds to the highest level of cyclic pressure where shakedown was achieved. The experimental upper bound corresponds to the first cyclic pressure level where shakedown was not achieved. The shakedown pressures predicted by the LMM show reasonable agreement with the experiments whilst retaining a level of conservatism. This conservatism is thought to arise from the perfectly plastic material used. The work hardening of the material, demonstrated by the Ultimate Tensile Strength values in Table 3.2, would result in a higher shakedown limit.

**Table 3.3 - Comparison of Shakedown Pressures**

Nozzle	LMM		Experiment		
	Lower Bound	Upper Bound	Lower Bound	Upper Bound	
5	4.53	4.58	4.82	5.17	(MPa)
6	4.12	4.16	4.48	4.82	(MPa)

Figure 3.14 shows the location of the plastic strains in Nozzle 5 predicted by the LMM, which are located at the nozzle-shell joint. This highlights the reverse plasticity mechanism which would be observed when the cyclic pressure exceeds the shakedown pressure. This location was also highlighted in the C.E.G.B. report, which provides further validation of the LMM analysis. A similar correlation was also observed with Nozzle 6.

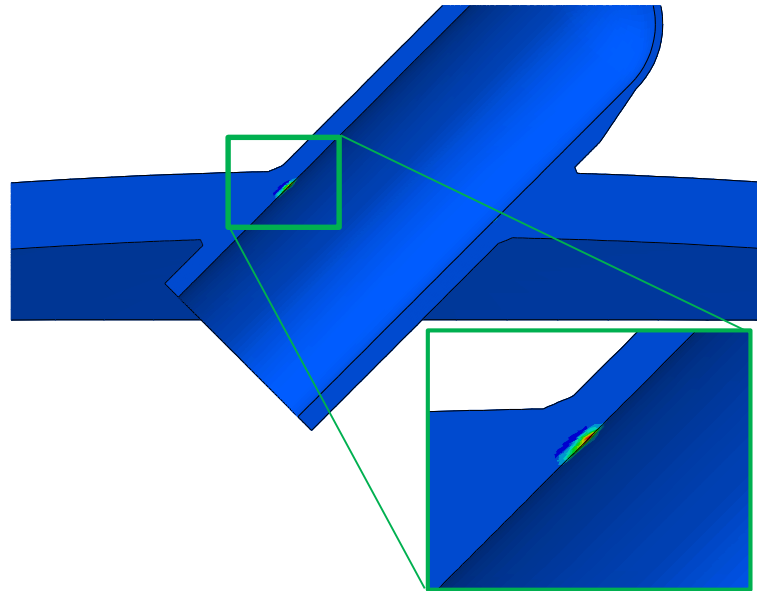


Figure 3.14 - Location of Reverse Plasticity in Nozzle 5

### 3.4 The LMM Strict Shakedown Method Applied to Pipe Bends

Having introduced and validated the LMM strict shakedown method in this chapter, this section introduces a more practical application of the method. Pipe bends are ubiquitous to any piping system and their analysis through use of the LMM offers the chance to demonstrate the capabilities and advantages of the method when applied to industrially relevant situations. Additionally, the strict shakedown behaviour of this geometry has received little attention in the literature, and so this study also aims to advance the knowledge of the behaviour of pipe bends subject to cyclic loading.

The cases explored here include 90 degree pipe bends subject to steady state internal pressure and either cyclic bending moments or cyclic thermal gradients. In the case of internal pressure and bending moments, the limit loads are also provided. A range of bend factors are considered and results are normalised so that the conclusions are as generally applicable as possible.

### 3.4.1 Existing Pipe Bend Solutions

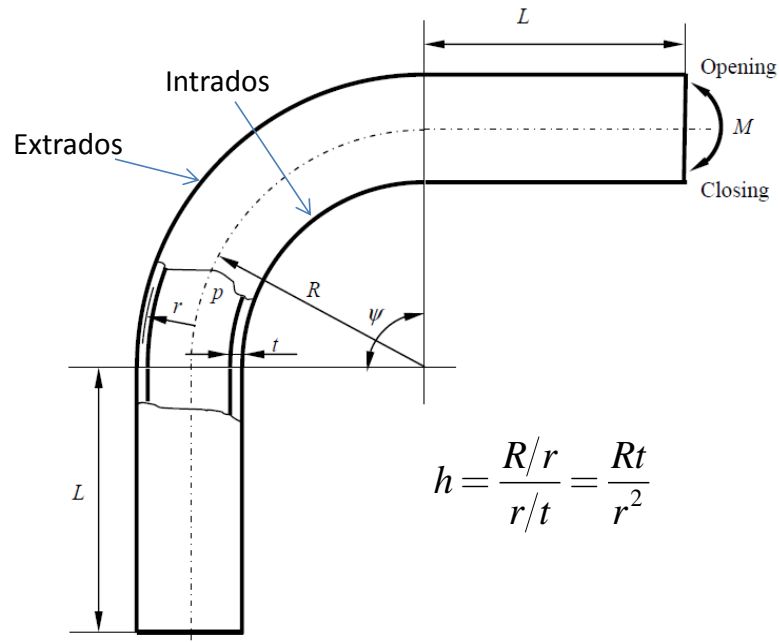


Figure 3.15 - Pipe Bend Geometry and h Value

Considerable attention has been given to calculation of limit loads of pipe bends over the years. A typical pipe bend, shown in Figure 3.15, is usually described in terms of two ratios,  $r/t$  and  $R/r$ , where  $r$  is the mean pipe radius,  $R$  is the bend radius and  $t$  is the wall thickness. The pipe bend factor,  $h$ , is given by combining these two ratios. The inside of the bend area is named the intrados, and the external area is named the extrados.

One of the first theoretical solutions for the limit load of pipe bends was that of Calladine [98], who derived an expression for the limit moment:

$$M_L = 1.19\pi^2 t \sigma_y h^{2/3} \text{ where } h \leq 0.5 \quad (3.31)$$

Goodall [99] derived an expression for the limit internal pressure

$$P_L = \sigma_y \frac{t}{r} \frac{\left(1 - \frac{r}{R}\right)}{\left(1 - \frac{r}{2R}\right)} \quad (3.32)$$

Both of the above theoretical expressions are based on thin shell theory and the Tresca yield criterion. Other than these equations, few other theoretical solutions could be found

for the plastic limit of this geometry. Instead, researchers have used extensive FEA to generate data for various ratios of  $R/r$  and  $r/t$ . These data points have then been plotted and equations derived from curve-fits of the data.

When carrying out these FEA analyses for this geometry under bending loads, it is common that the effects of non-linear geometry are taken into account. Doing this is an attempt to capture the geometric strengthening and weakening that is known to occur with this geometry. When a pipe bend is subject to opening or closing bending, the cross section of the bend changes as shown in Figure 3.16. This change in cross section increases/decreases the second moment of area which leads to the strengthening/weakening to further application of the bending moment. A typical, small strain, FEA analysis does not capture these effects and so FEA which includes the effects of non-linear geometry is common in the literature.

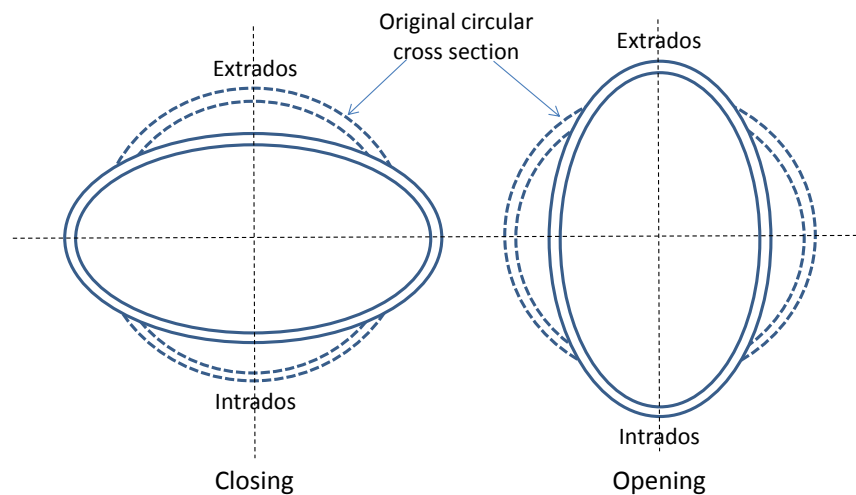


**Figure 3.16 - Pipe Bend Change in Cross Section Under Bending**

A recent review of the literature regarding the limit loads of pipe bends by Lei [100] highlighted some important conclusions. Firstly, the attached straight sections provide a significant level of reinforcement to the bend by allowing the plastic zone to spread. This increases the limit loads above those of equations (3.31) and (3.32). The second conclusion from this study concerned the limit load solutions available in the literature. The equations derived from FEA analyses, whilst providing a good fit to the data they are derived from, were not able to successfully predict the results from other authors. As a result of this, Lei derived a new set of equations to describe the limit moment, pressure and combined moment and pressure (which are given in Appendix A).

Despite the extensive volume of work regarding limit analysis and limit load solutions for mechanical loading, very little work has been published regarding the strict shakedown behaviour of this geometry. An experimental ratcheting study was performed for a single pipe bend geometry by Chen et al [101] so that material model calibration for FEA studies could be carried out. H.F. Abdalla et al [65] presented the strict shakedown behaviour of a single bend with  $R = 480\text{mm}$ ,  $r = 133.5\text{mm}$  and  $t = 3\text{mm}$  (giving  $R/r = 3.6$  and  $r/t = 44.5$ ). Further calculations are carried out by C.S Oh et al [66] for the strict shakedown of bends covering a large range of  $h$  for internal pressure and in-plane closing and opening bending. Other than these works, no further published shakedown calculations could be found for this geometry.

The numerical studies of both [65] and [66] use a version of the Nonlinear Superposition method outlined in section 2.6.1. By using this method, both groups were able to produce results which captured the nonlinear geometry aspects of the strict shakedown response by selecting this option for the elastic and elastic-plastic analyses that form the shakedown calculation. Figure 3.17 shows a typical comparison of the linear and nonlinear geometry shakedown results predicted by C.S Oh et al. It can be seen that the shakedown boundary for closing bending (nonlinear geometry) is greater than linear geometry, which is in turn greater than opening bending (nonlinear geometry), although it is not stated in [66] the nature of the bending to generate the linear geometry results.

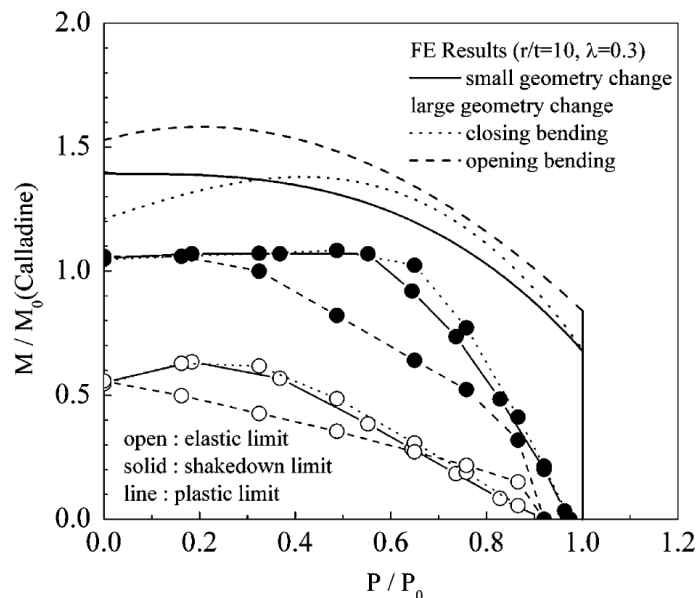


Figure 3.17 - Sample Results from [66]

The LMM is currently formulated for linear geometry only, but Figure 3.17 shows that there is some merit in producing these results. Firstly, the reverse plasticity limit at low levels of pressure loading limit is relatively unchanged for the linear geometry and nonlinear geometry for opening or closing bending. Additionally the limit load for internal pressure is unaffected by linear or nonlinear geometry (which is consistent with the findings in [100]). Furthermore, there are modifications to the strict shakedown theorems in the literature which take nonlinear geometry effects into account, for example [102][103]. Therefore results produced by the LMM would also form the baseline with which to compare nonlinear geometry results when these theorems are implemented in the LMM framework at a future date.

Cyclic thermal loading is common in plant components, and pipe bends are often subjected to cyclic gradients of temperature through the wall thickness. Despite this common loading condition, no published work could be found in the literature regarding the shakedown behaviour in this situation.

### **3.4.2 LMM Analysis**

The objective of this study is to use the LMM strict shakedown procedure to generate the limit loads and shakedown limits of pipe bends. Two cases are considered. The first is when the pipe is subjected to an internal pressure and in-plane closing, opening and reversed bending. The mechanisms of reverse plasticity and ratcheting are explored and a comparison between the shakedown behaviour of opening, closing and reversed bending is presented. The second case is where the pipe is subjected to an internal pressure and a cyclic temperature gradient through the wall thickness. The effect of temperature dependent yield stress is considered and the shakedown behaviour of pipe bends is compared to that of a straight pipe.

The results are presented in normalised form to make them as widely applicable as possible. The limit moment equations of Lei differ for opening and closing bending. The presence of reversed bending (i.e. involving opening and closing bending in the cycle) means that these equations cannot be used to normalise all the results. As a result of this, as well as the fact that the geometries with  $r/t = 5$  cannot be considered "thin" as an approximation, the results presented here are normalised against the limit pressure and moment for a thick walled straight pipe with the same mean radius and wall thickness:

$$P_L^s = \frac{2}{\sqrt{3}} \sigma_y \ln\left(\frac{r_o}{r_i}\right) \quad (3.33)$$

$$M_L^s = \frac{4}{3} \sigma_y (r_o^3 - r_i^3) \quad (3.34)$$

where  $r_o$  and  $r_i$  are the outer and inner radii of the pipe respectively. Limit load comparisons against the equations of Lei are also provided in section 3.4.4.3.

### 3.4.3 Description of FEA Model, Parametric Study and Loading

A three dimensional solid model was constructed in Abaqus. Due to the symmetry of the geometry, a one quarter model was used and symmetry boundary conditions were applied (see Figure 3.18). ABAQUS type C3D20R quadratic elements with reduced integration were used for the structural analysis and ABAQUS type DC3D20 elements were used for the heat transfer analysis.

To mesh the bend, at least three elements were used through the thickness, ten around the radius of the bend and twenty elements around the circumference of the pipe. A refinement study was conducted to validate the accuracy of the mesh used. Such a mesh was chosen to give sufficient density around the area of interest and to maintain reasonable element aspect ratios. The attached straight section was meshed with twenty elements along its length, which were biased to be smaller in the region of the bend.

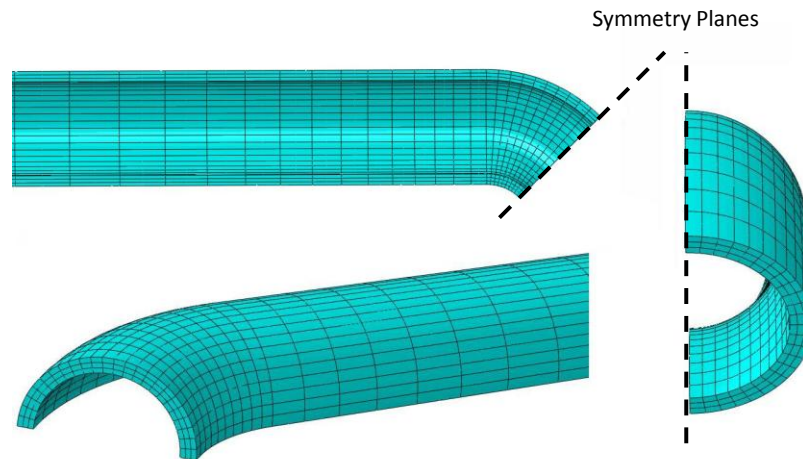
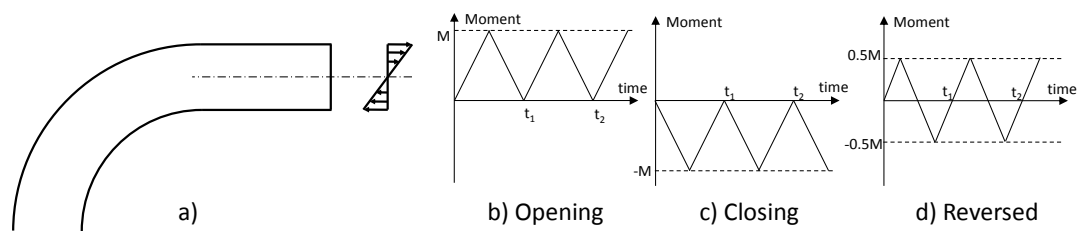


Figure 3.18 - Pipe Bend FEA Model Showing Symmetry Planes

The internal pressure,  $P$ , was applied at the inner surface assuming the closed end condition, with an equivalent axial tension applied at the free end of the straight section

to replicate the axial stress. The moment was applied as a linear pressure distribution at the free end of the straight section, which was applied using the user subroutine DLOAD in ABAQUS (Figure 3.19a).

When conducting a limit analysis, the pressure and moment loads were applied monotonically. When shakedown analysis was performed, the pressure was held at a constant value and the initial bending moment was cycled i) from zero to a maximum of  $M$  for opening bending ii) from zero to a minimum of  $-M$  for closing bending or iii) from  $-0.5M$  to  $+0.5M$  for reversed bending, shown in Figure 3.19.



**Figure 3.19 - Moment Loading and History**

When the case of internal pressure and cyclic thermal loading was considered, a steady state heat transfer analysis was conducted with  $T_o = 100^\circ\text{C}$  applied at the inner surface and  $0^\circ\text{C}$  at the outer surface, giving a linear temperature gradient through the wall thickness. The temperature distribution calculated by this heat transfer analysis was then applied to the model, which gives rise to thermal stresses in the bend. The free end of the pipe was constrained via equations to expand in-plane along its length, simulating the thermal expansion of a long pipe. The temperature gradient was cycled from zero to a maximum and back to zero over the time step.

Analysis of 9 geometries is presented with  $R/r = 2, 3$  and  $5$ , each of which with  $r/t = 5, 10$  and  $20$ , which gives  $0.1 \leq h \leq 1$ . In each case the attached straight sections were a length such that  $L/R = 8$ , which was found to be more than adequate to always provide the maximum reinforcement possible to the bend. In each case a Young's Modulus of  $200\text{GPa}$  and a Poisson's ratio of  $0.3$  was used. The steel is assumed to have a thermal expansion coefficient of  $1 \times 10^{-5} \text{ }^\circ\text{C}^{-1}$ . The yield stress is assumed to be temperature dependent, with data for this taken from PD5500 British Standard for unfired welded pressure vessel design [104], as shown in Table 3.4.

**Table 3.4 - Temperature Dependent Yield Stress**

Temperature (°C)	0	50	100	150	200	250	300	350
Yield Stress (MPa)	200	137	126	115	112	100	86	79

### 3.4.4 Internal Pressure and Moment Loading

Figure 3.20 presents the strict shakedown limit and limit load interaction curves for  $R/r = 2$  and  $r/t = 5$  under internal pressure and opening bending. It can be seen that the shakedown boundary follows a classic Bree-like shape whereby the reverse plasticity boundary is a constant value of cyclic bending. The limit load surface calculated by the LMM is shown and this has been verified at 5 points using ABAQUS elastic-plastic incremental analysis (using the Rik's method). The difference between the LMM and ABAQUS limit solutions is less than 1%, providing confidence that the LMM produces accurate results for these linear geometry analyses.

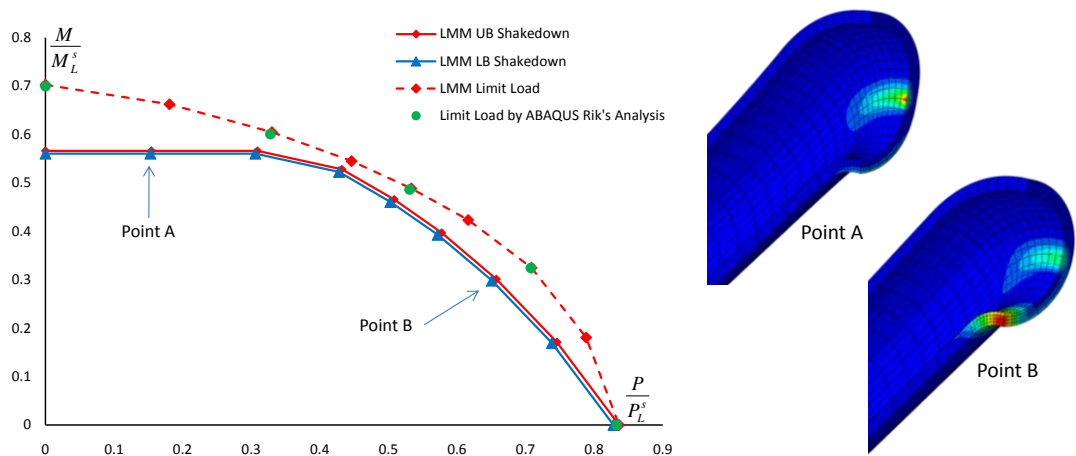


**Figure 3.20 -  $R/r=2$ ,  $r/t=5$  Limit load, Shakedown Limit and Location of Failure**

The contours of plastic strain resulting from the cyclic loading at points A and B are also shown in Figure 3.20, which correspond to the reverse plasticity limit and the ratchet limit respectively. These are the locations where ratcheting would occur if the loading was increased just beyond that point in the shakedown limit. The location corresponding to the reverse plasticity limit is restricted to a very small area at the flank of the pipe, with the strains accumulating at the inner surface. The location corresponding to the ratchet limit occurs globally at the intrados of the bend, with the strains initiating at the outer surface. This ratcheting location matches that found by Chen et al [101], giving further confidence in

the accuracy of the method. The reverse plasticity mechanism occurs mainly due to the location of the peak stress caused by the bending moment. The ratcheting mechanism occurs at the location of peak pressure stress, at the intrados of the bend.

Figure 3.21a shows a comparison between the linear geometry results obtained by C.S. Oh et al and the results obtained here for  $R/r=2$ ,  $r/t=10$  subject to internal pressure and cyclic opening bending. The data is normalised against equation (3.31) and the Goodall limit pressure using the von-Mises criterion (equation (3.32) multiplied by  $2/\sqrt{3}$ ). The method employed by C. S. Oh et al is a lower bound method and both the lower and upper bounds calculated by the LMM are shown in the Figure. Comparison of the two strict shakedown curves reveals that they produce comparable reverse plasticity boundaries but that the LMM predicts a significantly larger ratcheting boundary.

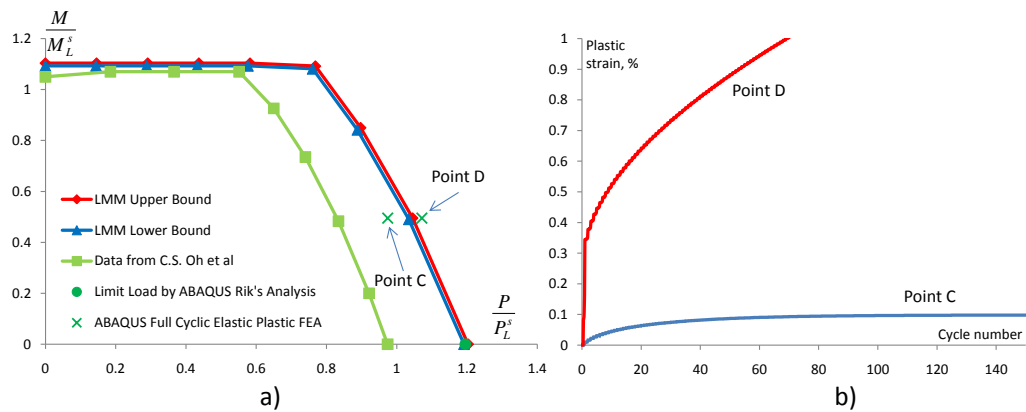


**Figure 3.21 - Comparison of the LMM with the Results in [66]**

In order to verify the accuracy of the LMM, the limit load for pressure loading was calculated using ABAQUS Rik's analysis and two points were chosen (labelled Point C and Point D in Figure 3.21a) for full cyclic analysis in ABAQUS. The limit pressure given by the Rik's analysis correlates well with the equivalent value calculated by the LMM, with a difference of less than 1% between the two solutions. The plastic strain histories for the cyclic loading at points C and D are shown in Figure 3.21b. These strains were taken from the position of maximum plastic strain, which was at the inner surface at the intrados of the bend. The plastic strain history of Point C shows that strict shakedown is achieved after approximately 100 cycles. Point D shows classic ratcheting behaviour, with the plastic strain increasing every cycle.

### 3.4.4.1 Effect of the Ratio $r/t$

Figure 3.22 shows the shakedown limit and limit load surfaces for fixed  $R/r$  values of 2, 3 and 5, and varying  $r/t$  values for an opening bending moment. The general trend for each geometry considered is similar. As  $r/t$  decreases (i.e. the pipe becomes thicker), the limit load surfaces expand, indicating larger loads to failure. Large increases in the limit moment are seen with decreasing  $r/t$  but comparatively little effect is observed in the normalised limit pressure. The graphs also reveal that the alternating plasticity boundary occurs at higher values of normalised moment with decreasing  $r/t$ .

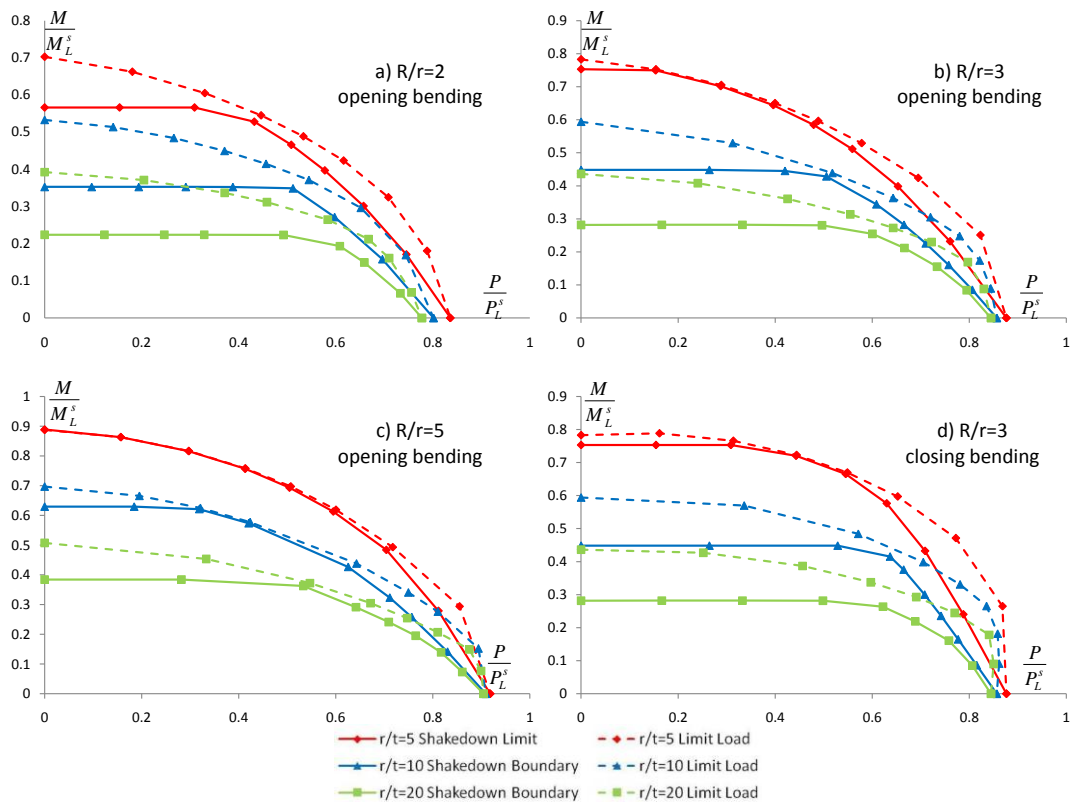


**Figure 3.22 - Effect of  $r/t$  on the Limit and Shakedown Boundaries**

One interesting observation is the margin between the limit load and the shakedown limit surfaces. In general, there is a significant margin between both lines at low pressures, which reduces to a minimum at around the point where alternating plasticity changes to ratcheting. At pressures larger than this the margin increases once more before converging to the limit load for pressure loading. As  $r/t$  becomes smaller, the margin between the two lines becomes smaller to the extent that there is almost no margin between the shakedown and limit loads for a large normalised pressure range for  $R/r = 3$ ,  $r/t = 5$  and  $R/r = 5$  and  $r/t = 5$ .

The same study was conducted for  $R/r = 3$  under closing bending, shown in Figure 3.22d. The trends observed for opening bending are also observed for closing bending.

### 3.4.4.2 Effect of the Ratio $R/r$

Figure 3.23 presents the same results as in Figure 3.22 for pipe bends subject to internal pressure and opening bending but in each graph  $r/t$  is fixed and the effects of changing  $R/r$  are observed. Each geometry exhibits similar trends. The limit load curve expands with increasing  $R/r$ , and shows an increase in both the limit moment and limit pressure towards a normalised value of 1. This correlates with the expected behaviour that as  $R/r \rightarrow \infty$  the behaviour of the bend will tend towards that of a straight pipe. In terms of the shakedown limit, increasing  $R/r$  increases the normalised moment with which alternating plasticity occurs. It is also observed that the margin between the limit load and shakedown limit curves reduces with increasing  $R/r$  in all cases.

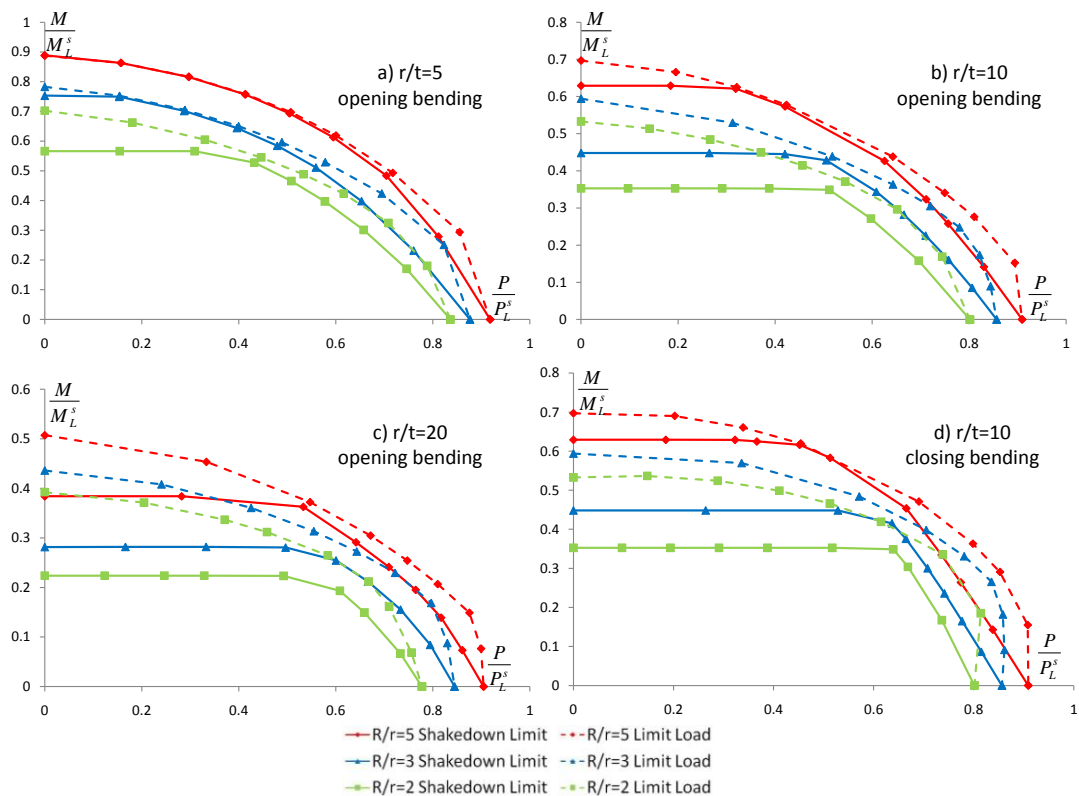


Figure 3.23 - Effect of  $R/r$  on the Shakedown Boundaries

The same study was undertaken with the closing bending case, using a fixed value of  $r/t = 10$ . Figure 3.23d shows that the same effects and trends are observed as per the opening bending cases.

### 3.4.4.3 Comparison of Opening, Closing and Reversed Bending

Figure 3.24 shows a comparison between closing, opening and reversed bending for  $r/t = 10$  and  $R/r = 2, 3$  and  $5$ . The bending moment range,  $\Delta M$ , is plotted rather than the peak value of moment,  $M$ , used in previous figures. In each case the limit load surface for closing bending is larger than that for opening bending but gives the same limit load for bending and pressure loading alone. Limit analysis of reversed bending is not possible due to the conflicting directions of opening and closing bending.

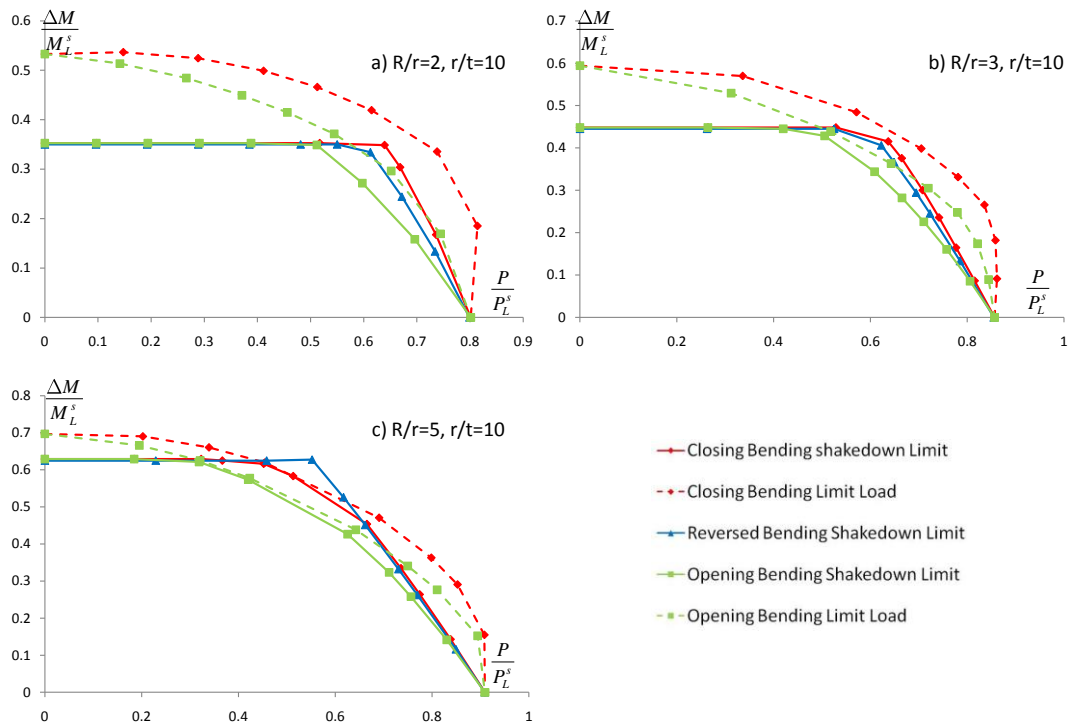


Figure 3.24 - Comparison of Opening, Closing and Reversed Bending

The strict shakedown limit curves show that the normalised moment at which reverse plasticity occurs does not change for any mode of bending. Closing bending has an increased ratcheting boundary over opening bending. The difference between the opening and closing bending ratcheting boundaries reduces with increasing  $R/r$ . The ratcheting boundary of reversed bending rests between that of opening and closing bending apart from the case of  $R/r=5$ , where reverse bending lies outside closing bending at the transition region between reverse plasticity and ratcheting.

Examination of the contour plots reveals that the location of the alternating plasticity mechanism does not change for opening, closing or reversed bending, and thus it is the

range of the bending stress which determines the alternating plasticity boundary rather than if it is tensile or compressive.

The case of the reversed bending strict shakedown limit being greater than closing bending for  $R/r=5$  (Figure 3.24c) can be explained since both the cyclic opening bending (Figure 3.19b) and closing bending (Figure 3.19c) are equivalent to the reverse bending (Figure 3.19d) superimposed on a constant mean bending moment. This mean moment causes a tensile stress at the intrados for opening bending and a compressive stress for closing bending. In the majority of the analyses performed in this paper, the addition of the stresses from the internal pressure and mean moment at the intrados is always tensile along the axis of the pipe, which results in the ratcheting mechanism beginning at the outer surface of the intrados. In the case of  $R/r=5$  for closing bending at high values of bending moment, the compressive stress from the mean moment is large enough to cause the sum of these stresses in the region to be compressive. This change to the stress causes the ratcheting mechanism to originate from the inner surface of the intrados. It is this change in ratcheting mechanism which reduces the shakedown envelope of closing bending below that of reversed bending for pressure values of  $0.45 < \left( \frac{P}{P_L^s} \right) < 0.66$ .

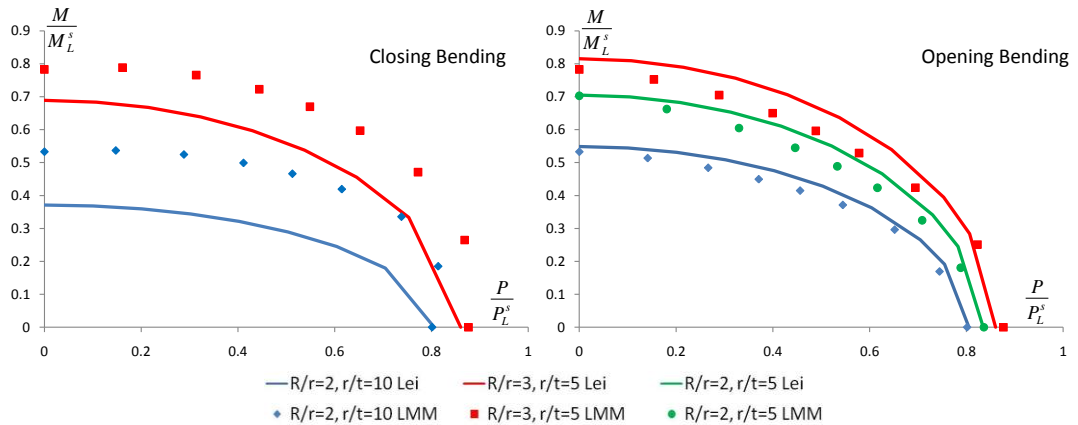


**Figure 3.25 - Comparison of LMM Results with the Equations of Lei [100]**

Figure 3.25 shows a comparison between some of the limit load surfaces calculated by the LMM and those given by the equations of Lei in Appendix A for combined pressure and moment loading (equation (A1.5)). It can be seen that the LMM results are generally conservative for opening bending. However the LMM results for closing bending are non-conservative compared to this equation. This highlights the need for the LMM to include a

nonlinear geometry option in the procedure so that cases such as this, where linear geometry is non-conservative, can be assessed accurately.

### 3.4.5 Internal Pressure and Thermal Loading

The applied temperature gradient through the wall ( $T_o=100^\circ\text{C}$  at the inner surface,  $0^\circ\text{C}$  at the outer surface) combined with the constraint that the free end expands in-plane creates an elastic stress which is linear through the thickness of the straight sections of pipe. The results presented here show the effects of  $R/r$  and  $r/t$  on the shakedown limit interaction curves. The internal pressures are normalised against equation (3.33) with a yield stress of 200MPa and the cyclic thermal loading,  $T$ , is normalised against the applied initial inner surface temperature  $T_o = 100^\circ\text{C}$ .

#### 3.4.5.1 Temperature Dependent Yield Stress

Figure 3.26 gives the shakedown boundaries for  $R/r=3$  and  $r/t=10$ , showing the difference between temperature dependent yield (given in Table 3.4) and temperature independent yield (value of 200MPa used). It is clear that where temperature dependency is strong, or where large temperatures are involved, it is important to consider this in the analysis. A significant reduction in the entire shakedown boundary is observed and the remainder of the results presented here therefore take temperature dependent yield stress into consideration.

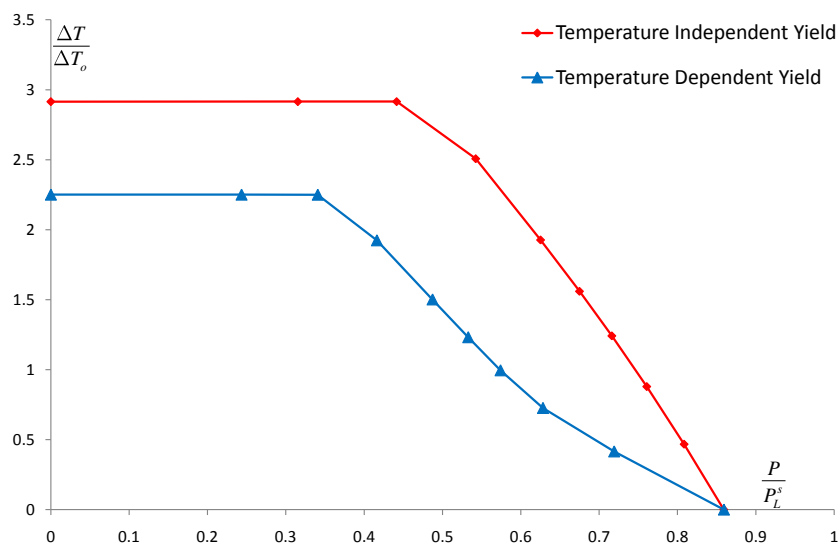


Figure 3.26 - Effect of Temperature Dependent Yield on the Strict Shakedown Limit for  $R/r=3$   $r/t=10$

### 3.4.5.2 Effect of R/r

Figure 3.27 gives a comparison of the shakedown boundaries with changing R/r and fixed r/t=10. Also included is the shakedown boundary for a straight pipe under the same loading. It can be seen that the shape of the shakedown envelopes for the pipe bend is very similar to that of the straight pipe. As R/r of the bend increases, the shakedown envelope tends towards that of the straight pipe. This is because as the radius of the bend becomes larger with respect to the pipe radius, the effect of the bend decreases, resulting in a lower stress concentration. When  $R/r \rightarrow \infty$  (i.e. a straight pipe) the concentration is zero. Overall, for the range of bends considered here, the reductions are relatively small when compared to a straight pipe. The most severe bend considered here,  $R/r = 2$ , has a reverse plasticity limit which is more than 90% that of the straight pipe and a ratcheting boundary which is at least 80% of the straight pipe.

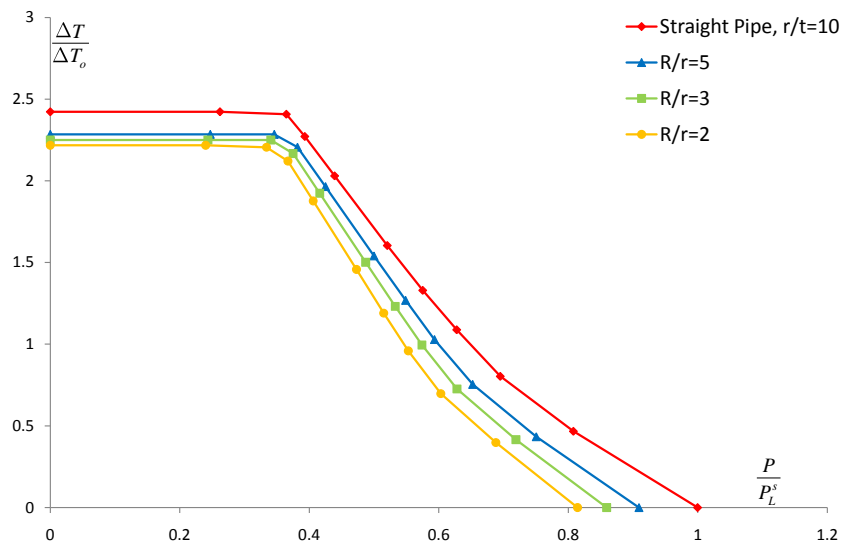


Figure 3.27 - Effect of R/r on Thermal Loading Strict Shakedown

### 3.4.5.3 Effect of r/t

Figure 3.28 shows the shakedown boundaries for fixed R/r = 3 and varying values of r/t = 5, 10 and 20, and also that of a straight pipe with r/t=10. This shows that only very marginal changes occur to the shakedown envelope over the thickness range considered. This is primarily because the magnitude of thermal stress created is relatively independent of thickness, with only thick pipes showing an increase in thermal stress (which causes the very slightly reduced reverse plasticity boundary for r/t=5 in Figure 3.28). Overall, the pipe

thickness has little effect on the normalised shakedown limit interaction diagram (clearly the absolute values will be affected).

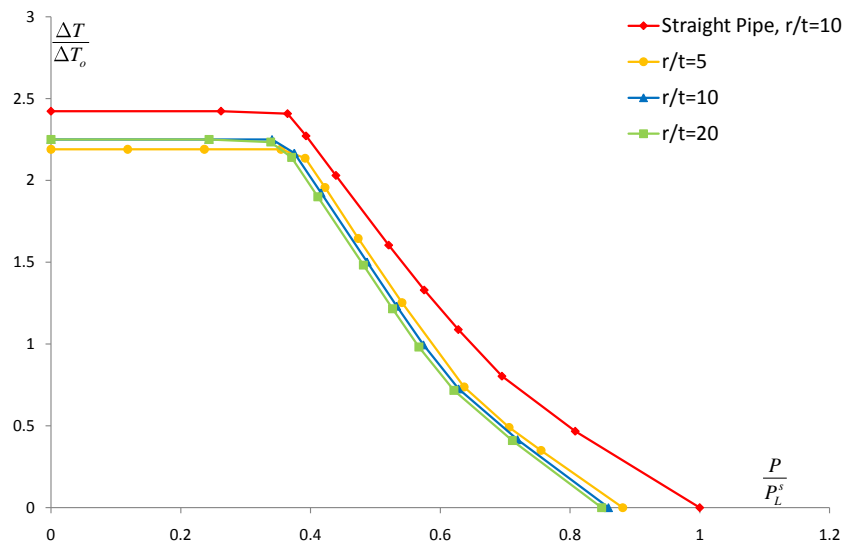


Figure 3.28 - Effect of  $r/t$  on Thermal Loading Strict Shakedown

### 3.4.6 Pipe Bend Conclusions

Pipe bends are known to ovalise during bending which leads to geometric strengthening and weakening to further bending moment application. However there is some merit in solutions generated by linear geometry calculations, including the reverse plasticity limit and limit pressure load. Furthermore, calculations using linear geometry are a useful baseline for when the modified bounding theorems for nonlinear geometry are implemented.

The LMM strict shakedown procedure has been applied to a parametric study of pipe bends as a demonstration of the investigations possible with this method. The linear geometry results have been validated against elastic-plastic FEA for both the limit loads and the shakedown limits. The effects of the ratios  $r/t$  and  $R/r$  have been considered to establish the effects of changing these ratios on the shakedown behaviour. Decreasing  $r/t$  causes an increase in the reverse plasticity limit and also reduces the margin between strict shakedown and limit load curves. Increasing  $R/r$  results in an increased reverse plasticity limit and also decreases the margin between strict shakedown and limit load curves. In these linear geometry results no difference in these trends was observed for opening or closing bending. The limit loads predicted by the LMM agree well with those from Abaqus Rik's analysis. These results compared to the empirically derived limit load solutions of Lei

[100] are conservative for opening bending, but are non-conservative for closing bending. This highlights the need for a nonlinear geometry theorem implementation in the LMM framework for situations when linear geometry calculations may be non-conservative.

Where thermal loading is involved, the effects of temperature dependent yield stress are important and should be included in the shakedown analysis. The effects of the thermal loading considered here reduced the strict shakedown boundary compared to that of a straight pipe, but the most severe bend considered here ( $R/r= 2$ ) still retained at least 80% of the strict shakedown strength of the equivalent straight pipe.

### **3.5 Summary and Discussion**

The LMM strict shakedown procedure has been established for a number of years and is a useful tool for calculation of the strict shakedown limit. The derivation and numerical implementation presented here from the work of Ponter shows how the plastic response of a material can be replicated by a series of linear solutions which satisfy the important conditions of the plasticity.

Validations of this method have been presented for a variety of situations. Comparison of the LMM against theoretical solutions of notched bars verifies the implementation of the method over the required dimensionalities. The solutions produced by the LMM agree well with the solutions of Miller and with Abaqus limit analysis. The Bree cylinder is used as a theoretical validation of the strict shakedown boundary, where lower and upper bound LMM solutions agree well with the limits derived by Bree and Bradford. These validations against theoretical solutions are taken forward by then comparing LMM solutions with experimental data. The limit loads of pipe intersections and shakedown pressures of nozzles in spherical shells calculated by the LMM compare favourably with the experimental results.

Finally the LMM has been applied to investigate the shakedown limits of pipe bends subject to internal pressure and either cyclic bending or cyclic thermal loading. This case study demonstrates the kind of investigations that are possible with the LMM due to the explicitly defined shakedown limits. The effect of changing geometry on the shakedown limits is presented in terms of the ratios  $r/t$  and  $R/r$ . This case study does, however, highlight that a nonlinear geometry option would be beneficial, and the implementation of such a theorem into the LMM framework could form the basis of future work with this method.

## **4 The LMM Global Shakedown Analysis Procedure**

### **4.1 Introduction**

The strict shakedown limit gives the margin to either reverse plasticity or ratchet and is a useful quantity to be able to calculate accurately. Strict shakedown is a desirable state for a component to be in, and the majority of components within EDF's nuclear fleet are within this limit. In high temperature operation, however, the yield stress of materials can reduce significantly which can lead to situations where the cyclic loading is outside of the strict shakedown limit.

The R5 procedure allows the component to operate in a global shakedown state, where some regions of the component exhibit a reverse plasticity response. In addition to the strict shakedown limit, it is therefore useful to be able to calculate the global shakedown limit, that is the boundary between reverse plasticity and ratcheting responses.

Ponter and Chen have derived such a method as part of the LMM framework [82][83]. Chen and Ponter then extended this method to include multiple load extremes in the cycle [29]. This method is an upper bound method and, as previously stated, it is desirable to have a complementary lower bound calculation to add conservatism for regular use by EDF engineers.

The purpose of this chapter is to describe the creation of a lower bound to the method of Ponter and Chen with a view to fulfilling objective 1 in section 1.6. Initially the upper bound method will be explained, followed by a theoretical derivation of the lower bound calculation. The implementation into the numerical procedure will then be described, and finally a description of the convergence improvements will be given.

### **4.2 LMM Upper Bound Global Shakedown Analysis**

#### **4.2.1 The General Cyclic State**

Similarly to the general cyclic state considered in section 3.2.1, we consider a body of volume,  $V$ , and surface,  $S$ , which is subject to a cyclic history of loading with a cycle time  $0 \leq t \leq \Delta t$ . The load history consists of mechanical loading which acts on part of the surface,  $S_T$ , and a temperature history which varies within the entire volume. The remaining surface,  $S_U$ , is constrained to have zero displacement rate (i.e.  $\dot{u} = 0$ ).

The load cycle can be expressed as the summation of steady state and time-varying components:

$$F(x,t) = \lambda \bar{F}(x) + P(x,t) + \theta(x,t) \quad (4.1)$$

Where  $P(x,t)$  and  $\theta(x,t)$  are the cyclic histories of mechanical load and temperature with cycle time  $\Delta t$ ,  $\bar{F}$  is a constant load independent of time and  $\lambda$  is a positive scalar load parameter. The linear elastic stress history associated with this load history is

$$\hat{\sigma}_{ij}(x,t) = \lambda \hat{\sigma}_{ij}^F(x,t) + \hat{\sigma}_{ij}^\Delta(x,t) \quad \text{where} \quad \hat{\sigma}_{ij}^\Delta = \hat{\sigma}_{ij}^P + \hat{\sigma}_{ij}^\theta \quad (4.2)$$

This cyclic problem will asymptotically approach a steady cyclic state where

$$\sigma_{ij}(t) = \sigma_{ij}(t + \Delta t) \quad \text{and} \quad \dot{\epsilon}_{ij}(t) = \dot{\epsilon}_{ij}(t + \Delta t) \quad (4.3)$$

This steady state cyclic solution,  $\sigma_{ij}(x,t)$ , can be expressed in terms of four components: the constant and cyclic applied elastic stresses,  $\lambda \hat{\sigma}_{ij}^F(x,t) + \hat{\sigma}_{ij}^\Delta(x,t)$ , the constant residual stress,  $\bar{\rho}_{ij}^r(x)$ , and the varying residual stress,  $\rho_{ij}^r(x,t)$  to give

$$\sigma_{ij}(x,t) = \lambda \hat{\sigma}_{ij}^F(x,t) + \hat{\sigma}_{ij}^\Delta(x,t) + \bar{\rho}_{ij}^r(x) + \rho_{ij}^r(x,t) \quad (4.4)$$

The constant residual stress,  $\bar{\rho}_{ij}^r(x)$ , is time independent and self equilibrating. The varying residual stress,  $\rho_{ij}^r(x,t)$ , represents the changes to the varying residual stress during the cycle due to the cyclic plasticity. If the component is not ratcheting then this varying residual stress must be identical in consecutive cycles and also satisfy

$$\rho_{ij}^r(x,0) = \rho_{ij}^r(x,\Delta t) = \bar{\rho}_{ij}^r(x) \quad (4.5)$$

Where  $\bar{\rho}_{ij}^r(x)$  is the constant component of  $\rho_{ij}^r$ . The material in question has a convex yield condition

$$f(\sigma_{ij}) \leq 0 \quad (4.6)$$

and the associated flow rule

$$\dot{\varepsilon}_{ij}^P = \dot{\alpha} \frac{df(\sigma_{ij})}{d\sigma_{ij}} \quad (4.7)$$

Then the maximum work principle also applies:

$$(\sigma_{ij}^c - \sigma_{ij}^*) \dot{\varepsilon}_{ij}^c \geq 0 \quad (4.8)$$

Where  $\sigma_{ij}^c$  denotes the stress at yield  $f(\sigma_{ij}^c) = 0$  and  $\sigma_{ij}^*$  represents any state of stress which satisfies the yield condition of (4.6).

#### 4.2.2 Upper Bound Theorem for Loading in Excess of Strict Shakedown

The shakedown bounding theorems of Melan and Koiter give a very rigorous set of criteria for the calculation of the shakedown limit. These criteria, however, are only applicable to strict shakedown. Therefore in order to obtain a limit on the global shakedown behaviour of a component, where the loading lies outside of the strict shakedown limit, further mathematical derivation was required. Ponter and Chen [82] provided one such derivation to create an upper bound theorem, which is summarised here.

Consider a class of strain rate histories,  $\dot{\varepsilon}_{ij}^c$ , which accumulate a strain field,  $\Delta\varepsilon_{ij}^c$ , over the cycle which is compatible with the displacement field  $\Delta u_i^c$ :

$$\Delta\varepsilon_{ij}^c = \int_0^{\Delta t} \dot{\varepsilon}_{ij}^c dt \quad (4.9)$$

Consider the upper bound strict shakedown theorem, but written in the following form

$$\int_V \int_0^{\Delta t} (\sigma_{ij}^c - \lambda^{UB} \hat{\sigma}_{ij}(x,t)) \dot{\varepsilon}_{ij}^c dt dV = 0 \quad (4.10)$$

Where  $\lambda_{UB}$  is greater than  $\lambda_s$ , which is the load multiplier at the strict shakedown limit. From this the functional,  $I(\dot{\varepsilon}_{ij}^c, \lambda)$ , is defined:

$$I(\dot{\varepsilon}_{ij}^c, \lambda) = \int_V \int_0^{\Delta t} (\sigma_{ij}^c - \lambda \hat{\sigma}_{ij}(x,t)) \dot{\varepsilon}_{ij}^c dt dV \quad (4.11)$$

Then it can be said that the load history is an upper bound to the strict shakedown limit if  $I(\dot{\epsilon}_{ij}^c, \lambda) \geq 0$ , and will equal the shakedown limit if  $I(\dot{\epsilon}_{ij}^c, \lambda_s) = 0$ .

In their derivation, Ponter and Chen expand this functional and place additional criteria on the stress fields, which allows the theorem to be extended beyond strict shakedown. These conditions are:

1) A cyclic history of residual stress,  $\rho_{ij}^r(x, t)$ , is defined corresponding to  $\dot{\epsilon}_{ij}^c$  such that

$$\dot{\epsilon}_{ij}^{cT} = C_{ijkl} \rho_{ij}^r + \dot{\epsilon}_{ij}^c \quad (4.12)$$

Where  $\dot{\epsilon}_{ij}^{cT}$  is also a kinematically admissible strain rate and  $\rho_{ij}^r(x, t)$  also satisfies condition (4.5) i.e.

$$\rho_{ij}^r(x, 0) = \rho_{ij}^r(x, \Delta t) = \bar{\rho}_{ij}^r(x) \quad (4.13)$$

Where  $\bar{\rho}_{ij}^r(x)$  is the constant component of  $\rho_{ij}^r(x, t)$ .

2) There exists a constant residual stress such that the total stress history

$$\sigma_{ij}^*(x, t) = \lambda \hat{\sigma}_{ij}(x, t) + \bar{\rho}_{ij}(x) + \rho_{ij}^r(x, t) \quad (4.14)$$

Satisfies the yield condition,  $f(\sigma_{ij}^*) \leq 0$ , during the entire cycle  $0 \leq t \leq \Delta t$ . These conditions lead to the functional  $I(\dot{\epsilon}_{ij}^c, \lambda)$  becoming

$$I(\dot{\epsilon}_{ij}^c, \lambda) = \int_V \int_0^{\Delta t} \left\{ \sigma_{ij}^c - (\lambda \hat{\sigma}_{ij}(x, t) + \bar{\rho}_{ij}(x) + \rho_{ij}^r(x, t)) \right\} \dot{\epsilon}_{ij}^c dt dV \quad (4.15)$$

The minimisation of  $I(\dot{\epsilon}_{ij}^c, \lambda)$  produces an upper bound to the global shakedown limit. This result allows the evaluation of loading which produces a stress field of the form of eqn (4.4), i.e. loading which is in excess of the strict shakedown limit. This result reduces to the strict shakedown theorem as the varying residual stress field becomes vanishingly small and

so proves that the upper bound strict shakedown theorem is a special case of a more general result.

### 4.2.3 The Two Stage Global Shakedown Limit Calculation

The functional of equation (4.15) requires the generation of two residual stress fields, one which is constant in time and the other which varies within the load cycle. Each of these residual stresses is associated with part of the applied loading. The varying part of the applied loading,  $\hat{\sigma}_{ij}^{\Delta}(x,t)$ , results in a closed cycle of plastic strains developing. Associated with this plastic strain cycle is the varying residual stress field,  $\rho_{ij}^r(x,t)$ . The steady state loading,  $\hat{\sigma}_{ij}^F$ , causes an additional constant residual stress field,  $\bar{\rho}_{ij}(x)$ , to form.

If it is possible to decompose the applied loading in this manner then the global shakedown limit can be evaluated using a two stage calculation process [82][83] where the functional (4.15) is also generated in two stages. This first stage considers the cyclic component of the applied loading to generate the varying residual stress field and varying plastic strains. By considering only the cyclic loading (4.15) becomes

$$I(\dot{\epsilon}_{ij}^c, \lambda) = \int_V \int_0^{\Delta t} \left\{ \sigma_{ij}^c - \left( \hat{\sigma}_{ij}^{\Delta}(x,t) + \rho_{ij}^r(x,t) \right) \right\} \dot{\epsilon}_{ij}^c dt dV \quad (4.16)$$

The second stage then finds the ratchet limit by adding the steady state portion of the load and calculating the constant residual stress field, which completes the stress fields in (4.15) to make

$$I(\dot{\epsilon}_{ij}^c, \lambda) = \int_V \int_0^{\Delta t} \left\{ \sigma_{ij}^c - \left( \lambda \hat{\sigma}_{ij}^F(x,t) + \hat{\sigma}_{ij}^{\Delta}(x,t) + \bar{\rho}_{ij}(x) + \rho_{ij}^r(x,t) \right) \right\} \dot{\epsilon}_{ij}^c dt dV \quad (4.17)$$

The advantage of decomposing the solution into two stages like this is that once stage 1 is complete, then the second stage is in fact a conventional shakedown analysis as described in chapter 3 where the stress history is augmented by the varying residual stress found in stage 1.

### 4.2.4 Numerical Implementation

The LMM global shakedown method is implemented in Abaqus in a similar way to the strict shakedown procedure, by using the UMAT and URDFIL subroutines. In this numerical

implementation the load history is also divided into a number of discrete vertices  $n=1,2,\dots,N$  with their corresponding time points,  $t_1, t_2,\dots,t_N$ . The loads, therefore, follow a series of straight line paths in load space (and the elastic stresses follow straight line paths in stress space). For a strictly convex yield surface the only instances where plastic strains can develop are at the vertices of the stress history, with the remainder of the load cycle spent within the yield surface. At each of these time points is an increment of plastic strain,  $\Delta\varepsilon_{ij}^n$ , which when summed over the cycle gives the total plastic strain increment

$$\Delta\varepsilon_{ij}^c = \sum_{n=1}^N \Delta\varepsilon_{ij}^n \quad (4.18)$$

#### 4.2.4.1 Stage 1 - Procedure for Establishing the Steady State Cycle

With the load cycle divided into discrete time points the functional  $I(\dot{\varepsilon}_{ij}^c, \lambda)$  of (4.16) can be approximated by the sum of the values of  $I^n$  at each time point in the cycle

$$I(\dot{\varepsilon}_{ij}^c, \lambda) = \sum_{n=1}^N I^n \quad (4.19)$$

Where, from (4.16)

$$I^n(\Delta\varepsilon_{ij}^n, \lambda) = \int_V \left\{ \sigma_{ij}^n - \left[ \hat{\sigma}_{ij}^{\Delta^n}(x) + \rho_{ij}^{r^n}(x) \right] \right\} \Delta\varepsilon_{ij}^n dV \quad (4.20)$$

And

$$\rho_{ij}^{r^n}(x_i) = \bar{\rho}_{ij}^r(x) + \sum_{n=1}^N \Delta\rho_{ij}^{r^n}(x) \quad (4.21)$$

$$\Delta\varepsilon_{ij}^{T^n} = C_{ijkl} \Delta\rho_{ij}^{r^n}(x) + \Delta\varepsilon_{ij}^n \quad (4.22)$$

Where the total strain increment  $\Delta\varepsilon_{ij}^{T^n}$  is compatible and the changing residual stress  $\Delta\rho_{ij}^{r^n}(x)$  satisfies equilibrium.

The iterative methodology adopted assumes a total number of load cycles, M, where each cycle  $m = 1, 2, \dots, M$ . Each load cycle contains a series of increments, N, which are associated with N time points in the load cycle so that each increment  $n=1, 2, \dots, N$ . The LMM methodology for the minimisation of  $I(\dot{\varepsilon}_{ij}^c, \lambda)$  in (4.19) uses the solution of a series of linear problems. The following procedure is outlined for an arbitrary point in the structure, x and at a single time point in the cycle, n. Assuming that an initial estimate of the strain increment,  $\Delta \varepsilon_{ijm}^n$ , for load cycle m at time point n is given, then the following procedure can be used to define the strain increment in the subsequent cycle m+1,  $\Delta \varepsilon_{ijm+1}^n$ . Similarly, an initial value of the varying residual stress for cycle m at time point  $t_n$ ,  $\rho_{ijm}^{r^n}$ , calculated in the previous increment is assumed to be known. The process then begins by calculating an updated linear coefficient,  $\mu_{m+1}^n$ , by linear matching

$$\mu_{m+1}^n = \mu_m^n \frac{\sigma_y}{\bar{\sigma}(\hat{\sigma}_{ij}^{\Delta^n} + \rho_{ijm}^{r^n})} \quad (4.23)$$

Where  $\mu_m^n$  is the iterative shear modulus and  $\sigma_y$  is the yield stress of the material. The new value of the strain increment  $\Delta \varepsilon_{ijm+1}^n$  is obtained through the solution to the following problem

$$\Delta \varepsilon_{ijm+1}^{T^n}{}' = \frac{1}{2\mu_1^n} \Delta \rho_{ijm+1}^{r^n}{}' + \Delta \varepsilon_{ijm+1}^n{}' \quad (4.24)$$

$$\Delta \varepsilon_{kkm+1}^{T^n} = \frac{1}{3K^n} \Delta \rho_{kkm+1}^{r^n} \quad (4.25)$$

$$\Delta \varepsilon_{ijm+1}^n{}' = \frac{1}{2\mu_{m+1}^n} \left\{ \hat{\sigma}_{ij}^{\Delta^n} + \rho_{ijm}^{r^{n-1}} + \Delta \rho_{ijm}^{r^n} \right\}' \quad (4.26)$$

Where  $K^n$  is the bulk modulus, which is obtained from material properties and  $\mu_1$  is the original shear modulus in cycle  $m=1$ . The history of residual stress,  $\rho_{ijm}^{r^{n-1}}$ , up to that time point is found by the cumulative sum of all previous increments of the varying residual stress during the cycle m:

$$\rho_{ij_m}^{r^{n-1}} = \bar{\rho}_{ij_m}^r + \Delta\rho_{ij_m}^{r^1} + \Delta\rho_{ij_m}^{r^2} + \dots + \Delta\rho_{ij_m}^{r^{n-1}} \quad (4.27)$$

A more detailed explanation of the entire procedure used to obtain the varying residual stress is given in Appendix B. Using equation (4.26) allows (4.24) to be written as

$$\Delta\varepsilon_{ij_{m+1}}^{T^n} = \left( \frac{1}{2\mu_1^n} + \frac{1}{2\mu_{m+1}^n} \right) \Delta\rho_{ij_{m+1}}^{r^n} + \frac{1}{2\mu_{m+1}^n} \left\{ \hat{\sigma}_{ij}^{\Delta^n} + \rho_{ij_m}^{r^{n-1}} \right\} \quad (4.28)$$

We define  $\bar{\mu}$  and  $\bar{K}$  as:

$$\frac{1}{\bar{\mu}} = \frac{1}{\mu_1^n} + \frac{1}{\mu_{m+1}^n} \quad \text{and} \quad \frac{1}{\bar{K}} = \frac{1}{K^n} \quad (4.29)$$

Which allows (4.25) and (4.28) to be simplified to

$$\Delta\rho_{ij_{m+1}}^{r^n} = 2\bar{\mu} \Delta\varepsilon_{ij_{m+1}}^{T^n} - \frac{\bar{\mu}}{\mu_{m+1}^n} \left\{ \hat{\sigma}_{ij}^{\Delta^n} + \rho_{ij_m}^{r^{n-1}} \right\} \quad (4.30)$$

$$\Delta\rho_{kk_{m+1}}^{r^n} = 3\bar{K} \Delta\varepsilon_{kk_{m+1}}^{T^n} \quad (4.31)$$

The solution of these equations can be solved in the UMAT and URDFIL subroutines. The problem is analogous to the standard Abaqus equation of the form

$$\Delta\rho_{m+1}^n = [J]_{m+1}^n \Delta\varepsilon_{m+1}^{T^n} - \Delta\sigma_{m+1}^{in^n} \quad (4.32)$$

Where the Jacobian for a 3D solid is given by

$$[J]_{m+1}^n = \frac{E(1-\nu)}{(1+\nu)(1-2\nu)} \begin{bmatrix} 1 & \frac{\nu}{1-\nu} & \frac{\nu}{1-\nu} & 0 & 0 & 0 \\ \frac{\nu}{1-\nu} & 1 & \frac{\nu}{1-\nu} & 0 & 0 & 0 \\ \frac{\nu}{1-\nu} & \frac{\nu}{1-\nu} & 1 & 0 & 0 & 0 \\ 0 & 0 & 0 & \frac{1-2\nu}{2(1-\nu)} & 0 & 0 \\ 0 & 0 & 0 & 0 & \frac{1-2\nu}{2(1-\nu)} & 0 \\ 0 & 0 & 0 & 0 & 0 & \frac{1-2\nu}{2(1-\nu)} \end{bmatrix} \quad (4.33)$$

And

$$\Delta\sigma_{m+1}^{in^n} = \frac{\bar{\mu}}{\mu_{m+1}^n} \left\{ \hat{\sigma}_{ij}^{\Delta^n} + \rho_{ijm}^{r^{n-1}} \right\}' \quad (4.34)$$

$$E = \frac{9\bar{K}\bar{\mu}}{3\bar{K} + \bar{\mu}} \quad \text{and} \quad \nu = \frac{3\bar{K} - 2\bar{\mu}}{2(3\bar{K} + \bar{\mu})} \quad (4.35)$$

Equations (4.23) to (4.35) have been implemented in Abaqus using a UMAT subroutine. The analysis is divided so that each increment of the Abaqus analysis solves one time point,  $n$ , in the load cycle so that each increment generates the strain increment and the change in residual stress associated with that time point. The history of residual stress is generated using the numerical procedure outlined in Appendix B. Therefore each  $N$  increments completes one cycle of loading. The completion of each load cycle generates increasingly accurate values of stress increment and changing residual stress, which reduces the value of the functional of equations (4.19) and (4.20). Continued iteration for  $M$  load cycles minimises this functional, hence producing a converged cyclic stress and strain state for the applied cyclic loading.

#### 4.2.4.2 Stage 2 - Calculation of the Global Shakedown Limit

When the above procedure converges then the varying residual stress field will be known along with the associated plastic strain range. As a result the first functional, equation (4.16) can be minimised. This leads onto the second stage in the procedure, which calculates the constant residual stress field,  $\bar{\rho}_{ij}$  associated with the addition of a constant load  $\hat{\sigma}_{ij}^F$ . The purpose of this second stage is to calculate the maximum level of additional constant loading which will not cause ratcheting, i.e. to find the global shakedown limit.

This stage of the calculation process can be performed using the existing strict shakedown method outlined in chapter 3 where the linear elastic solution is augmented by the varying residual stress. Therefore the stress field of equation (3.3) is modified and the input stress field to the strict shakedown method is now

$$\hat{\sigma}_{ij}(x,t) = \lambda \hat{\sigma}_{ij}^F(x) + \hat{\sigma}_{ij}^{\Delta}(x,t) + \rho_{ij}^r(x,t) \quad (4.36)$$

Where  $\lambda$  is a scalar multiplier to only the steady state loading. The iterative procedure given in equations (3.16) to (3.23) is used to determine the maximum level of this constant constant loading,  $\hat{\sigma}_{ij}^F(x_i)$ , and its associated constant residual stress field which will not cause ratcheting to occur. Only two changes are required to the procedure in section 3, namely to equations (3.19) and (3.23). Firstly equation (3.19) is updated to reflect the applied stress field of (4.36):

$$\sigma_{ij_{k+1}}^{in} = \bar{\mu}_{k+1} \left[ \sum_{n=1}^N \frac{1}{\mu_{k+1}^n} \lambda_k^{UB} \left( \hat{\sigma}_{ij}^F + \hat{\sigma}_{ij}^{\Delta^n} + \rho_{ij}^{r^n} \right) \right] \quad (4.37)$$

Where the upper bound load multiplier,  $\lambda_k^{UB}$ , is applied only to the steady state component of the loading. The magnitudes of the cyclic applied stress and varying residual stress,  $\hat{\sigma}_{ij}^{\Delta}$  and  $\rho_{ij}^r$  respectively, are assumed to be fixed during this calculation procedure. Secondly the upper bound multiplier of (3.23) is updated to reflect the fact that this cyclic loading is fixed in magnitude, which gives the following upper bound multiplier [29]

$$\lambda_{k+1}^{UB} = \frac{\int_V \sum_{n=1}^N \sigma_y \bar{\varepsilon}(\Delta \varepsilon_{ij}^n) dV - \int_V \sum_{n=1}^N \left[ \hat{\sigma}_{ij}^{\Delta^n} + \rho_{ij}^{r^n} \right] \Delta \varepsilon_{ij}^n dV}{\int_V \lambda_k^{UB} \hat{\sigma}_{ij}^F \left( \sum_{n=1}^N \Delta \varepsilon_{ij}^n \right) dV} \quad (4.38)$$

With these modifications in place the method of section 3 is able to monotonically converge towards the least upper bound load multiplier. This gives the maximum level of steady state loading which can be applied before ratcheting begins. The method outlined here has proven to be a robust and reliable global shakedown method which can be readily applied to industrially relevant components as discussed in section 2.6.3.

### 4.3 Lower Bounds to Global Shakedown

Melan's theorem has allowed lower bounds to the strict shakedown limit to be assessed for a number of years. The criteria of a self equilibrating residual stress and the non-violation of the yield function provide definitive shakedown/non-shakedown conditions which can be used to determine the strict shakedown status of the component in question.

The LMM strict and global shakedown procedures were originally derived as upper bound procedures. Recently the lower bounds were added, via Melan's theorem, to the strict shakedown procedure as a complementary calculation [28], which now means that the strict shakedown procedure calculates lower and upper bound load multipliers simultaneously. This addition of a lower bound has several advantages. Firstly, with conservatism being a key issue, the nuclear industry clearly favours lower bounds to the shakedown limit and so the LMM strict shakedown procedure therefore became a viable tool for use within EDF. The second advantage of a simultaneous calculation is the ability to compare the two solutions and judge convergence. Both lower and upper bounds should converge towards the exact shakedown limit, so the relative difference between the two load multipliers gives the user an indication of the current level of convergence and also provides confidence in the solution if this difference is small at the end of the solution. One of the primary objectives of this project is to add an analogous lower bound calculation into the global shakedown method. The benefits of this are similar to those for the strict shakedown procedure, namely the ability to use the method in the nuclear industry and the inherent self verification provided by simultaneous solution.

The remainder of this chapter details the creation, implementation and improvement of such a lower bound calculation. At present no formal lower bound theorem exists for loading in excess of the shakedown limit, and so this process then begins by setting out the theoretical foundation for the lower bound. This will be followed by describing the creation of the LMM global shakedown lower bound calculation. Finally the convergence properties of this lower bound will be investigated and improved upon.

## **4.4 A Lower Bound to the LMM Global Shakedown Procedure**

### **4.4.1 Conditions for a Lower Bound to Global Shakedown**

Melan's theorem, as given in section 2.3, states that a structure will be within strict shakedown if a constant residual stress field can be found such its superposition with the cyclic elastic stresses does not violate the yield condition at any point in the load cycle.

$$f(\hat{\sigma}_{ij}(x,t) + \bar{\rho}_{ij}(x)) \leq 0 \quad (4.39)$$

We begin by considering a component which is subject to an arbitrary cyclic loading history, with its corresponding elastic stress history,  $\hat{\sigma}_{ij}^{\Delta}(x,t)$ . Repeated cycles of this stress

history, if beyond the elastic limit, will cause an associated residual stress,  $\rho_{ij}^r(x,t)$ , to form. If the applied loading is within the strict shakedown limit then the time varying component of this residual stress will equal zero, and the lower bound strict shakedown theorem will apply. If the loading is beyond the strict shakedown limit then plastic strains will develop in every cycle, which in turn will cause the residual stress to include a time varying component. If there is a net increase in the plastic strain with each cycle then the component is ratcheting, however if the component is not ratcheting then some additional characteristics of the plastic strain and residual stress field may be observed. Firstly, the residual stress field will cause all load points in the cycle to satisfy the yield stress:

$$f(\hat{\sigma}_{ij}(x,t) + \rho_{ij}^r(x,t)) \leq 0 \quad (4.40)$$

If ratcheting is not occurring then any plastic strains which develop during the cycle must sum to zero i.e. a reverse plasticity mechanism. In the steady cyclic state this means that plastic strains in consecutive cycles must be identical

$$\varepsilon_{ij}^p(x,t_n^m) = \varepsilon_{ij}^p(x,t_n^{m+1}) \quad (4.41)$$

Where m is the cycle number and n is the time point in the cycle. The residual stress must also conform to the following behaviour:

$$\rho_{ij}^r(x,0) = \rho_{ij}^r(x,\Delta t) = \bar{\rho}_{ij}^r(x) \quad \text{and} \quad \rho_{ij}^r(x,t_n^m) = \rho_{ij}^r(x,t_n^{m+1}) \quad (4.42)$$

Where  $\bar{\rho}_{ij}^r(x)$  is the constant component of this residual stress. Therefore the residual stress will 1)only vary within the cycle time  $\Delta t$ , 2)will equal the constant component  $\bar{\rho}_{ij}^r(x)$  at the beginning and end of the cycle and 3)will be identical at each time point in subsequent cycles. If the stress fields are such that equation (4.40) is satisfied, the residual stress satisfies the conditions of (4.42) and the cyclic plastic strains satisfy (4.41) then the component is in global shakedown for the applied loading  $\hat{\sigma}_{ij}^\Delta(x,t)$ .

The conditions of (4.40), (4.41) and (4.42) are very useful as they provide a set of criteria by which the global shakedown condition can be judged for the given cyclic load history,  $\hat{\sigma}_{ij}^\Delta(x,t)$ . Having found the global shakedown status, the matter then remains of scaling

these loads, or a subset of them, to find the global shakedown limit. In strict shakedown this problem is simplified by only having to find a constant residual stress,  $\bar{\rho}_{ij}(x)$ , which satisfies yield. Therefore the entire load history can be scaled, updating  $\bar{\rho}_{ij}(x)$  as this is done, to find the strict shakedown limit. The theory states that if any  $\bar{\rho}_{ij}(x)$  can be found which satisfies the yield condition then strict shakedown has occurred. When loading is beyond strict shakedown, however, no such bounding theorem exists. Therefore each time the stress history was scaled, the varying residual stress and plastic strains associated with this would need to be re-evaluated and measured against conditions (4.40), (4.41) and (4.42), resulting in a lengthy process akin to the trial and error nature of traditional non-linear FEA.

The work of Polizzotto [105][106], which is based on earlier work by Ponter and Karadeniz [107], provides a neat solution to this issue. First consider that the volume,  $V$ , of the component to be divided into two regions.  $V_p$  is the region where alternating plastic strains occur and  $V_E$  is the remainder of the volume where the strains respond entirely elastically in the steady state. In [105], Polizzotto was able to show that if the two regions were considered separately then global shakedown would still be achieved as long as the volume  $V_E$  remained within strict shakedown without affecting the reverse plasticity of  $V_p$ . That is, additional loading can be applied to  $V$  if the additional stress fields do not affect the reverse plasticity of  $V_p$  and  $V_E$  remains in strict shakedown. This is a powerful idea because it allows the global shakedown limit to be determined directly by means of a modified strict shakedown assessment - if the strict shakedown limit can be found for the volume  $V_E$ , then the global shakedown limit has been found for  $V$ .

Therefore for a structure subject to  $\hat{\sigma}_{ij}^{\Delta}(x,t)$  which results in  $\rho_{ij}^r(x,t)$ , a lower bound to the global shakedown limit can be found for additional loading by satisfying the strict shakedown criteria in the volume which is not in reverse plasticity whilst  $V_p$  remains in reverse plasticity itself.

#### **4.4.2 Lower Bound in the LMM Global Shakedown Procedure**

The conditions described above for a lower bound to the global shakedown limit can be interpreted within the existing LMM structure. The two stage procedure adopted for the

upper bound calculation also lends itself to the inclusion of a lower bound based on the conditions of section 4.4.1.

Stage 1 of the process considers the cyclic component of the loading,  $\hat{\sigma}_{ij}^{\Delta}(x,t)$ , and calculates the steady state cyclic response including the varying residual stress field and the plastic strain range,  $\rho_{ij}^r(x,t)$  and  $\Delta\varepsilon_{ij}^p(x)$  respectively. At this point the lower bound conditions are satisfied if 1) the total cyclic stress history satisfies condition (4.40) over the entire structure for each point in the load cycle and 2) the varying residual stress satisfies conditions (4.41) and (4.42), thereby ensuring no net increase in strain in subsequent cycles. The stage 1 calculation is therefore unaltered by the presence of the lower bound checks because the minimisation of the functional (4.20) already incorporates these criteria, so no further calculations are required as long as convergence is met.

With a converged cyclic state, stage 2 then determines the maximum additional steady state loading,  $\lambda\hat{\sigma}_{ij}^F(x,t)$ , which will not cause ratcheting where  $\lambda$  is a scalar multiplier used during the solution. This additional load also causes an additional constant residual stress field,  $\bar{\rho}_{ij}(x)$ , to form. As described in section 4.2.4.2, each iteration scales the applied constant load using  $\lambda$  and the constant residual stress field associated with this additional load is calculated. This gives the total stress field at any point in the structure as the sum of the applied and residual stress fields:

$$\sigma_{ij}(x,t) = \hat{\sigma}_{ij}^F(x,t) + \hat{\sigma}_{ij}^{\Delta}(x,t) + \bar{\rho}_{ij}(x) + \rho_{ij}^r(x,t) \quad (4.43)$$

The nature of the constant residual stress field and the additional constant load, and the way in which they are calculated in this stage two calculation, satisfies the volume separation condition of Polizzotto. Consider the stress state of the structure after the stage 1 calculations are complete. Some part of the volume is in a reverse plastic state, and the remainder responds elastically. The stage two calculation then proceeds to add an additional constant load and calculate the corresponding constant residual stress. In regions which are already in a state of reverse plasticity, no further stress can be supported unless it is purely hydrostatic. Therefore the constant residual stress field associated with the additional load must be such that the net additional stress is zero or hydrostatic. In this way, a constant residual stress field forms which does not affect the reverse plasticity

status of the volume  $V_p$ , but still maintains strict shakedown within  $V_E$ . This is verified through numerical example in section 4.5.1.

Calculation of the lower bound global shakedown limit can be achieved with each iteration of stage 2 of the upper bound procedure. With each iteration the scaling of  $\hat{\sigma}_{ij}^F(x,t)$  and subsequent calculation of  $\bar{\rho}_{ij}(x)$  produces an updated total stress field. At any given point in the structure and time point in the cycle this stress field can be compared to yield to find the lower bound load multiplier,  $\lambda^{LB}$ :

$$f\left(\lambda^{LB}\hat{\sigma}_{ij}^F(x,t) + \bar{\rho}_{ij}(x) + \hat{\sigma}_{ij}^V(x,t)\right) \leq 0 \quad (4.44)$$

Where  $\hat{\sigma}_{ij}^V(x,t) = \hat{\sigma}_{ij}^\Delta(x,t) + \rho_{ij}^r(x,t)$  can be consolidated into a single entity - their magnitudes at each point in the load cycle has been assessed in stage 1 and remains at these levels for stage 2.  $\lambda^{LB}$  is the only unknown in equation (4.44) and so its value can be found for the point in the structure and time point in question. In the finite element solution this means solving equation (4.44) at every integration point for each point in the load cycle. The algebra involved in the expansion and solution of (4.44) is given in Appendix C, and results in the solution of a quadratic

$$A(\lambda^{LB})^2 + B\lambda^{LB} + C = 0 \quad \text{therefore} \quad \lambda^{LB} = \frac{-B \pm \sqrt{B^2 - 4AC}}{2A} \quad (4.45)$$

Where A, B and C are coefficients containing the eighteen stress components (three stress fields each with six components) and the yield stress. This gives the load multiplier, which if applied to the additional constant load, would make the effective stress at that point and load instance equal to or less than the yield stress. At the end of the increment, with  $\lambda^{LB}$  known for the whole structure at all load points, the minimum of these values is taken as the lower bound for the whole model. This gives the value of additional steady state loading which can be applied to the whole model which satisfies yield everywhere. Continued iteration of the LMM procedure produces improving estimates of the constant residual stress field, which in turn increases the lower bound multiplier.

## 4.5 Numerical Example

The lower bound described above has been implemented into the LMM global shakedown code as described in section 4.4.2, which completes the ability of the LMM to calculate lower and upper bounds to the strict and global shakedown limits. Simple numerical examples are presented here for two purposes. The first is to demonstrate that stage 2 of the global shakedown procedure conforms to the requirements set out by Polizzotto, in that the additional constant residual stress field must be such that the reverse plasticity region is not affected. The second purpose is to demonstrate the convergence properties of the newly derived method.

### 4.5.1 Verification of the Position of the Constant Residual Stress Field

It is assumed that stage 2 of the LMM global shakedown procedure conforms to the requirement that the constant residual stress field forms so that the reverse plasticity is not affected. The basic mechanics arguments put forward in section 4.4.2 would imply that this assumption is correct, but nonetheless there is no explicit instruction in the code for the regions of reverse plasticity to remain unaffected in the formulation of the residual stress. Therefore, this assumption is tested numerically by considering the Bree cylinder as described in section 3.3.2.

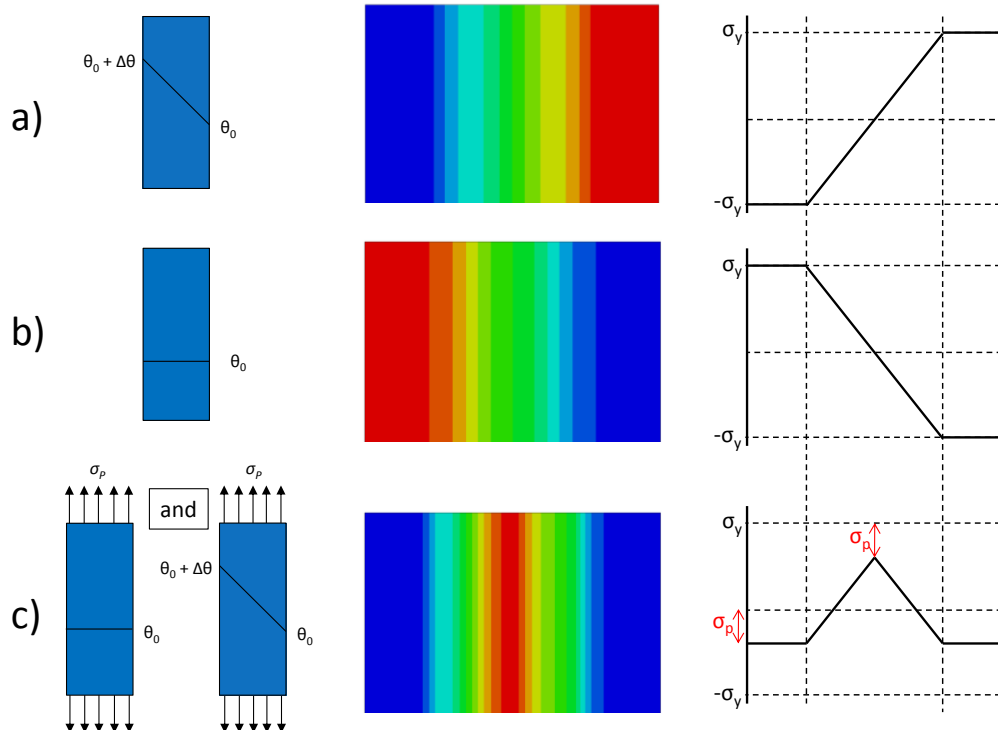


Figure 4.1 - Bree Stress Fields

In this case, the level of cyclic thermal loading considered in stage 1 of the LMM analysis creates an elastic stress range of 3 times the yield stress, which is sufficient to cause significant regions of reverse plasticity. An additional axial tension is applied in stage two. Figure 4.1a) and b) show the total stress fields generated by stage 1 of the LMM calculation at both extremes of the cyclic loading. Significant areas of yielding are observed at both extremes of the cycle. Figure 4.1c) then shows the constant residual stress field generated by stage two of the calculation when the additional axial tension is applied. It can be clearly seen that this constant residual stress forms such that the reverse plasticity is not affected. In the regions which are in reverse plasticity, this constant residual stress is equal in magnitude and opposite in sign to the applied tensile stress,  $\sigma_p$ . Therefore, because the tensile load is applied at all times the constant residual will cancel out  $\sigma_p$ , leaving the reverse plasticity regions unaltered. This test therefore verifies the assumption that the LMM follows the criteria set out by Polizzotto, and can therefore generate a lower bound to the global shakedown limit. A full analysis of the Bree cylinder is given in chapter 5.2.2.

#### 4.5.2 Plate with a Central Hole

To demonstrate the numerical procedures laid out in sections 4.2 and 4.4, the example of a plate with a central hole is analysed. Figure 4.2 shows the geometry, finite element mesh and load histories applied to the plate. The ratio between the diameter of the hole  $D$  and the length of the plate  $L$  is 0.2. The ratio between the thickness  $T$  and  $L$  is 0.05. Due to the symmetry of the geometry and loading, a quarter model is used with the appropriate boundary conditions. In addition, the free edges of the plate are constrained to expand in-plane to simulate the expansion of a large plate. The geometry is meshed with 642 elements of type C3D20R, a quadratic brick element with reduced integration (reduced integration is recommended in Abaqus for near incompressible solids).

The plate is subject to a cyclic temperature gradient between the bore of the hole and the outer edges. The temperature distribution as a function of radius is given in equation (4.46)

$$\theta(r,t) = \theta_0 + (\bar{\theta}(t) - \theta_0) \frac{\ln(2.5D/r)}{\ln(5)} \quad (4.46)$$

where  $D$  is the hole diameter and  $r$  is the radial distance from the centre of the hole, which approximates to a temperature of  $\theta = \bar{\theta}(t)$  at the bore of the hole and  $\theta_0$  at the edge of the plate. This gives a temperature difference between the bore of the hole and the edge of the

plate of  $\Delta\theta$ . The temperature difference between the bore and edges is cycled, resulting in the two load extremes used in the analysis. In addition to this cyclic thermal loading, a constant uniaxial tension,  $P$ , is applied along one edge of the plate. The plate material is perfectly plastic, has a young's modulus of 200GPa, a yield stress of 360MPa and a thermal expansion coefficient of  $5 \times 10^{-5} \text{ } ^\circ\text{C}^{-1}$ .

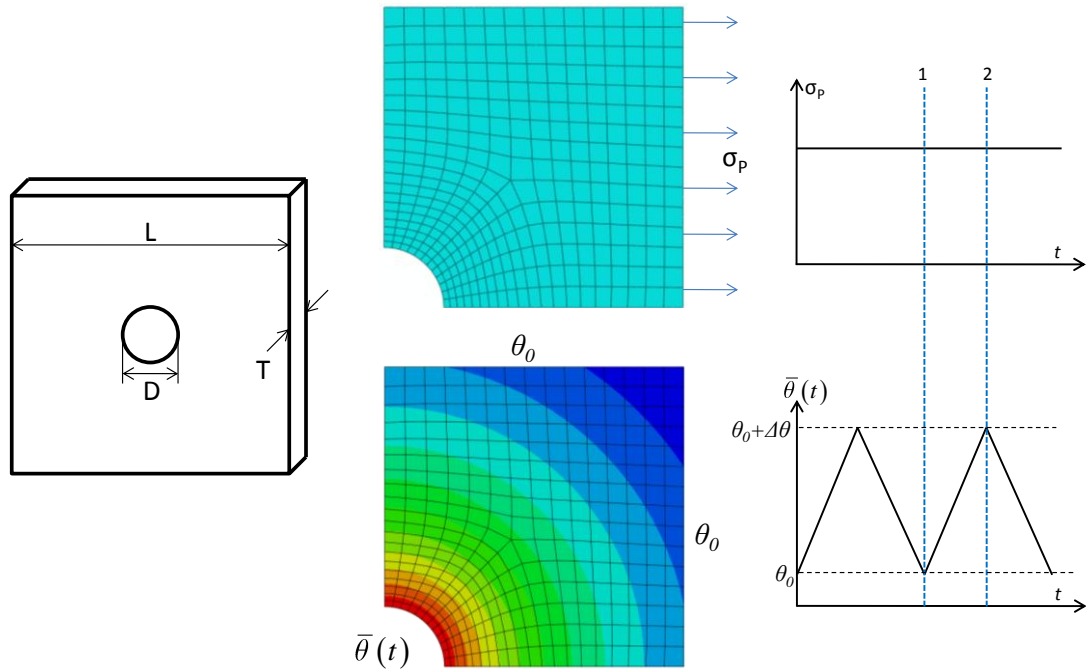


Figure 4.2 - Holed Plate Geometry, Mesh and Load History

The global shakedown interaction diagram for the plate is shown in Figure 4.3a where the applied temperature difference  $\Delta\theta$  is normalised against the reference temperature difference of  $\Delta\theta_0=100^\circ\text{C}$  and the uniaxial tension  $P$  is normalised against the yield stress of the material  $\sigma_y=360\text{MPa}$ . The reverse plasticity limit, calculated by the linear matching method shakedown procedure, is also shown in the figure and thus shows the capability of the linear matching method to calculate lower and upper bound strict and global shakedown limits. The interaction diagram follows the classic Bree-like shape, with lower and upper bound converging very closely.

The convergence of the lower and upper bounds at points A and B is shown in Figure 4.3b. In both cases the upper bound converges more quickly than the lower bound. This is due to the fact that the upper bound integrates energies over the volume (see equation (4.38)), diluting the effect of the stress concentration at the hole. The lower bound requires a greater number of iterations for the modulus adjustment procedure to redistribute the

stress and therefore satisfy the conditions set out in section 4.4.1. The convergence plot also shows that the lower bound at point B (within strict shakedown) converges more quickly than point A (which is global shakedown), which requires more increments than are shown in the figure to attain convergence. This is due to the fact that point B has no varying residual stress and thus a simpler stress state. Stage 1 of the calculation is still performed but converges almost instantly and moves onto stage 2. Point A, however, will have a significant level of varying residual stress and so will require more stage 1 increments to converge on these stresses. The more complex stress fields from stage 1 means that the lower bound requires longer to find a constant residual stress which satisfies yield at all points in the model. The plateaus seen in the convergence of the lower bounds are a result of the subroutine using the "best" value of lower bound calculated up to that increment. When the stress redistribution is taking place it is possible for the stress distributions to produce a worse lower bound than in the previous increment (especially within the first few increments when the rates of change of modulus and stress are high). As a result, the subroutines are programmed to use the best value of lower bound calculated up to that point.

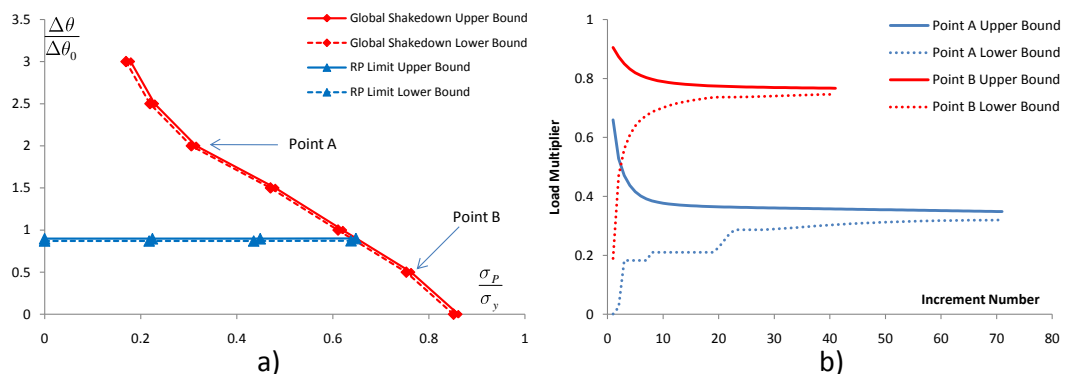


Figure 4.3 - Holed Plate Interaction Diagram and Convergence

## 4.6 Convergence Improvements

The poor convergence of the lower bound relative to the upper bound seen for Point B in Figure 4.3 can be attributed to the nature of lower bounds in finite element analysis. Being based on stress values at individual integration points will always leave lower bounds at the mercy of numerical errors (which are diluted by an upper bound procedure). The number of increments to find a converged lower bound in section 4.5.2 may be satisfactory for small models, but it is highly desirable to improve upon this for models of plant components with complex load histories.

### 4.6.1 Sources of Convergence Issues

Lower bounds can show poor convergence properties because of their reliance on stress values at individual integration points within the FE mesh. This is true to the point where a single integration point can be the sole inhibitor of lower bound convergence; in the lower bound search function explained at the end of section 4.4.2, the lowest value of  $\lambda^{LB}$  is the value taken as the lower bound for the whole model.

The inherent numerical error present in the stress values of finite element solutions will always be present. FEA is a displacement based method, with stress being a secondary calculation based on these displacements. In the LMM global shakedown assessment this is compounded by the fact that a two stage procedure is used. The convergence of both stages is based on numerical tolerances. Therefore whilst stage 1 may have converged to within the specified tolerance, there is still a margin for inaccuracies in the stress fields which are then carried forward into stage 2. In practice these errors are usually small for a converged solution, for example the stress at a particular point may be above the yield stress by less than 0.5%. To all intents and purposes the analyst would interpret this point as being at yield, but numerically these small errors can make the convergence of the stage 2 lower bound calculation a challenge.

Aside from the numerical issues, it is possible that some of the lower bound convergence issues are due to the estimates of the stress fields themselves. Figure 4.3b shows plateaus in the lower bound convergence. This is due to those increments generating a poorer estimate of the residual stress field, and so the best lower bound multiplier from previous increments is propagated. If these estimates of the stress fields could be improved then there would be a more monotonic increase in the lower bound with each increment.

Delving a little deeper into this issue, using the equations outlined in section 3.2 for the upper bound strict shakedown and stage 2 of the global shakedown, can reveal some possible causes in stress field inaccuracy. Revisiting these equations:

$$\mu_{k+1}^n = \frac{\sigma_y}{\bar{\varepsilon}_k^n} \quad \text{where} \quad \bar{\varepsilon}_k^n = \bar{\varepsilon}(\Delta\varepsilon_{ijk}^n) \quad (4.47)$$

And

$$\frac{1}{\bar{\mu}_{k+1}} = \sum_{n=1}^N \frac{1}{\mu_{k+1}^n} \quad (4.48)$$

Then:

$$\bar{\rho}_{ij_{k+1}} = [J]_{k+1} \Delta \varepsilon_{ij_{k+1}} - \sigma_{ij_{k+1}}^{in} \quad \text{where} \quad \sigma_{ij_{k+1}}^{in} = \bar{\mu}_{k+1} \left[ \sum_{n=1}^N \frac{1}{\mu_{k+1}^n} \lambda_{k+1}^{UB} \hat{\sigma}_{ij}^n \right] \quad (4.49)$$

It is clear from this sequence of calculations that the updated estimate of the residual stress field,  $\bar{\rho}_{ij_{k+1}}$ , is strongly linked to the values of the updated modulus  $\mu_{k+1}^n$  calculated at the beginning of the increment. The current scheme used in equation (4.47) matches the modulus of every integration point to the yield stress. In areas where the elastic stress is above yield, around stress raisers for example, then this scheme is ideal for quickly reducing the stress to satisfy the yield condition. In areas adjacent to this where the stress is lower, this scheme increases the stiffness to encourage stress to redistribute. In low stress areas which are remote from any stress raiser, however, it was hypothesised that this scheme could have the effect of over-stiffening the area, which could lead to distorted stress fields as a result. In addition to this, it was thought that the sudden large increase (in only a single increment in many cases) in modulus compared to the slower changes in high stress areas may be creating an imbalance which then requires further increments for the method to rectify.

With this in mind, several modifications to the matching scheme were tested numerically. In all cases the spirit of the original scheme was retained in that the yield stress was always used as the target stress. The modifications tested here attempted to remedy the over-stiffening issue by trialling different limits to the modulus values and also limits to the rates of change of modulus values.

#### 4.6.2 Proposed Solutions

The numerical limit of the maximum value of  $\mu$  in the LMM code is  $1 \times 10^8$  for models using units of Newtons and millimetres. This is applied uniformly in the FE model, so no integration point may have a stiffness which is greater than this value. This represents a stiffening of around 500 times for a typical steel with a young's modulus of 200 GPa (i.e.  $2 \times 10^5$  N/mm<sup>2</sup>), which is typical for steels and is assumed for the numerical experiments conducted here.

The first set of matching schemes proposed focused on this maximum value of  $\mu$ , and several limits were trialled. In order to tackle the over-stiffening in low stress regions the  $\mu$  limit was made a linear function of the stress at the integration point in question, shown graphically in Figure 4.4. A stress equal to or greater than yield would use  $\mu_{Max} = 1 \times 10^8$  as per the original code and a stress value of zero would have a maximum value as specified in Figure 4.4.

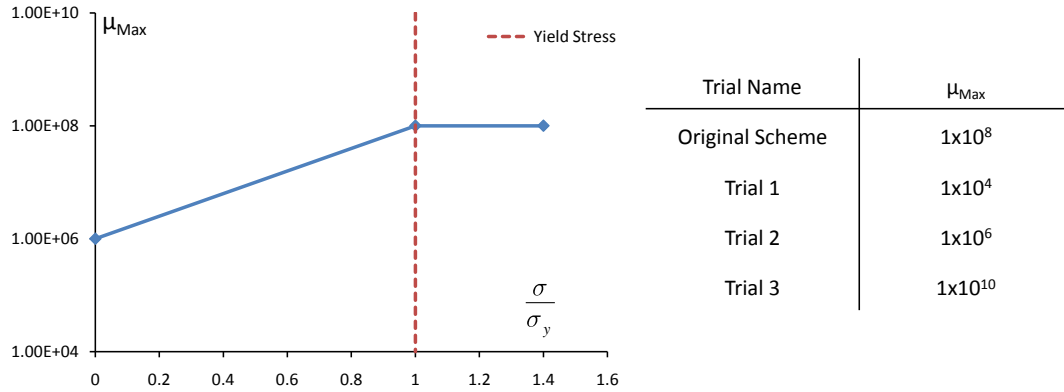


**Figure 4.4 - Setting  $\mu_{Max}$  as a Function of Stress**

Several schemes were also trialled which retained the uniform maximum value  $\mu_{Max} = 1 \times 10^8$ , but instead placed limits on the rate of change of  $\mu$  in each increment for integration points with stresses below yield. The rate of change of  $\mu$  is defined as the ratio of the previous value and current value:

$$\mu_{Rate} = \frac{\mu_{current}}{\mu_{previous}} \quad (4.50)$$

Integration points with a stress above yield were not included, leaving them to reduce to the yield stress as per the original scheme. The two methods used to enforce this limit to the rate of change are shown graphically in Figure 4.5.

Rates described as "flat" refer to all points below yield being limited to a maximum rate of change of the specified value, which is specified in Figure 4.5. The parabolic distribution limits the rate of change based on the stress level, which could target the desired areas more effectively. For areas with a very low stress, the rate of change would be small. For higher stressed areas the maximum rate would increase to encourage redistribution, and in highly stressed areas a low rate would apply because little redistribution would be required.

The parabolic distributions all have a  $\mu_{Rate} = 1$  when the stress is equal to zero or yield. The parabolic schemes are then defined by the max value of  $\mu_{Rate}$  which occurs at a stress value of half yield.

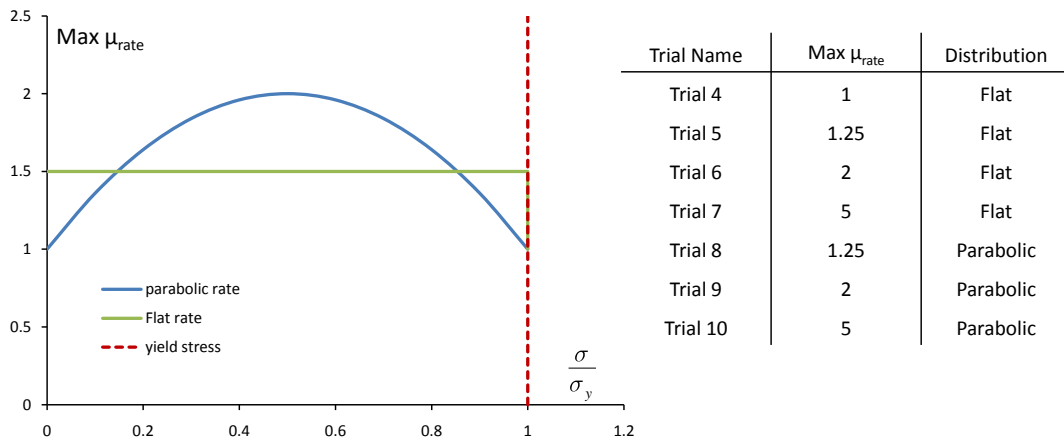


Figure 4.5 - Trial Schemes for Limiting  $\mu_{rate}$

### 4.6.3 Numerical Testing

The 10 matching schemes outlined above were implemented into the LMM subroutines for comparison with each other. Initially these trials were performed using the strict shakedown code (Points 1-3), and schemes which were successful in improving the stress field estimates were then brought forward for trialling in the global shakedown procedure (Points 4 and 5).

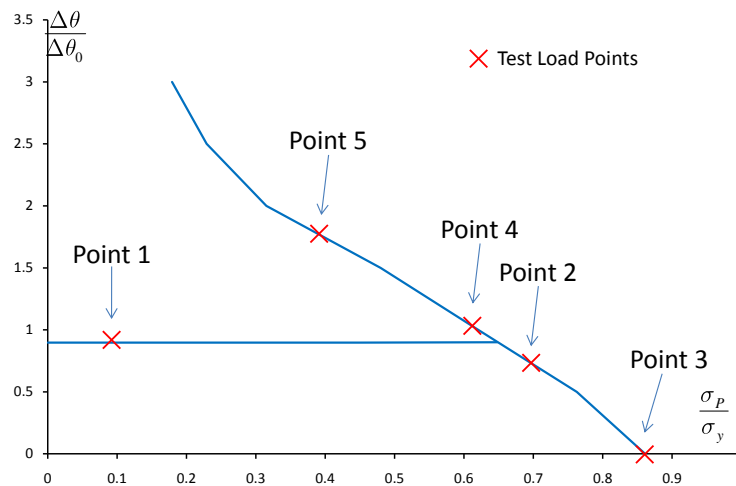


Figure 4.6 - Test Load Cases for the Holed Plate

The same holed plate problem as described in section 4.5.2 was used to perform the comparisons. Three points on the strict shakedown boundary were selected so that the effect of the matching schemes could be seen for both reverse plasticity and ratchet mechanisms. These three points are shown in Figure 4.6 and correspond to one point on the reverse plasticity limit (Point 1), one point on the ratchet limit (Point 2) and the limit load (Point 3). At these three points full elastic-plastic FEA was performed for 50 cycles to obtain the stress fields - this number of cycles was found to produce stress fields which changed very little between cycles. These stress fields were then used as the benchmark for comparison with the LMM.

The different matching schemes were implemented into the subroutines and solved using a convergence value of  $1e^{-4}$  (difference between consecutive upper bounds, see section 6.4). The stress fields produced were compared to those from step by step by comparing plots of the nodal equivalent stress along three lines in the finite element model. Path 1 runs along the left edge of the plate, Path 2 follows the circumference of the bore and Path 3 runs along the bottom of the plate. The location of these three lines is shown in Figure 4.7.

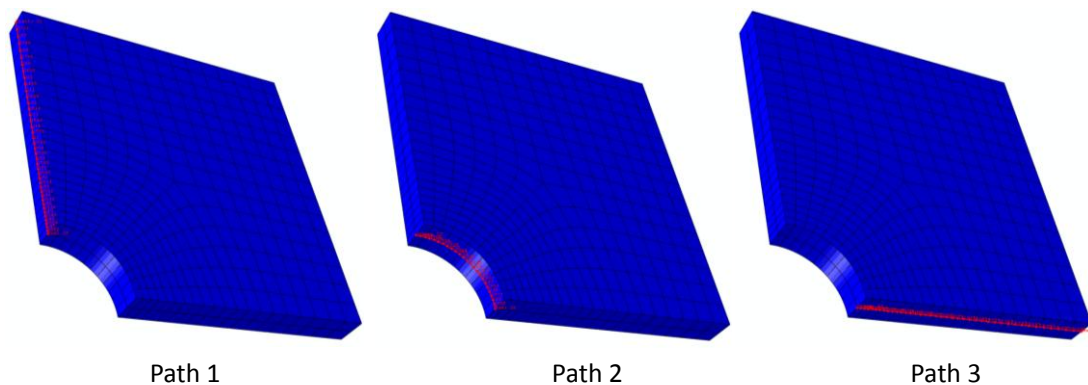
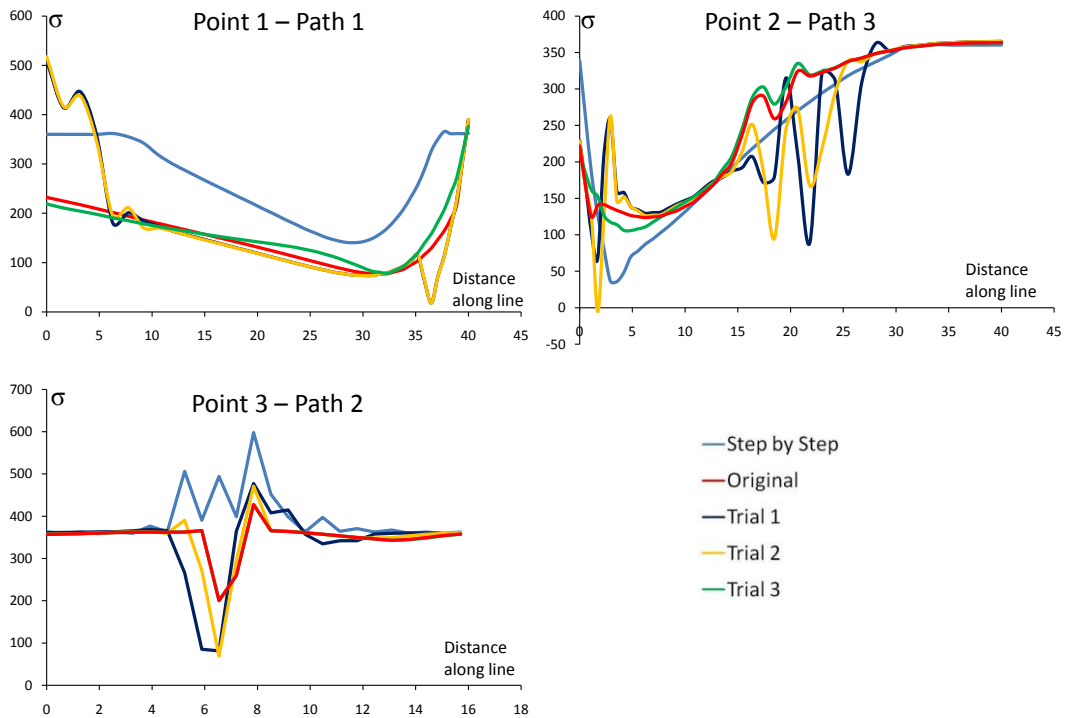


Figure 4.7 - Nodal Paths Used to Compare Stresses

#### 4.6.4 Results and Selection of Final Scheme

Considering the Trial 1, 2 and 3 results, the majority of the stress plots obtained showed no improvement or very little change in the stress fields calculated when compared to the original matching scheme. The points and node paths which displayed the most significant changes to these changes are displayed in Figure 4.8. In general, no single matching scheme from Trials 1, 2, or 3 showed an improvement over all load points and nodal paths considered. Schemes which displayed improvement in one path or load point were then shown to have a negative effect in others. From Figure 4.8 it can be seen that Trial 3 shows

an improvement to the predicted stresses when compared to those predicted by Step by Step analysis. This improvement is marginal, however.



**Figure 4.8 - Comparison of Trial 1,2 and 3 with the Original Scheme and Step by Step**

A similar situation was observed with Trials 4, 5, 6 and 7. In many situations these schemes showed little improvement or little change from the original scheme. Trial 4 was the exception to this, being the only scheme from these which gave stress results which were at least no worse than the original scheme. Trial 4 also gave an improvement in some load cases, two examples of which are shown in Figure 4.9, where the stresses generated more closely match the Step by Step stresses. Note in Figure 4.9 the results for Trials 5-7 and Original are coincident.

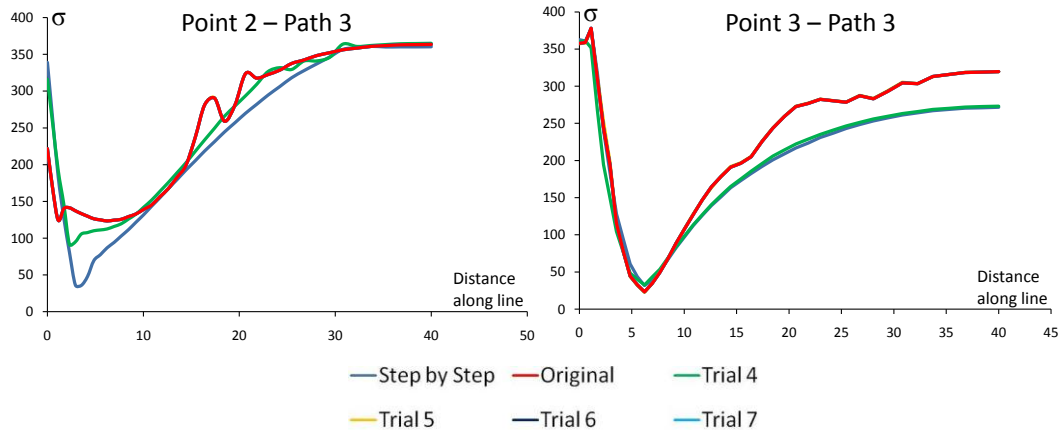


**Figure 4.9 - Comparison of Trials 4-7 with the Original Scheme and Step by Step Results**

The schemes of Trials 8-10 did not show any significant change to the results at any of the load points or nodal paths. Figure 4.10 shows two stress plots which are typical of the results for these three schemes (results for Trials 8-10 and the Original are coincident).

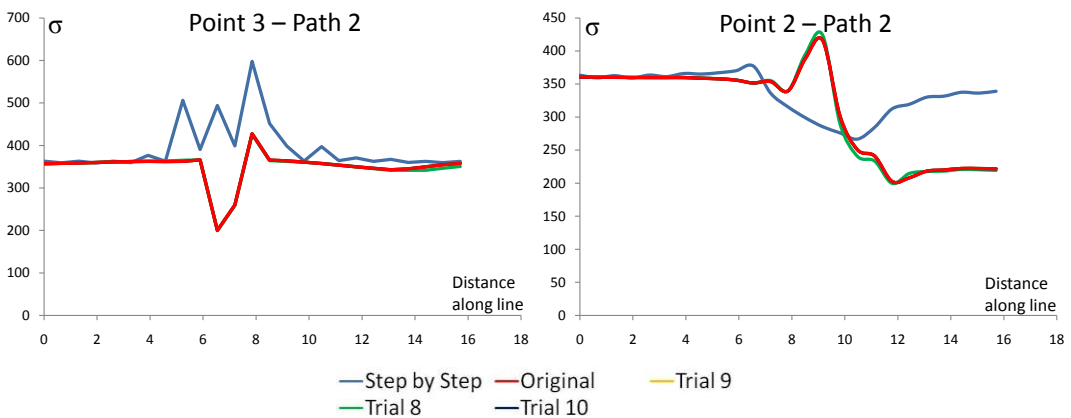


**Figure 4.10 - Comparison of Trials 8-10 with the Original Scheme and Step by Step Results**

The only scheme from these trials which could show even modest improvements was Trial 4. This scheme uses a  $\mu_{rate} = 1$  for a stress below yield, i.e. for stress which is below yield the modulus remains unchanged. Of the other schemes, none were able to produce improved stress fields for all load points and nodal paths. If improvements were seen, these were offset by poorer results in other nodal paths or load points. The Trial 4 scheme was brought forward for testing in stage 2 of the global shakedown code.

The global shakedown load multiplier convergence given by the original scheme and Trial 4 for Load Points 4 and 5 is given in Figure 4.11. From this comparison it can be seen that Trial 4 produces mixed results. In both cases the convergence of the upper bound is slowed.

This is to be expected because the changes in the stress fields are more localised, meaning that the energy changes per increment are smaller. The lower bound produced by the Trial 4 scheme shows an improvement for Load point 5, but has a detrimental effect for Load Point 4.

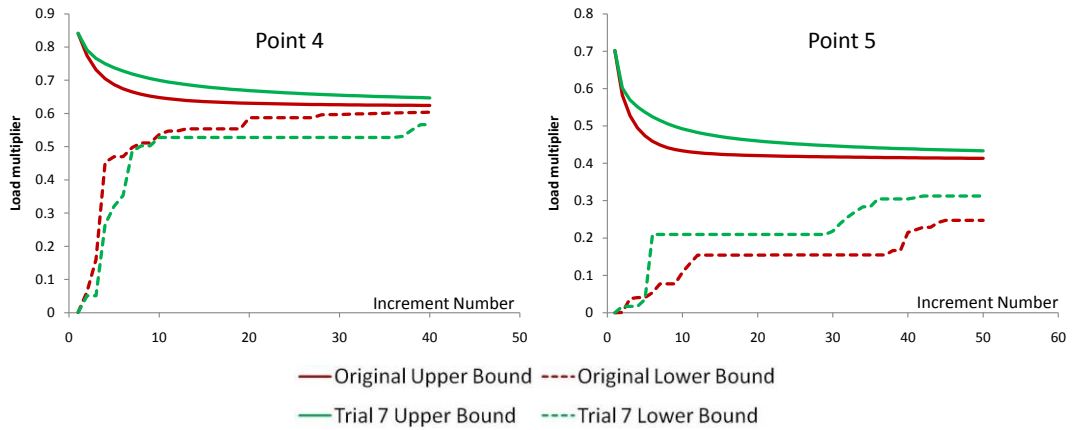


**Figure 4.11 - Load Multiplier Comparison of Original Scheme and Trial 4**

In addition to the Trial 4 scheme, a further elemental averaging scheme was tested in stage 2 of the global shakedown procedure. The element averaging scheme, rather than attempting to improve the lower bound by improving the stress field estimates, uses the original matching scheme and improves the lower bound by averaging the lower bound multipliers over each element. If single integration points are suffering from numerical issues then this scheme would aid the overall convergence of the solution by averaging this with the adjacent integration points. A comparison of Trial 4, elemental averaging and the (un-averaged) original scheme is shown in Figure 4.12 for Load Points 4 and 5.

The elemental averaging scheme is shown to produce favourable results for both cases. It has a smoothing effect to the lower bound convergence of Load Point 4 and a drastic improvement in the convergence of Load Point 5.

Based on these results the decision was taken to implement the elemental averaging of the lower bound in the global shakedown analysis procedure. This option is not strictly a lower bound because individual integration points may violate the yield condition, but if the finite element mesh is dense enough in the regions of interest then this approximation to the lower bound is thought to be acceptable given the large savings in solution time which are observed.

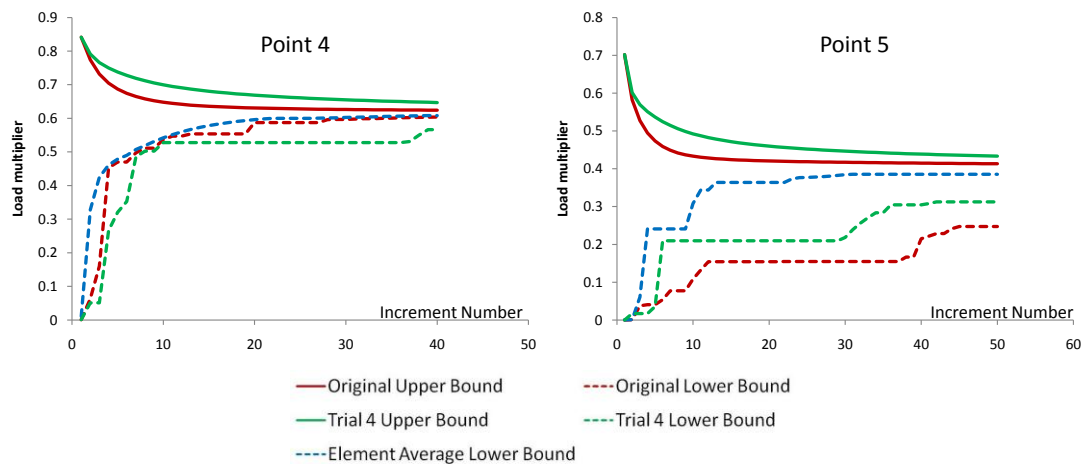


Figure 4.12 - Comparison of Elemental Averaging, Trial 4 and the Original Scheme

## 4.7 Summary and Discussion

The LMM global shakedown method created by Ponter and Chen is able to provide accurate upper bounds to the global shakedown limit. The creation of the lower bound calculation and the implementation into the LMM framework described in this chapter now means that the LMM is capable of producing lower and upper bound to both the strict and global shakedown limits. A lower bound solution provides the necessary conservatism required for regular use in the nuclear industry. This lower bound is calculated in parallel with the upper bound which provides a self verification of the solution. If both lower and upper bounds converge to a common value then the analyst can have confidence in this final solution.

Lower bound calculations within FEA are known to suffer from convergence issues due to numerical issues at individual integration points. Schemes to improve the stress fields generated by the LMM have been investigated with mixed results. Instead an element averaging of the lower bound multipliers has been selected to alleviate these convergence issues. Whilst this option only provides an approximation of the lower bound, it is thought that if the mesh density is high enough in areas of interest then the improved solution times justifies this choice.

## **5 Analyses and Validations of the LMM Global Shakedown Method**

### **5.1 Introduction**

The formulation and implementation of a lower bound to the global shakedown analysis procedure now means that the LMM is capable of providing lower and upper bound to both the strict and global shakedown limits. Validation of the strict shakedown procedure has been provided in Chapter 3, where several comparisons with theoretical, numerical and experimental results are presented.

This chapter presents a similar set of comparisons so that the Global Shakedown procedure may be validated in accordance with objective 2 in section 1.6. Some of the comparisons of Chapter 3 are revisited, such as the Bree Cylinder, to verify the implementation of the new lower bound calculation. In addition to these simpler comparisons, the global shakedown behaviour of a pipe intersection is investigated using the LMM and validated with step by step FEA. This example is a commonly analysed geometry in EDF and so proves that the LMM is worthy of regular use by EDF engineers.

### **5.2 Validations**

The LMM global shakedown method can be validated using the same examples as were used in section 3.3 to validate the strict shakedown procedure, namely the limit loads of notched bars and the Bree cylinder.

#### **5.2.1 Limit Loads of Notched Bars**

The limit loads of notched bars, originally used by Tipping [34], are once again used as a validation case. The global shakedown procedure is not intended for limit load calculation. The two stage calculation process means that some level of cyclic loading must be present in order for stage one to execute. Therefore, when in use in EDF, limit loads would be calculated using the strict shakedown procedure. For this validation case, however, the limit load can be approximated by the global shakedown procedure by setting the level of cyclic loading to a very small value. This will allow the validation of the newly added lower bound in a relatively simple setting before more complex situations are considered.

The four notched bar geometries of section 3.3.1 were analysed using the LMM global shakedown procedure to find the limit load for axial tension. The same finite element mesh, loads, boundary conditions and material properties were used. An cyclic axial load of

0.01% of the axial tension was applied in stage 1 of the procedure before the limit load was then calculated in stage 2. This level of cyclic loading was thought to be small enough so that the effect on the stage 2 calculation would be negligible. Convergence tolerances of  $1e-4$  and  $1e-5$  were used in stage 1 and stage 2 respectively (see section 6.4 for convergence options).

The load multipliers calculated by the global shakedown method are given in Table 5.1. For comparison the limit loads predicted by Abaqus limit analyses and the theoretical solutions of Miller. The load multipliers predicted by the strict shakedown procedure are also given.

**Table 5.1 - Comparison of Notched Bar Limit Load Solutions**

Solution	3D	Axisymmetric	Plane Strain	Plane Stress
Miller	0.3041	0.3041	0.8006	0.5565
Abaqus	0.3454	0.3454	0.8028	0.5573
LMM Strict Shakedown UB	0.3456	0.3456	0.8025	0.5583
LMM Strict Shakedown LB	0.3439	0.3439	0.7985	0.5555
LMM Global Shakedown UB	0.3451	0.3451	0.8024	0.5572
LMM Global Shakedown LB	0.3434	0.3433	0.7976	0.5545

The limit loads predicted by the global shakedown method agree well with the solutions of Miller and Abaqus limit analysis.

### 5.2.2 The Bree Cylinder

The Bree cylinder was used in chapter 3 as a useful example to validate the strict shakedown procedure. The strict shakedown procedure was able to accurately predict the theoretical strict shakedown limit of Bree and Bradford. These theoretical solutions also extend to the global shakedown limit, and so provide a useful example to verify the LMM in this regard, especially with the addition of a new lower bound.

In addition to this, Bradford has extended his global shakedown solutions in [95] and those of Bree [36] to include a temperature dependency in the yield stress [108]. Two yield stresses are used in this derivation, cold and hot, which are assumed to be uniform in the volume. The uniform hot yield stress applies when the linear temperature distribution is acting on the model, and the cold yield applies when this temperature distribution is removed. These temperature dependent global shakedown solutions are used as an additional comparison for the LMM.

The plane stress model used in section 3.3.2 was used once again with the same mesh, boundary conditions, material properties and loads (a steady state axial tension and a cyclic temperature difference between the inner and outer walls). Where the temperature dependent yield applies, a hot yield of 60% of the cold yield is used. The LMM global shakedown boundary is compared to the theoretical solution of Bree and the temperature dependent extension of Bradford in Figure 5.1. The limit load was approximated using the same technique used for the notched bar solutions. A cyclic thermal load of which gave a thermal stress range of 0.01% of the yield stress was used in stage 1, before stage 2 then found the limit load for the axial tension. Once again the vertical axis represents the level of cyclic thermal stress and the horizontal axis represents the level of steady state axial stress. Both axes have been normalised against the cold yield stress. A good agreement is seen between both solutions.

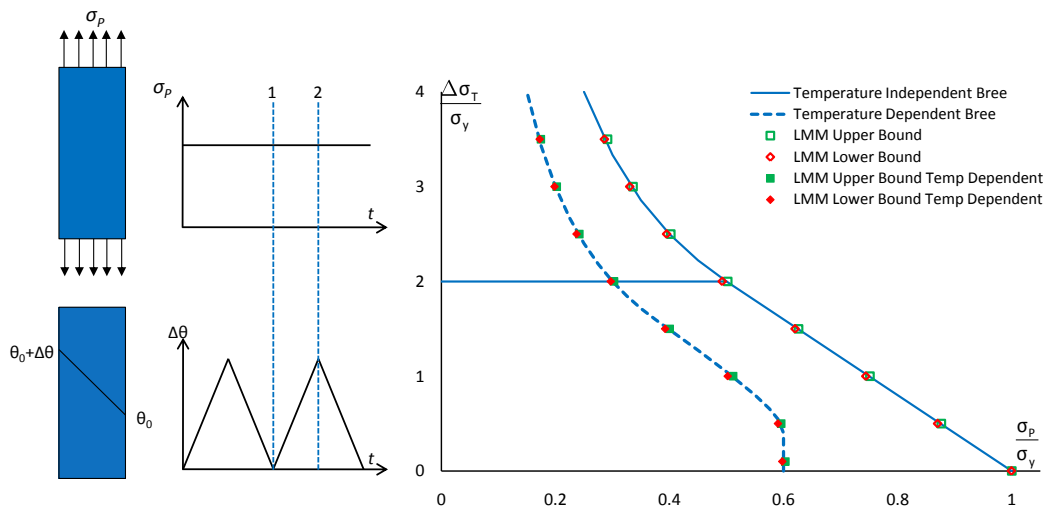
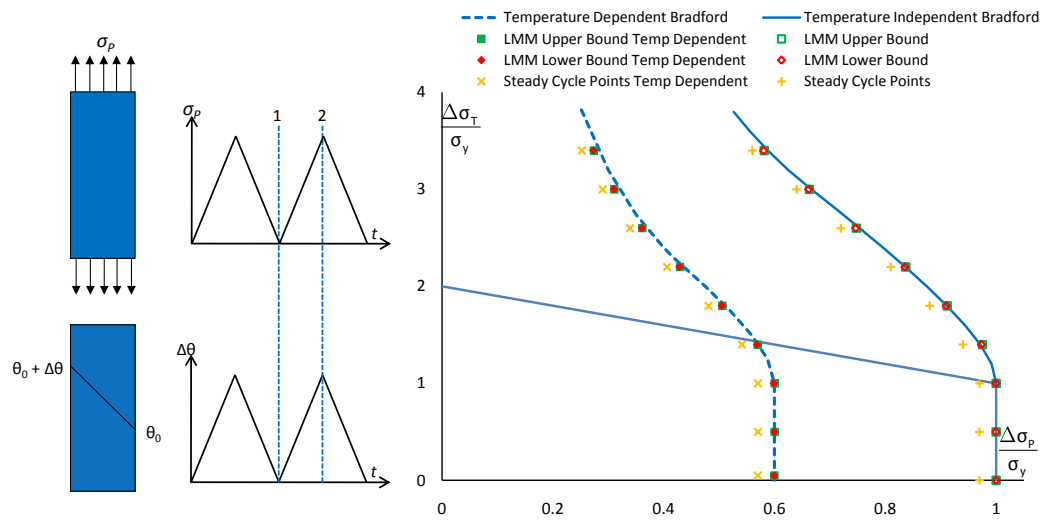


Figure 5.1 - Bree Cylinder Global Shakedown Results Comparison

The global shakedown limit for the modified loading conditions considered by Bradford in [95], and the extension to temperature dependent yield, has been calculated using the LMM and compared to the theoretical solutions in Figure 5.2. This situation has no steady state loading, and so the load decomposition typically required for the LMM two stage process cannot be achieved. Instead an approximation of the boundary is found. The level cyclic loading in stage 1 is chosen to be just inside the theoretical limit, shown as “steady cyclic points” in Figure 5.2. This means that a minimal steady state axial tension is added in stage 2 giving a reasonable approximation to the loading considered in the theoretical case.



**Figure 5.2 - Modified Bree Global Shakedown Results Comparison**

The vertical axis represents the cyclic thermal stress, and the horizontal axis represents the cyclic axial stress, and both are normalised against the cold yield stress. A slightly less favourable agreement is seen with these results, with the LMM tending to underestimate the global shakedown limit of Bradford. This example highlights the current limitation of the global shakedown to calculate the global shakedown limit based on steady state loading. This is being addressed by Lytwyn [109] where a global shakedown limit procedure is being developed for a generalised load cycle, similar to that of the strict shakedown procedure. Until this is complete, examples such as this must be approached with caution, and the strict shakedown procedure should be used where possible.

### 5.3 Global Shakedown of a Pipe Intersection

The examples above serve as a useful verification that the bounding theorems have been correctly implemented and that the method can reproduce the theoretical results. These

examples however, consider relatively simple loading and/or geometries. This makes them very useful for initial comparisons, but they do not represent the more complex geometries and load histories which are analysed within EDF. To ensure that the LMM will be a useful tool to EDF engineers a more representative component must be analysed and verified.

To this end the LMM global shakedown has been used to analyse a fictitious pipe intersection with a dissimilar material join. This geometry is commonly analysed with EDF, so fulfilling the requirement of realism. Furthermore there is little published work regarding the shakedown behaviour of pipe intersections, giving this study additional merit in furthering the understanding in this area.

Two scenarios are considered here. The first sees the intersection subject to steady state internal pressure and cyclic thermal loading. The thermal expansions of the materials in the dissimilar join serve to enhance the effects of the thermal loading in this case. The second scenario also has a steady state internal pressure and the cyclic loading is of the form of a bending moment applied to the branch pipe.

The thermally loaded case is extensively validated using elastic-plastic FEA to compare the global shakedown limit, plastic strain ranges and predicted failure mechanisms. The bending moment case is used to explore the behaviour of the intersection by altering material properties and observing the effect on the global shakedown limits.

### **5.3.1 Review of Existing Pipe Intersection Solutions**

The widespread use of pipe intersections has led to numerous studies of their behaviour over the years from early elastic analyses [110] through to more recent analyses considering creep effects including the effects of welded regions [111]. In particular, studies to calculate limit and plastic collapse loads are common for both internal pressure and bending modes. For example Hamilton et al [58] used the elastic compensation method to determine non-dimensionalised limit pressures for a number of intersection geometries. Another example includes the semi-theoretical limit solutions proposed by Kim et al [112] for internal pressure and bending moment loading. These equations use several geometric parameters to predict whether failure will occur in the nozzle, the main pipe or the intersection of the two for a monotonically applied bending moment or pressure.

Despite their common use in piping systems, very few studies have been published regarding this geometry subject to cyclic loading. A study by Nadarajah et al [59] used the

Elastic Compensation Method to conduct a parametric study of this geometry subject to internal pressure and cyclic bending moments. Systematically altering the mean radii and shell thicknesses of the pipe and nozzle allowed a variety of thin walled intersections (radius to thickness ratio between 50 and 200) to be analysed. Both the limit load surface and strict shakedown limit was calculated for each geometry using an elastic-perfectly plastic material model. The parametric studies found a strong interaction between the loads, with small nozzles (having a radius of less than one fifth of that of the main pipe) having a near linear interaction curve. Larger nozzles (i.e. with a radius of two fifths of the main pipe) still displayed a strong interaction between the loads, but had a circular interaction curve which is more akin to the conventional Bree like shakedown boundary.

In addition to this study, the strict shakedown response of a single thick walled pipe intersection was analysed in the EPERC Design by Analysis manual [113]. This geometry consisted of two materials and also contained the weld detail at the join between the nozzle and main pipe. Several analysis methods were used including the Elastic Compensation Method, direct analysis using elastic-plastic FEA and stress categorisation methods. The Elastic Compensation results presented for this case show little interaction between the bending moment and internal pressure. This is attributed to the thick shells, which serve to isolate the loadings from each other. Again, internal pressure and cyclic in-plane moments were considered. Apart from these studies, no further shakedown examples (whether strict or global) of this geometry could be found.

The intersection analysed here is more akin to the example in the EPERC Design by Analysis manual in that it is thick walled, manufactured from several materials and includes the geometry of the weld in the model. This should provide a similar complexity to many models analysed in EDF and prove the applicability of the LMM in an industrial setting.

### **5.3.2 The Pipe Intersection Model and Material Properties**

The pipe intersection analysed in this paper is shown in Figure 5.3. The small intersecting pipe is welded to the main pipe, with the weld itself modelled as a chamfer between the two shells (as per the EPERC example). The main pipe is made from 316 stainless steel, a common material in nuclear plant components. The intersecting pipe was chosen to be from low alloy steel SA508 and the weld material is Inconel 82/182. Recently the UK nuclear industry has been analysing the residual stresses present in this dissimilar weld with a view to investigating stress corrosion cracking [114–116].

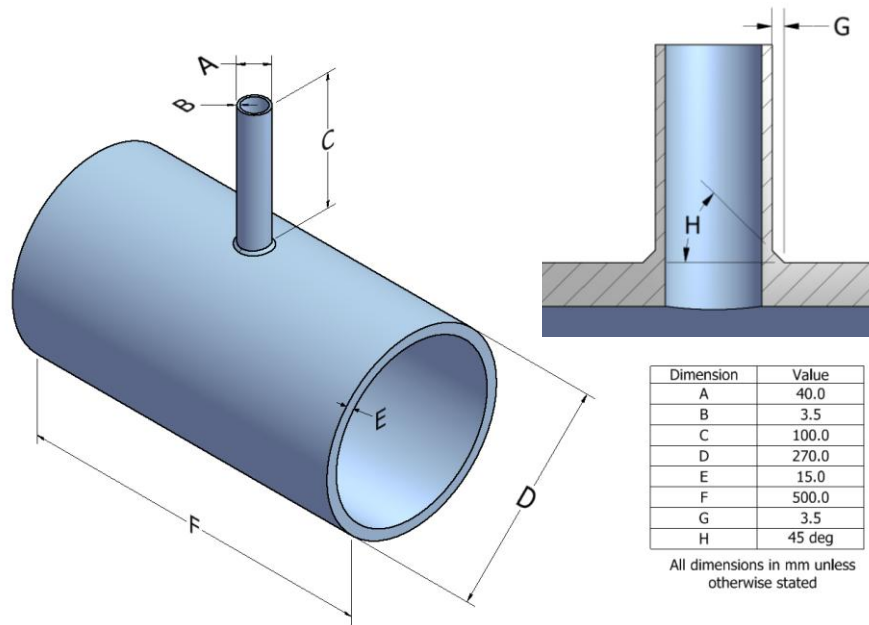


**Figure 5.3 - Pipe Intersection Geometry**

When conducting thermal analyses it is important to consider the effects of temperature dependent material properties. The temperature dependent yield stresses used for all three materials is shown in Table 5.2. During the analysis linear interpolation/extrapolation is used to calculate the yield stress at intermediate and outlying temperatures. The data for 316 and SA508 were taken from the British Standard [117] and a paper by Hurrell et al [118] respectively. Material data for the Inconel weld in the as-welded condition is limited, with the micromechanical tests of Kim et al [119] being the only elevated temperature tests which could be found. Linear extrapolation is performed to provide an approximation to the temperature dependency, which will give a more accurate solution than if temperature independent properties were assumed throughout the weld. An elastic perfectly plastic material which satisfies the von-Mises yield criterion is assumed throughout this work.

**Table 5.2 - Temperature Dependent Yield Stress Values**

Temperature (°C)	20	50	100	150	200	250	300	350	400	450
316	220	204	177	162	147	137	127	120	115	112
SA508	472		460		448		430		395	
Inconel 82/182	378.6						315.8*			

\*Yield stress taken at 320°C

The Linear Matching Method requires an elastic calculation to be performed for each point in the load cycle. This provides a starting point for the Linear Matching solution procedure. Temperature dependent yield stress is considered once the linear matching process has begun, but because the elastic solutions have been performed before this process a single value of thermal expansion must be assumed. This is fine for a single ratchet analysis at a fixed level of cyclic thermal load, but to create the Bree diagram a new set of elastic solutions would need to be created for each level of thermal loading considered. To avoid this, the worst case thermal expansion scenario was chosen.

When the temperature dependency of the thermal expansion coefficients of the materials in [116] is examined, it can be seen that the difference between the three values remains almost constant. The magnitude increases with increasing temperature, but does so uniformly for all three materials. Therefore, with a maximum temperature considered never larger than 600°C, the expansion values at this temperature were used for all thermal analyses conducted. Therefore values of  $1.8 \times 10^{-5}$  for 316,  $1.5 \times 10^{-5}$  for Inconel 82/182 and  $1.4 \times 10^{-5}$  for SA508 are used. This assumption gives conservative results in all cases.

Two separate load cases are considered for this pipe intersection. The first is a steady state internal pressure and a cyclic thermal load. The second load case is the combined action of a steady state internal pressure and a cyclic in plane bending moment.

### **5.3.3 Internal Pressure and Thermal Loading**

The thermal cycle chosen for this analysis has three load instances. The first point is where the intersection is at ambient temperature,  $\theta_0$ , throughout the entire structure. The second point is where the inner surface is at an elevated temperature,  $\theta_E$ , whilst the outer surface remains at ambient,  $\theta_0$ . This results in a linear temperature gradient through the wall of the pipe with a temperature difference  $\Delta\theta$ . The differential expansion of the inner and outer surfaces results in a linear distribution of elastic stress through the wall thickness. Finally, the case where the entire structure is held at a uniform elevated temperature,  $\theta_E$ , is considered. The different thermal expansion coefficients of the materials create thermal stresses at the material boundaries. In addition to this cyclic thermal loading, an internal pressure is applied. The closed end condition is assumed, which is applied in the model as an axial tension to both pipes. In addition, both free ends of the intersection are constrained to expand in plane, which simulates the expansion of a long pipe.

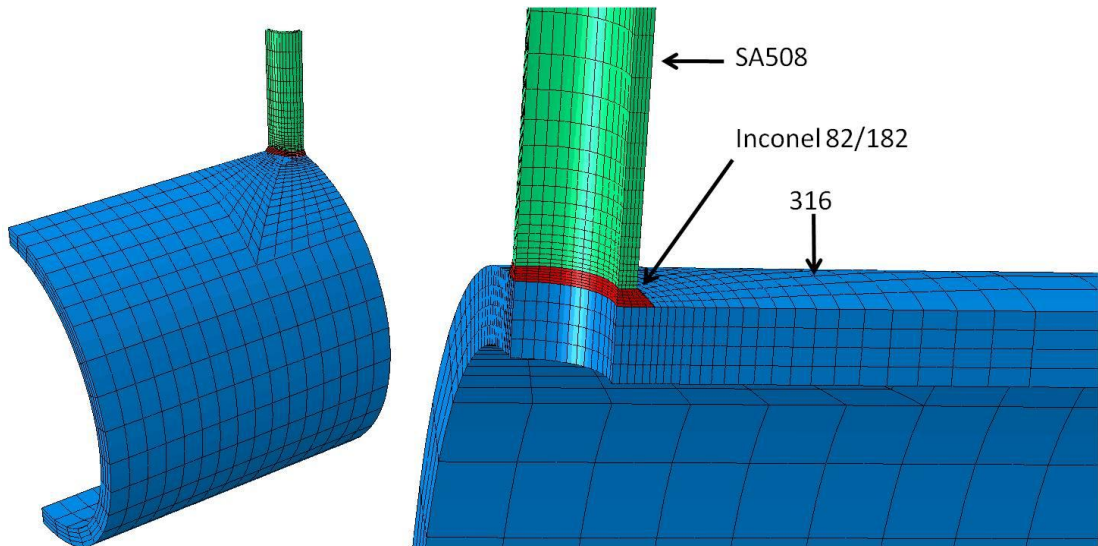


Figure 5.4 - Pipe Intersection Quarter Model and Mesh

Due to the symmetry present in the geometry and the applied loads, a quarter model with appropriate symmetry boundary conditions was used to model the pipe intersection. The mesh is refined in the region of the weld as all of the structural and material discontinuities are in this region. This gives the model a total of 4038 elements as shown in Figure 5.4. Element type DC3D20 elements used for the two heat transfer analyses. These temperature distributions were then applied as predefined fields in linear elastic structural analyses (using C3D20R elements), giving the stresses shown in Figure 5.5.

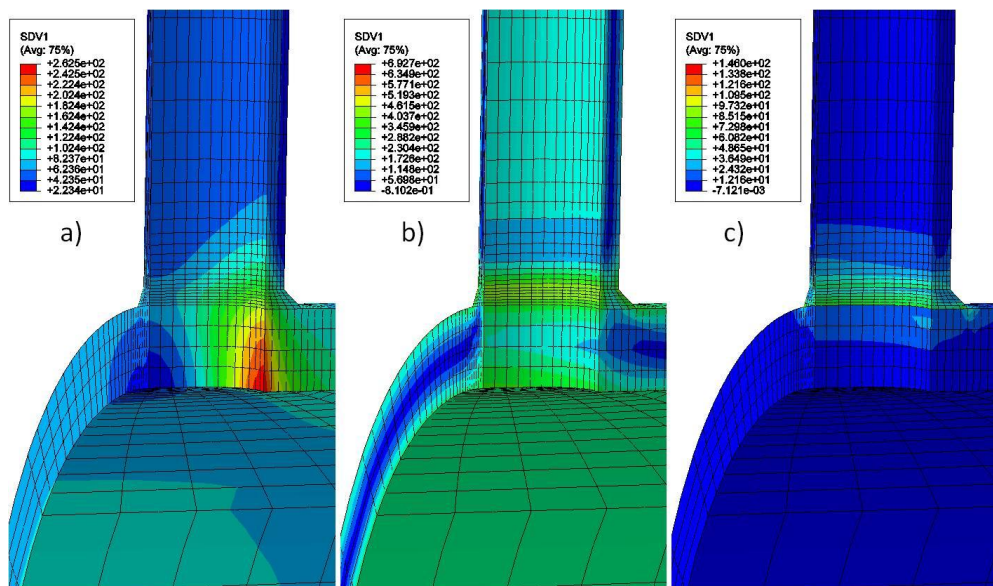


Figure 5.5 - Elastic Stresses due to a) Internal Pressure, b) Linear Temperature Difference and c) Uniform Elevated Temperature

These elastic stresses are used as the starting point for the LMM global shakedown analysis. In stage 1 the cyclic stresses are considered so that the reverse plasticity mechanism and plastic strain range can be calculated. Once this has been found, the maximum level of constant internal pressure which will not cause the component to ratchet is calculated. This calculation procedure was repeated for different levels of cyclic loading so that the global shakedown boundary could be created. The LMM strict shakedown procedure was also employed to calculate the reverse plasticity limit. This limit, which divides the regions of strict and global shakedown, completes the interaction diagram for the component and demonstrates the ability of the LMM to produce lower and upper bound limits for both shakedown and ratcheting.

### 5.3.3.1 Results

The interaction diagram for the constant internal pressure and the thermal cycle is shown in Figure 5.6. The applied constant internal pressure,  $P$ , is normalised against the initial applied internal pressure,  $P_0$ , of 10MPa. The applied temperature difference,  $\Delta\theta$ , is normalised against the initial applied temperature difference,  $\Delta\theta_0$ , of 100°C. Both temperature dependent and temperature independent results (using the yield stress at 20°C in Table 5.2) are plotted, which demonstrates the reduction in the shakedown limits caused by considering temperature dependent yield stress.

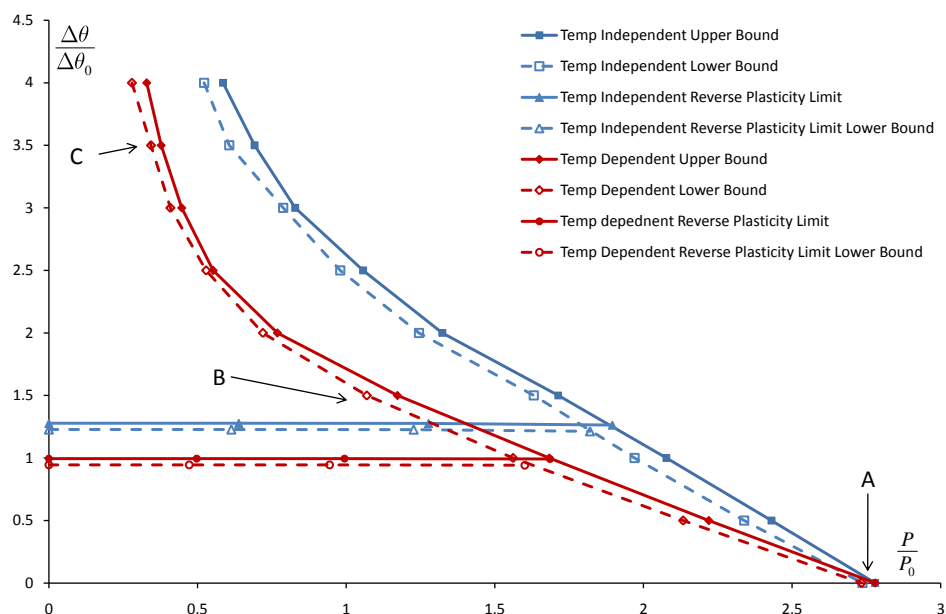
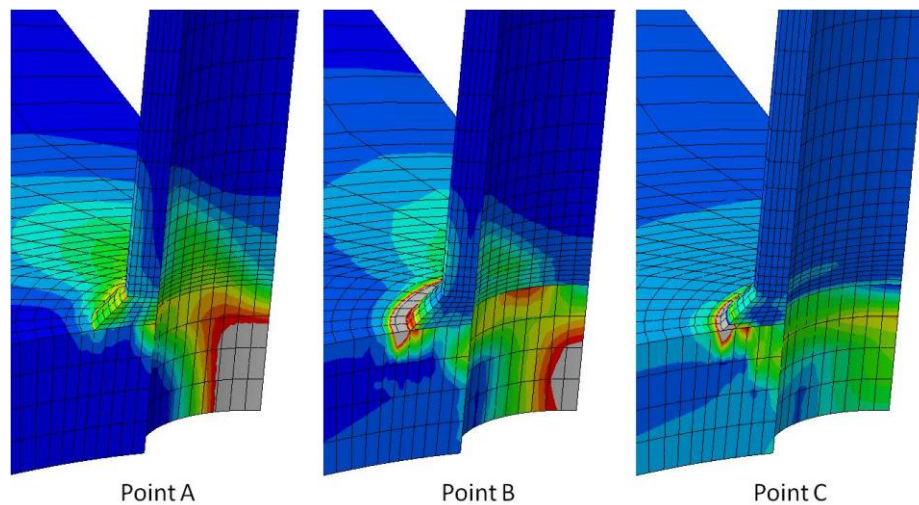


Figure 5.6 - Strict and Global Interaction Diagram

The point corresponding to zero cyclic load (point A in Figure 5.6) represents the limit load for internal pressure. The failure mechanism for this loading predicted by the LMM calculation is at the crotch corner, which is typical of this geometry subject to pressure loading. This mechanism dominates the failure at low levels of cyclic thermal loading. When the cyclic thermal load increases in magnitude (Point B), the material mismatch begins to play a more significant role in the failure. The difference in the thermal expansions causes a reverse plasticity mechanism at the material joins. When the internal pressure is applied, this then interacts with the concentration at the crotch corner to produce a failure mechanism which has a contribution from both loads.



**Figure 5.7 - Ratchet Mechanism at Point A, C and E**

At large levels of cyclic loading (point C), the material mismatch dominates the failure mechanism. The concentration due to the mismatch at these levels of thermal loading is such that even the severe stress raiser at the crotch corner is no longer a factor in the ratchet mechanism.

### **5.3.3.2 Validation**

Validation of these results has been achieved using elastic-plastic analysis in Abaqus. Figure 5.8 shows the results calculated by the LMM using temperature dependent results and the load points selected for full step by step analysis in Abaqus. Load points D, E, F and G are used to verify the ratchet boundary itself, and the points H to M are used to compare with the plastic strain ranges predicted by the LMM.

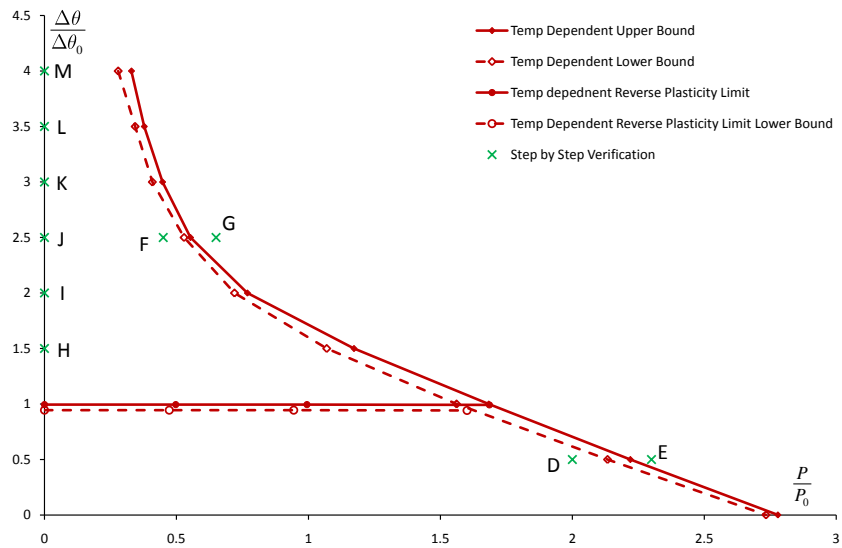


Figure 5.8 - Points Used for Comparison with Step by Step FEA

Point D lies within the elastic shakedown region, point F lies within the reverse plasticity region and the points E and G are beyond the ratchet limit. The step by step analyses were performed and the equivalent plastic strain at the most critical locations were checked to determine the cyclic response of the structure, and these correlate well with the ratchet bound predicted by the LMM. Figure 5.9a shows the plastic strain history for points D, E, F and G taken at the points of maximum plastic strain. Point D shows a strict shakedown response, the plastic strain ceasing to increase after ten cycles. Point E exhibits a clear ratcheting response. The plastic strain increases with every cycle at a constant rate, indicating a ratchet mechanism. Point G also shows a very strong ratchet mechanism.

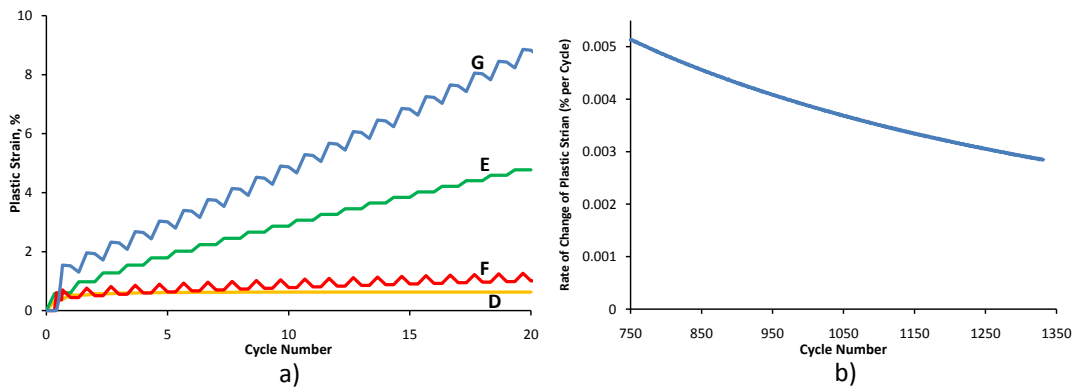
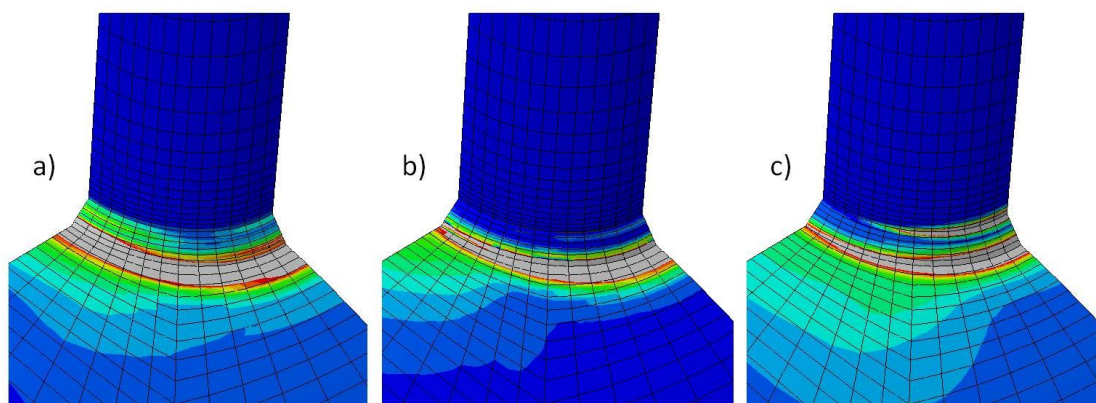


Figure 5.9 - Plastic Strain Response of Points D, E, F and G

The plastic strain history for point F should form a reverse plasticity mechanism, but it can be seen in Figure 5.9a that the plastic strain is still marginally increasing with each cycle.

Further Investigation of this load case reveals that, although the plastic strain is increasing within the cycles plotted, the rate of accumulation of plastic strain with each cycle is decreasing. Figure 5.9b plots the rate of change of plastic strain for point F when the analysis is performed for over 1000 cycles. It can be seen that the accumulation of plastic strain in each cycle falls to less than  $3 \times 10^{-3} \%$  per cycle and is still falling. If allowed to continue it is expected that this would fall to zero and a reverse plasticity mechanism would form. This result highlights the usefulness of the LMM in the analysis of cyclic problems in general. If step by step analysis were used alone, the result at point F may be interpreted as a ratcheting response. The LMM removes any ambiguity in these results, proving that the component is not ratcheting.

A qualitative verification of the LMM comes from its prediction of where the maximum plastic strains will occur. Figure 5.10 compares the equivalent plastic strain from points F, G and the corresponding point on the ratchet boundary at  $\Delta\theta/\Delta\theta_0 = 2.5$ . When comparing these contour plots an allowance must be made for the varying levels of internal pressure applied. Taking this into account the LMM predicts a plastic zone very similar to that from both step by step analyses, around the toe of the weld.



**Figure 5.10 - Predicted Failure Mechanism at a) Point F, b) the LMM at  $\Delta\theta/\Delta\theta_0 = 2.5$  and c) Point G**

The final validation presented here concerns the ability of the LMM to calculate plastic strain ranges. To do this, step by step analysis was carried out at points H to M in Figure 5.8. The location of the maximum plastic strain range in these analyses was found to be coincident with that predicted by the LMM at the same level of cyclic loading. Table 5.3 shows a comparison of the maximum plastic strain range calculated by both methods, and a very good agreement is observed.

**Table 5.3 - Comparison of Predicted Plastic Strain Ranges for Points H to M**

Normalised Cyclic Loading Level (from Figure 5.8)	Plastic Strain Range		% Difference
	Step by Step	LMM	
1.5 (H)	1.26E-03	1.27E-03	0.24
2 (I)	2.71E-03	2.71E-03	0.08
2.5 (J)	6.24E-03	6.19E-03	-0.74
3 (K)	9.54E-03	9.52E-03	-0.17
3.5 (L)	1.31E-02	1.31E-02	-0.09
4 (M)	1.69E-02	1.68E-02	-0.62

### 5.3.4 Internal Pressure and Moment Loading

The same geometry of pipe intersection was also analysed subject to a constant internal pressure and a cyclic in-plane bending moment. A half symmetry model was used, and once again the mesh was highly refined in the region of the weld. The length of the main pipe was reduced in an attempt to reduce the number of elements, giving the final model 4200 elements as shown in Figure 5.11a. Abaqus C3D20R elements were used for the analysis as per section 5.3.3. The cyclic bending moment is applied as a pure moment to the end of the branch pipe; the DLOAD subroutine was used to create a linear distribution of pressure across the branch which mimics the stress distribution of a pure bending moment. The pressure stress is near identical to Figure 5.5a and moment elastic solution is shown in Figure 5.11b.

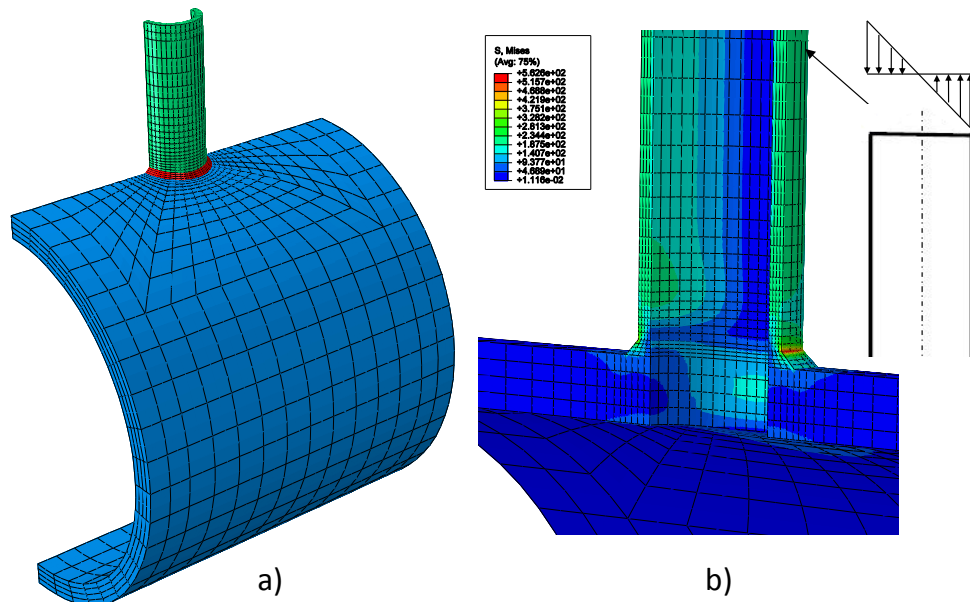


**Figure 5.11 - a) Half Model Mesh and b) Elastic Stress from Bending Moment**

### 5.3.4.1 Results

The ratchet interaction diagram was calculated for the dissimilar material pipe intersection subjected to this cyclic moment and constant internal pressure. This is shown in Figure 5.12, along with the reverse plasticity limit calculated by the LMM strict shakedown procedure. The applied constant internal pressure,  $P$ , is normalised against the initial applied internal pressure,  $P_0$ , of 10MPa. The applied cyclic moment,  $M$ , is normalised against the initial applied moment,  $M_0$ , of 741.95Nm. The form of the interaction diagram differs from that of Figure 5.8 in that there is a limit to the level of cyclic loading. This is typical of cyclic mechanical loads, which if large enough are able to cause limit state in the component.

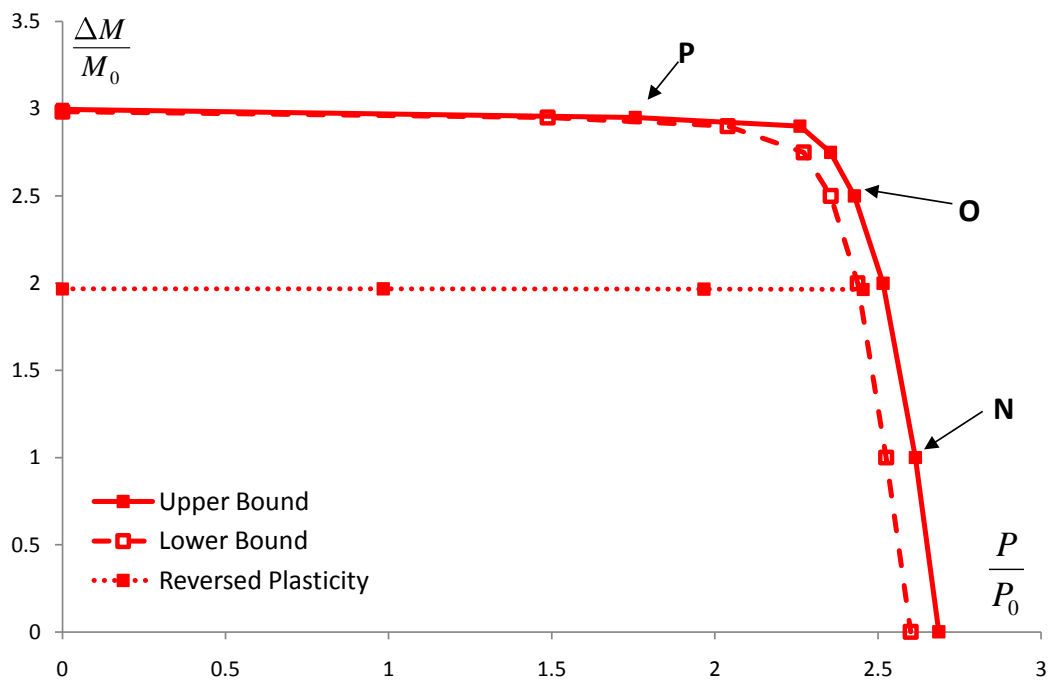
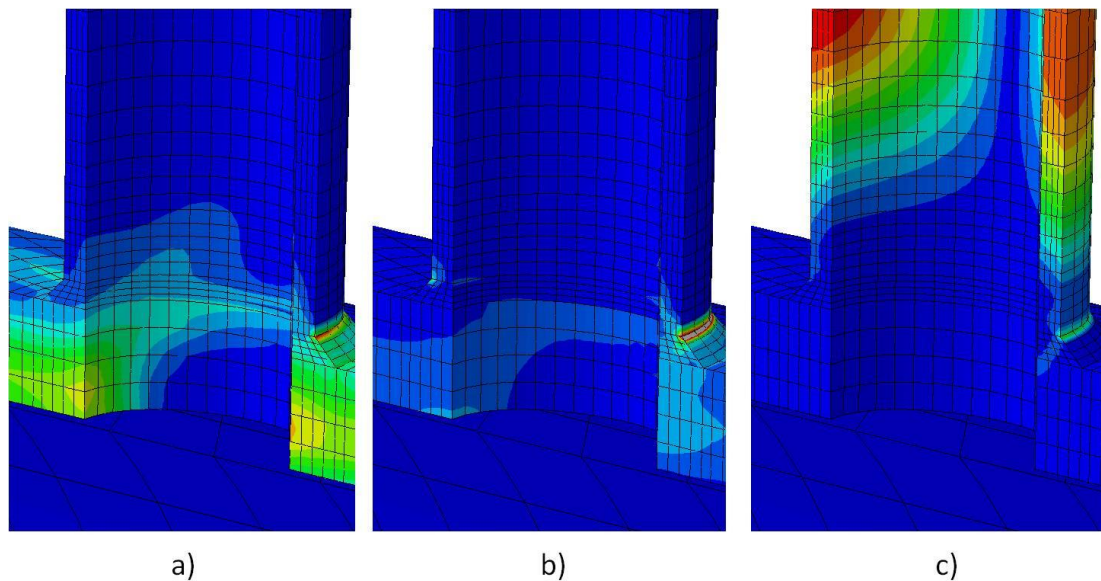


Figure 5.12 - Global Shakedown Interaction Diagram for Pressure Moment Loading

From this diagram it is instantly noticeable that there is little interaction between the pressure and moment loads. The ratchet boundary is relatively vertical at low levels of cyclic moment, and is relatively horizontal at low levels of constant pressure. This is easily explained by examining the elastic solutions. The internal pressure primarily affects the main pipe and the region around the crotch corner. There is a large stress concentration here, and all other stresses remain relatively low. Likewise the moment loading primarily affects the small pipe, causing comparatively small stresses in the main pipe. With both

loads acting relatively remotely from each other, an interaction is only possible when both loads reach high levels. This occurs at the "corner" of the interaction diagram, where both load levels are high.



**Figure 5.13 - Failure Mechanism at a) Point N, b) Point O and c) Point P**

This behaviour is reflected in the failure mechanisms seen in Figure 5.13. At low levels of cyclic moment, such as at point N, the failure mechanism resembles that of the limit load for pressure loading alone, where the crotch corner provides the source of the failure (Figure 5.13a). Similarly, at point P the large level of cyclic moment causes a failure pattern in the small pipe which is similar to that of the limit load of a beam in bending (Figure 5.13c). This result matches the failure mechanism seen in the EPERC example, where the failure is seen to occur in the branch pipe when subject to in-plane moment loading. Further verification comes from the work of Kim et al [112], which also predicts the limit load failure to occur in the branch pipe at this level of moment loading. At point O there is an interaction between the loads, as both become large enough to add significant levels of stress to the critical areas of the other load. The resulting failure mechanism is shown in Figure 5.13b, which combines the stress concentration at the weld from moment loading with the concentration at the crotch corner from pressure loading.

#### **5.3.4.2 Material Property Study**

In a finite element study, hypothetical situations can be explored to determine the effect various parameters have on the resulting behaviour. In the pipe intersection analysed here,

the room temperature yield stress of the SA508 small pipe is more than double that of the 316 of the main pipe, and the weld material yield is also significantly larger. It was postulated that if the yield stresses of the small pipe and weld were reduced then there may be more of an interaction between the two loads. Figure 5.14 shows the original results from Figure 5.12 with two further ratchet boundaries and their accompanying reverse plasticity limit. One is for the case where the entire pipe intersection is made from 316 steel (including the weld), named Case 1. The second is where the main pipe has properties of 316 and the small pipe and weld are given a yield stress which is 75% of that of 316, named Case 2.

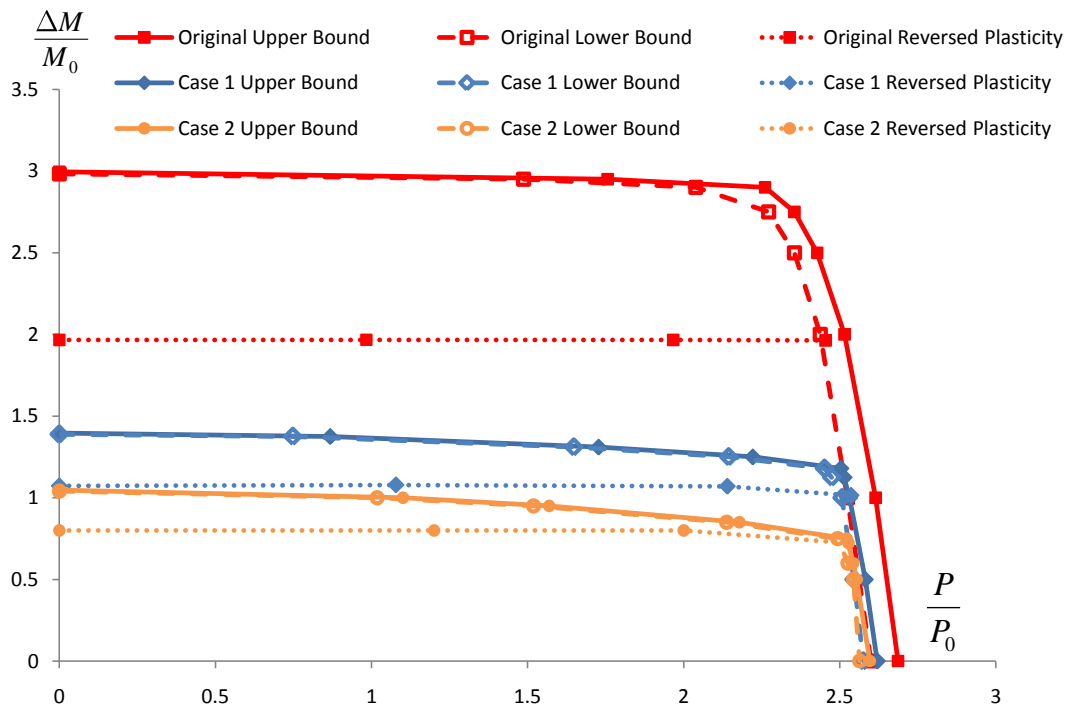


Figure 5.14 - Global Shakedown Interaction Diagram for Original Pipe, Case 1 and Case 2

Several observations can be made from this set of results. First of all, the limit load for internal pressure is not significantly affected. This is to be expected as the failure occurs at the crotch corner in the main pipe where the yield stress is unchanged from the original case. The gradient of the global shakedown bound at low levels of moment loading is unchanged, meaning that there is no change to the interaction of the loads at these levels of cyclic bending. To gain more of an insight into the interaction at higher levels of cyclic bending moment, the same results were plotted with the cyclic bending moment normalised against the limit moment for the small pipe,  $M_L$ . This is shown in Figure 5.15.

When the results are normalised in this way it is clear that the reduced yield stresses of Case 1 and Case 2 cause the interaction to begin at lower levels of normalised cyclic moment. This is confirmed by the contour plots in the transition region, which show the same shift in mechanism as in Figure 5.13 but at lower values of normalised cyclic bending moment.

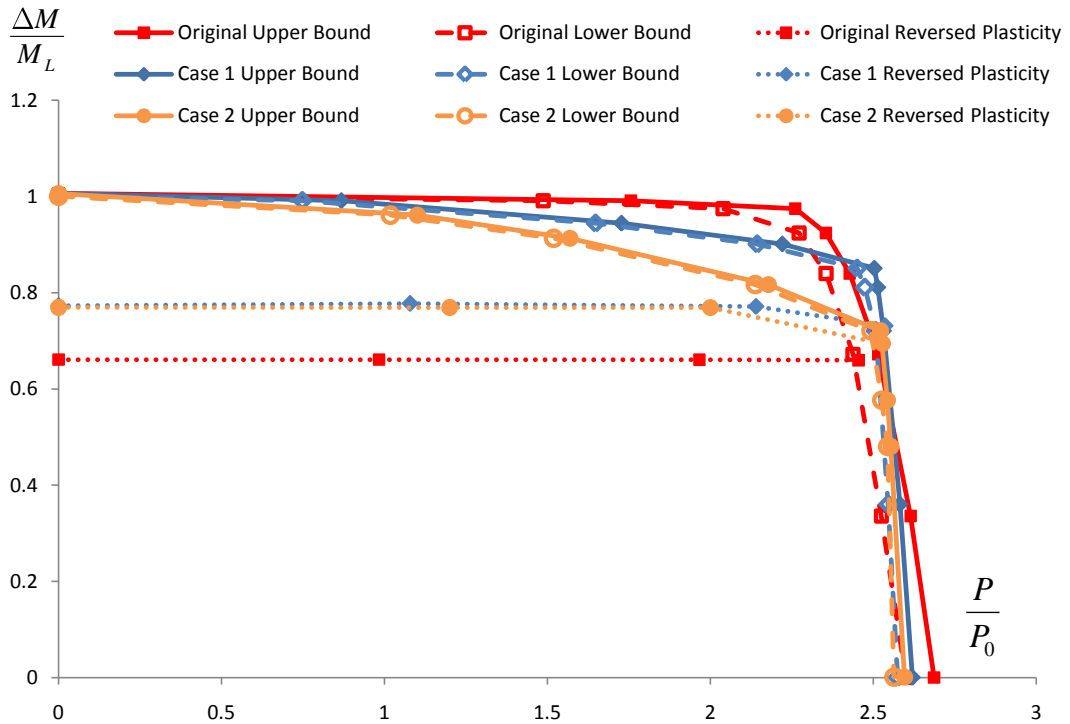


Figure 5.15 - Normalised Interaction Diagram of Original Pipe, Case 1 and Case 2

### 5.3.5 Pipe Intersection Summary

A pipe intersection with a dissimilar material joint was selected for global shakedown analysis using the LMM. This was chosen to represent a more industrially relevant geometry, and so prove that the LMM was suitable for use in EDF. The results for cyclic thermal loading and steady state internal pressure have been compared to elastic-plastic FEA with good agreement seen for the global shakedown limit, plastic strain ranges and predicted locations of failure.

The cyclic moment and steady state internal pressure loading results demonstrate the hypothetical situations and sensitivity studies possible using the LMM i.e. investigations into the behaviour of components under different circumstances, which is achieved in this case by altering the mechanical properties of the three materials. In an R5 assessment it is

recommended that a sensitivity study is performed to ensure the results are not significantly altered by minor variations in the input parameters. The changes to the properties conducted in section 5.3.4.2 is an extreme example of this, but represents the possibilities that exist when the LMM is utilised in this way.

## **5.4 Summary and Discussion**

Some Validations of the LMM global shakedown procedure have been presented in this chapter, and in general the LMM is able to produce favourable results. The limit loads of notched bars show an almost identical agreement with those of the strict shakedown procedure and Abaqus limit analysis, which in turn correlate well with the theoretical solutions. The Bree Cylinder case was revisited where the effects of temperature dependent material properties were also included. The LMM was able to predict the global shakedown limits for the original Bree loading very well. Where the loading of Bradford is concerned, when both loads are cyclic, an approximation of the global shakedown limit is obtained. Slightly less favourable results are seen, which highlights the limitations of the LMM where no steady state loading is applied.

The global shakedown behaviour of a pipe intersection with a dissimilar material join is also investigated. This shows the applicability of the LMM to geometries and loading which are more commonly seen in EDF. The interaction diagrams and plastic strain ranges produced for cyclic thermal loading by the LMM have been verified against step by step FEA and very favourable results are observed.

The sum of these comparisons contributes towards fulfilling criteria 2 from section 1.6, so that confidence can be built in the solutions provided by the LMM.

## **6 The Creation of a LMM Structural Analysis Tool**

### **6.1 Introduction**

One of the primary objectives of this project is to deliver the LMM in a form where it can be readily used by EDF engineers as an analysis tool. This will allow EDF engineers to access the LMM solution methods without having to make any of the changes to the subroutines required to run a LMM analysis as was previously required.

This chapter describes this analysis tool which includes the re-structuring of the user-subroutines and the creation of a graphical user interface. This will allow EDF engineers to perform LMM strict and global shakedown analyses of components with several options available within the analysis (such as temperature dependent material properties). This in itself is intended for regular use in EDF as a self contained analysis tool, but is also the starting point for a continuation project which will add further functionality based on recent developments of the LMM framework. Because of this, and for the sake of short term support of the code, this chapter and accompanying appendices aim to provide a comprehensive description of the structure of the LMM tool, subroutines and scripts.

### **6.2 Preliminary Considerations**

#### **6.2.1 Previous LMM Versions**

The original incarnation of the LMM code was created in the University of Leicester [120] and is still used for research purposes today. Several subroutines exist, and a LMM analysis consists of two stages. In the first stage an elastic analysis for each applied load and temperature distribution is performed using the elastic analysis UMAT subroutine. For each of these analyses the elastic stress tensor for each integration point is written to a text file, and the integration point temperature is written to a separate text file. The second stage of this analysis uses a second UMAT subroutine and these text files to perform the strict or global shakedown calculation. In this second stage some changes are required to the UMAT code in order to set up the analysis. For example, the number of integration points per element and the total number of elements in the model needed to be changed so that the arrays could be sized appropriately. The code defining the load cycle also requires updating, which reads the stress and temperature text files to generate the applied stresses at each point in the load cycle.

For an analysis using this set of subroutines both the elastic analyses and the shakedown calculation are submitted using the Abaqus batch command i.e. the Abaqus input file for the model is required. This input file is generated using Abaqus CAE for a complete model. The majority of the content of the input file is common between the elastic and shakedown calculations (such as geometry and boundary conditions). However there are some differences which must be performed manually (such as requesting the energy outputs associated with a UMAT subroutine).

As previously mentioned, a re-structuring of these subroutines was performed by Tipping [34] so that the LMM could be used with minimal code changes. The process of performing an analysis is similar to the original method in [120] in that the analysis retains the two stages of elastic and shakedown calculations, and text files are still used to pass the stresses and temperatures between the stages. The major difference with this procedure is that the load cycle is defined via a formatted text file which was read by the subroutines. This significantly reduces the code changes required for an analysis. However, the changes to the Abaqus input file still needed to be performed manually.

The creation of a formatted text file to configure the LMM analysis was a major step in the usability of the LMM, and in fact draws a parallel with the way in which any conventional Abaqus analysis operates. In an Abaqus analysis, the user creates the model in CAE and submits it for analysis. CAE then creates the formatted text file (the input file) which is passed to the Abaqus solver for solution. The text file for the LMM analysis is equivalent to the input file, the only difference being that it is created manually. The creation of a text file is also adopted here as it is a simple and robust method for passing information from the LMM user interface into the subroutines. The major difference in this work is that the text file is generated by the user interface rather than manually.

## **6.2.2 Customising Abaqus**

Abaqus contains a large number of options for the user to customise a model or analysis for their particular situation. To obtain user-generated solution options the user-subroutines can be used, which is how the LMM has been implemented. In addition to this Abaqus CAE contains the option to use scripts to perform operations on the model or results databases. These scripts are written in the Python open source scripting language [121], and Abaqus has extended this language to allow operations to be performed within CAE itself. These scripts can be used to perform all operations which are available through the CAE interface

(i.e. applying loads, meshing, plotting results etc) and can also query the model/odb for values. A typical example where scripts serve a useful function is in a sensitivity analysis, where an automatic process can vary a particular value in a model, re-submit for solution, query the results and decide whether a further iteration is required.

The use of python scripting within Abaqus is a very powerful tool, because options also exist to use this language to customise the CAE user interface itself. This can be achieved by creating either an entirely custom CAE interface or a plug-in to the standard CAE. The ability to create a custom GUI is a powerful tool as the modules and toolsets which are not desired can be removed and custom functions can be added. Abaqus Viewer is an example of this, where all the analysis toolsets and modules have been removed, leaving only the visualisation module for viewing output databases. Plug-ins form another useful avenue of adding functionality to the Abaqus CAE interface. Plug-ins can be created for a variety of purposes; commonly they are used to streamline tasks which are complex to perform or are performed regularly. An example of this is the automatic generation of geometries, such as the "Create Plate" plug-in which is contained within every standard installation of Abaqus CAE shown in Figure 6.1. This simple plug-in allows the user to enter the dimensions of the plate and, upon clicking OK, the scripts use these values to automatically create the desired plate.

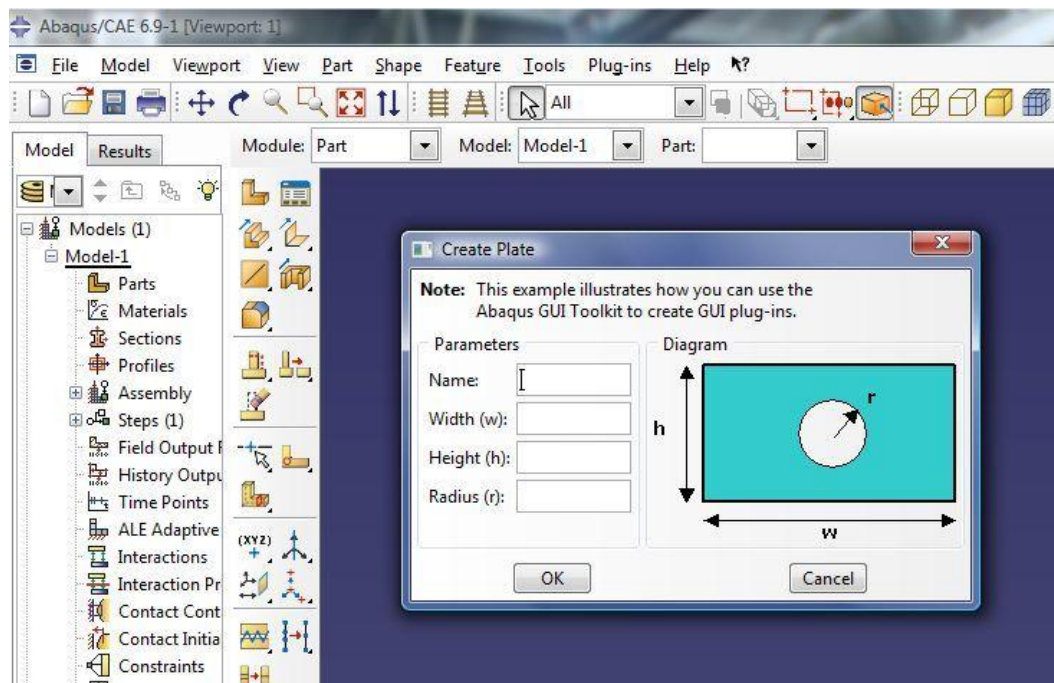


Figure 6.1 - The "Create Plate" Plug-in Dialog Box

For the LMM application a plug-in has been selected over a custom CAE interface. A plug-in can be accessed through the conventional CAE interface during normal use, whereas a custom CAE would need to be opened separately. An EDF engineer with an existing Abaqus model will be able to access the LMM through CAE, and the plug in will guide them through the process of entering the information needed to run a LMM analysis.

The creation of a plug-in to gather the required data and format the model will require a set of subroutines which are compatible with this model configuration and the text file used to pass in the data for the analysis. The re-structuring of the subroutines to accommodate this presents the opportunity to re-write them for multiple CPU solution, especially since even basic desktop computers now have dual or quad core as standard. Some features of the UMAT code written by Chen [120] and Tipping [34] are not amendable to solution with multiple CPUs, such as:

- Reading text files (for stress and temperature) from within a UMAT subroutine during the solution. This process becomes significantly slower when multiple cores are trying to access a single file. This slows the overall solution, defeating the purpose of multiple CPU solution.
- Using model sized arrays within UMAT to store the information for the entire model. Such arrays can be stored in common memory so that all CPUs have access to them, but the access would be slowed because only one CPU can access the array at a time. Instead a method which uses the Abaqus results files to store and access the data must be used instead.
- The use of SAVE statements, which means that the data in arrays is not saved between increments. Once again, the results files must be used to store and access information required between increments.

With all of these considerations, a plug-in has been created and the LMM subroutines have been re-written. The plug-in posts dialog boxes to gather the required information and data from the user. When the process is complete, the plug-in configures the model for the LMM analysis using scripts. The plug-in also writes the text file containing relevant data for the subroutines. The subroutines themselves have been re-written to allow multiple CPU solution in the UMAT routine.

The structure and function of the plug-in is dictated by many of the features of the subroutines and their re-structuring for multiple CPU solution. Therefore the subroutines will be described first, followed by a description of the plug-in created to use them.

### 6.3 Re-structuring of the Subroutines

Figure 6.2 shows the general structure of a LMM solution with the new set of subroutines.

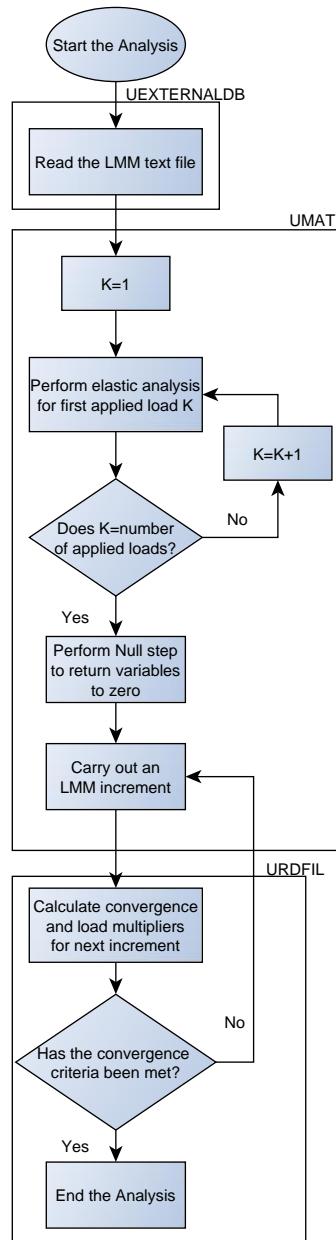


Figure 6.2 - Overall Structure of a LMM Solution

The starting point of this process assumes that the plug-in has created a formatted text file containing information about the analysis such as the convergence tolerance, analysis type, load cycle and temperature dependent material data. The reading of this text file uses the Abaqus UEXTERNALDB subroutine. This subroutine is called at the beginning of every analysis by Abaqus before the solution begins and also at the end of the analysis. It is intended for communication with external files and software and uses only a single CPU, regardless of how many are requested for the actual solution stage. This makes this subroutine ideal for reading the LMM text file produced by the plug-in.

When UEXTERNALDB has completed reading the text file at the beginning of the analysis, then the solution begins. This means that the UMAT subroutine is called for each integration point which has been defined as a User-material from within Abaqus CAE. Defining areas of the model as a User-material within Abaqus CAE tells the solver to look to the UMAT subroutine for the material behaviour of those areas. This solution stage of the analysis uses the number of CPUs requested by the user, and so this UMAT subroutine must be coded to accommodate this.

As part of the restructuring, all the elastic calculations for the applied loads and the LMM calculation itself have been incorporated into a single Abaqus analysis. Each elastic calculation is carried out as a single analysis step within this Abaqus analysis, with the LMM calculation being performed in the final analysis step. This consolidation into a single Abaqus analysis means that the passing of stresses and temperatures in text files is no longer required. Instead the results file itself can be used for storage and access of this information. When defining a User-material in Abaqus CAE, the user is able to specify the number of Solution-Dependent State Variables (SDV) for that material. This is the number of memory spaces available to the UMAT in the output database file, and so is commonly used to provide contour plots of user defined variable fields calculated during the UMAT solution. However, the direct access that UMAT has to the SDVs means that they can also be used as a way of storing values and data to be used during the analysis. This has been used to pass elastic stresses and temperatures between the elastic analyses and the LMM analysis, removing the need for text files and therefore removing this restriction to multiple CPU solution.

Returning to Figure 6.2, the UMAT subroutine is divided into elastic and LMM sections. An elastic analysis is performed for each applied load and the stresses and temperatures are

stored in the SDV slots. When all applied loads have been considered, an intermediate "null" step is included. This allows key variables in the subroutine to return to zero before commencing the LMM solution. The LMM solution itself uses the stresses and temperatures from the SDVs along with the load cycle and material property data read in the UEXTERNALDB subroutine to perform the calculations.

Within the LMM solution stage, the data previously stored in model-sized arrays is now stored using the SDVs. Abaqus itself manages the multiple CPUs accessing the results files as it would during any analysis which uses multiple CPUs. These existing methods for managing multiple CPU solution means that the UMAT subroutine can use Abaqus itself to manage the multiple CPUs accessing the data simultaneously. The alternative, placing these model-sized arrays into common memory, would mean the CPUs would have to queue for access to the array and could produce unpredictable results.

The URDFIL subroutine is called by Abaqus at the end of every increment, and so is used here to perform a number of tasks. Firstly, the URDFIL can be used to access the results file and so is able to obtain the volume integrals required to calculate the upper bound multipliers of equations (3.23) and (4.38). Being called at the end of the increment means that the URDFIL is used to provide a summary of the increment to the user to give an indication of how the solution is progressing. Finally, the URDFIL routine can also be used to terminate an analysis. Convergence calculations are performed in URDFIL and if the convergence criteria are satisfied then the analysis is ended. If convergence is not met, then the solution continues for a further increment where the UMAT is called and the LMM calculations are performed once again.

With these subroutines there are three LMM analyses possible: strict shakedown, steady state cycle only and steady state cycle + ratchet limit (i.e. the global shakedown limit). The subroutines have been programmed to be flexible and allow as many options as possible within these three analyses. These options are summarised in Table 6.1. A full description of all the subroutines is provided in Appendix D. This set of subroutines requires that the Abaqus model is configured in a certain way (e.g. one analysis step per applied load) and so provides a set of requirements which has dictated the design of the plug-in and its operation.

**Table 6.1 - Functions Available in Each LMM Analysis**

Analysis Option	Strict Shakedown	Steady State Cycle Only	Steady State Cycle + Ratchet Limit
All structural continuum element types (3D, axisymmetric, plane strain and plane stress)	✓	✓	✓
Temperature dependent Young's modulus and yield stress	✓	✓	✓
Perfect Plasticity Material Model	✓	✓	✓
Ramberg-Osgood Material Model (which may also be temperature dependent)		✓	✓
Any number of points possible in the load cycle	✓	✓	✓
Ability to select which loads to scale during solution	✓		✓
Two convergence options (see section 6.4)	✓		✓

#### **6.4 Graphical User Interface via an Abaqus Plug-in**

Upon selecting the LMM plug-in from the "plug-ins" menu in Abaqus CAE, the user is then guided through the process seen in Figure 6.3, which is implemented within the framework of Figure E-1 in Appendix E. The Main dialog box is posted which prompts the user to select which model from within the current CAE session they would like to analyse and which type of LMM analysis - strict shakedown, steady state cycle or steady state cycle + ratchet limit. Selecting a steady state cycle analysis means that only stage 1 of the global shakedown procedure is performed to give the steady cyclic state of the component along with the associated strain ranges. The second stage, to find the global shakedown limit is not performed.

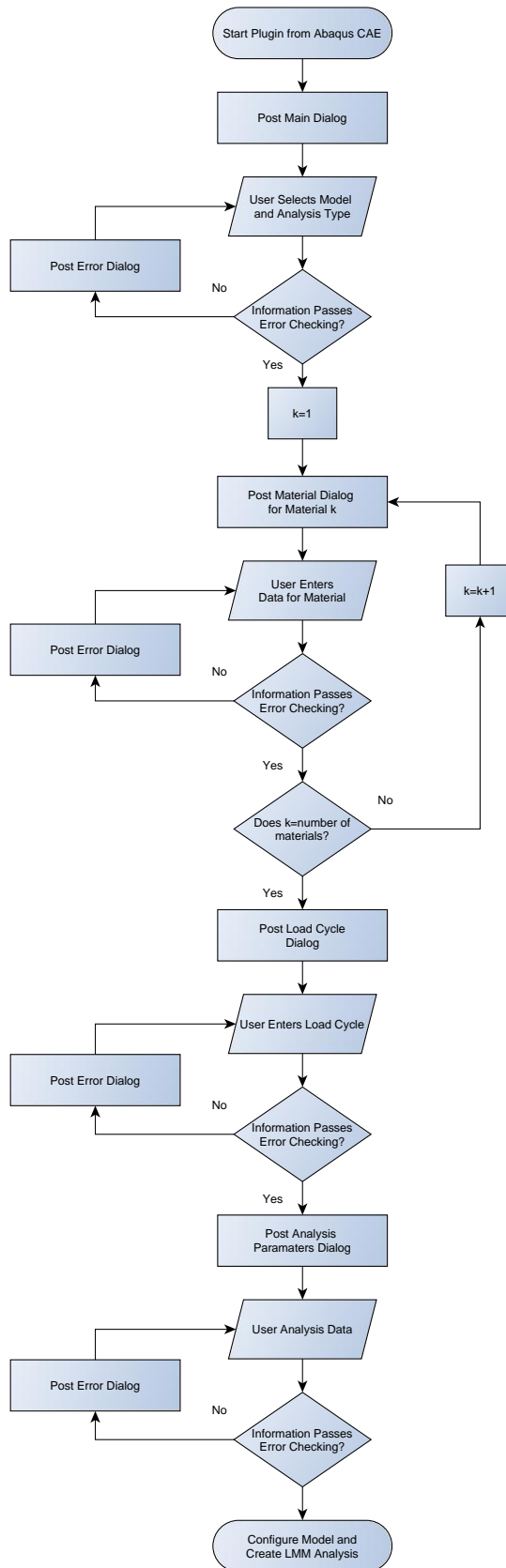
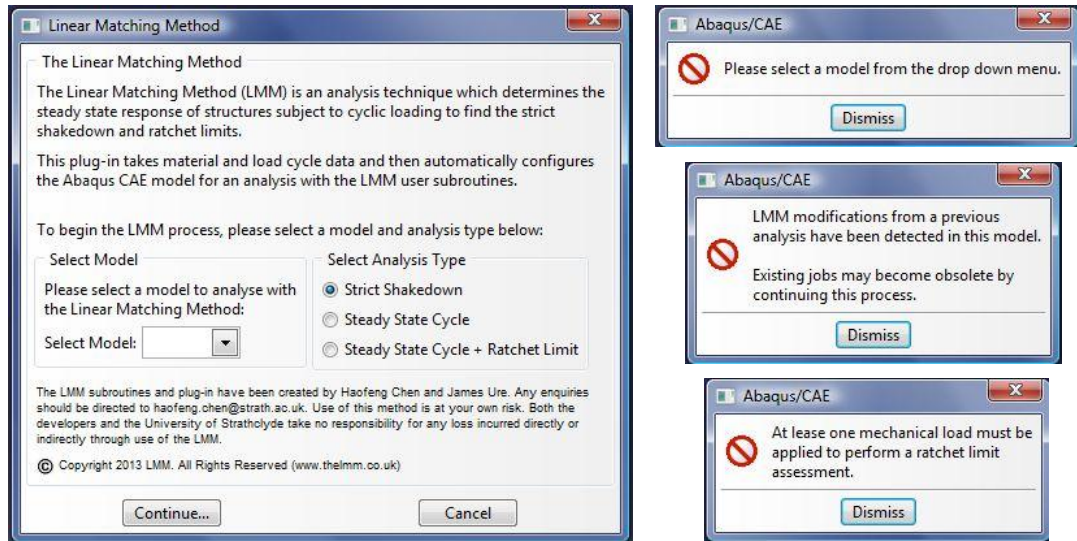


Figure 6.3 - High Level Overview of LMM Plug-in from the Users Perspective

With the information from this dialog, background scripts perform a series of checks on the selected model to ensure it is possible to perform a LMM analysis successfully. This includes very basic checks, such as ensuring the component is meshed. It also includes checks more specific to the LMM, such as ensuring that at least one mechanical load is applied when a ratchet limit analysis is selected. Any error found is displayed to the user so that it may be remedied. The Main dialog box and example error boxes are shown in Figure 6.4.



**Figure 6.4 - Main Dialog Box and Possible Error Messages**

Upon passing these checks, a series of subsequent dialogs are posted. This begins with the material data. A Material dialog box is posted for each material which is used in the current model. Within each of these dialogs the user is prompted to enter the Young's modulus, yield stress, Poisson's ratio and the thermal expansion coefficient. The Young's modulus and yield stress may be temperature dependent, which is enabled by selecting this in the check box. In many situations the model will have already been used in a previous analysis, meaning material property data has already been defined in CAE. If this is the case the "Extract" function can be used, which queries the current material for the four properties required for the LMM analysis and populates the dialog box accordingly. The Material dialog box is shown in Figure 6.5, alongside some of the possible error messages.

When either a steady state cycle or steady state cycle + ratchet analysis is chosen the user has the option of using a Ramberg-Osgood model in stage 1 of this calculation. In this case

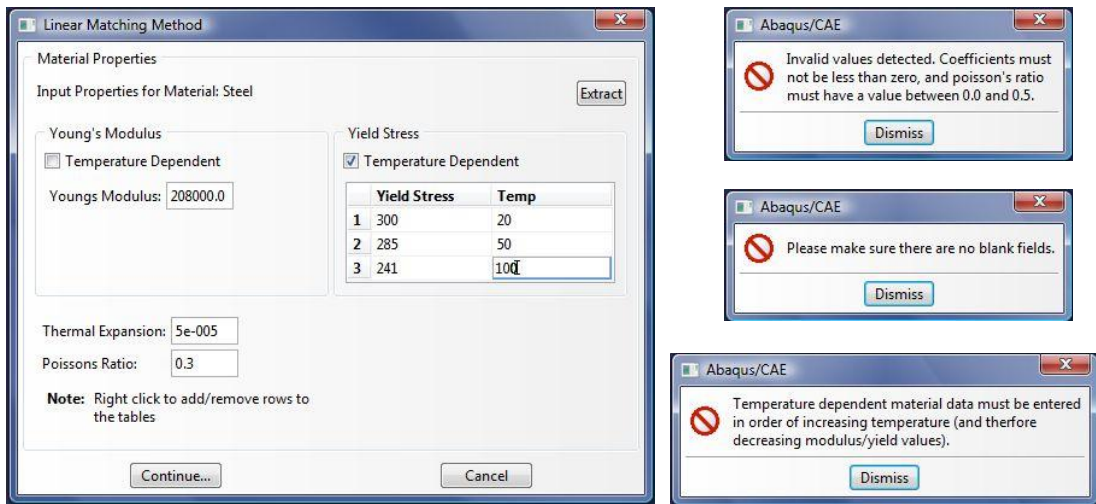


Figure 6.5 - Material Properties Dialog Box and Possible Error Messages

the Material dialog is shown in Figure 6.6a. The Ramberg-Osgood parameters may be temperature dependent or independent in the same way as the modulus and yield. A function is also included to link the R-O parameters to the yield stress. This function calculates the 0.2% proof stress from the R-O parameters entered and populates the yield stress fields accordingly. Additional advice is available for the R-O model by selecting the "Tip" button, which displays the box shown in Figure 6.6b.

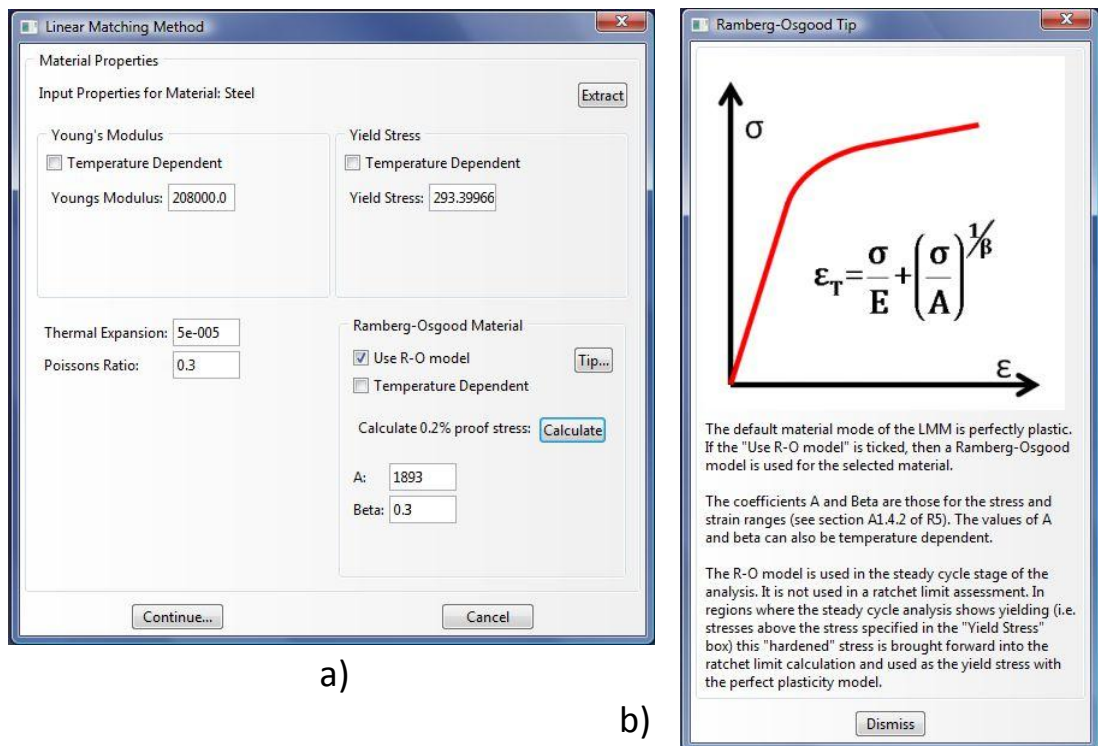


Figure 6.6 - a) Material Properties Dialog with Ramberg Osgood Option and b) "Tip" Box

A Material dialog box is shown for each active material in the model (i.e. each material which has been assigned into a section assignment in the parts). When this is complete, the plug-in moves on from materials to the load cycle.

The Loadcycle dialog boxes shown in Figure 6.7 are broadly the same for all analysis types, but contain some small differences. If a strict shakedown analysis is selected, Figure 6.7a will be shown. For a steady state cycle the load scaling box in Figure 6.7b will be shown instead, and for a steady state cycle + ratchet the load scaling options of Figure 6.7c apply.

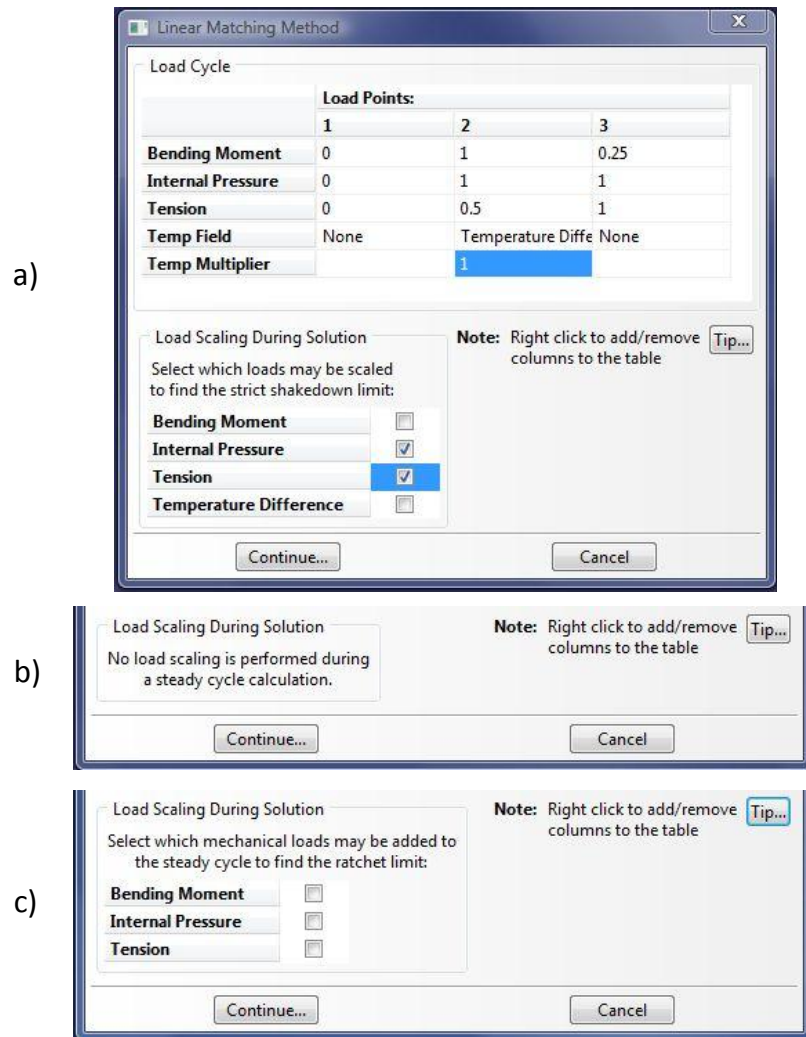


Figure 6.7 - Loadcycle Dialog and Load Scaling Options

In all cases the Loadcycle table at the top of the box is present. This table allows the user to define the load cycle by adding any number of time points and scaling the loads to the appropriate level for that time point in the cycle. At each time point a temperature field can also be applied by selecting desired predefined field from the drop-down list. Selecting the

"Tip" button displays a box with additional information on populating this table and a simple worked example as shown in Figure 6.8.

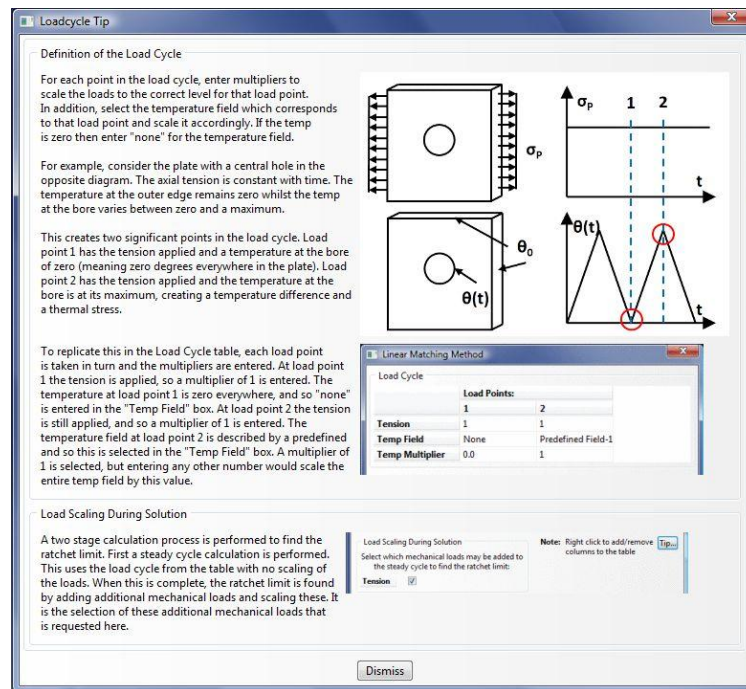


Figure 6.8 - "Tip" Box for Loadcycle

The subtle difference between the three analysis options comes when selecting the loads which may be scaled. In a strict shakedown analysis, any of the applied loads and temperature may be selected for scaling. These loads and temperature fields will be scaled by the load multiplier,  $\lambda$ , to find the strict shakedown limit. The loads which are not checked as scalable are left at the magnitudes given in the load cycle table.

A steady state cycle analysis has no option for scaling loads. This is because no load multiplier exists in stage 1 of the global shakedown procedure. The load levels given in the table are fixed at those values and the stage 1 procedure determines the steady state response due to this load cycle.

Stage 2 of the global shakedown procedure requires that an additional steady state load is applied to find the global shakedown limit. Therefore the user may select which of these loads are to be added as additional loads in stage 2. The "Tip" box also contains advice on the load scaling for each analysis type.

The Analysis Parameters dialog shown in Figure 6.9 is the final dialog box and gathers the data required to create the analysis (such as the job name and working directory) and the

solution controls (convergence level and maximum number of increments. The current working directory is automatically detected and displayed, but the user may choose to change this. Default values of convergence levels are also displayed for inexperienced users.

There are different convergence options available depending on the analysis type chosen. A strict shakedown analysis can use either the difference between consecutive upper bounds (which historically was the way convergence was judged) or can use the % difference between lower and upper bounds. A steady state cycle convergence is based on volume integrals of modulus between consecutive increments. If there is little change in this value then the stress fields are not changing and so have reached a converged steady state behaviour. The value of convergence in the dialog box represents the percentage change of this volume integral in consecutive increments. A ratchet limit analysis requires convergence values for both stages of the procedure. Stage 1 is identical to that of a steady state cycle analysis, and the convergence options for stage 2 are identical to those for the strict shakedown analysis. Once again, the "Tip" box gives additional information and help to the user if required.

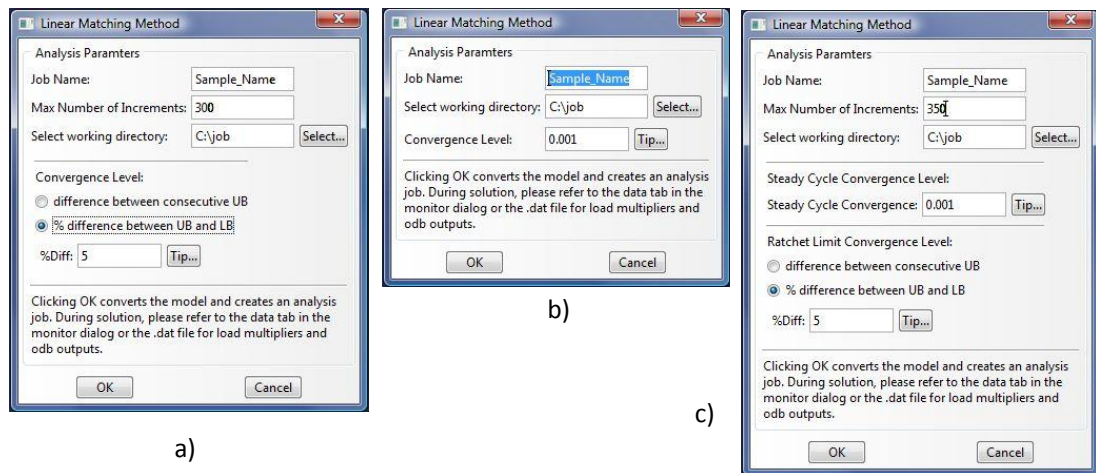


**Figure 6.9 - Analysis Parameters Dialog Boxes for a) Strict Shakedown, b) Steady State Cycle and c) Steady State Cycle + Ratchet**

If the data entered in the Analysis Parameters box passes the error checking stage, then the user interface portion of the plug-in is complete. In total the dialog boxes will have gathered the following information: model name, analysis type, material properties (temperature dependent), load cycle, which loads are scalable, job name, max number of increments, convergence criteria and working directory. The next stage of the plug-in is to

use this information to configure the Abaqus model and write the LMM text file containing the information for the subroutines. The changes to the model have been designed so that the original model is entirely recoverable i.e. nothing of the original model is deleted. Instead items are suppressed or copied so that the LMM configuration of the model can be applied. All the model data is passed into a set of scripts which write relevant information to the LMM text file and perform a series of changes to the model. Firstly, the LMM text file is created and populated with information about the analysis. An example of this is shown in Table 6.2.

**Table 6.2 - LMM Text File Example**

LMM Text File	Explanation
<pre> Analysis Type: STRICT_SHAKEDOWN  Max Number of Increments: 350  Convergence (%Diff) 5.00000  Dimensionality THREE_D  Number of Applied Loads 4 Number of Load Instances 2  Load:Bending Moment NOT_SCALABLE 0.00000 1.00000 Load:Internal Pressure SCALABLE 0.00000 1.00000 Load:Tension SCALABLE 0.00000 0.50000 Load:Temperature Difference NOT_SCALABLE 0.00000 1.00000 </pre>	<p>The analysis type. May also have a value of STEADY_CYCLE_ONLY or STEADY_CYCLE_AND_RATCHET</p> <p>Max number of increments defined by the user should convergence prove elusive</p> <p>The convergence option chosen and the value. The (%Diff) flag is present when the percentage difference convergence option is used. It is not present when the difference between upper bounds is selected</p> <p>Dimensionality flag. May also have a value of THREE_D, AXISYMMETRIC, PLANE_STRESS or PLANE_STRAIN.</p> <p>The number of loads (including temperature distributions) and load instances in the cycle</p> <p>The multipliers for each load as entered in the Loadcycle table. The LMM uses these multipliers to construct the load cycle in the code and so determine the elastic stress at each load point. The SCALABLE/NOT_SCALABLE flag dictates whether the load can be scaled using the calculated <math>\lambda</math> in each increment.</p>

Once this information has been written to the LMM text file, the next stage is to configure the loads and boundary conditions in the Abaqus CAE model. Two basic requirements dictate the way in which this is achieved. The first requirement is that the elastic stress for each applied load must be known so that superposition can be used to construct the load cycle in the subroutines. The second requirement is that the same boundary conditions are used for all elastic analyses and the shakedown/steady cycle/ratchet analysis. Therefore one analysis step is created for each of these applied loads and predefined fields and the corresponding load or field is applied in isolation in that step. Figure 6.10 shows example Load Manager and Predefined Field Manager tables from Abaqus to illustrate this. A "Null" analysis step is created where no loads are applied, which allows the subroutines to return key variables to zero. The final analysis step created is for the shakedown/steady cycle/global shakedown analysis. This situation allows the LMM subroutines to obtain the elastic stresses for each load in turn, return the subroutine variables to zero and then carry out the shakedown/steady cycle/ratchet analysis. The boundary conditions are moved to the first step and set to propagate through the entire analysis. The original analysis steps are suppressed, allowing the user to recover the original state of the model.

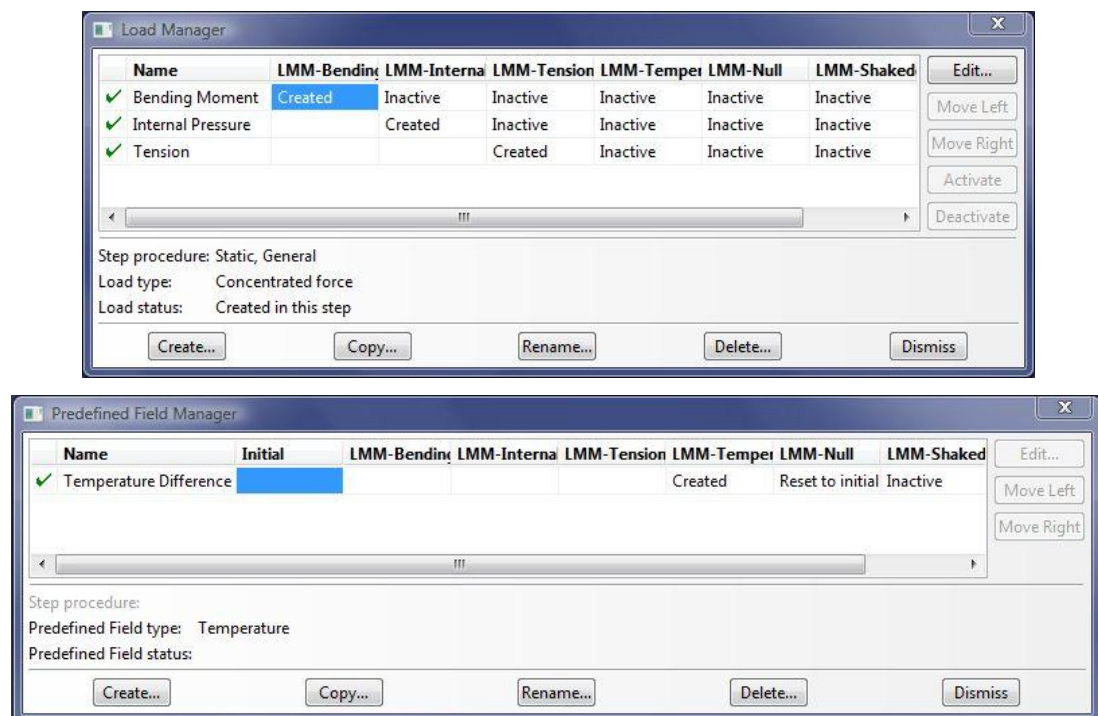


Figure 6.10 - Load and Predefined Field Manager Dialogs

The materials are the next area to receive attention. The LMM requires a User-material to be defined in Abaqus to link with the UMAT subroutine. In Abaqus CAE a copy of each

active material is made which is defined as a User-material for the LMM analysis. The original material is retained so that the user may recover the original material properties. Values for temperature independent Young's modulus, Poisson's ratio, yield stress and the Ramberg-Osgood parameters are entered as constants in this material. A User-material is only able to include multiple constants, not tables. Therefore if a property is temperature dependent then a value of zero is entered for this constant and the temperature dependent values are appended to the bottom of the LMM text file. An example of this is given in Table 6.3.

**Table 6.3 - Material Properties Section of the LMM Text File**

LMM Text File	Explanation
<pre>Material Properties: Number of materials: 3</pre>	<p>The number of materials is printed so that UEXTERNALDB knows how many materials to look for in the file</p>
<pre>Material:SA508 Temperature Independent Modulus Temperature Independent Yield Stress Perfectly Plastic Material</pre>	<p>The material name is printed to be read by UEXTERNALDB. The modulus and yield for each material may be either: Temperature Independent or Temperature Dependent. Temp independent values are written to the User Material in Abaqus</p>
<pre>Material:INCONEL 82/182 Temperature Independent Modulus Temperature Dependent Yield Stress: 2 3.7860000000e+002      20.000 3.1580000000e+002      320.000 Perfectly Plastic Material</pre>	<p>Where temperature dependent properties are found, these are printed in a formatted way so that UEXTERNALDB is able to read them.</p>
<pre>Material:STEEL 316 Temperature Independent Modulus Temperature Independent Yield Stress Temperature Independent Ramberg-Osgood</pre>	<p>For each material, the words Perfectly Plastic Material Are printed unless a Ramberg-Osgood material is selected. Where a Ramberg-Osgood model is used with temperature dependent properties then a formatted list of these is provided in the same way as modulus or yield. Otherwise it is declared as temperature independent and the values are written in the User Material.</p>

After the materials configuration, the field and output requests are created. Once again any original requests in the model are suppressed rather than deleted. The most important of the LMM output requests is the variable SDV, which is the user-defined outputs from the UMAT subroutine. Requesting this output allows the user to view contour plots of the variables calculated within the UMAT routine, and so it is vital that this is included.

In addition to the field and history outputs, the energy file output must be requested so that the volume integrals needed for the upper bound load multiplier of equation (3.23) can be accessed. The only way to achieve this is by adding commands to the keyword block for the model, which contains all the commands printed to the input file when the analysis begins (shown in Figure 6.11). Part of this script inserts the commands to the keyword block as if a user had manually typed them. To recover the initial state of the model a user simply clicks the button "Discard All Edits", which removes any user-added commands.

The final script creates the LMM analysis job with the correct subroutine for the analysis type selected. When created, the user may edit the job in the same way as any other Abaqus job by selecting the number of CPUs to solve with, queue options etc. Finally the user may submit the analysis for solution.

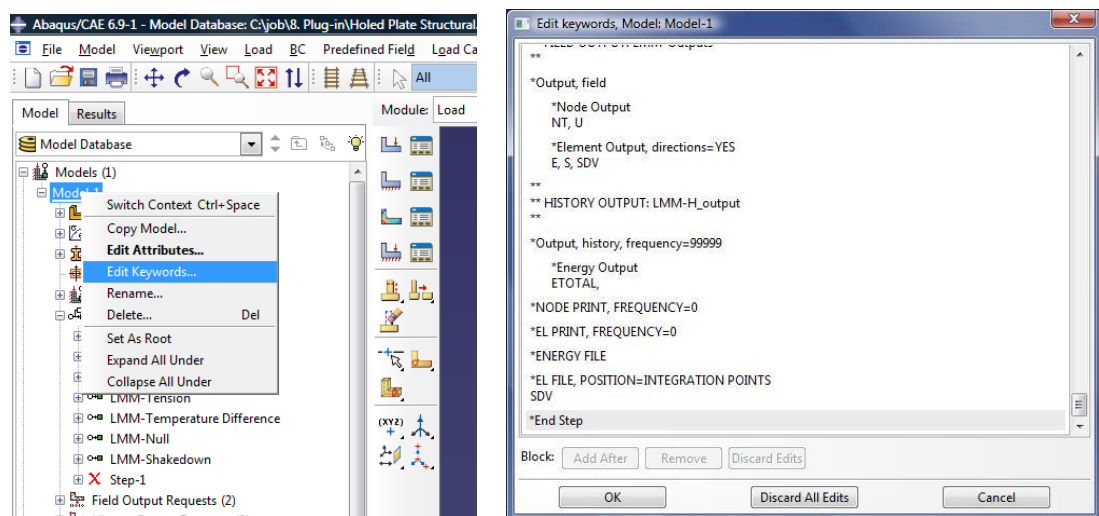


**Figure 6.11 - Keyword Block After the \*ENERGY FILE Command has been Added**

Whilst solving any Abaqus job the progress of the solution may be seen in the "Monitor" dialog box. Information such as the current step and increment are displayed along with any warnings and errors encountered. The URDFIL subroutine contains code which prints additional information about the LMM to the Data file which can be read by this dialog box.

During the solution, the lower and upper bound load multipliers and convergence levels are printed for the current increment so the user can see the progress of the solution. When the analysis is complete a summary is printed which declares the shakedown status of the model, the final values of the load multipliers and lists the SDV numbering so the user can view contour plots of the results. A sample summary given in the Monitor dialog box is shown in Figure 6.12.

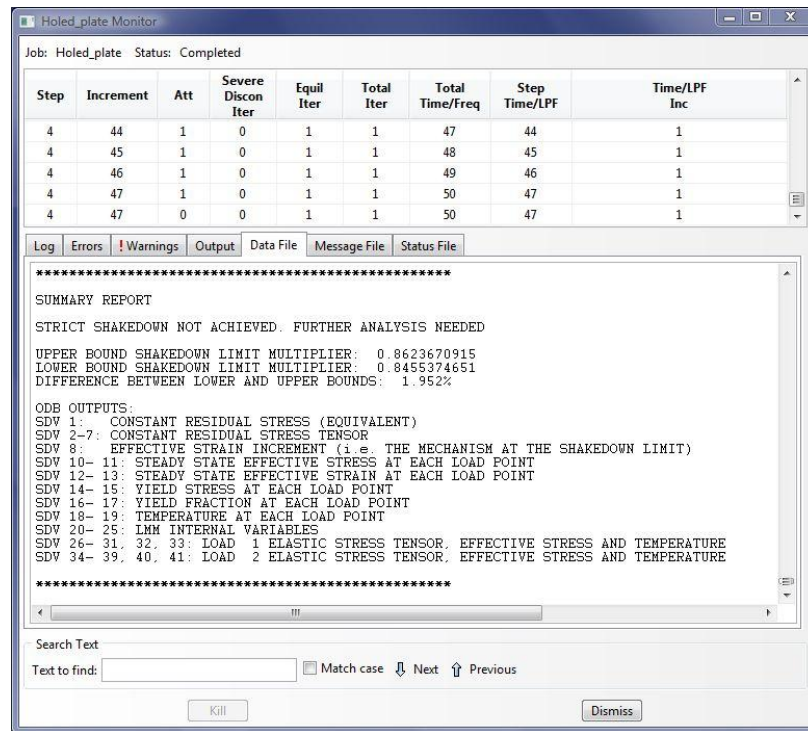


Figure 6.12 - Monitor Dialog Box Showing the LMM Summary Report

When complete, the user may view contour plots of the results in the same way as any other Abaqus analysis.

## 6.5 Installation and Testing

The plug-in and subroutines described here have been installed on the EDF computer system. An extended visit to the EDF offices allowed time for an independent user to extensively test the LMM tool and give feedback on any problems encountered or additional functions which would be of benefit.

This external perspective was a valuable asset. As mentioned in section 6.4 a lot of effort was invested in error checking of the inputs of each dialog box. However it is very difficult for a single programmer to foresee every eventuality or combination of events which could

lead to an error. The testing within EDF highlighted some additional situations which should be avoided and minor errors with the plug-in itself, and these were rectified on site when they arose.

This testing also highlighted some small additional functions which would be beneficial in regular use. For example in Figure 6.6a the function which calculates the 0.2% proof stress was added in this way. Therefore the plug-in overall has been tailored based on the requests of EDF, making the tool more convenient for their engineers to use. EDF are now satisfied with the current tool.

## **6.6 Summary and Discussion**

This chapter has described the development of the LMM into a tool which can be used on a regular basis by EDF engineers. This has involved re-structuring the subroutines for multiple CPU solution and developing a plug-in for Abaqus CAE.

This plug-in has been created to provide an intuitive and simple way to perform a LMM analysis. The data for the analysis is gathered through Abaqus CAE, which is a familiar environment for EDF engineers. The plug-in implements all of the functionality possible in the subroutines, and includes extensive error checking to ensure that only permissible combinations of options are used. The plug-in and subroutines have been written so that the configuration of the subroutines for each analysis is performed automatically, thus making a LMM analysis more convenient and less prone to errors.

As mentioned in the introduction to this chapter, the analysis tool created here is to form the basis of a continuation project. This project will extend the capabilities of the LMM to include the effects of creep in the cycle (see section 8.2 for further details). These extensions will allow the analysis tool to have a wider applicability to structural integrity analyses both in EDF and other organisations dealing with structural integrity issues.

## 7 Application of the Complete LMM Analysis Tool

This chapter demonstrates the use of the LMM analysis tool described in the previous chapter. This serves two purposes. Firstly it acts as a worked example of a LMM analysis within the context of an R5 assessment. Secondly it acts as another verification of the LMM. In the example shown here the use of elastic plastic FEA was necessary to demonstrate shakedown and so these results are compared to the LMM.

The example used is that of a header branch pipe from one of the EDF AGR stations. The assessment of this component was performed by T. Siddall in [122]. Proof of shakedown proved problematic during the integrity assessment which makes this an ideal example for a LMM analysis. A full description of the background to the analysis conducted is given in [122]. The important aspects of this background are summarised in this chapter, followed by a description of the FEA model. The analyses conducted in [122] are described, which are based on the R5 procedure and some elastic-plastic calculations. The setup and submission of the LMM analysis of the header is described, followed by a comparison of the results with the R5 and elastic-plastic FEA results.

### 7.1 Background

It was required to demonstrate sufficient margin against ratcheting for the secondary header tees in the cold reheat system of the AGR. A schematic of such a header is shown in Figure 7.1, where the main pipe has two parallel branch pipes. There are a number of these secondary headers in this system. They have all been designed with the same wall thicknesses, but two variations exist with regards to the distance between the two branch pipes.

NDT was performed on a number of the headers to determine the current wall thicknesses. This inspection showed a significant variation in these wall thicknesses, where the minimum main and branch pipe thicknesses were found to be 20mm and 10.7mm respectively. It should be noted that these minimum thicknesses were not observed in the same header.

In order to prove shakedown in all of the headers whilst keeping the number of analyses to a minimum a worst case model was created. The minimum wall thicknesses observed from the NDT of all the headers were used in this model despite their occurrence in different headers. This gives an inherent conservatism in the model.

This worst case model also considered the possibility of an interaction between the two branch pipes. There are two header geometries, the difference between them being the dimension F (3153.3mm and 4169.3mm). It was shown in [122] that the smaller of these two designs could show an interaction of the stresses between the two branches whereas the larger design would not. Therefore as a conservative approach the smaller branch geometry was used.

The design conditions of the header are an internal pressure of 4.55MPa, which is limited by a safety relief valve upstream of the header, and a temperature of 382.2°C. The analysis assumes that the pipework operates between two relatively steady state conditions of cold shutdown and hot pressurised, which was confirmed by plant temperature and pressure data. Therefore no cold-pressurised or thermal shock conditions are considered.

In addition to the pressure and temperature, the headers experience bending moments due to interaction with the rest of the piping system. The applied bending moments at the cold shutdown and hot pressurised conditions were analysed using the PSA5 software for the entire cold reheat piping system. There was a variation in the bending moments seen across all the headers in the system, and so the worst case bending moments were chosen as a conservative option for this model.

## 7.2 Finite Element Model

### 7.2.1 Geometry

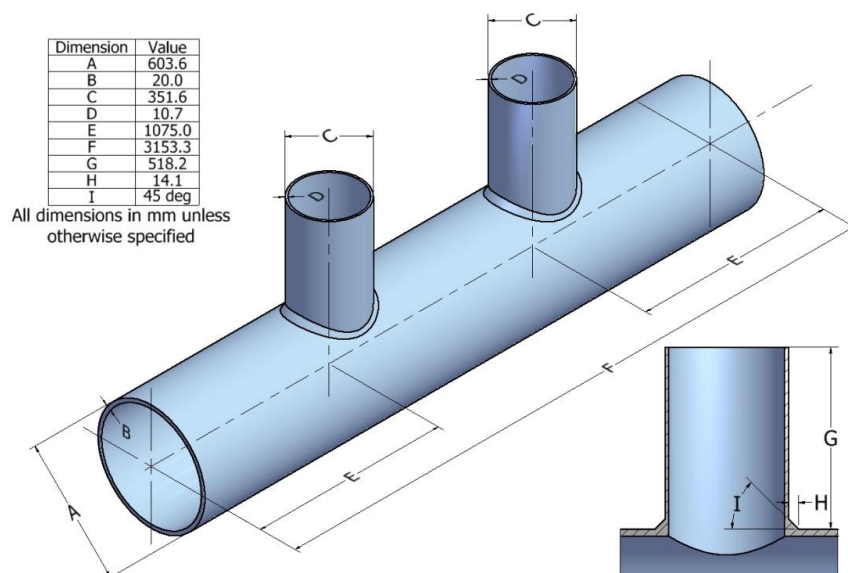


Figure 7.1 - Geometry and Dimensions of Header

The dimensions of the header geometry used are shown in Figure 7.1, and the model and mesh were created to match that of [122] as closely as possible. The weld is modelled as a 45 degree chamfer with a leg length of 14.1mm. This gives a weld cap dimension of 20mm, which was the minimum observed in the inspection data. Although symmetry exists in this geometry, the applied bending moments are not symmetrical. Therefore symmetry could not be used.

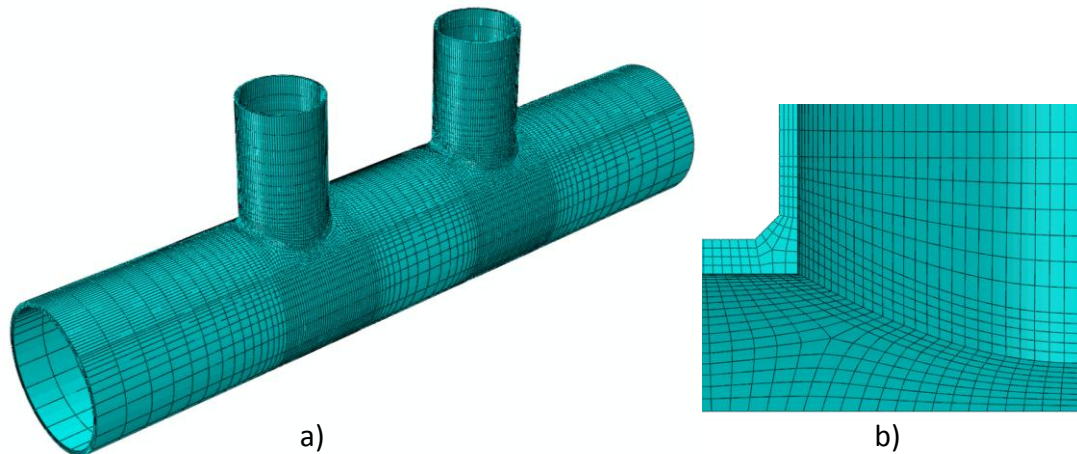


Figure 7.2 - a) Header Mesh b) Weld Mesh Detail

The FEA model is meshed with the Abaqus quadratic brick element C3D20R, as shown in Figure 7.2a. The mesh is biased to be denser in the region of the intersection and weld, resulting in a total of 52240 elements in the model. The weld region is meshed as shown in Figure 7.2b, which results in no element warnings for internal angles or aspect ratio.

## 7.2.2 Material Properties

Table 7.1 - Temperature Dependent Material Properties for the Header Branch

Temperature (°C)	Yield Stress, $\sigma_y$ (MPa)	Shakedown Yield Stress, $K_s\sigma_y$ (MPa)	Ultimate Tensile Strength (MPa)	Young's Modulus (GPa)
20	247.1	180.4	419	210
382.2	139.7	125.7	389.5	185.9

Table 7.1 shows the young's modulus and yield stress at 20°C and 382.2°C. For a shakedown assessment R5 also includes a factor,  $K_s$ , on the yield stress. This represents the ability of the material to harden or soften during repeated cycles of loading. The header pipework is

produced from BS-3602-HFS-27S carbon steel. The  $K_s$  factor for carbon steels given in R5 is 0.73 at 20°C and 0.9 for temperatures above 150°C. This gives the shakedown yield stresses in Table 7.1.

### 7.2.3 Loads and Boundary Conditions

The internal pressure of 4.55MPa is applied to all internal surfaces of the model. The closed end condition is replicated by applying the equivalent axial tension to the ends of the main and branch pipes as a tensile pressure. The two temperature extremes of 20°C and 382.2°C are assumed to be entirely uniform with no temperature differences within the model. Therefore these are modelled using uniform predefined fields.

The FEA model makes use of reference points and rigid kinematic MPC constraints as a convenient way of applying bending moments and boundary conditions to the model. These are shown in Figure 7.3. To maintain consistency the naming convention used here is the same as [122]. In all cases these constraints allow for radial expansion of the pipes due to internal pressure.

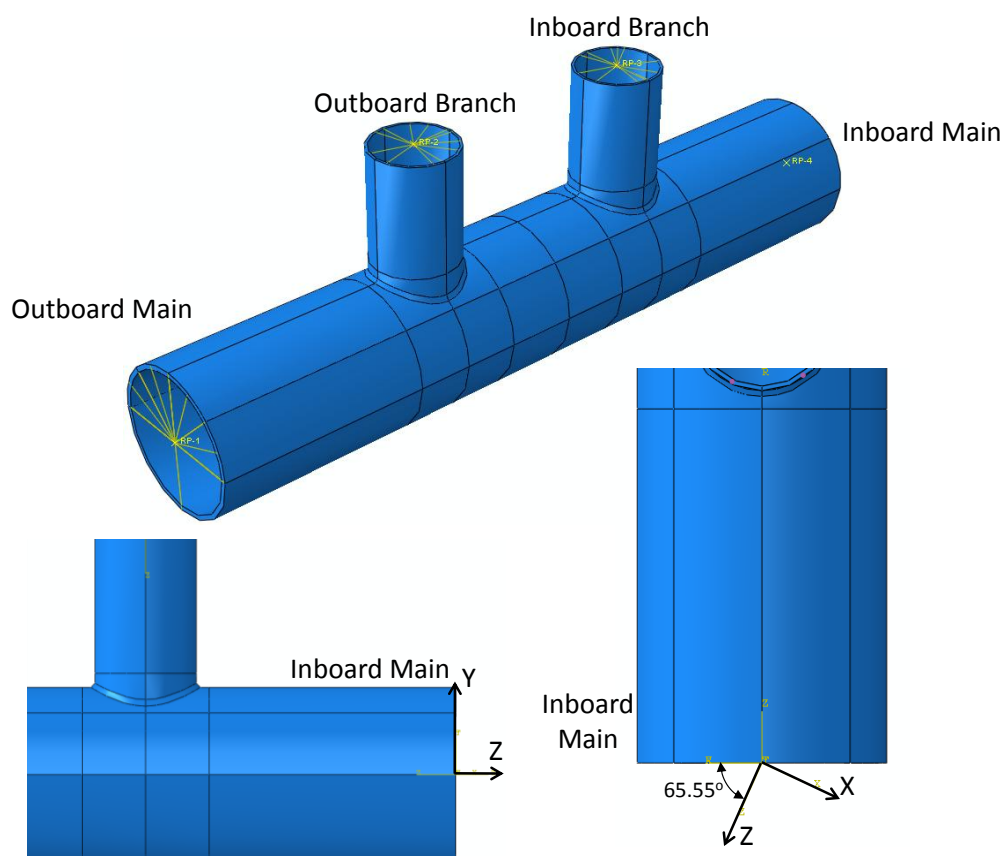


Figure 7.3 - Reference Points, Multi-Point Constraints and Moment Coordinate System

The worst case bending moments from the PSA5 analysis are given in Table 7.2. The PSA5 analysis has its own global co-ordinate system which differs from that of Abaqus. Therefore a Cartesian coordinate system was created in at the Inboard Main reference point so that the moments from PSA5 could be directly applied to the model. This coordinate system is shown in Figure 7.3. The model is constrained by fully fixing the Outboard Main Reference Point in all degrees of freedom.

**Table 7.2 - Bending Moments Applied to Model (all in Nm)**

	Cold Shutdown			Hot Pressure		
Location	$M_x$	$M_y$	$M_z$	$M_x$	$M_y$	$M_z$
Inboard Main	23033	-2823	-6580	-35978	4287	15550
Inboard Branch	-26508	2076	6314	14715	-2952	-5103
Outboard Branch	-15019	-344	8705	4363	-1289	-2750

### 7.3 EDF Shakedown Analysis

To perform the R5 Volume 2/3 shakedown calculations the stresses need to be linearised across the section in question. In [122] the stress classification line shown in Figure 7.4 proved to be most severe, and so those results are presented here. This line is at the outboard side of the inboard branch pipe.

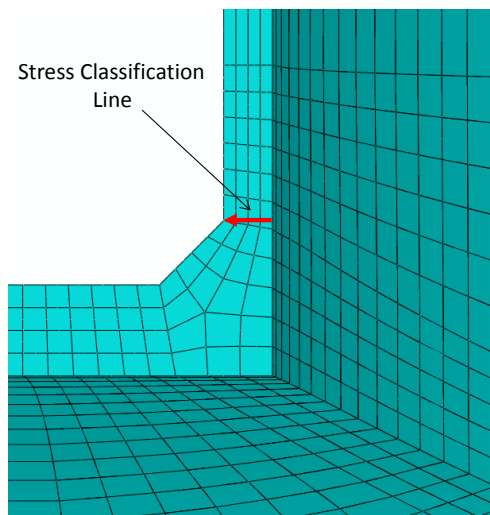


**Figure 7.4 - Stress Classification Line for Linearised Stresses**

### 7.3.1 R5 Simple Checks

The checks in R5 Volume 2/3 were used to determine the shakedown status of the component, beginning with the simple checks in R5 section 6.6. This check assumed that the residual stress field is null. The shakedown condition is met if the linearised elastic stresses are less than the modified yield stress:

$$\hat{\sigma}_{lin}(x,t) \leq K_s \sigma_y \quad (7.1)$$

An elastic analysis was performed for the cold shutdown and hot pressurised states. Figure 7.5 shows a contour plot of the von-Mises equivalent stress at the hot-pressurised condition, where the contour limit has been set to the shakedown yield stress of 125.7MPa. It can be seen that a significant region around the intersections has exceeded this limit, shown in grey. The linearised stresses across the classification line in Figure 7.4 exceed the yield stress: the von-Mises equivalent membrane + bending stress at the inner and outer surfaces are 278MPa and 246MPa respectively. This is in excess of the modified yield and so shakedown cannot be demonstrated using the simplified check.

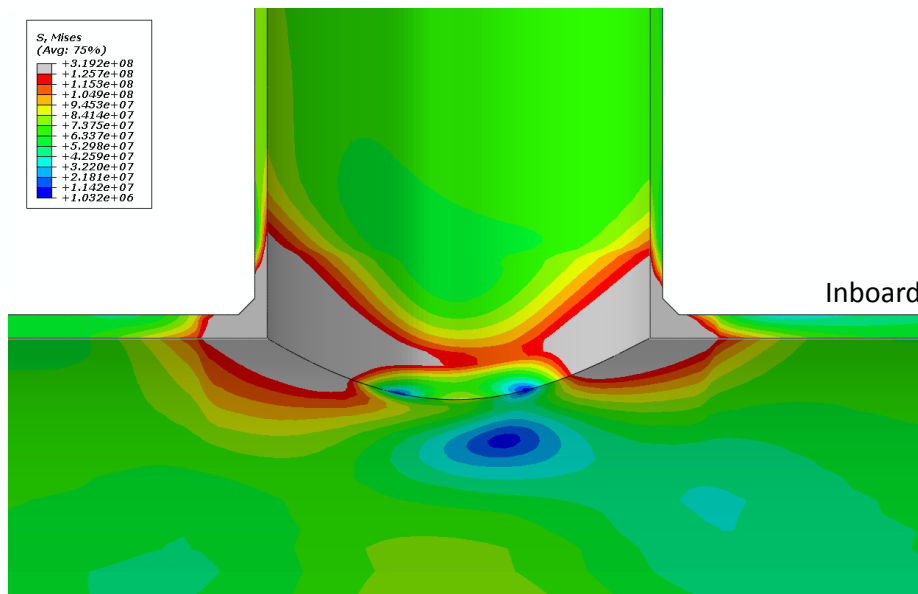


Figure 7.5 - Elastic Stress at the Hot Pressure Condition

### 7.3.2 R5 Shakedown Check Involving a Residual Stress Field

To generate a residual stress field the elastic analysis in section 7.3.1 was extended to an elastic perfectly-plastic analysis with the unmodified yield stress at 382.2°C (i.e. 139.7MPa). The internal pressure and associated axial tensions were applied along with the hot

moments to generate the elastic-plastic response at this state. Following this plastic deformation, all the loads were removed which left the resultant residual stress field shown in Figure 7.6.

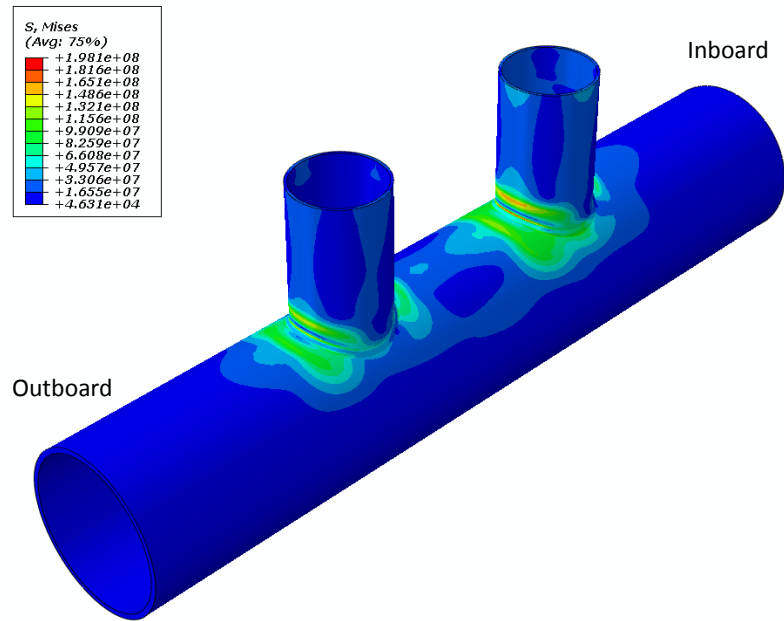


Figure 7.6 - Residual Stress State after Removal of all Loads (temp 382.2 degrees)

When this route is adopted in R5 the stress across the section (including the residual stress field) must satisfy

$$\bar{\sigma}_s(x,t) \leq K_s \sigma_y \quad (7.2)$$

Where  $\bar{\sigma}_s$  is the sum of the applied elastic and residual stresses. If  $\bar{\sigma}_s$  is a linearised stress distribution, as was used in [122], then equation (7.2) must be satisfied over the entire classification line. The superposition of the elastic and residual stresses at the hot pressure condition resulted in membrane + bending stresses of 183MPa and 188MPa at the inner and outer surfaces respectively. This is greatly in excess of  $K_s \sigma_y$  at 382.2°C (125.7MPa) and so fails the shakedown criteria of R5.

### 7.3.3 Elastic-Plastic FEA

Exhaustion of the simplified criteria in R5 meant that cyclic elastic-plastic FEA was required to demonstrate shakedown. An elastic perfectly-plastic material was used with the unmodified yield stresses at 20°C and 382.2°C. The model was cycled between the two states of cold shutdown and hot pressure. Figure 7.7 shows the plastic strain contours after

the final cycle and highlights the location of peak plastic strain (in the branch side weld toe in the inboard branch). The plastic strain in this most critical location is also plotted in Figure 7.7. It can be seen that the plastic strain stabilises after the first cycle and so the header is within strict shakedown.

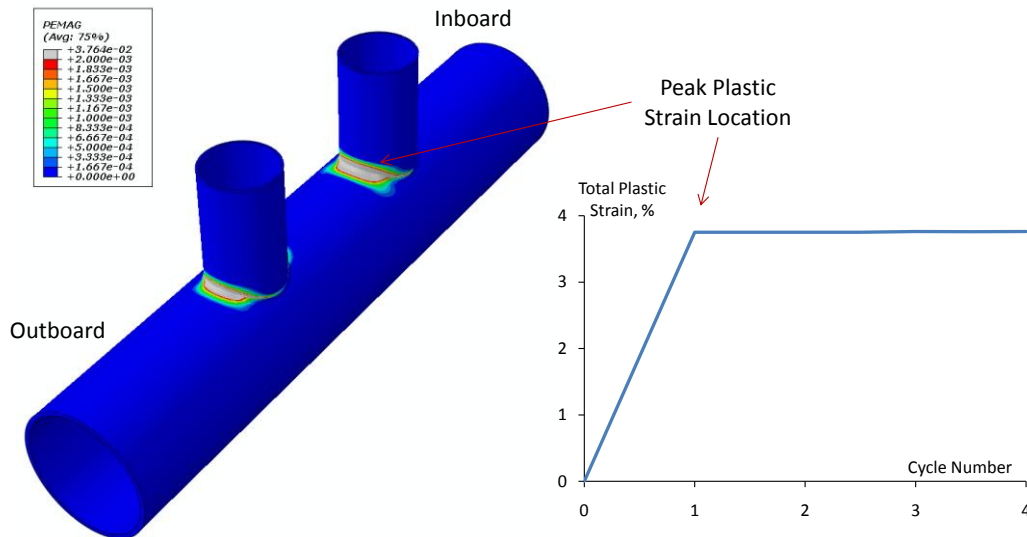


Figure 7.7 - Contour of Plastic Strain and Plastic Strain History At the Critical Location

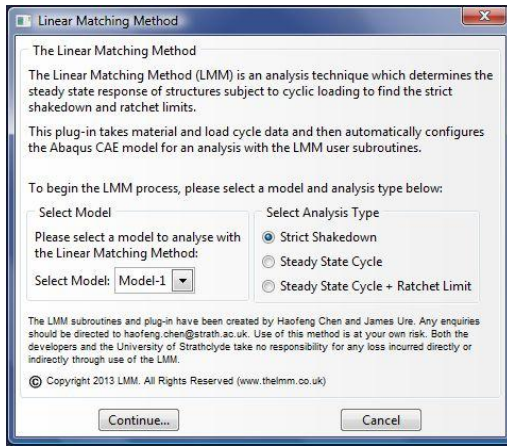
## 7.4 Analysis using the LMM

This header branch has been re-analysed using the newly developed LMM tool. The steps used in this section to construct the LMM analysis are detailed so as to act as a worked example of a LMM analysis. The results are then compared to the EDF analysis.

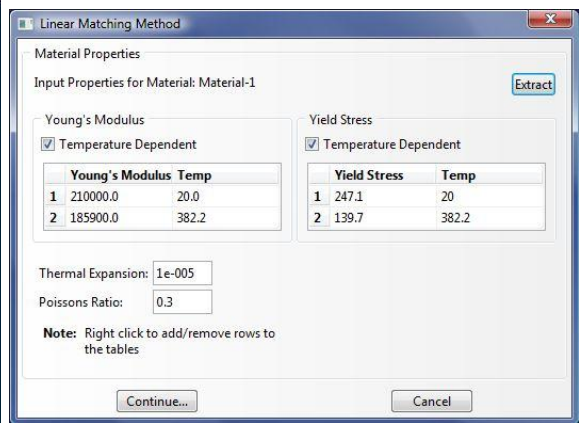
### 7.4.1 Strict Shakedown Analysis

The FEA model of section 7.2 was used for a LMM strict shakedown analysis. Figure 7.8a shows the first dialog box of the LMM plug-in, which shows the selection of the model and a strict shakedown analysis.

Only one material is defined in this model, therefore a single material properties dialog is shown. Figure 7.8b shows the materials dialog with the temperature dependent properties. Only two temperature dependent properties are used so the third line of the tables is deleted. The Young's modulus and Poisson's ratio were already defined for the elastic analysis, and so the "Extract" function was used to populate the dialog box. The elevated temperature in the model is uniform and so no thermal stresses will be generated. Therefore an arbitrary thermal expansion coefficient is entered.

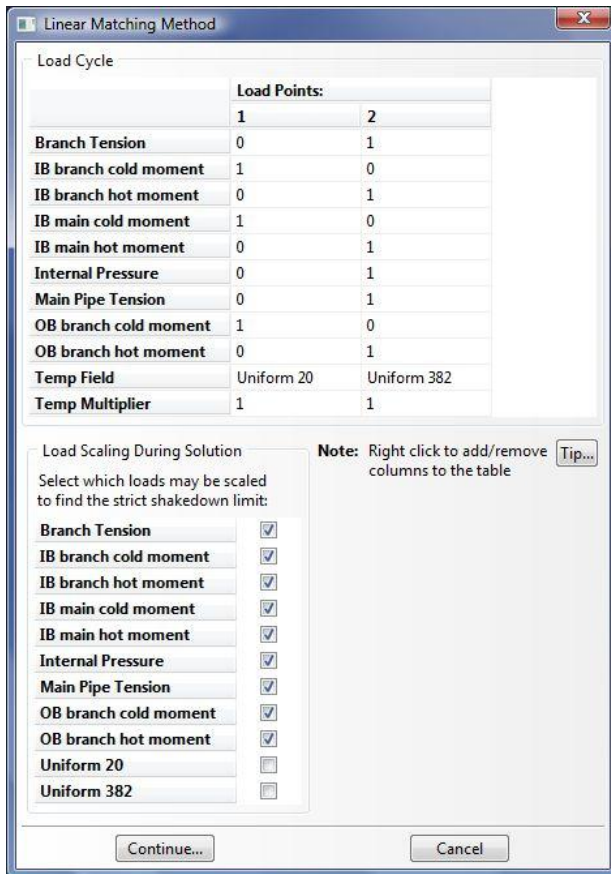


a)

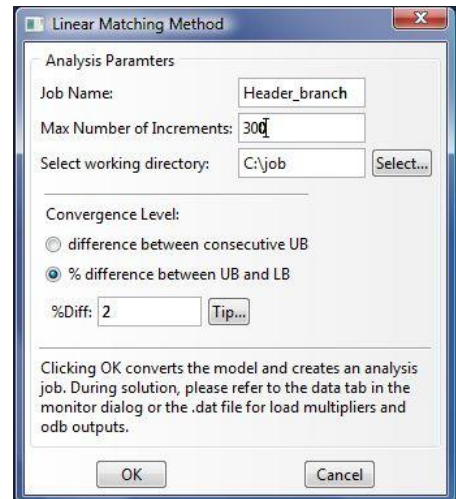


b)

Figure 7.8 - a) Main Dialog Box and b) Materials Dialog Box



a)



b)

Figure 7.9 - a) Load Cycle Dialog and b) Job Dialog

Figure 7.9a shows the Load Cycle dialog box. The load cycle for this component is assumed to vary between the two conditions of cold shutdown and hot pressure. Therefore two points in the load cycle table are required. The cold moments are applied with a multiplier

of 1.0 in the first load instance along with the 20°C temperature field. The hot moments, internal pressure and axial tensions associated with this are not applied and so have a multiplier of zero. In the second load instance, the cold moments have a multiplier of zero. The hot moments, internal pressure and its associated axial tensions are given a multiplier of 1.0. The second load instance is given the 382.2°C temperature field. All loads are allowed to be scaled during the solution. Therefore the resulting shakedown load multiplier will be the level by which all these loads can be scaled to be exactly at the shakedown limit. The two temperature fields are not included in this scaling, which means that the yield stresses at both load points will remain unaffected.

The final dialog, shown in Figure 7.9b, is used to name the analysis, set the working directory, and specify the number of increments and convergence. This is a relatively large model and so a maximum of 300 increments was set. If convergence has not occurred in this time then the analysis is terminated to prevent the files becoming too large. A 2% difference between lower and upper bounds was chosen as the convergence tolerance. This value is thought sufficient to ensure converged lower and upper bounds without allowing the solution time to become excessive.

With the data entered into the dialog, the LMM scripts configure the model as described in section 6.4. The analysis job is created in CAE, and at this point the model is ready for a LMM analysis. At this point the job definition created by the LMM was modified to solve on multiple CPUs, and then it was submitted for analysis.

The convergence tolerance was met in 118 increments of the LMM solution with upper and lower bound multipliers of 1.117 and 1.096, as shown in Figure 7.10. Therefore the applied loads could be increased by approximately 10% whilst still achieving strict shakedown. This result confirms that the header is in strict shakedown as observed in the cyclic elastic plastic FEA. Figure 7.11 compares the contour plots of plastic strain predicted by the LMM and elastic plastic FEA. The LMM results are given at the strict shakedown limit, and the Abaqus results are for the specified loading. Nevertheless, a good agreement is observed.

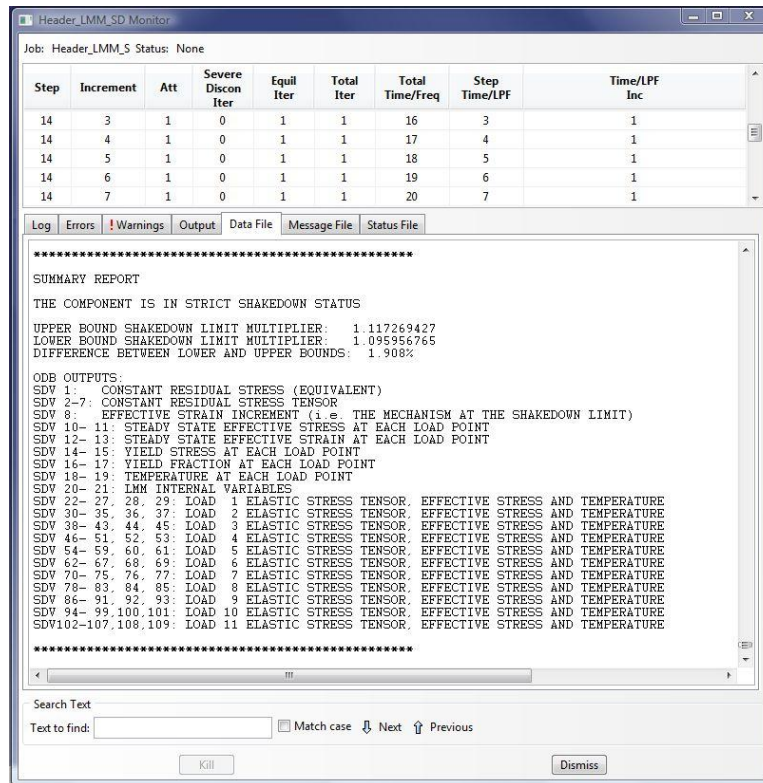


Figure 7.10 - Abaqus Monitor Dialog for the Strict Shakedown Analysis

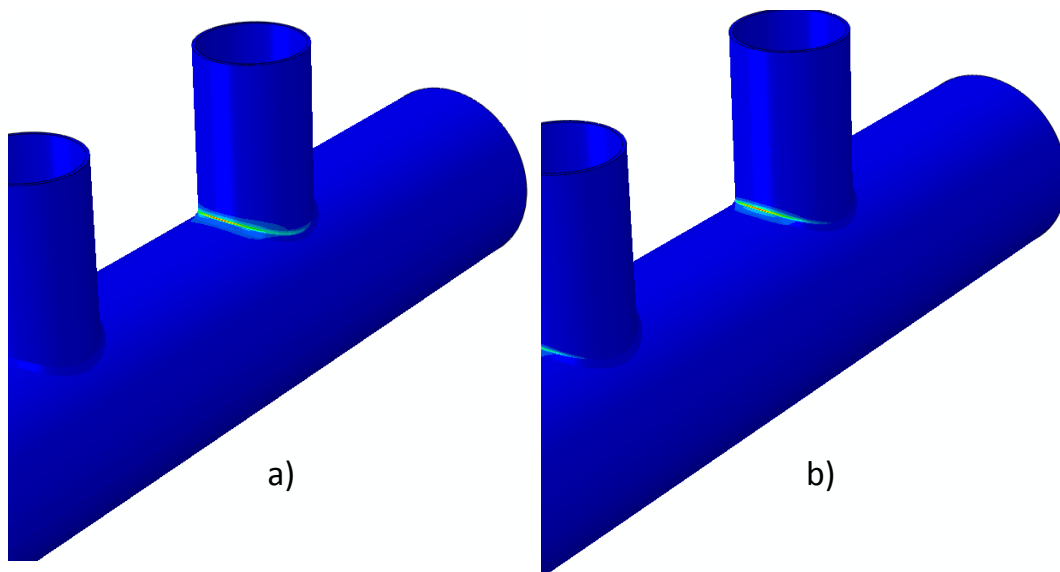


Figure 7.11 - a) LMM Mechanism Prediction at the Strict Shakedown Limit and b) Location of Peak Plastic Strain from Elastic-Plastic Analysis

The elastic plastic analysis of [122] described in section 7.3.3 used the unmodified yield stress to prove shakedown, and this has been validated with the LMM analysis using the

same values of yield stress. However the R5 assessments use a modified value of yield to account for cyclic softening. The header components see a very low number of cycles – plant data shows around 6 cycles per year. Therefore it is questionable whether the steel would see enough cycles to soften by any significant level. Nevertheless it is prudent to check the shakedown status using  $K_s \sigma_y$ .

The LMM analysis was repeated using the shakedown yield stresses from Table 7.1. The resulting lower and upper bound shakedown multipliers are 0.867 and 0.886 respectively. Therefore the header is not in strict shakedown and further analysis is required to ensure that it is not ratcheting.

#### 7.4.2 Steady State Cycle and Global Shakedown Limit

Since strict shakedown could not be achieved when the  $K_s \sigma_y$  values of yield stress were used, the model must either be in global shakedown or ratcheting. To find out which, the model was analysed using the LMM global shakedown procedure. The LMM plug-in was started once again within Abaqus CAE. Figure 7.12 shows the Main and Material dialog boxes, which are nearly identical to that of the strict shakedown analysis. In this case, the Ramberg-Osgood model is not used due to lack of material data.

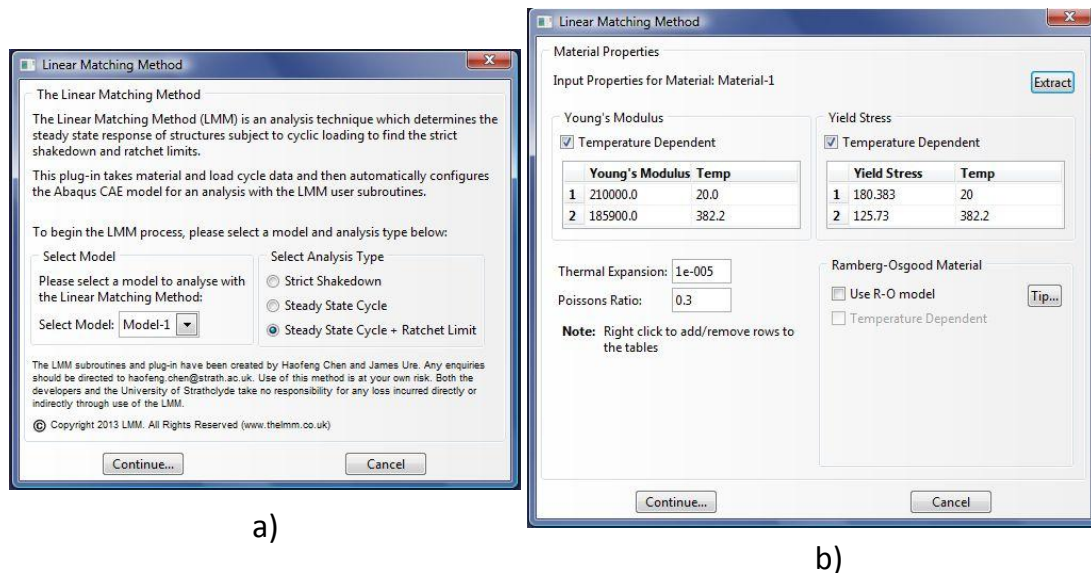


Figure 7.12 - Steady Cycle and Ratchet Limit a) Main and b) Materials Dialogs

The load cycle is identical to that of the strict shakedown analysis. This means that the stage 1 calculation will give the stabilised cycle for these loads and the strain ranges to use

in a low cycle fatigue calculation. At this point the global shakedown calculation differs from the strict shakedown. In the strict shakedown analysis all the loads were scaled, which gives the level by which the entire load case should be scaled to be at the strict shakedown limit. The global shakedown procedure, however, adds the selected extra loading to all load points to find the global shakedown limit. The additional loads must be selected carefully to ensure the ratchet limit is meaningful. In this case the internal pressure and associated axial tensions were selected to be added in stage 2, shown in Figure 7.13a. This means that the ratchet limit multiplier will correspond to the level of additional pressure loading that will not cause ratcheting. If it was deemed that the safety margin against an increase in cold or hot moments was needed, then these could be selected instead.

The global shakedown analysis required two convergence values. A steady cycle convergence value of  $1e^{-4}$  was used to obtain a stabilised cycle. A 5% difference in lower and upper bound was chosen for stage 2 in order to reduce the number of increments required. Figure 7.13b shows the Job dialog box. The model was then solved.

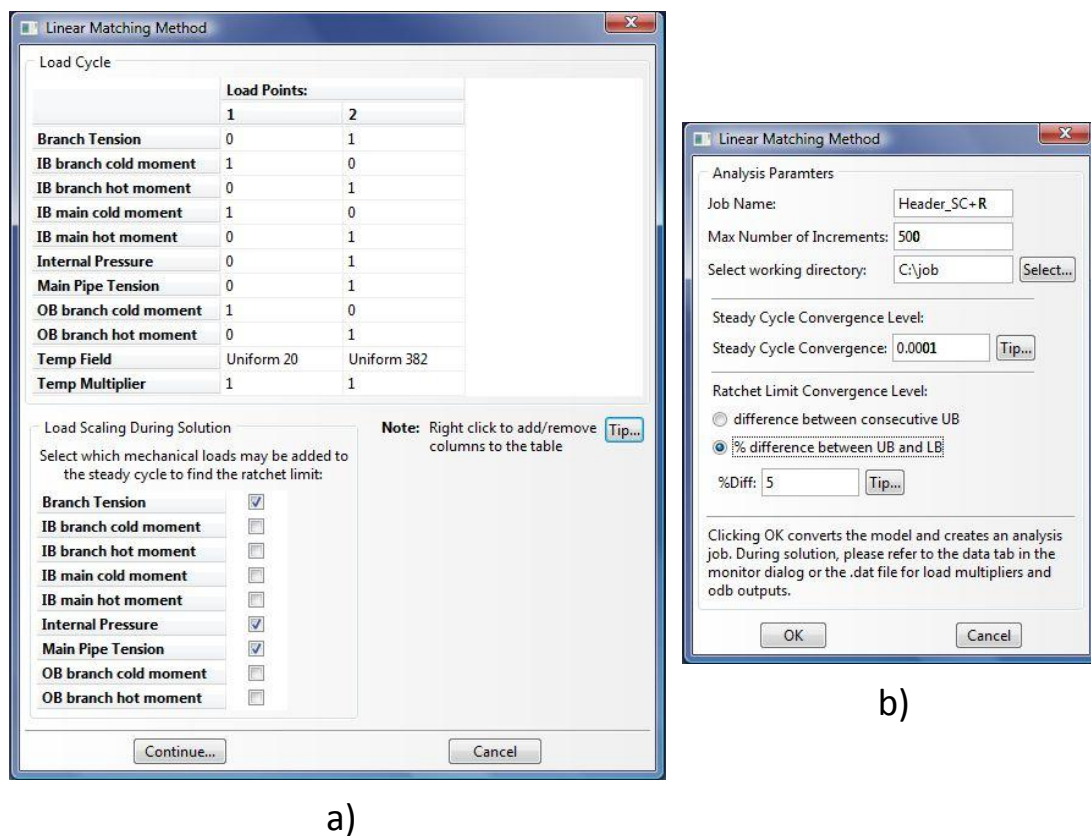


Figure 7.13 - Steady Cycle and Ratchet a) Load Cycle Dialog and b) Job Dialog

The lower and upper load multipliers given by this analysis were 0.024 and 0.087 respectively, which correspond to an allowable increase in pressure of 2.4% and 8.7% respectively. This means that an increase in pressure of 0.4MPa (using the upper bound multiplier) can be sustained before ratcheting. The difference in the load multipliers is greater than the 5% specified in the plug-in and is a result of the analysis being terminated due to the size of the results files, which were becoming large. The purpose of the stage 2 analysis was to demonstrate if the header is in global shakedown, therefore any positive load multiplier indicates this. Examining the load multipliers during the solution shows that the upper bound has converged very well, with little change seen between consecutive increments. The lower bound, even with the convergence improvements of section 4.6, showed a slow convergence with the inboard branch weld toe being the source of the problem. Despite this, the lower bound shows that at least 0.11MPa of internal pressure can be added before ratcheting will begin and continued solution would approach the converged upper bound value. Based on this the header was judged to be within global shakedown and the analysis was terminated.

Two elastic plastic analyses were conducted to validate this result. The first analysis considered the exact load history seen by the header. Figure 7.14a shows the contours of plastic strain at the weld of the inboard branch given by this elastic plastic analysis and the LMM at the hot end of the cycle, and a good agreement is observed. The plastic strain history at the point of the highest plastic strain in the elastic plastic analysis is plotted in Figure 7.14b, which shows that the header is operating in global shakedown. The plastic strain range at this location given by the LMM and the elastic plastic analysis are  $9.75e-4$  and  $8.97e-4$  respectively, which shows that the LMM gives a conservative estimate of this.

The second elastic plastic analysis was conducted to validate the location of the global shakedown limit predicted by stage 2 of the LMM calculation. This analysis considered an increase in the internal pressure and tensions of 9%, taking the load cycle just beyond the global shakedown limit predicted by the LMM upper bound. Figure 7.15 shows the plastic strain history, which shows an accumulation of plastic strain until a plastic hinge forms during the 12th cycle and the analysis halts

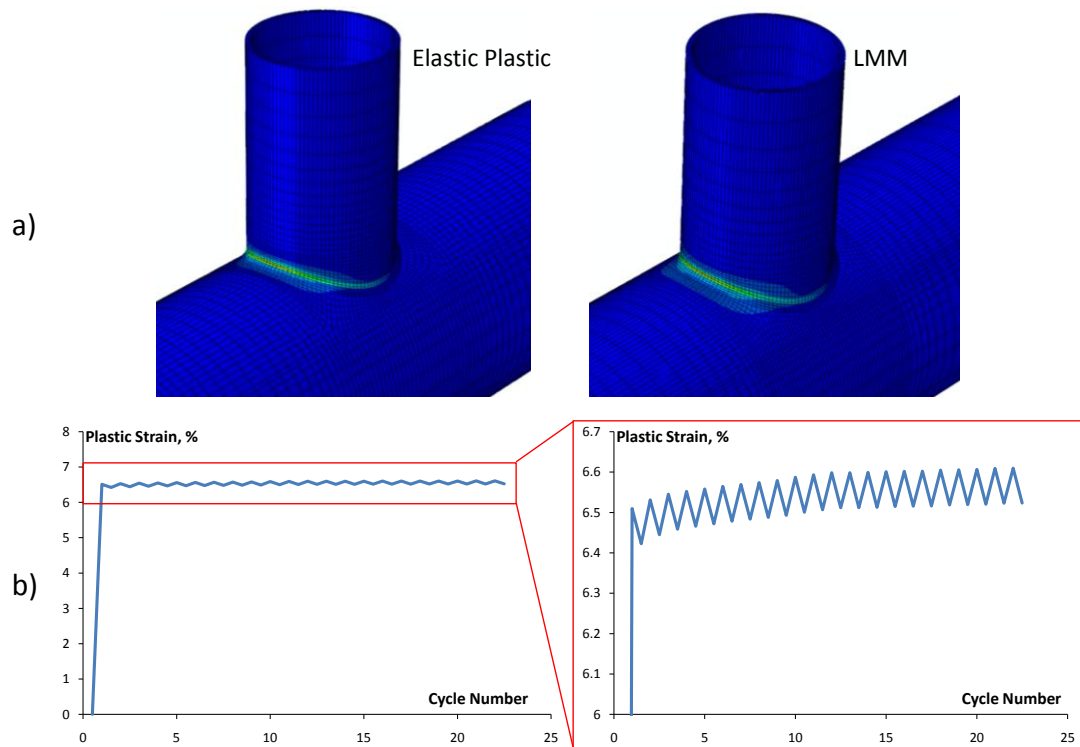


Figure 7.14 - a) Contour Plot of Plastic Strain and b) Plastic Strain History of Elastic Plastic Analysis.

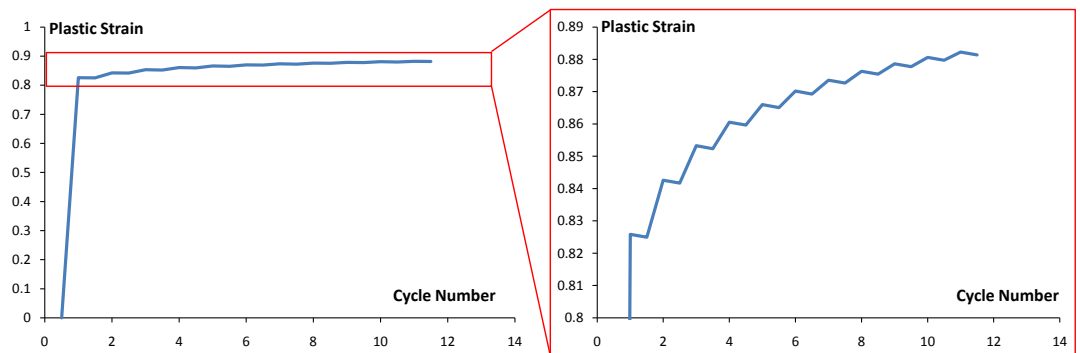


Figure 7.15 - Plastic Strain History of the Second Elastic Plastic Analysis

These analyses show that the header operates in global shakedown, but is very close to the global shakedown limit. A relatively small increase in the pressure would result in ratcheting behaviour. Despite this, further evidence to substantiate the global shakedown status of the component comes from the available material properties. Table 7.1 shows that significant work hardening occurs in this material, which is not taken into account in any of the analyses conducted here. If a Ramberg-Osgood model were available then this could be used in stage 1 of the global shakedown calculation. This hardening would bring the header further away from the global shakedown limit (possibly even to within strict shakedown) which supports the global shakedown status of the header.

## 7.5 Summary and Discussion

This chapter has revisited the analysis of a header branch pipe performed by EDF. The original analysis of this component used the R5 procedure, but these checks could not demonstrate that the header was in shakedown. Elastic plastic analysis was performed and showed that the header was in strict shakedown.

The LMM has been used in this chapter to re-analyse the header. This provides a worked example of the newly created LMM plug-in. The steps involved in running the LMM strict shakedown analysis and the outputs it produces are described. The LMM results concur with that of the elastic plastic analysis, which show that the header is in strict shakedown when the unmodified yield stress is assumed. However strict shakedown is not achieved if the R5  $K_s$  factor is applied.

The LMM global shakedown analysis proved that the header is in global shakedown but, with the perfectly plastic material assumed, a relatively small increase in the internal pressure would cause ratcheting. Elastic plastic analyses verify the plastic strain locations, plastic strain range and global shakedown limit predicted by the LMM. This chapter therefore also adds to the validation objective of this thesis by adding one further practical application of the LMM to the number of existing examples. The model used for this analysis is one of the largest used in any LMM analysis, and the resulting global shakedown output files became large as a result. Future development of the plug-in and subroutines should include work to reduce the size of these outputs.

## **8 Conclusions, Discussion and Future Work**

### **8.1 Summary of the Thesis**

The Linear Matching Method has been in development for a number of years, and has been used primarily as a research tool within an academic environment. The work presented in this thesis centres around the development of the LMM for use within an industrial context. The changes and developments to the LMM which allow this to happen were defined by three objectives:

1. Addition of conservative lower bounds to the LMM framework
2. Provide validations of the solutions produced by the LMM
3. Create a graphical user interface to the LMM

The LMM strict and global shakedown procedures were originally derived as upper bound procedures. Whilst upper bounds offer advantages in terms of solution convergence, the nuclear industry has a clear preference for the conservatism offered by lower bound solutions to the shakedown limit. A lower bound to the strict shakedown procedure was added before the start of this project, and so the effort in this thesis was focused on creating an analogous lower bound to the global shakedown method.

The process of creating this lower bound began by setting out the theoretical foundations - no formal lower bound theorem for global shakedown exists, and so the work of Polizzotto was used to construct the basis of a lower bound for the LMM. These theoretical foundations were developed into a numerical calculation which was implemented into the global shakedown procedure. The resulting method produces the lower and upper bound load multipliers simultaneously, which allows the user to judge convergence of the solution as it progresses. It also gives confidence in the final solution if the two multipliers have converged closely. Improvements to the convergence of the lower bound were investigated through different modulus matching schemes, but with inconclusive results. An elemental average of the lower bound was found to give the best approximation to the lower bound whilst improving the speed of convergence dramatically. This now means that the LMM has the capability to calculate the lower and upper bounds to both the strict and global shakedown limit.

Ease of use of the LMM was a primary concern with this project. The LMM, implemented using subroutines in Abaqus, can be a difficult tool to use for those with little programming

experience, especially since some code changes were required for each analysis. The plug-in created for Abaqus now provides a convenient way for the user to perform a LMM analysis because the required data is entered into dialog boxes within the familiar Abaqus CAE environment. The need for code changes has been removed, with the analysis being configured by passing a text file between Abaqus CAE and the subroutines. The subroutines themselves have been re-written to allow solution on multiple CPUs, an improvement over the previous single CPU versions of the code. The plug-in and subroutines have been installed on the EDF computer system and have undergone testing by an independent user. This resulted in some minor adjustments, additional error checking and extra functionality to tailor the plug-in for use in EDF.

Chapter 7 of this thesis re-visits an existing EDF analysis to demonstrate the use of the final LMM analysis tool. This gives a worked example of the plug-in to demonstrate how to interpret the material properties and applied loads for a LMM analysis. The results are compared to the R5 assessment and elastic plastic analysis which demonstrates the applicability of the LMM to assessments performed by EDF. For future development and support of the code, the subroutines and plug-in scripts have been described in detail in Appendix D and Appendix E respectively.

A number of LMM analyses have been performed throughout this thesis, which have been compared with theoretical, numerical or experimental data. The general purpose of these analyses is to validate parts of the LMM framework, add confidence in the results it produces and determine its current limitations. These comparisons will add to existing published comparisons, and over time the increasing number of these will prove the capabilities of the method and highlight areas for future development.

Comparisons with theoretical solutions are given for the limit loads of notched bars and the Bree cylinder shakedown limits. These comparisons, with their simple geometries and loading, allows the implementation of the bounding theorems to be tested. This includes the newly developed lower bound to the global shakedown limit. The notched bar examples provide an extra function by allowing the different dimensionalities to be verified. In all cases a good agreement between the LMM and the theoretical solutions is seen. This is the case even for the the Bree cylinder with modified loading, provided by Bradford [95], where an approximation of the load cycle was required for the current LMM global shakedown method.

Elastic plastic analyses provide a convenient way to validate the LMM solutions. The primary role of the LMM is to provide the same (and more) results as are possible with elastic plastic analysis but with shorter solution times. Since elastic plastic FEA is a trusted method within EDF, a favourable comparison of the LMM with this method is considered to be a suitable method of validation. The examples of pipe bends, pipe intersections and the header branch have all been analysed using the LMM and compared to elastic plastic analyses. A good agreement is seen in all cases, whether that be the location of the shakedown limits, the location of the mechanism or individual values such as the peak plastic strain range.

The LMM is to be used for the analysis of plant components, therefore comparison of the LMM with experimental/plant data is a crucial final stage to the validation exercise. This thesis presents a comparison of the LMM strict shakedown procedure with experimental limit loads of pipe intersections and strict shakedown pressure of nozzles in spherical shells. The LMM was able to conservatively predict these limit loads and shakedown limits, which is an encouraging result in terms of regular industrial use.

## **8.2 Future work**

The work presented in this thesis opens several avenues for improvements and further work. In particular there is considerable scope for additional validations with experimental comparisons, extending the capabilities of the LMM and for implementing more functionality in the plug-in for general structural integrity assessments.

There is a continuous need for validation of the method against experimental data. The experimental limit loads and shakedown limits provide a starting point for this, but there is a lot of scope for extending this area of the validations. Some areas to consider include:

- Thermally load examples. The temperature dependency of material properties is a useful function within the LMM, and thermal loading is a common occurrence in power plant components.
- Published tests exist for limit loads and strict shakedown limits, but very few examples could be found for loading which is beyond strict shakedown, i.e. tests to find the global shakedown limit.
- Tests were found in the literature which consider creep dwells in the load cycle. These may be useful for the continuation project which follows this one (see below)

Building a bank of validation cases will give more confidence in the capabilities of the method, and will serve to validate any new functionality added to the framework.

In Section 3.4, the analysis of pipe bends subject to bending moments highlighted that small deformation theory used by the LMM may not always be conservative. Work has been conducted by some authors to extend the shakedown bounding theorems to include the effects of large deformation, for example Gross and Weege [102] and Polizzotto and Borino [103]. If enough demand is found for large deformation shakedown solutions then work to include these theorems into the LMM framework would be beneficial.

At present a concurrent EngD project (student: Michael Lytwyn) is tackling developments to the global shakedown method so as to allow a generalised load cycle rather than the two stage process currently used [109]. Several examples used during this thesis have involved situations where the load cycle cannot be easily decomposed into cyclic and steady state components. The modified Bree loading mentioned earlier in this section is one such example. Another, more practical, situation where this is also true is in the analysis of the header branch in chapter 7. None of the loads present in the analysis propagated through all load points. A global shakedown method which could scale the loading in the same way as the current strict shakedown method would be highly beneficial in these cases. Rather than adding extra loads, this method would scale the load cycle itself resulting in a global shakedown limit linked directly to this load cycle. When complete, and an associated lower bound calculation is available, this method could add to the current global shakedown method used in the plug-in to make this shakedown analysis tool more versatile.

Relatively recently Chen and Ponter [84] and Gorash and Chen [90][91] have made progress with the LMM which allows the inclusion of creep into the steady cycle calculation. When a creep dwell, and the associated stress relaxation, is part of the cyclic loading the steady state behaviour becomes very difficult to determine. These developments to the LMM code allow the calculation of, among other things, the stabilised cyclic stresses, the plastic strain range and creep strain per cycle. This opens up a number of possibilities for structural integrity applications - R5 volume 2/3 uses these parameters to calculate the creep damage, fatigue damage, the creep fatigue interaction and ultimately determine if a crack will initiate in the component.

The development of a plug-in for the LMM in this project, combined with the developments by Gorash and Chen, has prompted the creation of a follow on project with EDF. Overall this project aims to take the current plug-in and develop it into a more comprehensive structural integrity tool with the LMM as the basis. Specifically it aims to:

- Include creep rupture calculations (both calculating the time to rupture for a given load cycle or calculating the maximum loading which will give the desired time to rupture)
- Carry out theoretical developments to develop the work of Chen and Ponter [84] and Gorash and Chen [90][91] to include more creep models (such as the strain hardening models adopted by EDF)
- Extend the plug-in to include these options for routine use in EDF

The plug-in and subroutines described in this thesis will serve as a starting point for this continuation project.

## 9 References

- [1] British Energy Generation Ltd, *R5: Assessment procedure for the high temperature response of structures*, Rev 3. 2003.
- [2] R. A. Ainsworth, "R5 procedures for assessing structural integrity of components under creep and creep-fatigue conditions," *International Materials Reviews*, vol. 51, no. 2, pp. 107–126, Apr. 2006.
- [3] J. Wood, *Nuclear Power*, 1st Ed. Stevenage: The Institute of Engineering and Technology, 2007.
- [4] P. Norman, "N01 - Reactor Physics and Criticality Course Notes." Univeristy of Birmingham, Nuclear Technology Education Consortium, 2010.
- [5] EDF Energy, "Our Nuclear Power Stations," 2013. [Online]. Available: <http://www.edfenergy.com/about-us/energy-generation/nuclear-generation/nuclear-power-stations/>. [Accessed: 01-Jun-2013].
- [6] Magnox Ltd, "Magnox Ltd, Wylfa Facts and Figures." [Online]. Available: <http://www.magnoxsites.co.uk/our-sites/wylfa/facts-and-figures>. [Accessed: 01-Aug-2013].
- [7] Department of Trade and Industry, "Our energy future - creating a low carbon economy," 2003.
- [8] Department of Trade and Industry, "Meeting the Energy Challenge - A White Paper on Energy," 2007.
- [9] Department for Business Enterprise and Regulatory Reform, "Meeting the Energy Challenge: A White Paper on Nuclear Power," 2008.
- [10] Office for Nuclear Regulation, "Information on ONR," 2013.
- [11] Office for Nuclear Regulation, "Background - The Generic Design Assessment process," 2013. [Online]. Available: <http://www.hse.gov.uk/newreactors/background.htm>. [Accessed: 02-Jun-2013].
- [12] EDF Energy, "New Nuclear: Building a reliable and affordable energy supply," 2013. [Online]. Available: <http://www.edfenergy.com/about-us/energy-generation/new-nuclear/>. [Accessed: 02-Jun-2013].
- [13] Office for Nuclear Regulation, "Current reactors being assessed," 2013. [Online]. Available: <http://www.hse.gov.uk/newreactors/gda-ukepr-ap1000.htm>. [Accessed: 02-Jun-2013].
- [14] Office for Nuclear Regulation, "Regulators to assess new nuclear reactor design," 2013. [Online]. Available: <http://news.hse.gov.uk/onr/2013/01/new-nuclear-reactor-design/>. [Accessed: 01-Jun-2013].

- [15] "UK regulators gear up for ABWR review," *Nuclear Engineering International*, Apr-2013. [Online]. Available: <http://www.neimagazine.com/news/newsuk-regulators-gear-up-for-abwr-review/>. [Accessed: 24-Jun-2013].
- [16] World Nuclear News, "Olkiluoto 3 delayed beyond 2014," 2012. [Online]. Available: [http://www.world-nuclear-news.org/NN-Olkiluoto\\_3\\_delayed\\_beyond\\_2014-1707124.html](http://www.world-nuclear-news.org/NN-Olkiluoto_3_delayed_beyond_2014-1707124.html). [Accessed: 03-Jun-2013].
- [17] The Guardian, "Construction schedule on Chinese third-generation nuclear plants races ahead of European models," 2010. [Online]. Available: <http://www.guardian.co.uk/environment/2010/dec/28/china-areva-taishan-nuclear-thibault>. [Accessed: 04-Jun-2013].
- [18] International Atomic Energy Agency, "Power Reactor Information System - KASHIWAZAKI KARIWA-6." [Online]. Available: <http://www.iaea.org/PRIS/CountryStatistics/ReactorDetails.aspx?current=383>. [Accessed: 24-Jun-2013].
- [19] International Atomic Energy Agency, "Power Reactor Information System - KASHIWAZAKI KARIWA-7." [Online]. Available: <http://www.iaea.org/PRIS/CountryStatistics/ReactorDetails.aspx?current=384>. [Accessed: 24-Jun-2013].
- [20] P. Benham, R. Crawford, and C. Armstrong, *Mechanics of Engineering Materials*, 2nd Ed. London: Pearson Education, 1996.
- [21] D. W. Dean, R. A. Ainsworth, and S. E. Booth, "Development and use of the R5 procedures for the assessment of defects in high temperature plant," *International Journal of Pressure Vessels and Piping*, vol. 78, no. 11–12, pp. 963–976, Nov. 2001.
- [22] "EDF to extend UK AGR life by five years; Heysham and Hartlepool are first winners," *Nuclear Engineering International*, 2010. [Online]. Available: <http://www.neimagazine.com/news/newsedf-to-extend-uk-agr-life-by-five-years-heysham-and-hartlepool-are-first-winners>. [Accessed: 24-Jun-2013].
- [23] EDF Energy, "EDF Energy announces seven year life extension to Hinkley Point B and Hunterston B nuclear power stations," 2012. [Online]. Available: <http://www.edfenergy.com/media-centre/press-news/EDF-Energy-announces-seven-year-life-extension-to-Hinkley-Point-B-and-Hunterston-B-nuclear-power-stations.shtml>. [Accessed: 24-Jun-2013].
- [24] "EDF plans longer life extensions for UK AGRs," *Nuclear Engineering International*, 2012. [Online]. Available: <http://www.neimagazine.com/news/newsedf-plans-longer-life-extensions-for-uk-agrs>. [Accessed: 24-Jun-2013].
- [25] R. a. Ainsworth and D. G. Hooton, "R6 and R5 procedures: The way forward," *International Journal of Pressure Vessels and Piping*, vol. 85, no. 3, pp. 175–182, Mar. 2008.

- [26] J. Shi and S. Booth, "An Investigation of Effects of Welding Residual Stresses on Creep Crack Growth for a Low Alloy Butt Weld," in *13th International Conference on Pressure Vessel Technology*, 2012.
- [27] M. J. Chevalier, D. J. Smith, and D. W. Dean, "The reliability of structural systems operating at high temperature: Replacing engineering judgement with operational experience," *International Journal of Pressure Vessels and Piping*, vol. 98, pp. 65–75, Oct. 2012.
- [28] H. Chen, "Lower and Upper Bound Shakedown Analysis of Structures With Temperature-Dependent Yield Stress," *Journal of Pressure Vessel Technology*, vol. 132, no. 1, p. 011202, 2010.
- [29] H. Chen and A. R. S. Ponter, "A Direct Method on the Evaluation of Ratchet Limit," *Journal of Pressure Vessel Technology*, vol. 132, no. 4, p. 041202, 2010.
- [30] D. Mackenzie, J. T. Boyle, and R. Hamilton, "The elastic compensation method for limit and shakedown analysis: a review," *The Journal of Strain Analysis for Engineering Design*, vol. 35, no. 3, pp. 171–188, Jan. 2000.
- [31] Dassault Systemes, "Abaqus 6.9 User Manual." 2009.
- [32] H. F. Chen and A. R. S. Ponter, "Integrity assessment of a 3D tubeplate using the linear matching method. Part 1. Shakedown, reverse plasticity and ratchetting," *International Journal of Pressure Vessels and Piping*, vol. 82, no. 2, pp. 85–94, Feb. 2005.
- [33] H. F. Chen and A. R. S. Ponter, "Integrity assessment of a 3D tubeplate using the linear matching method. Part 2: Creep relaxation and reverse plasticity," *International Journal of Pressure Vessels and Piping*, vol. 82, no. 2, pp. 95–104, Feb. 2005.
- [34] D. Tipping, "The Linear Matching Method: A Guide to the ABAQUS User Subroutines, British Energy Generation Ltd Report E/REP/BBGB/0017/GEN/07," 2008.
- [35] M. Boulbibane and a. R. S. Ponter, "Extension of the linear matching method to geotechnical problems," *Computer Methods in Applied Mechanics and Engineering*, vol. 194, no. 45–47, pp. 4633–4650, Nov. 2005.
- [36] J. Bree, "Elastic-plastic behaviour of thin tubes subjected to internal pressure and intermittent high-heat fluxes with application to fast-nuclear-reactor fuel elements," *The Journal of Strain Analysis for Engineering Design*, vol. 2, no. 3, pp. 226–238, Jul. 1967.
- [37] American Society of Mechanical Engineers, *ASME Boiler & Pressure Vessel Code Section 8 Division 2*. New York: , 2010.
- [38] E. Melan, "Theorie statisch unbestimmter systeme aus ideal-plastischem baustoff," *Sitzungsber. d. Akad. d. Wiss*, vol. 145, no. 2A, pp. 195–218, 1936.

- [39] W. T. Koiter, "General theorems for elastic plastic solids," in *Progress in solid mechanics*, J. Sneddon and R. Hill, Eds. Amsterdam: , 1960, pp. 167–221.
- [40] B. Karihaloo and W. G. Knauss, Eds., *Comprehensive Structural Integrity Volume 2*. Elsevier Pergamon, 2003.
- [41] British Energy Generation Ltd, *R6: Assessment of the integrity of structures containing defects*, Rev 4. 2004.
- [42] T. M. L. Nguyen-Tajan, B. Pommier, H. Maitournam, M. Houari, L. Verger, Z. Z. Du, and M. Snyman, "Determination of the stabilized response of a structure undergoing cyclic thermal-mechanical loads by a direct cyclic method," in *Abaqus Users' Conference*, 2003.
- [43] M. Martin, "Application of Direct Cyclic Analysis to the Prediction of Plastic Shakedown of Nuclear Power Plant Components," in *ASME 2008 Pressure Vessels and Piping Conference Volume 2: Computer Applications/Technology and Bolted Joints*, 2008, pp. 265–275.
- [44] P. Carter, "Analysis of cyclic creep and rupture. Part 2: calculation of cyclic reference stresses and ratcheting interaction diagrams," *International Journal of Pressure Vessels and Piping*, vol. 82, no. 1, pp. 27–33, Jan. 2005.
- [45] D. K. Vu, a. M. Yan, and H. Nguyen-Dang, "A primal–dual algorithm for shakedown analysis of structures," *Computer Methods in Applied Mechanics and Engineering*, vol. 193, no. 42–44, pp. 4663–4674, Oct. 2004.
- [46] V. D. Khoi, A.-M. Yan, and N.-D. Hung, "A dual form for discretized kinematic formulation in shakedown analysis," *International Journal of Solids and Structures*, vol. 41, no. 1, pp. 267–277, Jan. 2004.
- [47] M. Staat and M. Heitzer, "LISA — a European project for FEM-based limit and shakedown analysis," vol. 206, pp. 151–166, 2001.
- [48] M. Staat and M. Heitzer, *Numerical Methods for Limit and Shakedown Analysis: Deterministic and Probabilistic Problems*, 15th ed., vol. 15. Jülich: John von Neumann Institute for Computing, 2002.
- [49] Y. Yamamoto, S. Asada, and A. Okamoto, "Round Robin Calculations of Collapse Loads—A Torispherical Pressure Vessel Head With a Conical Transition," *Journal of Pressure Vessel Technology*, vol. 119, no. 4, pp. 503–509, 1997.
- [50] M. Heitzer, "Structural Optimization with FEM-based Shakedown Analyses," *Journal of Global Optimization*, vol. 24, no. 3, pp. 371–384, 2002.
- [51] G. Maier, J. Pastor, A. R. S. Ponter, and D. Weichert, "Direct Methods of Limit and Shakedown Analysis," in *Comprehensive Structural Integrity Volume 3*, R. de Borst and H. A. Mang, Eds. Amsterdam: Elsevier Pergamon, 2003, pp. 637–684.

- [52] R. Seshadri, "Inelastic evaluation of mechanical and structural components using the generalized local stress strain method of analysis," *Nuclear Engineering and Design*, vol. 153, no. 2–3, pp. 287–303, Jan. 1995.
- [53] R. Seshadri and S. P. Mangalaramanan, "Lower bound limit loads using variational concepts: the  $\alpha$ -method," *International Journal of Pressure Vessels and Piping*, vol. 71, no. 2, pp. 93–106, Apr. 1997.
- [54] D. L. Marriott, "Evaluation of deformation or load control of stresses under inelastic conditions using elastic finite element stress analysis," in *ASME Pressure Vessels and Piping Conference*, 1988, pp. 3–9.
- [55] D. Mackenzie and J. T. Boyle, "A method of estimating limit loads by iterative elastic analysis. I—Simple examples," *International Journal of Pressure Vessels and Piping*, vol. 53, no. 1, pp. 77–95, Jan. 1992.
- [56] C. Nadarajah, D. Mackenzie, and J. T. Boyle, "A method of estimating limit loads by iterative elastic analysis. II—Nozzle sphere intersections with internal pressure and radial load," *International Journal of Pressure Vessels and Piping*, vol. 53, no. 1, pp. 97–119, Jan. 1992.
- [57] J. Shi, D. Mackenzie, and J. T. Boyle, "A method of estimating limit loads by iterative elastic analysis. III—Torispherical heads under internal pressure," *International Journal of Pressure Vessels and Piping*, vol. 53, no. 1, pp. 121–142, Jan. 1992.
- [58] R. Hamilton, D. Mackenzie, J. Shi, and J. T. Boyle, "Simplified lower bound limit analysis of pressurised cylinder/cylinder intersections using generalised yield criteria," *International Journal of Pressure Vessels and Piping*, vol. 67, no. 2, pp. 219–226, Jul. 1996.
- [59] C. Nadarajah, D. Mackenzie, and J. T. Boyle, "Limit and shakedown analysis of nozzle/cylinder intersections under internal pressure and in-plane moment loading," *International Journal of Pressure Vessels and Piping*, vol. 68, no. 3, pp. 261–272, Oct. 1996.
- [60] D. Mackenzie, J. Shi, and J. T. Boyle, "Finite element modelling for limit analysis by the elastic compensation method," *Computers & Structures*, vol. 51, no. 4, pp. 403–410, May 1994.
- [61] M. Muscat, R. Hamilton, and J. T. Boyle, "Shakedown analysis for complex loading using superposition," *The Journal of Strain Analysis for Engineering Design*, vol. 37, no. 5, pp. 399–412, Jan. 2002.
- [62] M. Muscat, D. Mackenzie, and R. Hamilton, "Evaluating shakedown under proportional loading by non-linear static analysis," *Computers & Structures*, vol. 81, no. 17, pp. 1727–1737, Aug. 2003.
- [63] M. Muscat and D. Mackenzie, "Elastic-Shakedown Analysis of Axisymmetric Nozzles," *Journal of Pressure Vessel Technology*, vol. 125, no. 4, p. 365, 2003.

- [64] P. Makulsawatudom, D. Mackenzie, and R. Hamilton, "Shakedown behaviour of thick cylindrical vessels with crossholes," *Proceedings of the Institution of Mechanical Engineers, Part E: Journal of Process Mechanical Engineering*, vol. 218, no. 3, pp. 133–141, Jan. 2004.
- [65] H. F. Abdalla, M. M. Megahed, and M. Y. A. Younan, "Shakedown Limits of a 90-Degree Pipe Bend Using Small and Large Displacement Formulations," *Journal of Pressure Vessel Technology*, vol. 129, no. 2, p. 287, 2007.
- [66] C.-S. Oh, Y.-J. Kim, and C.-Y. Park, "Shakedown limit loads for elbows under internal pressure and cyclic in-plane bending," *International Journal of Pressure Vessels and Piping*, vol. 85, no. 6, pp. 394–405, Jun. 2008.
- [67] A. R. S. Ponter and K. F. Carter, "Limit state solutions, based upon linear elastic solutions with a spatially varying elastic modulus," *Computer Methods in Applied Mechanics and Engineering*, vol. 140, no. 3–4, pp. 237–258, Jan. 1997.
- [68] A. R. S. Ponter and K. F. Carter, "Shakedown state simulation techniques based on linear elastic solutions," *Computer Methods in Applied Mechanics and Engineering*, vol. 140, no. 3–4, pp. 259–279, Jan. 1997.
- [69] A. R. S. Ponter, P. Fuschi, and M. Engelhardt, "Limit analysis for a general class of yield conditions," *European Journal of Mechanics - A/Solids*, vol. 19, no. 3, pp. 401–421, May 2000.
- [70] A. R. S. Ponter and M. Engelhardt, "Shakedown limits for a general yield condition: implementation and application for a Von Mises yield condition," *European Journal of Mechanics - A/Solids*, vol. 19, no. 3, pp. 423–445, May 2000.
- [71] H. F. Chen and A. R. S. Ponter, "Shakedown and limit analyses for 3-D structures using the linear matching method," *International Journal of Pressure Vessels and Piping*, vol. 78, no. 6, pp. 443–451, Jun. 2001.
- [72] H. Chen and A. R. S. Ponter, "Structural integrity assessment of superheater outlet penetration tubeplate," *International Journal of Pressure Vessels and Piping*, vol. 86, no. 7, pp. 412–419, Jul. 2009.
- [73] T. Li, H. Chen, W. Chen, and J. Ure, "On the shakedown analysis of welded pipes," *International Journal of Pressure Vessels and Piping*, vol. 88, no. 8–9, pp. 301–310, Aug. 2011.
- [74] H. Chen, W. Chen, T. Li, and J. Ure, "Shakedown Behaviour of Composite Cylinders With Cross Hole," in *ASME 2010 Pressure Vessels and Piping Conference: Volume 2*, 2010, pp. 89–98.
- [75] M. Martin and D. Rice, "A Hybrid Procedure for Ratchet Boundary Prediction," in *ASME 2009 Pressure Vessels and Piping Conference Volume 1: Codes and Standards*, 2009, pp. 81–88.

- [76] A. Jappy, D. Mackenzie, and H. Chen, "A Fully Implicit, Lower Bound, Multi-Axial Solution Strategy for Direct Ratchet Boundary Evaluation: Theoretical Development," in *ASME 2012 Pressure Vessels and Piping Conference Volume 3: Design and Analysis*, 2012, pp. 577–585.
- [77] A. Jappy, D. Mackenzie, and H. Chen, "A Fully Implicit, Lower Bound, Multi-Axial Solution Strategy for Direct Ratchet Boundary Evaluation: Implementation and Comparison," in *ASME 2012 Pressure Vessels and Piping Conference Volume 3: Design and Analysis*, 2012, pp. 587–595.
- [78] R. Adibi-Asl and W. Reinhardt, "Non-cyclic shakedown/ratcheting boundary determination – Part 1: Analytical approach," *International Journal of Pressure Vessels and Piping*, vol. 88, no. 8–9, pp. 311–320, Aug. 2011.
- [79] R. Adibi-Asl and W. Reinhardt, "Non-cyclic shakedown/ratcheting boundary determination - Part 2: Numerical implementation," *International Journal of Pressure Vessels and Piping*, vol. 88, no. 8–9, pp. 321–329, Aug. 2011.
- [80] R. Adibi-Asl and W. Reinhardt, "Ratchet Boundary Determination Using a Noncyclic Method," *Journal of Pressure Vessel Technology*, vol. 132, no. 2, p. 021201, 2010.
- [81] R. Adibi-Asl and W. Reinhardt, "Shakedown/Ratcheting Boundary Determination Using Iterative Linear Elastic Schemes," in *ASME 2009 Pressure Vessels and Piping Conference Volume 1: Codes and Standards*, 2009, pp. 109–119.
- [82] A. R. S. Ponter and H. Chen, "A minimum theorem for cyclic load in excess of shakedown, with application to the evaluation of a ratchet limit," *European Journal of Mechanics - A/Solids*, vol. 20, no. 4, pp. 539–553, Jul. 2001.
- [83] H. Chen and A. R. S. Ponter, "A method for the evaluation of a ratchet limit and the amplitude of plastic strain for bodies subjected to cyclic loading," *European Journal of Mechanics - A/Solids*, vol. 20, no. 4, pp. 555–571, Jul. 2001.
- [84] H. Chen and A. R. S. Ponter, "Linear matching method on the evaluation of plastic and creep behaviours for bodies subjected to cyclic thermal and mechanical loading," *International Journal for Numerical Methods in Engineering*, vol. 68, no. 1, pp. 13–32, Oct. 2006.
- [85] W. Chen, H. Chen, T. Li, and J. Ure, "Limit, Shakedown and Ratchet Analyses of Defective Pipeline Under Internal Pressure and Cyclic Thermal Loading," in *ASME 2011 Pressure Vessels and Piping Conference: Volume 2*, 2011, pp. 311–320.
- [86] T. Li, H. Chen, W. Chen, and J. Ure, "On the Ratchet Analysis of a Cracked Welded Pipe," *Journal of Pressure Vessel Technology*, vol. 134, no. 1, p. 011203, 2012.
- [87] M. Lytwyn, H. Chen, and M. Martin, "Linear Matching Method for ratchet limit prediction in comparison to Rolls-Royce's Hierarchical Finite Element Framework," in *13th International Conference on Pressure Vessel Technology*, 2012.

- [88] M. Martin, L. Rawson, and D. Rice, "A Hierarchical Finite Element Framework for the Assessment of Pressure Vessels to the ASME III Code," in *ASME 2010 Pressure Vessels and Piping Conference: Volume 1*, 2010, pp. 125–135.
- [89] M. Martin, C. Watson, and K. Wright, "Review of ASME III Code Case for the Application of Finite Element Based Limit Load Analysis," in *ASME 2011 Pressure Vessels and Piping Conference: Volume 1*, 2011, pp. 513–518.
- [90] Y. Gorash and H. Chen, "Creep-fatigue life assessment of cruciform weldments using the linear matching method," *International Journal of Pressure Vessels and Piping*, vol. 104, pp. 1–13, Apr. 2013.
- [91] Y. Gorash and H. Chen, "A parametric study on creep-fatigue strength of welded joints using the linear matching method," *International Journal of Fatigue*, vol. 55, pp. 112–125, Oct. 2013.
- [92] H. Reece-Barkell, M. Stevens, D. J. Tipping, and J. Sole, "Shakedown and Ratcheting Assessment of a Tubeplate Using the Linear Matching Method," in *ASME 2012 Pressure Vessels and Piping Conference Volume 1: Codes and Standards*, 2012, pp. 405–412.
- [93] M. Engelhardt, "Computational Modelling of Shakedown," PhD Thesis, University of Leicester, 1999.
- [94] A. G. Miller, "Review of limit loads of structures containing defects," *International Journal of Pressure Vessels and Piping*, vol. 32, no. 1–4, pp. 197–327, Jan. 1988.
- [95] R. A. W. Bradford, "The Bree problem with primary load cycling in-phase with the secondary load," *International Journal of Pressure Vessels and Piping*, vol. 99–100, pp. 44–50, Nov. 2012.
- [96] F. Ellyin, "Experimental investigation of limit loads of nozzles in cylindrical vessels," *Welding Research Council Bulletin*, vol. 219, pp. 1–14, 1976.
- [97] E. Procter and R. F. Flinders, "Shakedown investigations on partial penetration welded nozzles in a spherical shell," *Nuclear Engineering and Design*, vol. 8, no. 1, pp. 171–185, Jul. 1968.
- [98] C. R. Calladine, "Limit analysis of curved tubes," *Journal of Mechanical Engineering Science*, vol. 16, no. 2, pp. 85–87, Apr. 1974.
- [99] I. W. Goodall, "Lower bound limit analysis of curved tubes loaded by combined internal pressure and in-plane bending moment, CEGB Report RD/B/N4360," 1978.
- [100] Y. Lei, "Review of limit load solutions for defect-free pipe bends, British Energy Generation Ltd Report E/REP/BBGB/0034/GEN/08," 2009.

- [101] X. Chen, B. Gao, and G. Chen, "Ratcheting Study of Pressurized Elbows Subjected to Reversed In-Plane Bending," *Journal of Pressure Vessel Technology*, vol. 128, no. 4, p. 525, 2006.
- [102] J. Gross-Weege, "A unified formulation of statical shakedown criteria for geometrically nonlinear problems," *International Journal of Plasticity*, vol. 6, no. 4, pp. 433–447, Jan. 1990.
- [103] C. Polizzotto and G. Borino, "Shakedown and steady-state responses of elastic-plastic solids in large displacements," *International Journal of Solids and Structures*, vol. 33, no. 23, pp. 3415–3437, Sep. 1996.
- [104] British Standards Institute, "PD5500: Specification for Unfired fusion welded pressure vessels," 2006.
- [105] C. Polizzotto, "A Study on Plastic Shakedown of Structures: Part I—Basic Properties," *Journal of Applied Mechanics*, vol. 60, no. 2, p. 318, 1993.
- [106] C. Polizzotto, "A Study on Plastic Shakedown of Structures: Part II—Theorems," *Journal of Applied Mechanics*, vol. 60, no. 2, p. 324, 1993.
- [107] A. R. S. Ponter and S. Karadeniz, "An Extended Shakedown Theory for Structures That Suffer Cyclic Thermal Loading, Part 1: Theory," *Journal of Applied Mechanics*, vol. 52, no. 4, p. 877, 1985.
- [108] R. A. W. Bradford, "An alternative method for assessing creep ratchet for the Bree and Modified Bree problems with sustained thermal load, EDF Energy Draft Report," 2013.
- [109] Dalton Nuclear Institute, "Project Opportunities within the Nuclear EngD Programme." [Online]. Available: <http://www.dalton.manchester.ac.uk/images/subr/files/Engdwebsiteprojectlist.pdf>. [Accessed: 01-Aug-2013].
- [110] J. G. Lekkerkerker, "The determination of elastic stresses near cylinder-to-cylinder intersections," *Nuclear Engineering and Design*, vol. 20, no. 1, pp. 57–84, Jun. 1972.
- [111] J. Han, Y. Kim, and K. Lee, "Effect of Creep Mismatch Factor on Stress Redistribution in Welded Branch Pipes," in *ASME 2010 Pressure Vessels and Piping Conference: Volume 5*, 2010, pp. 411–420.
- [112] Y.-J. Kim, K.-H. Lee, and C.-Y. Park, "Limit loads for thin-walled piping branch junctions under internal pressure and in-plane bending," *International Journal of Pressure Vessels and Piping*, vol. 83, no. 9, pp. 645–653, Sep. 2006.
- [113] European Pressure Equipment Research Council, "Design by Analysis Manual," 1999.
- [114] F. W. Brust, T. Zhang, D.-J. Shim, S. Kalyanam, G. Wilkowski, M. Smith, and A. Goodfellow, "Summary of Weld Residual Stress Analyses for Dissimilar Metal Weld

Nozzles,” in *ASME 2010 Pressure Vessels and Piping Conference: Volume 6, Parts A and B*, 2010, pp. 1521–1529.

- [115] M. C. Smith, O. Muránsky, P. J. Bendeich, and L. Edwards, “The Impact of Key Simulation Variables on Predicted Residual Stresses in Pressuriser Nozzle Dissimilar Metal Weld Mock-Ups: Part 1—Simulation,” in *ASME 2010 Pressure Vessels and Piping Conference: Volume 6, Parts A and B*, 2010, pp. 1483–1494.
- [116] M. C. Smith, O. Muransky, A. Goodfellow, E. Kingston, P. Freyer, S. Marlette, G. M. Wilkowski, B. Brust, and D.-J. Shim, “The Impact of Key Simulation Variables on Predicted Residual Stresses in Pressuriser Nozzle Dissimilar Metal Weld Mock-Ups: Part 2—Comparison of Simulation and Measurements,” in *ASME 2010 Pressure Vessels and Piping Conference: Volume 6, Parts A and B*, 2010, pp. 1495–1511.
- [117] British Standards Institute, “BS EN 10028-7 Flat products made of steels for pressure purposes Part 7-Stainless Steels,” 2007.
- [118] P. R. Hurrell, N. A. Leggatt, and R. J. Dennis, “Residual Stress Analysis of Tube Attachment Weld in Pressure Vessel Forging: Comparison of FE Predictions and Measurements,” in *Volume 6: Materials and Fabrication*, 2005, vol. 2005, pp. 771–780.
- [119] J. W. Kim, K. Lee, J. S. Kim, and T. S. Byun, “Local mechanical properties of Alloy 82/182 dissimilar weld joint between SA508 Gr.1a and F316 SS at RT and 320°C,” *Journal of Nuclear Materials*, vol. 384, no. 3, pp. 212–221, Feb. 2009.
- [120] A. R. S. Ponter and H. Chen, “Linear Matching Method on Structural Integrity Assessment - User Guide,” University of Leicester, 2004.
- [121] Python Software Foundation, “Python Programming Language – Official Website.” [Online]. Available: <http://www.python.org/>. [Accessed: 24-Jul-2013].
- [122] T. Siddall, “Finite Element Modelling and Shakedown Assessment of Cold Reheat Secondary Header Branches, British Energy Generation Ltd Report E/REP/BBJB/0087/AGR/09,” 2011.

## Appendix A. Equations for limit pressure and moment of a pipe bend

This appendix lists the equations derived by Lei in [100] for the limit pressure and moment of pipe bends. Begin by defining the limit pressure and limit moment for a thin straight pipe as

$$P_L^s = \frac{2}{\sqrt{3}} \frac{\sigma_y t}{r} \quad \text{and} \quad M_L^s = 4r^2 t \sigma_y \quad (\text{A1.1})$$

Then the limit internal pressure is given by:

$$\frac{P_L}{P_L^s} = \begin{cases} c \left( \frac{R}{r} \right)^n & \text{for } 1.5 \leq \frac{R}{r} < 6 \\ 1 - \frac{r}{R} & \text{for } \frac{R}{r} \geq 6 \\ 1 - \frac{r}{2R} & \end{cases} \quad \text{and} \quad \begin{cases} c = 0.8447 - 0.0099 \frac{r}{t} \\ n = 0.0373 + 0.0075 \frac{r}{t} \end{cases} \quad \text{for } 5 \leq \frac{r}{t} \leq 15$$

$$\begin{cases} c = 0.6962 \\ n = 0.1498 \end{cases} \quad \text{for } 5 \leq \frac{r}{t} \leq 1. \quad (\text{A1.2})$$

The limit in-plane opening bending moment is given by:

$$\frac{M_L}{M_L^s} = 1.04h^{1/3} - 0.0594 \quad \text{for } 0.1 \leq h \leq 0.6 \quad (\text{A1.3})$$

And the limit in-plane closing bending moment is given by:

$$\begin{cases} \frac{M_L}{M_L^s} = \left(1 + \frac{0.22}{h^{1.028+0.12R/r}}\right)^{-1} & \text{for } h \leq 1 \\ \frac{M_L}{M_L^s} = \left(1 + \frac{0.22}{h^{1.313}}\right)^{-1} & \text{for } h > 1 \end{cases} \quad (\text{A1.4})$$

Where combined pressure and bending moments are applied, the following limit locus is defined:

$$\frac{M_L}{(M_L)_{P=0}} = \sqrt{1 - \left(\frac{P}{(P_L)_{M=0}}\right)^2} \quad (\text{A1.5})$$

Where  $(M_L)_{P=0}$  is the limit moment with no pressure loading (equation (A1.3) or (A1.4)) and  $(P_L)_{M=0}$  is the limit pressure with no moment loading (equation (A1.2)).

## Appendix B. Iterative Evaluation of the Varying Residual Stress Field

The procedure for obtaining the varying residual stress field involves a load cycle which has N load instances where  $n=1,2,\dots,N$ , which is associated with N increments in the solution procedure. This cycle repeats M times so that  $m=1,2,\dots,M$ . The iterative procedure is as follows:

### During Load Cycle m=1:

Increment 1:  $\Delta\rho_{ij_1}^{r1}$ , which results from the applied elastic stress  $\sigma_{ij}^{\Delta^1}$ , is evaluated.

Increment 2:  $\Delta\rho_{ij_1}^{r2}$ , which results from the applied stress  $\sigma_{ij}^{\Delta^2} + \Delta\rho_{ij_1}^{r1}$ , is evaluated.

Increment N:  $\Delta\rho_{ij_1}^{rN}$ , which results from the applied stress

$\sigma_{ij}^{\Delta^N} + \Delta\rho_{ij_1}^{r1} + \Delta\rho_{ij_1}^{r2} + \dots + \Delta\rho_{ij_1}^{rN-1}$  is evaluated.

### During Load Cycle m=2

Increment N+1:  $\Delta\rho_{ij_2}^{r1}$  resulting from  $\sigma_{ij}^{\Delta^1} + \left[ \Delta\rho_{ij_1}^{r1} + \Delta\rho_{ij_1}^{r2} + \dots + \Delta\rho_{ij_1}^{rN} \right]$  is evaluated

Increment N+2:  $\Delta\rho_{ij_2}^{r2}$  resulting from  $\sigma_{ij}^{\Delta^2} + \left[ \Delta\rho_{ij_1}^{r1} + \Delta\rho_{ij_1}^{r2} + \dots + \Delta\rho_{ij_1}^{rN} \right] + \Delta\rho_{ij_2}^{r1}$  is evaluated

Increment 2N:  $\Delta\rho_{ij_2}^{rN}$  which results from the applied stress

$\sigma_{ij}^{\Delta^N} + \left[ \Delta\rho_{ij_1}^{r1} + \Delta\rho_{ij_1}^{r2} + \dots + \Delta\rho_{ij_1}^{rN} \right] + \Delta\rho_{ij_2}^{r1} + \Delta\rho_{ij_2}^{r2} + \dots + \Delta\rho_{ij_2}^{rN-1}$  is evaluated

### During Load Cycle m=M:

Increment MN-N+1:  $\Delta\rho_{ij_M}^{r1}$  resulting from  $\sigma_{ij}^{\Delta^1} + \sum_{n=1}^N \Delta\rho_{ij_1}^{r_n} + \dots + \sum_{n=1}^N \Delta\rho_{ij_{M-1}}^{r_n}$  is

evaluated

Increment MN-N+2:  $\Delta\rho_{ijM}^{r,2}$  resulting from  $\sigma_{ij}^{\Delta^2} + \sum_{n=1}^N \Delta\rho_{ij1}^{r,n} + \dots + \sum_{n=1}^N \Delta\rho_{ijM-1}^{r,n} + \Delta\rho_{ijM}^{r,1}$

is evaluated

Increment MN:  $\Delta\rho_{ijM}^{r,N}$  resulting from  $\sigma_{ij}^{\Delta^N} + \sum_{n=1}^N \Delta\rho_{ij1}^{r,n} + \dots + \sum_{n=1}^N \Delta\rho_{ijM-1}^{r,n} + \sum_{n=1}^{N-1} \Delta\rho_{ijM}^{r,n}$

If a convergent solution is obtained which is inside the ratchet limit then the sum of the increments of residual stress over the final cycle M must tend to zero:

$$\sum_{n=1}^N \Delta\rho_{ijM}^{r,n} = 0$$

Therefore the steady state component of this residual stress is given by

$$\bar{\rho}_{ij}^r = \sum_{n=1}^N \Delta\rho_{ij1}^{r,n} + \dots + \sum_{n=1}^N \Delta\rho_{ijM-1}^{r,n}$$

And the accumulated residual stress at a particular time point in the cycle is therefore the sum of the constant part  $\bar{\rho}_{ij}^r$  and varying part for that time point:

$$\rho_{ij}^r(t_n) = \bar{\rho}_{ij}^r + \sum_{n=1}^N \Delta\rho_{ij}^{r,n}$$

Which is equivalent to equation (4.27) used in the numerical procedure.

## Appendix C. Algebraic Expansion of Equation (4.44)

Equation (4.43) describes the total stress field in the structure, and is re-iterated here for convenience

$$\sigma_{ij}(x,t) = \hat{\sigma}_{ij}^F(x,t) + \hat{\sigma}_{ij}^\Delta(x,t) + \bar{\rho}_{ij}(x) + \rho_{ij}^r(x,t) \quad (C1.1)$$

The stage 1 calculation does not scale the applied cyclic stresses and find the varying residual stress associated with that fixed level of cyclic loading. Therefore when these stresses are brought forward to stage 2, they can be considered as a single stress field:

$$\hat{\sigma}_{ij}^V(x,t) = \hat{\sigma}_{ij}^\Delta(x,t) + \rho_{ij}^r(x,t) \quad (C1.2)$$

During the stage 2 calculation equation (4.44) must be satisfied for the loading to be within global shakedown:

$$f\left(\lambda^{LB} \hat{\sigma}_{ij}^F(x,t) + \bar{\rho}_{ij}(x) + \hat{\sigma}_{ij}^V(x,t)\right) \leq 0 \quad (C1.3)$$

Numerically this means checking the yield condition has not been violated at all integration points in the model and at all time points in the cycle. To find the global shakedown limit  $\lambda^{LB}$  should be scaled so that the effective stress equals the yield stress. As  $\lambda^{LB}$  is the only unknown in equation (4.44) it can be rearranged to find  $\lambda^{LB}$  and give the lower bound multiplier for that integration point and time point in the load cycle. Each of the three stresses in equation (C1.3) is described by six components, which gives a total of eighteen stresses. The von-Mises yield function is used, so equation (C1.3) expands to:

$$\begin{aligned} \frac{2}{3}\sigma_{yield}^2 = & \left[ \left( \lambda_{LB} \hat{\sigma}_x^F + \bar{\rho}_x + \hat{\sigma}_x^V \right) - \sigma_H \right] + \left[ \left( \lambda_{LB} \hat{\sigma}_y^F + \bar{\rho}_y + \hat{\sigma}_y^V \right) - \sigma_H \right] \\ & + \left[ \left( \lambda_{LB} \hat{\sigma}_z^F + \bar{\rho}_z + \hat{\sigma}_z^V \right) - \sigma_H \right] + \left( \lambda_{LB} \hat{\sigma}_{xy}^F + \bar{\rho}_{xy} + \hat{\sigma}_{xy}^V \right) \\ & + \left( \lambda_{LB} \hat{\sigma}_{yz}^F + \bar{\rho}_{yz} + \hat{\sigma}_{yz}^V \right) + \left( \lambda_{LB} \hat{\sigma}_{xz}^F + \bar{\rho}_{xz} + \hat{\sigma}_{xz}^V \right) \end{aligned} \quad (C1.4)$$

Where  $\sigma_H$  is the hydrostatic stress:

$$\sigma_H = \left( \frac{(\lambda_{LB} \hat{\sigma}_x^F + \bar{\rho}_x + \hat{\sigma}_x^V) + (\lambda_{LB} \hat{\sigma}_y^F + \bar{\rho}_y + \hat{\sigma}_y^V) + (\lambda_{LB} \hat{\sigma}_z^F + \bar{\rho}_z + \hat{\sigma}_z^V)}{3} \right) \quad (C1.5)$$

Re-arranging for  $\lambda^{LB}$  results in a quadratic:

$$A(\lambda_{LB})^2 + B\lambda_{LB} + C = 0 \quad (C1.6)$$

Where the coefficients A, B and C are:

$$A = -\frac{2}{3}\hat{\sigma}_x^F \hat{\sigma}_y^F + 2(\hat{\sigma}_{xy}^F)^2 + \frac{2}{3}(\hat{\sigma}_x^F)^2 + 2(\hat{\sigma}_{xz}^F)^2 - \frac{2}{3}\hat{\sigma}_x^F \hat{\sigma}_z^F + \frac{2}{3}(\hat{\sigma}_y^F)^2 + \frac{2}{3}(\hat{\sigma}_z^F)^2 + \frac{2}{3}\hat{\sigma}_y^F \hat{\sigma}_z^F + \frac{2}{3}(\hat{\sigma}_{yz}^F)^2 \quad (C1.7)$$

$$B = -\frac{2}{3}\bar{\rho}_y \hat{\sigma}_z^F + 4\hat{\sigma}_{yz}^F \bar{\rho}_{yz} + 4\hat{\sigma}_{xz}^F \hat{\sigma}_{xz}^V - \frac{2}{3}\hat{\sigma}_x^F \bar{\rho}_y + \frac{4}{3}\hat{\sigma}_y^F \bar{\rho}_y + 4\hat{\sigma}_{xy}^F \hat{\sigma}_{xy}^V - \frac{2}{3}\hat{\sigma}_x^V \hat{\sigma}_y^F + \frac{4}{3}\hat{\sigma}_z^F \hat{\sigma}_z^V + 4\hat{\sigma}_{xz}^F \bar{\rho}_{xz} - \frac{2}{3}\hat{\sigma}_x^F \hat{\sigma}_y^V + \frac{4}{3}\hat{\sigma}_z^F \bar{\rho}_z + \frac{4}{3}\hat{\sigma}_x^F \hat{\sigma}_x^V + \frac{4}{3}\hat{\sigma}_y^F \hat{\sigma}_y^V - \frac{2}{3}\bar{\rho}_x \hat{\sigma}_z^F + \frac{4}{3}\hat{\sigma}_x^F \bar{\rho}_x - \frac{2}{3}\hat{\sigma}_y^V \hat{\sigma}_z^F - \frac{2}{3}\bar{\rho}_x \hat{\sigma}_y^F + 4\hat{\sigma}_{xy}^F \bar{\rho}_{xy} - \frac{2}{3}\hat{\sigma}_x^V \hat{\sigma}_z^F + 4\hat{\sigma}_{yz}^F \hat{\sigma}_{yz}^V - \frac{2}{3}\hat{\sigma}_y^F \bar{\rho}_z - \frac{2}{3}\hat{\sigma}_x^F \hat{\sigma}_z^V - \frac{2}{3}\hat{\sigma}_y^F \hat{\sigma}_z^V - \frac{2}{3}\hat{\sigma}_x^F \bar{\rho}_z \quad (C1.8)$$

$$C = 2(\hat{\sigma}_{yz}^V)^2 - \frac{2}{3}\hat{\sigma}_y^V \bar{\rho}_z + \frac{2}{3}(\bar{\rho}_x)^2 + \frac{2}{3}(\bar{\rho}_z)^2 + 2(\hat{\sigma}_{xz}^V)^2 - \frac{2}{3}\bar{\rho}_y \hat{\sigma}_z^V - \frac{2}{3}\bar{\rho}_y \bar{\rho}_z + 4\hat{\sigma}_{xy}^V \bar{\rho}_{xy} - \frac{2}{3}\hat{\sigma}_x^V \hat{\sigma}_z^V - \frac{2}{3}\hat{\sigma}_x^V \bar{\rho}_z - \frac{2}{3}\bar{\rho}_x \hat{\sigma}_z^V - \frac{2}{3}\bar{\rho}_x \bar{\rho}_z + \frac{4}{3}\hat{\sigma}_z^V \bar{\rho}_z + 2(\hat{\sigma}_z^V)^2 + \frac{2}{3}(\bar{\rho}_{xy})^2 + \frac{2}{3}(\bar{\rho}_{xz})^2 + 2(\hat{\sigma}_{xy}^V)^2 - \frac{2}{3}\bar{\rho}_x \hat{\sigma}_y^V - \frac{2}{3}\hat{\sigma}_x^V \hat{\sigma}_y^V - \frac{2}{3}\bar{\rho}_x \bar{\rho}_y + 4\hat{\sigma}_{xz}^V \bar{\rho}_{xz} + \frac{4}{3}\hat{\sigma}_y^V \bar{\rho}_y - \frac{2}{3}\hat{\sigma}_x^V \bar{\rho}_y + 2(\hat{\sigma}_x^V)^2 + 2(\hat{\sigma}_y^V)^2 + \frac{4}{3}\hat{\sigma}_x^V \bar{\rho}_x - \frac{2}{3}\hat{\sigma}_y^V \hat{\sigma}_z^V + \frac{2}{3}(\bar{\rho}_{yz})^2 + \frac{4}{3}\hat{\sigma}_{yz}^V \bar{\rho}_{yz} + \frac{2}{3}(\bar{\rho}_y)^2 - \frac{2}{3}(\sigma_{yield})^2 \quad (C1.9)$$

where x, y, z, xy, xz and yz are the direct and shear components of stress.

## **Appendix D. The LMM Subroutines**

This appendix gives details of each of the LMM subroutines and the calculations and tasks they perform. This appendix should give a better understanding of the code for support and future development.

### **UEXTERNALDB(LOP,LRESTART,TIME,DTIME,KSTEP,KINC)**

The UEXTERNALDB subroutine is called by Abaqus once at the beginning of the analysis (LOP=0), at the start of each increment (LOP=1), the end of each increment (LOP=2) and the end of the analysis (LOP=3).

This subroutine is used at the beginning of the analysis (LOP=0) to read the LMM text file created by the plug-in. It is also used at the end of the analysis (LOP=3) to properly close this text file.

The structure of the subroutine is broadly similar for all three analysis types. There are some minor differences between the strict shakedown code and the steady cycle and ratchet code which relates to the slightly different data required by these analyses. For example the Ramberg-Osgood model is only implemented in the steady cycle and ratchet code. Table D-1 summarises the order in which the values are read from the text file and the respective differences between the strict shakedown and steady cycle and ratchet codes.

The values read by UEXTERNALDB are placed into COMMON blocks. This means that this data can be shared with the UMAT and URDFIL subroutines.

### **The UMAT Subroutine<sup>1</sup>**

This subroutine is where the bulk of the LMM calculations take place. The initial stress tensor (STRESS), initial strain (STRAN) and strain increment (DSTRAN) are passed into UMAT at the beginning of the increment. The UMAT subroutine must then return the updated stress tensor (STRESS) and Jacobian matrix (DDSDDE). UMAT is called for each integration point which has been assigned a User-material, and at each integration point it is called at least twice during an increment.

---

<sup>1</sup> See the Abaqus User Subroutines Reference Manual in [31] for a full argument list for UMAT

**Table D-1 - UEXTERNALDB operations**

Strict Shakedown Only	Common to Both	Steady Cycle and Ratchet Only
	Analysis type	
	Maximum number of increments	
Convergence type and value		Steady cycle convergence value
		Global shakedown convergence value (if this analysis is selected)
	Dimensionality of the model	
	Number of applied loads	
	Number of load instances	
	Multipliers for each load and whether it is scalable or not	
	Number of materials	
	For each material read the temperature dependent modulus and yield stress (if any)	
		Read if this material has a Ramberg-Osgood model associated with it, and if it does then read the temperature dependent parameters (if any)

The UMAT subroutine is used for several tasks within the LMM framework. It is used to calculate the elastic stresses for each applied load. It is also used to perform an increment of the strict shakedown/steady cycle/steady cycle and ratchet analysis, depending on which is selected. There are two files which contain the LMM UMATs and the associated URDFIL subroutine, and each UMAT is further divided into subroutines to perform these different aspects of the LMM solution.

- LMM\_Shakedown\_Multi\_Process.for. In this file the UMAT is divided into two subroutines named ELASTIC and SHAKEDOWN.
- LMM\_Steady\_Cycle\_and\_Ratcher.for. In this file the UMAT is divided into three subroutines: ELASTIC, STEADYCYCLE and RATCHET.

When the solution begins the UMAT is called and in all cases the ELASTIC subroutine is used to carry out an elastic analysis for each applied load. Once complete, the ELASTIC subroutine is called once more during the null step which has no applied loads. This allows key variables, such as the strain increment (DSTRAN), to return to zero before the LMM solution commences with one of the other subroutines.

A UMAT subroutine uses an array of Solution-Dependent State Variables (STATEV) to store values calculated. The STATEV array is passed into UMAT at the beginning of the increment and contains the values calculated at the end of the previous increment (or propagates the values if they are unchanged in the previous increment). These are used to provide the user with contour plots in the odb file for a number of variables such as stresses and strains. The STATEV array is also used within the calculation procedures to pass variables between consecutive increments.

UMAT contains three variables, SSE, SPD and SCD, which have no effect on the solution but are intended for energy output. The LMM uses these values because they can be extracted in URDFIL as volume integrals of the values needed for the upper bound load multiplier.

### **ELASTIC**

In both files the ELASTIC subroutine replicates a standard elastic analysis in Abaqus. The reason that this analysis is performed using UMAT rather than using Abaqus itself is so that the stress tensor and temperature for each applied load can be stored in the STATEV array. This allows the subsequent SHAKEDOWN/STEADYCYCLE/RATCHET subroutine access to these values. The STATEV numbering is determined by the number of applied loads.

### **SHAKEDOWN**

The SHAKEDOWN subroutine follows the calculations given in chapter 3 to perform a single LMM strict shakedown increment. The major steps of the code are as follows:

1. Initialise variables and ensure they equal zero to begin a new increment
2. If this is the first increment then set the upper bound load multiplier to 1.0
3. Call LOADCYCLE to obtain the elastic stress and temperature at each point in the load cycle
4. If temperature dependent yield is defined then call YIELDSTRESS to obtain the yield stress. Otherwise the yield stress equals the User-material property

5. In the first increment the Shear modulus is obtained by  $1/\text{young's modulus}$ . If this is temperature dependent then call MODULUS to obtain this value.
6. After the first increment the shear modulus is obtained by dividing the effective strain by the yield stress (equation (3.16))
7. The value of  $\sigma_{ij}^{in,k+1}$  is calculated according to equation (3.19) using the values of shear modulus and applied stress.
8. JACOBIAN is called to form the stiffness matrix (DDSDDE)
9. The estimate of the constant residual stress field,  $\bar{\rho}_{ij}^{k+1}$ , is obtained by equation (3.20)
10. RLOWER is called to calculate the lower bound multiplier
11. Provide Abaqus with a STRESS tensor which is compatible with the Jacobian and strain increments. This stress has no meaning in the LMM solution.
12. Call COMPLIANCE to obtain the compliance matrix and then calculate the strains according to equation (3.21). If the problem is plane stress then calculate the out of plane strain.
13. Write the energy values of equation (3.22) to the variables SSE, SPD and SCD. These will be extracted as volume integrals in the URDFIL when all integration points have been considered in UMAT.
14. Calculate the effective strain increment. The magnitude of this value is unimportant and not used in the calculation procedure. Instead, the contour plot of this value shows the location of the reverse plasticity or ratchet mechanism.

### **STEADYCYCLE**

The STEADYCYCLE subroutine performs stage 1 of the global shakedown analysis as given in section 4.2.4.1. As mentioned in this section, the numerical implementation of this procedure interprets one Abaqus increment as one point in the load cycle. Therefore a load cycle with N points will need N Abaqus increments to analyse it once. If this is repeated over M cycles then a convergent solution is obtained. The major steps in the code are as follows:

1. Initiate key variables and set their value to zero
2. One increment is used per point on the load cycle. Therefore the current point in the load cycle is determined by the remainder of the current increment number

divided by the number of points in the load cycle (which is given by the MOD intrinsic function in Fortran)

3. Call SCLOADCYCLE to obtain the elastic stress and temperature for the load cycle point in question
4. Add the varying residual stress increment calculated in the previous increment to the RSTRESS variable. This gives the current total varying residual stress as given in equation (4.27). See Appendix B for further details on the cumulative total method used to obtain the varying residual stress.
5. When a complete cycle has been evaluated (i.e. when the method is back to the start of the load cycle again) then the current value of RSTRESS is equal to the constant component of the varying residual stress.
6. Calculate the yield stress for this increment. The first time around the load cycle the yield stress entered in the plug-in is used (and if this is temperature dependent then YIELDSTRESS is called). If a Ramberg-Osgood model has been selected then it is only after the first time around the load cycle that this is used. If this is not selected then the yield stress is calculated in the same way as during the first time round the load cycle.
7. If the young's modulus is temperature dependent then call MODULUS to obtain this value. Then use this value to calculate the multi-axial young's modulus and bulk modulus.
8. During the first time round the load cycle the multi-axial young's modulus is used. In subsequent iterations after the first cycle then modulus adjustment is performed according to equation (4.23)
9. Calculate  $\bar{\mu}$  and  $\bar{K}$  as per equation (4.29)
10. Calculate STRESSIN, which corresponds to  $\Delta\sigma_{m+1}^{in}$  in equation (4.34)
11. Calculate E and  $\nu$  from equation (4.35) and populate the Jacobian by calling JACOBIAN
12. Calculate the varying residual stress increment by solving equation (4.32)
13. Provide Abaqus with a STRESS tensor which is compatible with the Jacobian and strain increments. This stress has no meaning in the LMM solution
14. Calculate the plastic strain increment

15. When a complete load cycle has been calculated then the ratchet strain can be computed by summing the plastic strain increments. These plastic strain increments are re-called from the STATEV array into the array PTSTRAN. This is then used to sum the plastic strain increments over the load cycle, with the remainder being the ratchet strain.
16. Call COMPLAINCE to obtain the compliance matrix and then calculate the elastic strains
17. Calculate the elastic strain range when a complete load cycle has been calculated. First the elastic strains from all load points are re-called from the STATEV array into the ETSTRAN array. These elastic strain components are used to find the maximum elastic strain range between any two load points in the cycle, which is given as the elastic strain range for that point.
18. If a complete load cycle has been considered then the plastic strain range can be calculated. The plastic strain at each load point is given by the sum of the plastic strain increments up to that point. These are used to find the maximum difference in plastic strain between any two load points.
19. A similar process is used for total strain range, which uses the sum of elastic and plastic strains.
20. The shear modulus is summed over the cycle and the inverse is written to the variable SSE to be read by the URDFIL subroutine.

### **RATCHET**

If the global shakedown limit is requested by the user, then the RATCHET code is called once the stage 1 calculation using the STEADYCYCLE subroutine is complete. The RATCHET subroutine is very similar to the SHAKEDOWN subroutine

1. Initiate key variables and set their value to zero
2. If it is the first increment in the global shakedown analysis then set the upper bound increment to 1.0
3. Call RLOADCYCLE to obtain the stress of the additional constant loads added to the cyclic stresses from stage 1
4. If temperature dependent yield is defined then call YIELDSTRESS to obtain the yield stress. Otherwise the yield stress equals the User-material property

5. If a Ramberg-Osgood material was used in stage 1 then find out if hardening has occurred during any point in the load cycle. If it has then use the hardened yield stress for that point in the load cycle. If no hardening has occurred then use the yield stress as calculated in number 4 above
6. In the first increment the Shear modulus is obtained by 1/young's modulus. If this is temperature dependent then call MODULUS to obtain this value.
7. After the first increment the shear modulus is obtained by dividing the effective strain by the yield stress
8. The value of  $\sigma_{ij}^{in,k+1}$  is calculated according to equation (3.19) using the values of shear modulus and applied stress
9. JACOBIAN is called to form the stiffness matrix (DDSDDE)
10. The estimate of the constant residual stress field,  $\bar{\rho}_{ij}^{k+1}$ , is obtained by equation (3.20)
11. The total stress is calculated and RLOWER is called to calculate the lower bound load multiplier
12. Provide Abaqus with a STRESS tensor which is compatible with the Jacobian and strain increments. This stress has no meaning in the LMM solution.
13. Call COMPLIANCE to obtain the compliance matrix and then calculate the strains according to equation (3.21). If the problem is plane stress then calculate the out of plane strain.
14. Write the energy values of equation (3.22) to the variables SSE, SPD and SCD. These will be extracted as volume integrals in the URDFIL when all integration points have been considered in UMAT
15. Calculate the effective strain increment. This magnitude of this value is unimportant and not used in the calculation procedure. Instead, the contour plot of this value shows the location of the ratchet mechanism

**URDFIL(LSTOP,LOVRWRT,KSTEP,KINC,DTIME,TIME)**

The URDFIL subroutine performs a number of functions in a LMM analysis. It is called by Abaqus at the end of the increment after the solution has completed. The Abaqus utility routines DBFILE and POSFIL can be used within URDFIL to access the results file.

### **URDFIL for Strict Shakedown**

The URDFIL routine is only used during the shakedown step, i.e. no actions are taken during the elastic or null steps. During each shakedown increment the following actions are taken by looping over the results for each element and integration point:

1. Call DBFILE and POSFIL to access the results
2. Extract the elemental lower bound multiplier
3. Add this multiplier to the running total for the element
4. When all integration points in the element have been added then take the average
5. Zero off the counter to begin the total for the next element
6. Extract the volume integrals for equation (3.23)

When this loop is complete the lower bound multiplier is finalised for the increment. If the element average lower bound value is greater than 99.5% of the upper bound then the integration point value is used instead. The upper bound multiplier is calculated from the volume integrals.

At this point a section of code is in place to detect a change in the mechanism of the model. During a normal solution the best value of the lower bound is displayed, and over consecutive increments this tends towards the upper bound. If a change in mechanism occurs then the upper bound will reduce and, due to the best lower bound restriction, can drop below the lower bound. If this is the case then the best lower bound restriction is removed and the convergence is judged using consecutive upper bounds.

The convergence calculations are the final task in the URDFIL. The convergence condition selected by the user must be satisfied for five consecutive increments, at which point the analysis is terminated.

### **URDFIL for Steady Cycle and Ratchet**

Similarly to the strict shakedown, URDFIL is only used during the steady cycle and ratchet step. The variable CURRANALYSIS is used to indicate whether the solution is currently using the STEADYCYCLE or RATCHET subroutine.

When URDFIL is called after an increment which used the STEADYCYCLE subroutine:

1. Call DBFILE and POSFIL to access the results

2. Calculate the ratio of ratchet strain to plastic strain range. Issue warning if this is too high
3. Calculate convergence by extracting the relevant volume integral

If the convergence criterion is met for 5 consecutive increments or the increment number is 40 times the number of load instances then the steady cycle calculation is complete. If the user has not requested the ratchet limit then the analysis terminates and the analysis information is printed to the data file. If the ratchet limit is requested then the variable CURRANALYSIS is updated and the analysis continues using the RATCHET subroutine. After each increment which uses this subroutine:

1. Call DBFILE and POSFIL to access the results
2. Extract the elemental lower bound multiplier
3. Add this multiplier to the running total for the element
4. When all integration points in the element have been added then take the average
5. Zero off the counter to begin the total for the next element
6. Extract the volume integrals for equation (4.38)

When this loop is complete the lower bound multiplier is finalised for the increment. This is done in the same way as for the strict shakedown where if the element average lower bound value is greater than 99.5% of the upper bound then the integration point value is used instead. The upper bound multiplier is calculated from the volume integrals.

The same mechanism shift code is also present in this URDFIL which posts a warning to the user, removes the best lower bound and continues using the convergence based on the consecutive upper bounds.

The analysis terminates when the convergence criteria is met for five consecutive increments or the maximum number of increments is met.

#### **JACOBIAN(ITYPE,PNU,YM,DDSDDE,NTENS,NDI)**

This subroutine forms the jacobian matrix. It is dependent on the dimensionality of the model

For 3D elements:

$$[J] = \frac{E}{(1+\nu)(1-2\nu)} \begin{bmatrix} (1-\nu) & \nu & \nu & 0 & 0 & 0 \\ \nu & (1-\nu) & \nu & 0 & 0 & 0 \\ \nu & \nu & (1-\nu) & 0 & 0 & 0 \\ 0 & 0 & 0 & \frac{(1-2\nu)}{2} & 0 & 0 \\ 0 & 0 & 0 & 0 & \frac{(1-2\nu)}{2} & 0 \\ 0 & 0 & 0 & 0 & 0 & \frac{(1-2\nu)}{2} \end{bmatrix}$$

For plane strain and axisymmetric elements:

$$[J] = \frac{E}{(1+\nu)(1-2\nu)} \begin{bmatrix} (1-\nu) & \nu & \nu & 0 \\ \nu & (1-\nu) & \nu & 0 \\ \nu & \nu & (1-\nu) & 0 \\ 0 & 0 & 0 & \frac{(1-2\nu)}{2} \end{bmatrix}$$

For plane stress elements:

$$[J] = \frac{E}{1-\nu^2} \begin{bmatrix} 1 & \nu & 0 \\ \nu & 1 & 0 \\ 0 & 0 & \frac{(1-\nu)}{2} \end{bmatrix}$$

Argument	Description
ITYPE	Dimensionality of the model (0=3D, 1=plane strain 2=plane stress, 3=axisymmetric)
PNU	Poisson's ratio
DDSDDE	The Jacobian matrix
NTENS	Number of stress components (for 3D NTENS=6, for plane strain and axisymmetric NTENS=4 and for plane stress NTENS=3)
NDI	Number of direct stress components (for 3D, plane strain and axisymmetric NDI =3 and for plane stress NDI =2)

**COMPLIANCE(SM,PNU,NTENS,NDI,COMP,ITYPE)**

This subroutine forms the compliance matrix. It is dependent on the dimensionality of the model. For 3D elements:

$$[C] = \frac{1}{E} \begin{bmatrix} 1 & -\nu & -\nu & 0 & 0 & 0 \\ -\nu & 1 & -\nu & 0 & 0 & 0 \\ -\nu & -\nu & 1 & 0 & 0 & 0 \\ 0 & 0 & 0 & 2(1+\nu) & 0 & 0 \\ 0 & 0 & 0 & 0 & 2(1+\nu) & 0 \\ 0 & 0 & 0 & 0 & 0 & 2(1+\nu) \end{bmatrix}$$

For plane strain elements

$$[C] = \frac{1+\nu}{E} \begin{bmatrix} (1-\nu) & -\nu & 0 \\ -\nu & (1-\nu) & 0 \\ 0 & 0 & 0 \\ 0 & 0 & 0 \\ 0 & 0 & 0 \\ 0 & 0 & 2 \end{bmatrix}$$

For axisymmetric elements

$$[C] = \frac{1}{E} \begin{bmatrix} 1 & -\nu & -\nu & 0 \\ -\nu & 1 & -\nu & 0 \\ -\nu & -\nu & 1 & 0 \\ 0 & 0 & 0 & 2(1+\nu) \end{bmatrix}$$

For plane stress elements

$$[C] = \frac{1}{E} \begin{bmatrix} 1 & -\nu & 0 \\ -\nu & 1 & 0 \\ 0 & 0 & 2(1+\nu) \end{bmatrix}$$

Argument	Description
SM	1/Young's modulus
PNU	Poisson's ratio
NTENS	Number of strain components (e.g. for 3D NTENS=6)
NDI	Number of direct strain components
COMP	The compliance matrix
ITYPE	Dimensionality of the model

#### **VMSTRS(VMSTRESS,NTENS,ITYPE)**

Calculates the von-Mises equivalent stress for the given stress tensor using the following equation:

$$\sigma_{ij} = \sqrt{\frac{3}{2} \left[ (\sigma_x - \sigma_H)^2 + (\sigma_y - \sigma_H)^2 + (\sigma_z - \sigma_H)^2 + 2(\sigma_{xy}^2 + \sigma_{xz}^2 + \sigma_{yz}^2) \right]}$$

$$\sigma_H = \frac{\sigma_x + \sigma_y + \sigma_z}{3}$$

Argument	Description
VMSTRESS	Stress tensor
NTENS	Number of stress components (e.g. for 3D NTENS=6)
ITYPE	Dimensionality of the model

**VMSTRN(VMSTRAN,NTENS,ITYPE,OUTPLNSTRN,HYD)**

Calculates the equivalent strain for the given strain tensor. If the strains are not deviatoric then the following equation is used:

$$\varepsilon_{ij} = \sqrt{\frac{2}{3} \left[ (\varepsilon_x - \varepsilon_H)^2 + (\varepsilon_y - \varepsilon_H)^2 + (\varepsilon_z - \varepsilon_H)^2 + 0.5(\gamma_{xy}^2 + \gamma_{xz}^2 + \gamma_{yz}^2) \right]}$$

$$\varepsilon_H = \frac{\varepsilon_x + \varepsilon_y + \varepsilon_z}{3}$$

If the strains are already deviatoric then the following equation is used:

$$\varepsilon_{ij} = \sqrt{\frac{2}{3} \left[ \varepsilon_x^2 + \varepsilon_y^2 + \varepsilon_z^2 + 2(\varepsilon_{xy}^2 + \varepsilon_{xz}^2 + \varepsilon_{yz}^2) \right]}$$

Argument	Description
VMSTRAN	Strain tensor
NTENS	Number of stress components (e.g. for 3D NTENS=6)
ITYPE	Dimensionality of the model
OUTPLNSTRN	Out of plane strain for plane stress elements
HYD	Flag to indicate whether the strains are deviatoric or not

**YIELDSTRESS(CMNAME,TDYIELD,TEMP)**

Calculates the temperature dependent yield stress. Temperatures and temperature dependent values are passed in via a common block from UEXTERNALDB. This subroutine uses the ZZPRIN subroutine to linearly interpolate to find the yield stress for the given temperature.

Argument	Description
CMNAME	Name of material at current integration point
TDYIELD	Value of yield stress passed back into main subroutine
TEMP	Temperature at the current integration point

**RAMBERG(CMNAME,YIELD,TEMP,ATI,BETATI,PLSTRAIN,RONAMES)**

This subroutine calculates the hardened “yield” stress based on the Ramberg-Osgood model

$$\varepsilon_{plastic} = \left( \frac{\sigma}{A} \right)^{1/\beta}$$

If the parameters A and  $\beta$  are temperature dependent then temperature dependent values are passed in via a common block from UEXTERNALDB. The ZZPRIN subroutine is then used to linearly interpolate these values before use in the above equation.

Argument	Description
CMNAME	Name of material at current integration point
YIELD	Hardened yield stress passed back into main routine
TEMP	Temperature at the current integration point
ATI	Temperature independent value of A
BETATI	Temperature independent value of $\beta$
PLSTRAIN	Plastic strain
RONAMES	List of materials for which a R-O model defined

**MODULUS(CMNAME,TDMOD,TEMP)**

Calculates the temperature dependent modulus. Temperatures and temperature dependent values are passed in via a common block from UEXTERNALDB. This subroutine uses the ZZPRIN subroutine to linearly interpolate to find the yield stress for the given temperature.

Argument	Description
CMNAME	Name of material at current integration point
TDMOD	Value of modulus passed back into main subroutine
TEMP	Temperature at the current integration point

**LOADCYCLE(STATEV,NSTATV,KINC,NTENS,DEV,NSO,NLOADS,M,SLOAD,ELAFIX,ELASCL,TEM)**

This subroutine is used during a strict shakedown assessment to give the elastic stress tensor of the applied loads for each point in the load cycle.

Firstly, the elastic stresses and temperatures for each applied load (calculated by the ELASTIC subroutine) are read from the STATEV array. If this load is marked as scalable then the stresses and temperature for that load are scaled by the current upper bound load multiplier. Superposition is used with the load multipliers to calculate the total applied elastic stress at each load point. Additional arrays are also created containing only scaled stresses and only unscaled stresses - these are used when calculating the upper bound load multiplier in the URDFIL subroutine.

Argument	Description
STATEV	The array containing the solution dependent variables in the UMAT subroutine
NSTATV	The number of spaces in the STATEV array
KINC	The increment number
NTENS	Number of stress components
DEV	Elastic stress tensor for each point in the load cycle.
NSO	Number of points in the load cycle
NLOADS	Number of applied loads
M	Array of load multipliers given by the user in the plug-in
SLOAD	Vector containing flags indicating whether loads are scalable during the solution or not
ELAFIX	Elastic stresses which are not scaled during the solution
ELASCL	Elastic stresses which are scaled during the solution
TEM	Temperature at each load point

**RLOADCYCLE(STATEV,NSTATV,KINC,NTENS,DEV,NSO,NLOADS,SLOAD,STRFIX,STRSCL,TEM,ESTART)**

This subroutine is used during stage 2 of a global shakedown analysis. It takes the stresses and temperatures calculated by the STEADYCYCLE subroutine and adds the steady state loads chosen by the user in the plug-in.

Firstly the total stress from each load point (calculated by STEADYCYCLE) is read from the STATEV array. The stresses from the additional steady state loads are scaled by the upper bound load multiplier. The stress for each load point is found by superposition of the stresses from STEADYCYCLE and the additional steady state loads.

Argument	Description
STATEV	The array containing the solution dependent variables in the UMAT subroutine
NSTATV	The number of spaces in the STATEV array
KINC	The increment number
NTENS	Number of stress components
DEV	Elastic stress tensor for each point in the load cycle.
NSO	Number of points in the load cycle
NLOADS	Number of applied loads
SLOAD	Vector containing flags indicating whether loads have been selected to be added as additional steady state loads
STRFIX	Elastic stresses from the STEADYCYCLE subroutine
STRSCL	Elastic stresses from loads which have been selected to be added as additional steady state loads
TEM	Temperature at each load point
ESTART	The NSTATV number at which the elastic solutions begin.

**SCLOADCYCLE(STATEV,NSTATV,KINC,NTENS,DEV,NSO,NLOADS,M,SLOAD,TEM,ILOAD,NOEL,NPT,ESTART)**

This subroutine is used during a steady cycle analysis or during stage 1 of a global shakedown analysis.

Firstly the elastic stresses are read from the STATEV array. They are then scaled according to the multipliers given in the plug-in. Superposition is used to obtain the elastic stress at each point in the load cycle. The temperature at each load point is also read from the STATEV array.

Argument	Description
STATEV	The array containing the solution dependent variables in the

	UMAT subroutine
NSTATV	The number of spaces in the STATEV array
KINC	The increment number
NTENS	Number of stress components
DEV	Elastic stress tensor for each point in the load cycle.
NSO	Number of points in the load cycle
NLOADS	Number of applied loads
M	Array of load multipliers given by the user in the plug-in
SLOAD	Vector containing flags indicating whether loads are scalable during the solution or not
TEM	Temperature at each load point
ILOAD	Load point number
NOEL	Element number
NPT	Integration point number
ESTART	The NSTATV number at which the elastic solutions begin.

**DEVIATORIC(ITYPE,STRESSES,DEVOSTR,NTENS,NDI)**

Finds the deviatoric stresses of the given stress tensor STRESSES. The hydrostatic stress is found:

$$\sigma_H = \frac{\sigma_x + \sigma_y + \sigma_z}{3}$$

And the deviatoric stresses are found by subtracting the hydrostatic stress from the direct components

$$\sigma'_{ii} = \sigma_{ii} - \sigma_H$$

Where the shear components remain unchanged.

Argument	Description
ITYPE	Dimensionality of the model
STRESSES	Stress tensor containing hydrostatic stress (i.e. not deviatoric)
DEVOSTR	Tensor of deviatoric stresses
NTENS	Number of stress components
NDI	Number of direct stress components

**RLOWER(STRSCL,STRFIX,CSTRESS,YIELD,YLAMACO,NTENS,NSO,ITYPE,STATEV,NSTATV,  
NOEL,NPT,LMMANTYPE,I)**

This subroutine is used in a strict shakedown assessment and also in stage 2 of the global shakedown assessment. It calculates the lower bound multiplier on the selected loads.

A check is performed for no or negligible scalable loads (which would cause the calculation to fail). If this is passed then the quadratic of Appendix C is solved. The coefficients A, B and C are found from the stress components and the roots of the quadratic are found. The largest positive root is taken to be the lower bound multiplier for that load point and is stored in the STATEV array. If it is not possible to find a positive root then a flag is stored in the STATEV array.

Argument	Description
STRSCL	Array of scalable stresses. In a strict shakedown analysis these stresses are from the loads which have been ticked as scalable. In stage 2 of global shakedown these stresses are the additional steady state stresses.
STRFIX	Array of fixed stresses. In a strict shakedown assessment these are the stresses selected not to be scalable. In stage 2 global shakedown these are the stresses from the steady cycle calculation.
CSTRESS	Constant residual stress tensor
YIELD	Yield stress at each load point
YLAMACO	Calculated lower bound multiplier
NTENS	Number of stress components
NSO	Number of points in the load cycle
ITYPE	Dimensionality of the model
STATEV	The array containing the solution dependent variables in the

	UMAT subroutine
NSTATV	The number of spaces in the STATEV array
NOEL	Element number
NPT	Integration point number
LMMANTYPE	Flag indicating if the analysis is strict shakedown or stage 2 of global shakedown
I	Load point number

**ZZPRIN(LENGTH,PVALS,TVALS,TMAX,TMIN,VALT,FLAG,PROP)**

Performs linear interpolation when tabular temperature dependent material properties are entered.

Argument	Description
LENGTH	Length of the arrays PVALS and TVALS i.e. the number of temperature dependent properties entered
PVALS	Vector containing temperature dependent values
TVALS	Vector containing temperatures
TMAX	Max temperature for valid extrapolation (set to 50 degrees above highest value in TVALS)
TMIN	Min temperature for valid extrapolation (set to 50 degrees below lowest value in TVALS)
VALT	Temperature at the point in question
FLAG	False if VALT outside allowable temperature range $TMIN < VALT < TMAX$
PROP	Linearly interpolated property value at temperature VALT

## **Appendix E. Structure of the LMM Plug-in**

The purpose of this appendix is to give a more detailed description of the LMM plug-in and its structure. This appendix does not describe how to create a plug-in, although the structure of a generic plug-in is briefly given to better describe the functioning of the LMM.

Firstly the overall structure of the LMM plug-in is described within the context of the Abaqus plug-in system. Next the code which constitutes the dialog boxes themselves is described. Finally all the scripts which perform the peripheral and supplemental operations are described.

### **E.1 Structure of the LMM Abaqus Plug-in**

Abaqus has a well established structure which any user-defined plug-ins must conform to. This includes certain methods which are called in a specified order, as shown in Figure E-1. The python class which contains all of these methods is called the Mode, and in the case of the LMM plug-in a Form Mode is used.

The form contains numerous data structures called keywords which store data as the plug-in process continues. Any number of keywords may be defined in the form depending on the amount of data required for the purpose. When the last dialog has been posted and completed then the form takes the data contained in these keywords and sends it in a command string to the designated target. Put simply, the form is a process for gathering the required data into the keywords so it can send a command string. The data is gathered by posting dialog boxes and running scripts. The dialog boxes contain widgets (such as text fields, tables and check boxes) which are connected directly to keywords in the form which takes the user's input and directly populates the keywords.

To create a plug-in some or all of the methods in Figure E-1 may be over-written to perform the functions desired. The methods which have been re-written for the LMM plug-in are coloured red. Those which remain in their original implementation are coloured blue.

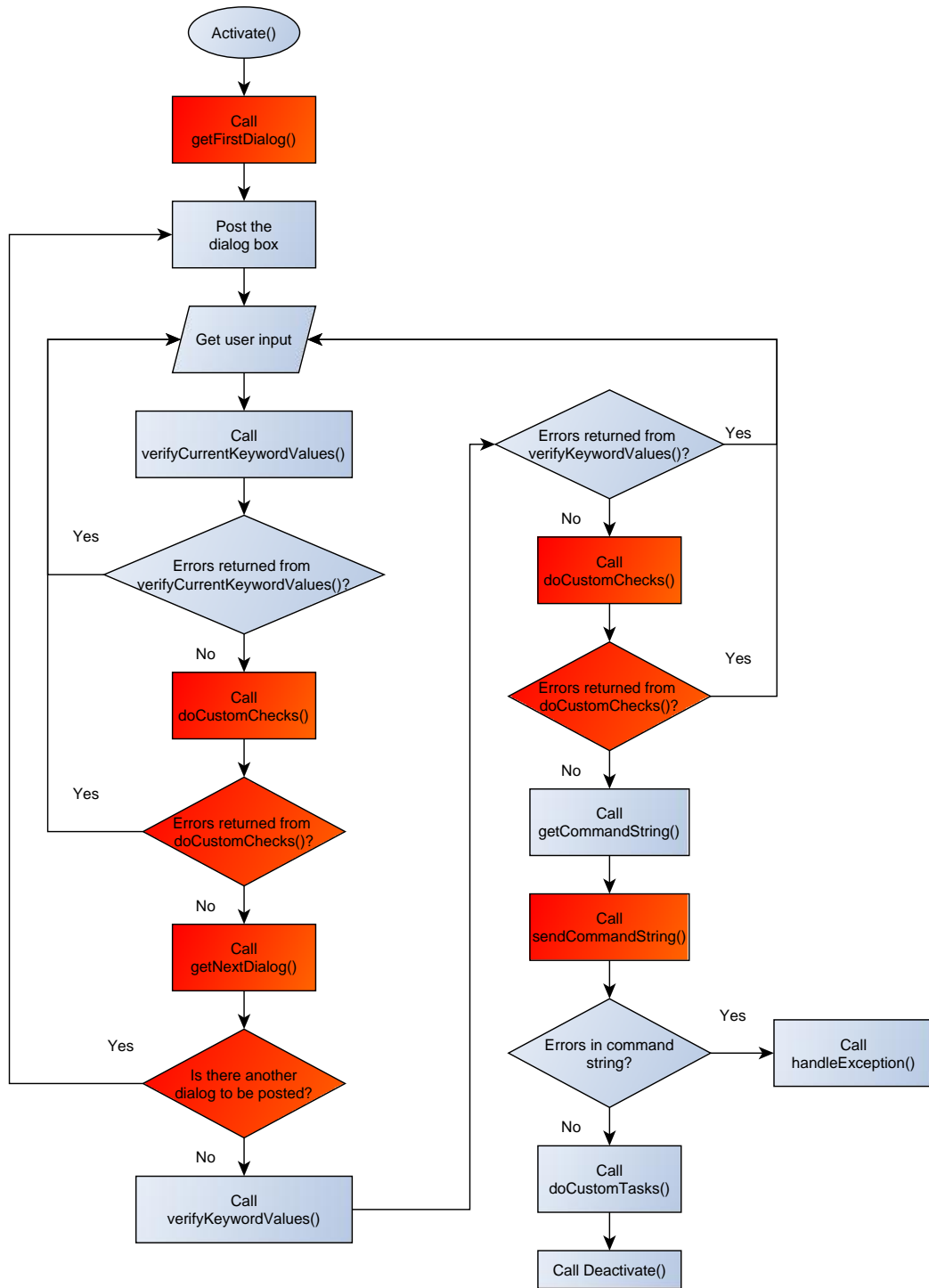


**Figure E-1 - Structure of a Generic Abaqus Plug-in**

The process is activated when the user invokes the plug-in through CAE. The `getFirstDialog()` contains code which determines the first dialog box to be displayed to the user. Dialog boxes themselves are defined independently of the process in Figure E-1 and are called and posted when required. After posting the first dialog box and obtaining the

user input, two stages of error checking are performed. The first, `verifyCurrentKeywordValues()`, performs basic checking of the values. For example it checks that text has not been entered in a field which requires an integer. The `doCustomChecks()` method is originally empty by default, and so the user can use this to add in additional error checking. `doCustomChecks()` has been extensively used in the LMM plug-in to check the validity of the values. If errors are returned by either of these scripts then an error is posted and the user is returned to the dialog box to rectify the error. If no errors are found then the process moves onto the `getNextDialog()` method, which determines the next dialog (if any) to be posted. Once again the data entered by the user is checked by `verifyCurrentKeywordValues()` and `doCustomChecks()` with an error posted for invalid entries.

When `getNextDialog()` has posted the last dialog box and the data has been successfully checked, then all the data entered is assembled into the command string which, in the case of the LMM plug-in, is sent to a series of scripts for model configuration.

#### **`getFirstDialog(self)`**

For any plug-in it is compulsory to write this method. For the LMM this script first finds the file path of the current model and queries `self.modelTgt` for the previous file path. `LMM_newModelCheck` is called and these are passed in as arguments. Finally, the first dialog is posted, `LMM_main`.

#### **`getNextDialog(self, previousDb)`**

This script uses the argument `previousDb` to determine the next dialog box to display. After `LMM_main` the materials dialog, `LMM_mats`, is posted. A counter is also started. Each materials dialog posted adds one to the counter, which is compared to the number of materials in the model. Each subsequent time `getNextDialog` is called these two numbers are compared and a `LMM_mats` dialog is posted until they are equal.

When the counter equals the number of materials, the script `LMM_remove_mats` is called to remove any materials data from the keywords which is no longer needed (for example if the material has been deleted from CAE, then it should be deleted from the keywords as well). After this script has run then the `LMM_loadCycle` dialog is posted.

If the loadCycle box is the previousDb then LMM\_job is posted, which is the final dialog box in the plug-in.

### doCustomChecks(self)

This method is used extensively in the LMM plug-in for checking of data. It is called to perform checks for every dialog box. If these checks are not passed, then doCustomChecks does not allow the dialog box to be unposted. Instead an error message is shown to the user indicating the source of the error and the dialog box remains so that the error can be fixed.

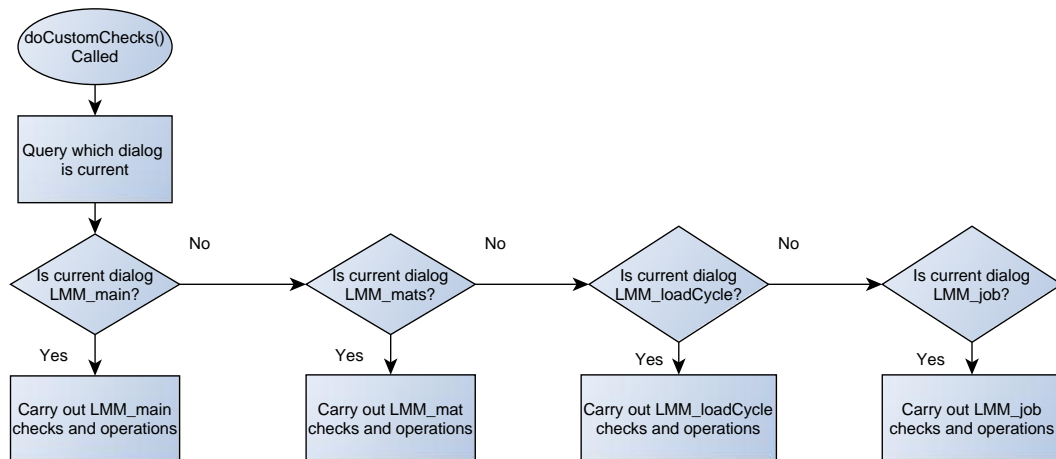


Figure E-2 - doCustomChecks Dialog Box Decision

A different stream of error checking is invoked depending on which dialog box is currently being displayed, shown in Figure E-2 above. Each stream is shown graphically in Figure E-3a and b and Figure E-4a and b.

The checks for LMM\_main follow a fairly sequential path. A series of scripts is called which checks a different aspect of the model. First the dialog box itself is checked by LMM\_main\_checks() to make sure the user has entered the data correctly. An error is posted if this is not the case. Otherwise the series of scripts is called. These each return an integer value. Any value above zero indicates a different type of error which allows the error message to be tailored to the situation. If all error flags are zero then doCustomChecks is complete for this dialog and returns to the form.

The checks for material data are less sequential due to the many options available in this dialog box. Normally the widgets in the dialog are connected directly to the keywords. In

this case the data from many text fields and tables must be stored in a single tuple keyword, and so the conventional connection between widget and keyword cannot be used. Instead the data from this dialog must be manually extracted, checked in the usual way, and then manually populated in the keywords.

Beginning with the modulus, the dialog is queried for this data. Depending on its temperature dependency LMM\_matTI\_checks or LMM\_matTD\_checks is called for error checking. This is repeated for the yield stress. The thermal expansion and Poisson's ratio are always temperature independent. If a steady cycle or ratchet analysis is chosen and a Ramberg-Osgood is selected then these values are queried and error checked. If no errors are found (i.e. an error flag of zero) then the materials tuple keywords are searched for any existing data for the current material. Any data found is deleted and replaced with the data from the dialog box.

The loadCycle dialog suffers from a similar problem to the materials in that the conventional widget-keyword connection cannot be used. This is due to errors when the table is re-posted but with a different number of rows or columns. Therefore the data in the dialog is manually extracted, error checked and then the tuple keywords are manually populated.

When the data has been extracted, LMM\_loadCycle\_checks is called to perform the error checking. If the error checking is passed (i.e. an error flag of zero) then the data in the load cycle keywords is deleted entirely and replaced with the data from the dialog box.

The LMM\_job dialog box connects the widgets directly to the keywords and so these values can be queried directly. LMM\_job\_checks performs the error checking and Errors are posted for any mistakes made. If the job name selected by the user already exists in the current model then the user is asked if they would like to overwrite it.

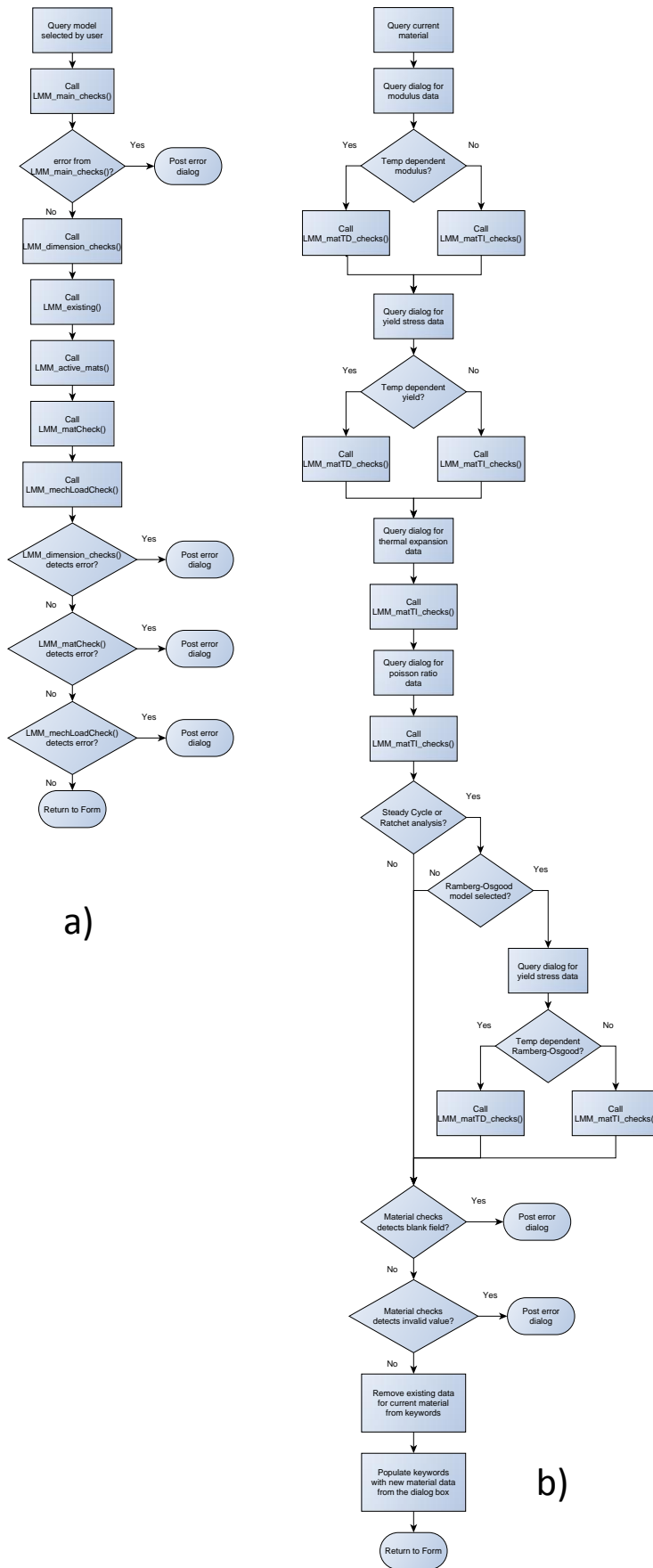


Figure E-3 - doCustomChecks for a)LMM\_main and b)LMM\_mats dialog boxes

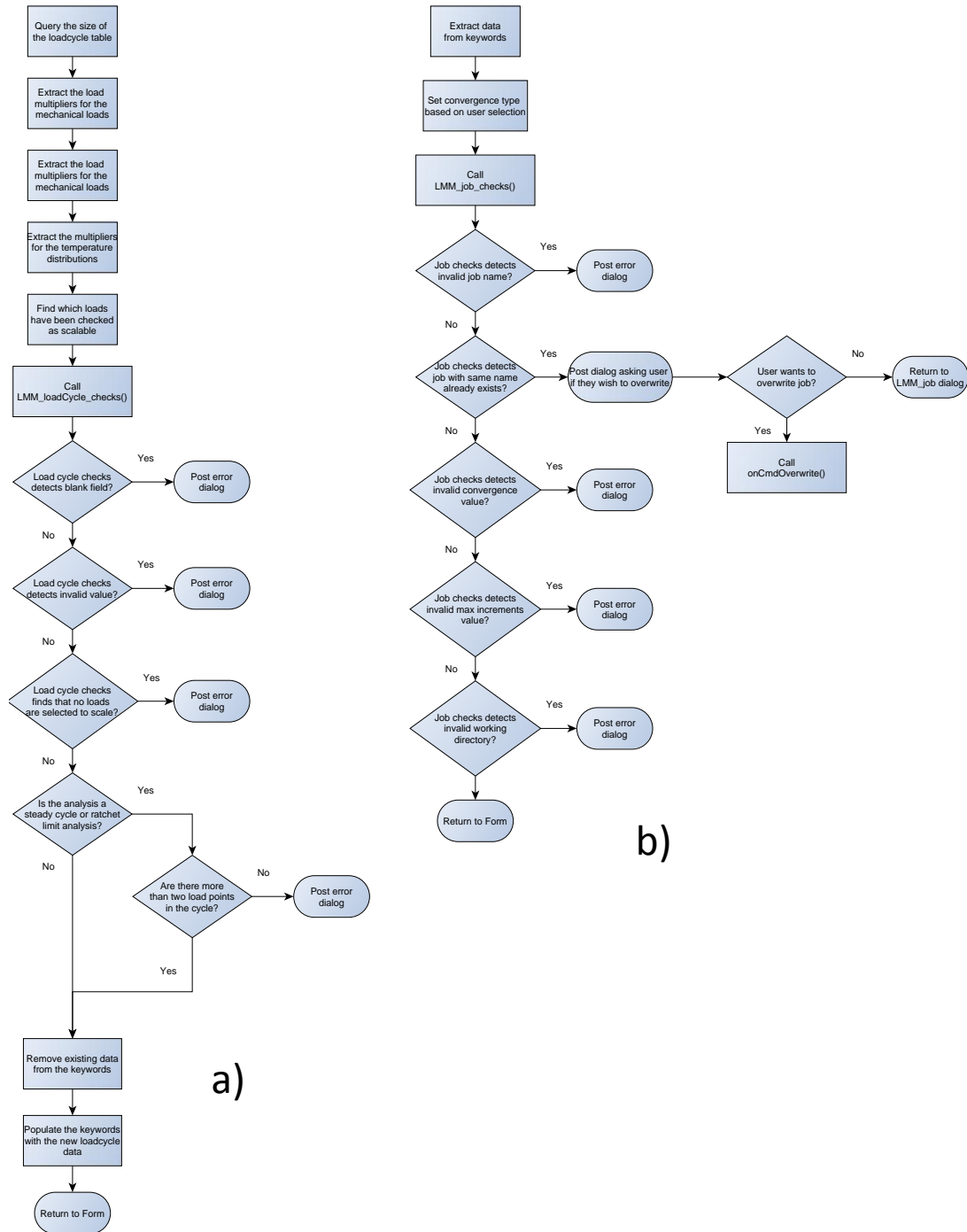


Figure E-4 - doCustomChecks for a) LMM\_loadCycle and b) LMM\_job

### Sending the Command String

When doCustomChecks has completed the checks for the final dialog box then the form has gathered all the information for the keywords. These are then assembled into a command string and sent to LMMMainScript. This script is the governing script for a series of

operations which are performed on the model and to write the LMM text file for the subroutines. The final result of these operations is a model which has been configured for the analysis, an analysis job created and the text file printed in the working directory.

## **E.2 Dialog Boxes**

The posting of dialog boxes is controlled by the `getFirstDialog()` or `getNextDialog()` scripts shown in Figure E-1. When posted, a dialog box will display the widgets which have been arranged according to layout managers.

The code written to display these widgets is performed once. Dialogs also have a `processUpdates` method associated with them, which allows actions to be performed on the dialog whilst it is posted. For example some buttons may be stippled based on whether a check box in the dialog has been ticked. The `processUpdates()` script is continuously called by Abaqus CAE whilst the dialog box is displayed which allows these updates to happen instantly. However it also means that time consuming tasks should not be completed here or the plug-in and CAE will become slow.

### **LMM\_main Dialog Box and Scripts**

This dialog is present to introduce the LMM to the user and allow them to select the model and analysis type to be carried out.

The `processUpdates` is used here to determine if previous LMM modifications have been made to the selected model. The model name selected from the drop down menu in the dialog is passed into the `LMM_existing` script. If this detects that the LMM has already been used on this model then an error dialog box is posted.

### **LMM\_mats Dialog Box and Scripts**

This dialog is posted once for each material in the analysis. It contains four main areas – Young's modulus, yield stress, Poisson's ratio & thermal expansion and finally Ramberg-Osgood. The Ramberg-Osgood section is only available for steady cycle or ratchet limit analyses.

The Young's modulus and yield stress areas are governed by similar code. A text field is used for temperature independent values, and a table is used for temperature dependency. The user may select temperature dependent or independent via a check box. This check

box is linked to an FXswitcher in the processUpdates script which swaps the view of the text box/table according to the state of the check box. When the dialog box is first called the keywords are queried for existing data which determines the initial state of the FXswitcher and populates the values.

The thermal expansion and Poisson's ratio are given in text fields. The keywords are queried for existing data for the current material and this is entered into the text fields if it exists.

The Ramberg-Osgood area is only shown if the analysis type is steady cycle or steady cycle + ratchet limit. It contains two switchers. The first toggles the use of the model. This displays or hides the widgets used to enter the coefficients. Within this switcher is a second switcher which toggles the use of temperature dependent properties. This area of the dialog also contains a "Tip" button, which displays a help box to explain this material model to the user.

The processUpdates for this dialog is used entirely to control the FX switchers based on the condition of the check boxes. In addition to this, two automatic functions are included in this dialog box: "Extract" which extracts any existing material data from the CAE model and "Calculate" which calculates the 0.2% proof stress from the Ramberg-Osgood parameters and populates the yield stress area of the dialog box.

The Extract function is initiated by clicking the Extract button which calls the onCmdSelect method. This method queries the dialog box to determine if there are values present in any of the widgets. If values are found then a question is posted asking the user if they wish to continue and overwrite these values. Clicking "no" cancels this process. Clicking "Yes", or if no values are found then LMM\_extract\_CAE\_Matprops is called to query the CAE file for properties. This is followed by the populateValues method which fills in the widgets with the extracted values.

The Calculate function is initiated by clicking on the Calculate button in the Ramberg-Osgood area of the dialog. This calls the onProofSelect method which checks for incomplete Ramberg-Osgood parameters which, if found, displays an error. The onProofSelect also checks for existing values in the yield stress widgets. If values are found then a question is posted asking the user if they wish to continue and overwrite these values. Clicking "no" cancels this process. Clicking "Yes", or if no values are found, the calcProof method is called

to give the proof stresses followed by the populateProof method to populate the yield stress widgets.

### **LMM\_loadCycle Dialog Box and Scripts**

This dialog is posted to gather the load cycle multipliers for each load and predefined field. It also allows the user to choose which loads area scalable in a strict shakedown or ratchet analysis.

First the model is queried to obtain the names of the loads and predefined fields, which are put into tab separated lists (which is needed for the table headings). The keywords are queried to find the number of columns to show in the table, where one column equals one load point in the cycle. When the table has been constructed then it is populated with any existing data from the keywords.

The second half of the dialog allows the user to select which loads are scaled during solution. This depends on the analysis type chosen in the LMM\_Main dialog box. If a strict shakedown assessment is chosen then all of the loads and predefined fields are displayed. In a steady cycle analysis none of the loads are displayed as no scaling occurs during this calculation. If a steady cycle + ratchet is selected then only the mechanical loads are shown. A help box is displayed when the user clicks "Tip", which gives advice on this load scaling situation.

The processUpdates for this dialog deals with the formatting of the table. When columns are added or removed by the user the heading above the table must span over all columns. If a column is added then a drop down list must be added in the "Temp Field" row so that the user has this option in the new column.

### **LMM\_job Dialog Box an Scripts**

This dialog is the final in the series and is the last step in the user interface. Text fields are used for the job name, max number of increments and the working directory. The current working directory is automatically detected and displayed. Clicking the "Select" button displays a file selector dialog so the user can navigate to a new working directory if desired.

The convergence options displayed depend on the analysis chosen in the LMM\_Main dialog. Strict shakedown has two options: the difference between consecutive upper

bounds and the percentage difference between lower and upper bounds. A steady cycle analysis uses the difference in modulus between consecutive increments as its only convergence option. A steady cycle + ratchet analysis needs two convergence values, one for each stage of the analysis. Convergence for stage 1 is identical to that of the steady cycle analysis described above. Convergence for stage two has the same two options as the strict shakedown analysis.

The convergence for strict shakedown and stage 2 of the ratchet analysis contains an FXswitcher to swap the text field depending on the user's selection. Both of these text fields are linked to an AFXfloatTarget in the form, which allows different default values to be displayed for each text field. The processUpdates for this dialog manages the FXswitcher based on the two radio buttons.

A help box is displayed by clicking on the "Tip" button. The help content changes depending on the analysis type chosen and explains the convergence options to the user.

### **E.3 Supplemental Scripts**

This file contains several scripts which perform error checking of the values in the dialog boxes.

#### **LMM\_main\_checks(mdl)**

This script performs a very basic check on the LMM\_Main dialog box. It checks that the user has selected a model from the drop down menu and it is not blank.

#### **LMM\_dimension\_checks(mdl)**

This script determines the dimensionality of the model and to make sure that the model does not contain mixed dimensionalities (e.g. plane stress and plane strain).

Each instance in the assembly is queried in turn to find if it is 3D, axisymmetric or 2D planar. If it is 2D planar then the element is queried to find out if it is plane strain or plane stress. The dimensionality of each instance is stored in a list which is then examined. If every instance is not identical then an error is returned. The dimensionality of the model is also returned to populate the jobInfoKw keyword.

#### **LMM\_matTI\_checks(value,poisFlag)**

This script checks the temperature independent material properties are valid. A single number is passed in by the variable **value**. Firstly the script checks that **value** is not blank, that it is a floating point number and that it is non-negative. The **poisFlag** variable indicates if the current value being checked is the Poisson's ratio. If it is then the extra condition that it cannot be greater than 0.5 is applied.

#### **LMM\_matTD\_checks(valuesTD,temps,roFlag=0)**

A script to check the validity of temperature dependent values. The variable valuesTD contains the temperature dependent values and temps contains the temperatures. Both of these lists are checked for blank values, non-floating point numbers and negative numbers. The roFlag variable indicates if the data currently being checked is for a Ramberg-Osgood model or not. If it is not, then the data must be in order of increasing temperature (and therefore decreasing value). This does not strictly apply to a Ramberg-Osgood material, and so this restriction is not applied to this material.

#### **LMM\_loadCycle\_checks(cycle,scl,tempCycle,analysisType,mechLoadFlag)**

This script checks the load cycle for invalid entries. The load cycle table in the dialog box is divided into the mechanical loads at the top and two lines for the temperature field and its multiplier at the bottom. If mechanical loads have been applied in the model, as indicated by the mechLoadFlag variable, then these multipliers are checked for blank values and that they are floating point numbers. If the analysis is strict shakedown or steady cycle + ratchet, which is indicated by the variable analysisType, then the scl list is checked to make sure at least one load has been selected for scaling.

The temperature fields and their multipliers are then checked. Blank fields return an error. A temperature field which has been assigned without a multiplier also returns an error.

Finally a check is made to ensure that that a steady cycle analysis or steady cycle + ratchet analysis contains at least two points in the load cycle.

#### **LMM\_job\_checks(job,wDir,existingJobs,loadInst,analysisType,convType,SCconv,conv)**

This script checks the final dialog box for errors in the name, convergence, max number of increments and working directory. Firstly the job name is checked. This follows the same

rules as are enforced when creating a job in Abaqus CAE (therefore the script LMM\_solution will be able to create a job with a legal name).

Next a check is performed to find if a job with that name already exists (this is used to post an overwrite question to the user in doCustomChecks script). Blank values are checked for, and if a steady cycle + ratchet analysis is being performed then the maximum number of increments must be greater than the  $(40 * \text{the number of load instances})$  that the steady cycle requires.

The convergence values are checked depending on the analysis type chosen. An analysis involving a steady cycle stage checks that this convergence is a floating point number between 0.0 and 1.0. A strict shakedown or steady cycle + ratchet has two options for convergence. The consecutive upper bound convergence option is checked for a floating point number between 0.0 and 1.0. The % difference option is checked for a floating point number between 0.0 and 100.0.

Finally the working directory field is checked to ensure it is not blank.

#### **LMM\_activeMats(model)**

In abaqus CAE it is possible to define a number of materials and then not use them in the analysis. This script queries the model to create a list of materials which are currently being used so that only these are considered by subsequent parts of the plug-in.

The script begins by querying the assembly to create a list of all the parts which are present in the assembly. For each of these assembled parts, the section assignments are queried to create a list of unsuppressed sections (with no duplicate sections). Finally, this list of sections is queried to create a list of materials which have been assigned to these sections (with no duplicate materials)

This list of materials used in the model is returned.

#### **LMM\_existing(model)**

This script queries the selected model to find if LMM modifications have already been made. Specifically it queries the step names. If 'LMM' is in the title then the LMM has been used on this model before.

### **LMM\_matCheck(materials, model)**

In Abaqus CAE it is possible to re-name or delete a material and then not update the section definitions that this material was assigned to. Therefore when Abaqus solves the model, the section will reference a material which is not there. This script takes the list, **materials**, and checks that each of these exists within the CAE model.

### **LMM\_remove\_mats(self,materials)**

If there are materials which are no longer part of the CAE model, then this script ensures that no data associated with these materials remains in the keywords.

The temperature independent keywords are considered first. Each of the keywords is searched and if the material is not in the **materials** list then its data is removed. Similar action is taken with the temperature dependent keywords. In this case, a search is performed to find out how many data entries are associated with the rogue material.

### **LMM\_newModelCheck(self,fPath,oldfPath)**

This script applies if a LMM analysis is performed on a model, and then another model is opened in the same CAE session also for a LMM analysis. This script compares the filepaths of the current model and that of the model last acted on by the plug-in. If these two values are different then all data in the keywords is removed, allowing this new model to start fresh. If it is the same model, then the data in the keywords is retained so that the user does not have to re-enter all the information in the dialog boxes.

The current filepath is updated in the AFXStringTarget named self.modelTgt. Therefore the current model filepath will be passed in as the previous filepath the next time the plug-in is called.

### **LMM\_extract\_CAE\_Matprops(model,matName)**

The material definitions in the model may contain data which are relevant to the LMM analysis, such as Young's modulus. This script has been written to extract such material data, so that the user does not have to re-enter it in the materials dialog box.

First the script determines whether to take the data from the material or the "original" material (see LMM\_Mats for details of creating copies of the material definitions). When

this has been established then several “try” statements determine if the material has elastic, plastic or thermal expansion data which can be extracted. Each of these is then taken in turn, extracting the data which is compatible with the LMM analysis:

- The Young’s modulus must be isotropic and not contain any field variables. In addition, the LMM does not support temperature dependent Poisson's ratio and so these values are not extracted from temperature dependent data
- The plastic data must be isotropic, not contain any field variables and cannot be rate dependent.
- The thermal expansion data must be isotropic, not contain any field variables, cannot be from the UEXPAN subroutine and cannot be temperature dependent.

All data which passes these checks is extracted into tables and returned.

#### **LMM\_mechLoadCheck(model,anType)**

When a steady cycle + ratchet limit analysis is selected at least one mechanical load must be applied in the model so that stage 2 in the subroutines can find the ratchet limit. This script checks that at least one mechanical load is applied in the model.

#### **LMM\_openModelCheck(model)**

The LMM plug-in has been designed to operate on existing models which are ready to be submitted for analysis. This script performs a quick check to ensure that the user is not invoking the LMM plug-in on a new/blank model.

#### **E.4 Scripts Called Once the Command String is Sent - LMMScripts.py**

This file contains all the scripts which are used once the user-interface portion of the plug-in is complete. In other words, these scripts perform the model configuration and create the LMM text file based on the information from the dialog boxes.

#### **LMMMainScript(...All keywords as arguments...)**

This script performs some initial preparatory work and then acts as the governing script for all operations which happen after the user-interface is complete. The preparation work includes tasks such as creating lists of the loads and predefined fields in the model, setting the working directory, naming the LMM text file and determining the number of state

dependent variables required by UMAT subroutine. When these tasks are complete, the following scripts are called in this order:

1. LMM\_loadcycle
2. LMM\_loads
3. LMM\_Mats
4. LMM\_Output
5. LMM\_solution

### **LMM\_loadcycle(...)**

This script writes the majority of the data to the LMM text file (everything bar the material properties). Table 6.2 is an example of the data which would be printed by this script.

First the script creates the text file with the name of the job + "LMM\_LC". The analysis type is written followed by the maximum number of increments specified by the user. The convergence tolerance is written (both tolerances for a steady cycle + ratchet). A percentage difference option is marked with the flag "%Diff" to differentiate it. The dimensionality of the model is then written.

The number of loads and load instances is written so that the UEXTERNALDB knows how many times to loop in order to read all the loads. The first load is named along with a flag indicating if it is scalable during the solution or not. The multipliers for that load are then written. This is repeated for all loads and predefined fields.

### **LMM\_loads(model,appLoads,preDef,BCs,jobInfo)**

This script formats the loads, predefined fields and boundary conditions in the CAE model in the following order:

1. Create a new "placeholder" step and place it first after the "Initial" step.
2. Move all loads, predefined fields and boundary conditions so that they are created in this step. This means that all the remaining steps may be operated on, suppressed or deleted without fear of deleting any loads or boundary conditions.
3. Delete any step with a name beginning in "LMM-". This is from a previous LMM analysis and will not be needed.
4. Suppress non-LMM steps

5. Create a static-general step for each of the loads and predefined fields and name it after the associated load or field. Also create the “null” and “shakedown” steps.
6. Move the loads and fields to their corresponding step.
7. Move the boundary conditions and suppressed loads to the first step which is not the placeholder.
8. Modify each load so that it is created in its corresponding step, but inactive in all subsequent steps. Similarly for the predefined fields configure them so that they are created in their corresponding step, but reset to initial in subsequent steps. This means that only one load or predefined field is active in any given step, and no loads are active in the “null” and “shakedown” steps.

### **LMM\_Mats(...)**

This script creates the User-materials needed by the UMAT subroutine. Where temperature dependent properties exist then this script also prints these to the LMM text file.

Firstly, the number of materials is written to the LMM text file. Then the active materials in the model are copied and the originals are renamed with “-Original” in their name so that the user can recover them if necessary.

The remainder of the script is contained within a large **for** loop. Each material is considered in turn and the following actions are performed:

1. Delete the material and create new with the same name. This is the quickest way to ensure the material has no properties defined.
2. Query the modulus data passed in from LMMMainScript. If it is temperature independent then write this to the LMM text file and put the value into the User-material. If temperature dependent values are used then write these and their temperatures to the LMM text file and write a zero in the User-material.
3. Repeat 2. for the yield stress and Ramberg-Osgood.
4. Write the Poisson's ratio and thermal expansion to the User-material.

When all materials have been considered in this loop, then the LMM text file is closed.

### **LMM\_Output(model,anType)**

This script creates the correct output requests for the LMM analysis. The existing requests are suppressed so they can be recovered. The LMM does not require history outputs, but a minimal one is created to prevent Abaqus CAE showing a warning to the user.

Output to the energy file is requested in this script. The only way to achieve this is to edit the keyword block i.e. no command exists to perform this directly. Lines of text are printed at the end of the keyword block to make these requests. This must be the last action taken before creating the job – these lines of text are only valid at the end of the keyword block. Any further manipulation of the model would add commands after these, making them invalid.

### **LMM\_solution(modelSel,jobInfo,anType)**

This short script creates the analysis job with the correct subroutine for the analysis chosen. This is the final script in the entire plug-in, and once complete the user will have an analysis job which is ready to submit for solution.